INL/MIS-13-30314 Rev. 4

September 2017

Assessment of BISON:
A Nuclear Fuel Performance Analysis Code
BISON Release 1.4

Idaho National Laboratory
Fuel Modeling and Simulation Department
Idaho Falls, Idaho 83415

INL/MIS-13-30314 Rev. 4

Assessment of BISON: A Nuclear Fuel Performance Code

Idaho National Laboratory
Fuel Modeling and Simulation Department
Idaho Falls, Idaho 83415

September 2017

Prepared for the
U.S. Department of Energy
Office of Nuclear Energy
Under U.S. Department of Energy-Idaho Operations Office
Contract DE-AC07-99ID13727

Assessment of BISON: A Nuclear Fuel Performance Analysis Code Rev. 4

Fuels Modeling & Simulation Department
Idaho National Laboratory
Idaho Falls, ID

June 2018

Abstract

A high-level summary of an effort to assess the predictive capability of BISON, a nuclear fuel performance code, is presented. This assessment was focused mainly on LWR fuel, and to a lesser degree, TRISO particle fuel. A comparison of BISON simulation results to a variety of experimental measurements of instrumented LWR fuel rods are shown. The source of LWR experimental data is primarily from the IAEA's FUMEX program. Benchmark simulation results of TRISO-coated particles are compared to BISON simulations. The TRISO benchmark simulations originate from the IAEA Coordinated Research Program. A brief discussion of material models and modeling approaches is also presented. There was a concerted effort to avoid model tuning to a particular set of experimental measurements. The material models and approaches were reviewed by the BISON team, and a subset of these were used for all the BISON simulations. As such, the BISON results shown in this assessment document are best-estimate as of fall 2017.

Overall, BISON simulations compare quite well with LWR experimental measurements and benchmark TRISO simulations. Discussion of future development and assessment efforts are also presented. More detailed versions of each assessment case are documented and can be found at the INL BISON repository.

Contents

1 Introduction

BISON is a modern finite-element based nuclear fuel performance code that has been under development at the Idaho National Laboratory since 2009 [1]. The code is applicable to both steady and transient fuel behavior and can be used to analyze either 1D spherical, 1.5D axisymmetric, 2D axisymmetric or 3D geometries. BISON has been applied to a variety of fuel forms including Light Water Reactor (LWR) fuel rods [1], TRISO-coated particle fuel [2], metallic fuel in both rod [3] and plate geometries, and is currently working on expanding MOX fuel capabilities.

From the beginning, the development of BISON and related software has been accompanied by the creation of numerous verification tests in which specific features of the code are tested to see if they compute the correct analytical or known solution. There are currently over 800 of these regression tests for the MOOSE/BISON code hierarchy. During code development, the tests are run frequently (typically several times a day) and the solutions checked on a variety of computer platforms.

In addition, efforts have begun to assess BISON's ability to predict fuel behavior by comparison to data from a variety of instrumented LWR fuel rods and by code comparison for a series of TRISO-coated particle fuel benchmark cases. This assessment effort has been invaluable, leading to the discovery of development oversights not apparent from the simpler regression tests. Additionally it has led to improved confidence in BISON's ability to predict nuclear fuel behavior.

Recently a reduced dimension capability for fuel rods, the 1.5 dimension (1.5D) capability, has been developed to address the need for fast running simulations of typical LWR fuel rods [4]. The 1.5D simulation capability has been validated with 2D-RZ axisymmetric simulations for a select number of LWR cases [4].

To date, the BISON LWR validation database includes 73 integral fuel rod assessment cases, covering normal reactor operating conditions and power ramp tests. These cases were selected to assess the code's ability to simulate a variety of physical behaviors including thermal response both early in life and during power ramping, fission gas release, and mechanical behavior including cladding elongation and pellet clad mechanical interaction (PCMI). In addition to these, the BISON LWR validation database comprises several cases for accident fuel rod behavior. These include 59 accident scenario simulations including; cladding-only assessment cases for cladding ballooning and burst failure under LOCA conditions, integral fuel rod LOCA cases, and a RIA accident case with code to code comparisons.

Many of these assessment cases grew out of participation in the International Atomic Energy Agency (IAEA) sponsored FUMEX-III and FUMAC Coordinated Research Projects [5, 6] and are priority cases from FUMEX-II [7], FUMEX-III, or FUMAC. Other cases were chosen based on recommendations from nuclear fuel experts.

For TRISO-coated particle fuel, a set of 13 benchmark cases have been considered which compare BISON results to those from other fuel performance codes, under normal operation and operational transients. These cases originated as part of an IAEA Coordinated Research Program (CRP-6) on High Temperature Gas Reactor (HTGR) fuel [8].

Chapters 2, 3, and 4 summarize the LWR, TRISO, and 1.5D cases, respectively. Each LWR assessment case is discussed in further detail in the attached appendices. Each result reported within is based on BISON 1.4 and can be run on a MacPro workstation. All cases can also be run, and do run nightly, on the INL high performance computer FALCON.

2 Light Water Reactor Fuel

2.1 Assessment Cases

As summarized in Table 2.1, 73 integral fuel rod LWR assessment cases covering normal reactor operating conditions and power ramp tests have been simulated. Indicated in the table are the measured quantities for comparison, namely fuel centerline temperature (FCT) at beginnng of life (BOL), throughout life (TL), and during power ramps (Ramps), fission gas release (FGR), cladding elongation (Clad-Elong), and cladding outer diameter following pellet clad mechanical interaction (PCMI).

Table 2.1: Summary table of BISON LWR assessment cases.

Experiment	Rod	FCT BOL	FCT TL	FCT Ramps	FGR	Clad Elong	Clad-Dia (PCMI)
IFA-431	1,2,3	X					
IFA-432	1,2,3	X					
IFA-515.10	A1	X	X				
US PWR 16x16	TSQ002,TSQ022		X		X		X
IFA-519	DH,DK						
IFA-534	18,19				X		
IFA-535.5/6	809,810				X	X	
IFA-597.3	7,8			X	X	X	
IFA-562	15,16,17		X		X		
IFA-636	5					X	X
Risø-2	GEm				X		X
Risø-3	II3,II5,GE7,AN2,AN8				X		X
Risø-3	AN3,AN4			X	X		
AREVA Idealized Case					X		
HBEP	6 Rods				X		
R.E. Ginna	2,4				X		
FUMEX-II Simplified Cases	27(1),(2a),(2b),(2c),(2d)				X		
OSIRIS	J12,H09						X
REGATE					X		X
Super-Ramp	11 rods				X		X
TRIBULATION	BN1/3,BN1/4,BN3/15				X	X	X
Calvert Cliffs	13 rods				X	X	X

In addition, Table 2.2 summarizes 58 assessment cases for accident fuel rod behavior with detailed results in Section 2.6.

Table 2.2: Summary table of BISON LWR accident fuel rod behavior assessment cases.

Experiment	Rod	Burst	LOCA	RIA
IFA-650	2,10		X	
CABRI REP NA	2,3,5,10			X
Hardy Tube Test	3 rods	X		
PUZRY	31 rods	X		
REBEKA	8 rods	X		
OECD RIA Benchmark	5			X
NSRR FK	9 rods			X

2.2 Material and Behavioral Models

This section briefly reviews the BISON material and behavior models used in analyzing the LWR assessment cases. Theoretical details may be found in the BISON Theory Manual [9], and descriptions of the input options for the models are in the BISON User's Manual [10].

Burnup Evolution of burnup is typically driven by a table of rod averaged linear power at given times in the analysis. Axial variations are described in a simialr manner. The radial power profile is modeled according to [11] and [12]. This model computes the evolution of the concentrations of various heavy metal isotopes locally across the radius of the fuel pellet and the coupled evolution of the radial power and burnup distributions. (See [9, Power, Burnup, and Related Models][10, Burnup].)

Contact Mechanical contact is enforced using node/face constraints. The penalty algorithm is commonly used. The interaction is enforced with a frictionless model. (See [9, Mechanical Contact][10, Mechanical Contact].)

Elastic An elastic material law is used for the fuel. A creep model is available but was not chosen due to the fact that it predicts excessive creep as a result of excessively high stresses in the absence of a cracking model. Typical parameters are 2×10^{11} N/m^2 for Young's modulus and 0.345 for Poisson's ratio. The coefficient of thermal expansion is 10×10^{-6} m/m/K. (See [10, Solid Mechanics Models].)

GrainRadiusAux When a polycrystalline material is subject to high temperatures, larger grains tend to grow at the expense of the smaller ones. As a consequence, the latter gradually disappear, thus reducing the total number of grains per unit volume and increasing the average grain size. The granular structure of the fuel affects physical processes such as fission gas behavior (Section 2.4). A simple empirical model [13] is implemented in BISON for calculating grain growth in UO_2 fuel. (See [9, Grain Growth][10, Other AuxKernels].)

HeatConductionMaterial The general HeatConductionMaterial is used to set the thermal conductivity and specific heat for the clad. Thermal conductivity is set at 16 W/m/K, and specific heat is 330 J/kg/K. (See [10, Thermal Models].)

MechZry The MechZry model is capable of tracking primary, thermal, and irradiation-induced creep in clad. Typical parameters are 7.5×10^{10} N/m^2 for Young's modulus and 0.3 for Poisson's ratio. The coefficient of thermal expansion is 5×10^{-6} m/m/K.The Franklin irradiation growth model is also incorporated into this material model. (See [9, Thermal and Irradiation Creep; Limbäck Creep Model][10, Solid Mechanics Models].)

RelocationUO2 RelocationUO2 accounts for cracking and relocation of fuel pellet fragments in the radial direction. This model is necessary for accurate modeling of LWR fuel. (See [9, Relocation][10, Solid Mechanics Models].)

Sifgrs The Simple Integrated Fission Gas Release and Swelling (Sifgrs) model is intended for consistently evaluating the kinetics of both fission gas swelling and release in UO_2. (See [9, Fission Gas Behavior][10, Fission Gas Models].)

ThermalContact The transfer of heat from the fuel to the cladding is accomplished via the ThermalContact model. The model is based on [14]. This model includes a computation of the conductivity of the gas using the MATPRO model [15], increased conductance due to mechanical contact [14], and radiant heat transfer. Temperature jump distance is computed [16]. Typical roughness values are 1 μm for the clad and 2 μm for the fuel, with a roughness coefficient of 3.2. (See [9, Gap Heat Transfer][10, Thermal Contact].)

ThermalFuel The ThermalFuel model incorporates several empirical fits for thermal conductivity of UO_2. The assessment cases were run with the NFIR correlation [17]. The NFIR model contains a temperature dependent thermal recovery function that accounts for self-annealing of defects in the fuel as it heats up. The ultimate effect of the self-annealing is a slight increase of the thermal conductivity over a range of temperatures up to $\sim$1200 K. (See [9, Thermal Properties][10, Thermal Models].)

2.3 Thermal Behavior

The ability to accurately predict fuel rod thermal behavior is essential for fuel performance analysis. Temperatures drive many other important physical phenomena, such as fission gas release and clad thermal creep. Peak fuel temperatures are of primary importance in determining fuel rod performance and lifetime.

2.3.1 Beginning of Life

Seven of the rods simulated to date considered only the first rise to power, also referred to as beginning of life (BOL). Temperature comparisons during the first rise to power are significant as they isolate several important aspects of fuel rod behavior before complexities associated with higher burnups are encountered. Proper prediction of BOL centerline temperatures requires accurate models for the fuel and clad thermal conductivity, gap heat transfer, thermal expansion of both the fuel and the clad materials (to predict an accurate gap width), and fuel relocation. Figure 2.1 summarizes the BOL fuel centerline temperature comparisons for all cases considered. Plotted is the measured versus predicted temperature as the rod power is increased during power-up. The solid line indicates a perfect comparison, and the dashed lines indicate $\pm$10 percent error. For all BOL cases considered to date, BISON does a good job of predicting the fuel centerline temperature.

2.3.2 Through Life

Four experimental cases in Table 2.1 contained through life temperature data, IFA-515.10 Rod A1 and IFA-562 Rods 15, 16 and 17 [18, 19] . The four cases were composed of annular UO_2 fuel pellets enclosed in a Zircaloy-2 cladding. The through life temperature measurements were obtained using centerline expansion thermometers (ET) that were placed inside the inner diameter of the fuel stack. These ETs spanned the entire length of the fuel stack and therefore provided average fuel centerline measurements. The temperature is derived from the expansion of the ET that is measured by a LVDT. These rods were irradiated to high burnups (75.5 MWd/kgUO_2 for IFA-515.10 Rod A1 and an average of 49.4 MWd/kgUO_2 for the IFA-562.2 rods) to assess temperature evolution as a function of burnup. To more accurately assess BISON's capabilities of predicting temperature through life, measured vs. predicted plots are given for four different burnup increments: $0 \leq Bu < 20$, $20 \leq Bu < 40$, $40 \leq Bu < 60$, and $Bu \geq 60$ MWd/kgUO_2 as shown in Figure 2.2.

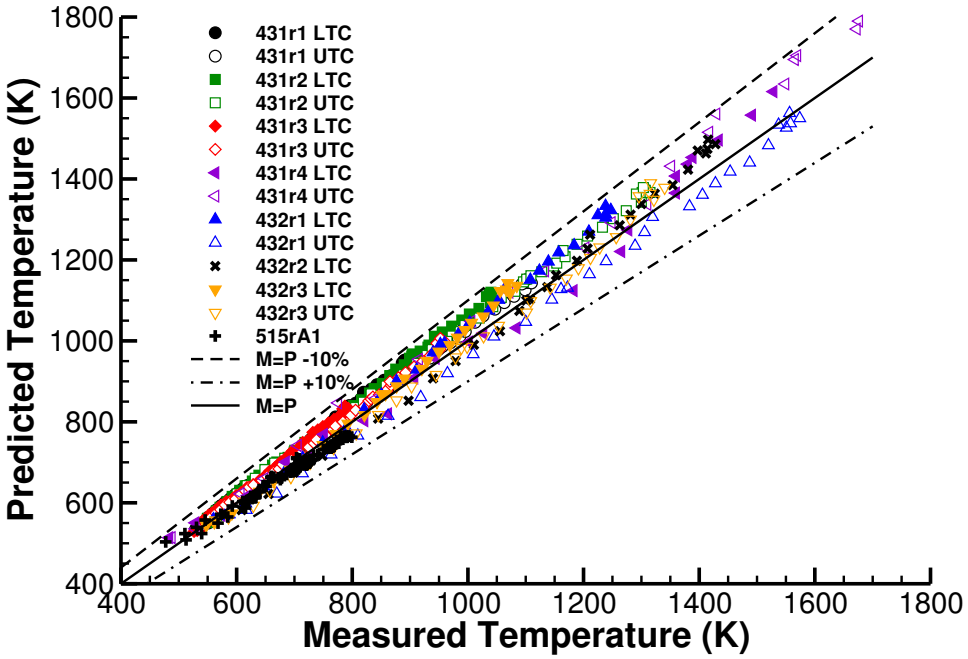

Figure 2.1: BOL measured vs. predicted fuel centerline temperature for rods 1, 2, and 3 in IFA-431, IFA-432, and IFA-515.10 Rod A1. LTC and UTC stand for lower and upper thermocouple measurements, respectively.

Considering IFA-515.10 Rod A1 it is observed the temperature predictions show similar behavior for all burnup ranges illustrated in Figures 2.2(a), 2.2(b), 2.2(c), and 2.2(d) as illustrated by the blue circles. At low temperatures BISON matches the experiment quite well with the majority of points falling close to the M=P line. At higher temperatures BISON primarily under predicts the centerline temperature with a few points falling outside the $\pm 10\%$ range. Even in the high burnup region shown in Figure 2.2(d) almost all data points fall within the $\pm 10\%$ range indicating that the thermal conductivity degradation as a function of burnup is accurately captured. Overall BISON predicts the centerline temperature quite well through life for IFA-515.10 Rod A1 considering the complexities associated fuel and cladding evolution over such long irradiation times.

Contrarily to the the IFA-515.10 irradiation, the rods analyzed from the IFA-562.2 experiment illustrate that BISON primarily over predicts the temperature with less scatter in the points for all burnup ranges. As expected all the IFA-562.2 rods have very similar predicted temperatures since the power histories were similar. The reason for including two simulations of Rod 17 with two different assumed fuel roughnesses, denoted by R_f, is to highlight the changes in predictions based solely on the interpretation of the experiment. The documentation for the IFA-562.2 rods did not provide an as-fabricated fuel roughness and therefore the roughness was assumed to be the BISON default value of 2 μm. This default value is used for any validation case for which a fuel roughness is not provided. The chosen value of 0.2 μm was the reported value for the IFA-515.10 experiment [18]. Comparing the two data sets for Rod 17 in Figure 2.2 it is observed that the simulation with the lower surface roughnesses predicts lower fuel centerline temperatures. The deviation between the two simulations becomes larger as irradiation progresses. This is because at higher burnups the fuel has come into contact with the cladding and the fuel roughness plays a crucial role in the solid-solid conductance term of the heat transfer coefficient between the fuel and cladding. What this simple study illustrates is that the interpretation of the experimental documentation can have a significant impact on predictions of the fuel performance code. The purpose of a mechanistic fuel performance code is to provide predictions without any tuning of parameters. In order to do this experiments should provide all of the details associated with the experiment including uncertainties such that model predictions can be assessed against the uncertainty within the experimental measurements.

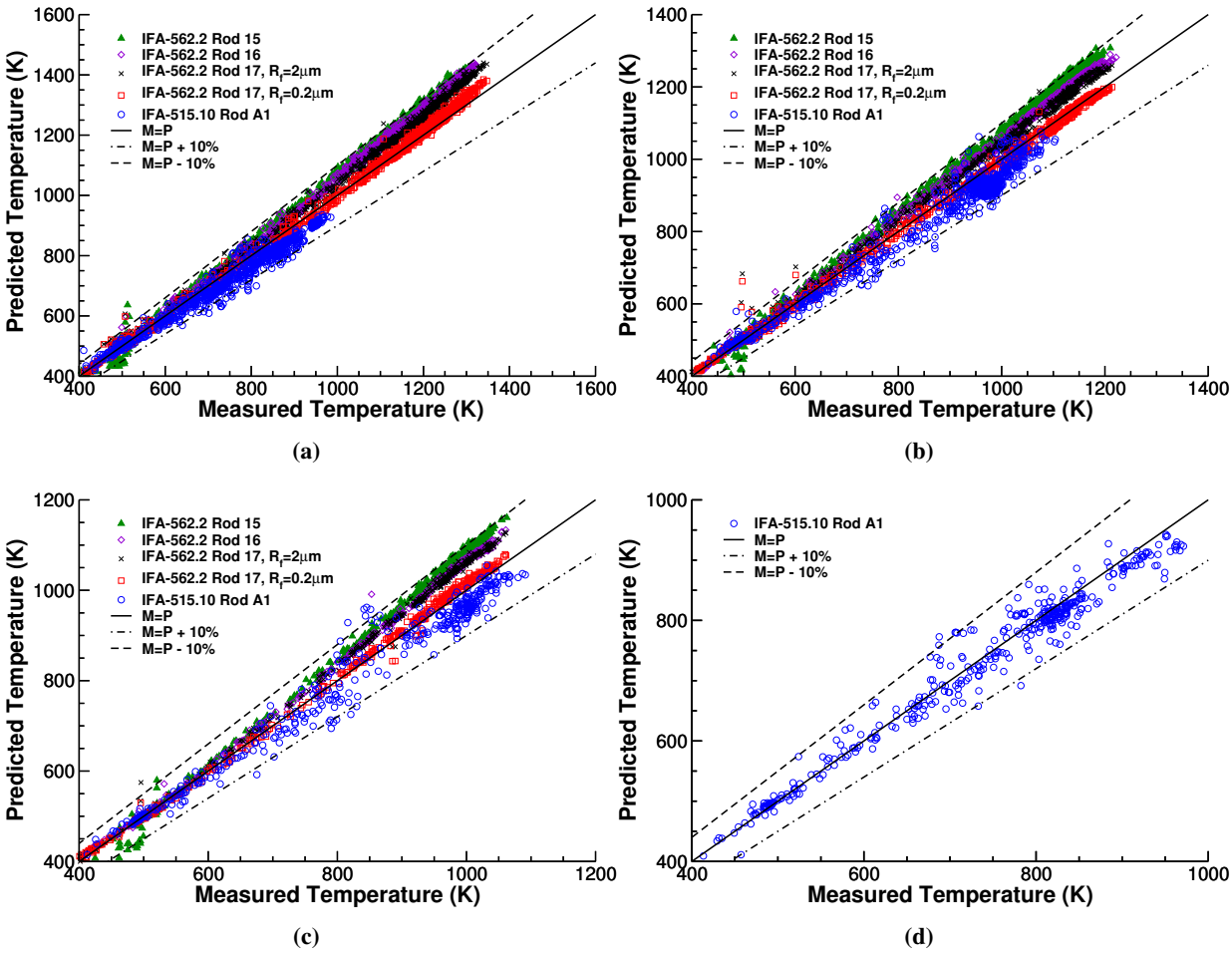

Figure 2.2: Comparison of the measured vs. predicted fuel centerline temperature for through life rods for four different burnup ranges: (a) $0 \leq Bu < 20$, (b) $20 \leq Bu < 40$, (c) $40 \leq Bu < 60$, and (d) $Bu \geq 60$ MWd/kgUO$_2$. The R$_f$ parameter in the IFA-562.2 Rod 17 series labels indicate the fuel roughness used in the simulation.

2.3.3 Ramp Tests

Similar to Figs. 2.1 and 2.2, Fig. 2.3 compares measured and predicted fuel centerline temperatures for the five ramp test experiments. Comparisons are reasonable, with some points falling outside the $\pm 10\%$ error bands. Note that focusing only on data from the Risø-3 experiments indicates a tendency to over predict temperature at low power and under predict temperature at high power. However, the single Halden experiment (IFA-597.3 rod 8) shows no such trend. Additional ramp test comparisons are needed (and in progress) to better understand this observation.

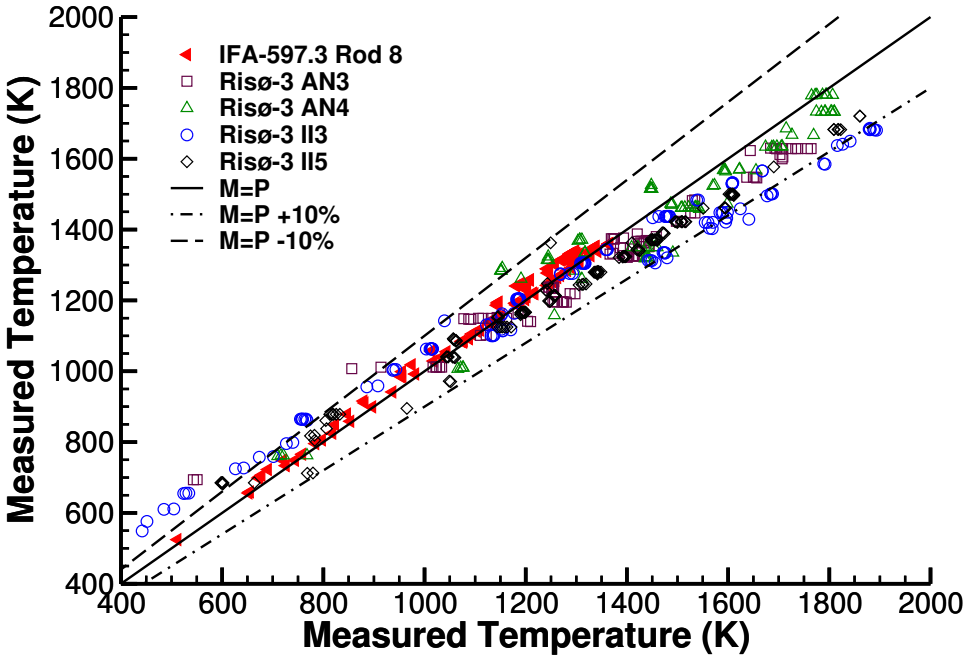

Figure 2.3: Comparison of the measured vs. predicted fuel centerline temperature for fuel rods that experienced power ramps.

2.3.4 Thermal Behavior Summary

BOL, through-life, and ramp temperature measurements of LWR experiments were compared to BISON simulation results in order to evaluate the models used in BISON. The comparisons show the BISON calculations are reasonably close to experimental measurements. This is significant because fuel temperatures strongly affect important physical processes such as fission gas release and clad creep and directly determine fuel rod life.

2.4 Fission Gas Behavior

The processes induced by the generation of the fission gases xenon and krypton in nuclear fuel have a strong impact on the thermo-mechanical performance of the fuel rods. On the one hand, the fission gases tend to precipitate into bubbles resulting in fuel swelling, which promotes pellet-cladding gap closure and the ensuing pellet-cladding mechanical interaction (PCMI). On the other hand, fission gas release (FGR) to the fuel rod free volume causes pressure build-up and thermal conductivity degradation of the rod filling gas.

A Simple Integrated Fission Gas Release and Swelling (Sifgrs) model is available in BISON for the coupled fission gas swelling and release in UO_2. The model is founded on a physics-based description of the relevant processes, while retaining a level of complexity consistent with the application to engineering-scale nuclear fuel analysis. The Sifgrs model draws on and extends the approach described in [20].

The mutual dependence between fission gas behavior and grain growth is taken into account in Sifgrs through coupling with the grain growth model (Section 2.2).

As a first step, the model was implemented and tested in BISON for the analysis of FGR only [20]. More recently, the calculation of the fission gas swelling as coupled with the FGR has been introduced and matched with the mechanical analysis in BISON. Testing of the full Sifgrs fission gas release and swelling model is underway. First results are presented in this report, including comparisons with the empirical fission swelling model from MATPRO [15], also available in BISON.

The Vitanza Criterion was simulated to determine the burnup dependent threshold temperature at which more than 1% FGR can be expected. BISON falls within the ranges of other well-known fuel performance codes as shown in Figure 2.4.

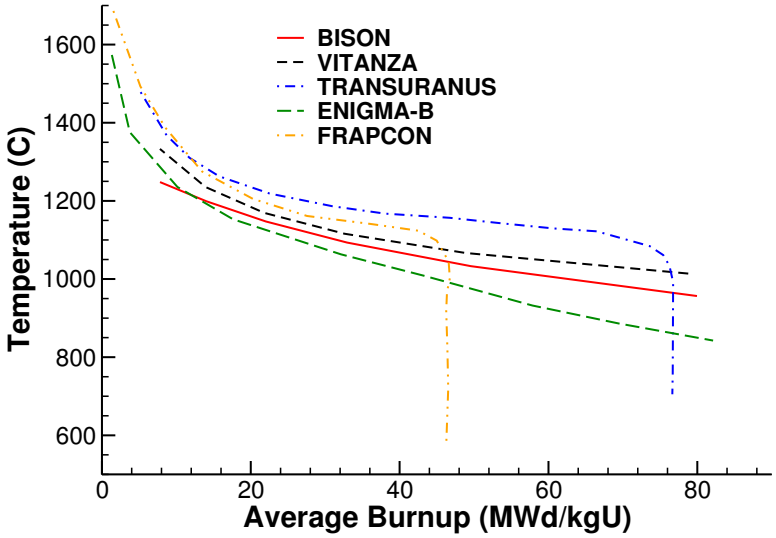

Figure 2.4: 27(1) BISON and other code results compared to Vitanza criteria [21].

FGR comparisons were performed with multiple assessment cases (see Table 2.1). To best summarize a majority of these comparisons, a measured versus predicted plot of the end of life total fission gas release for normal operations/bump tested rods is shown in Figure 2.5.

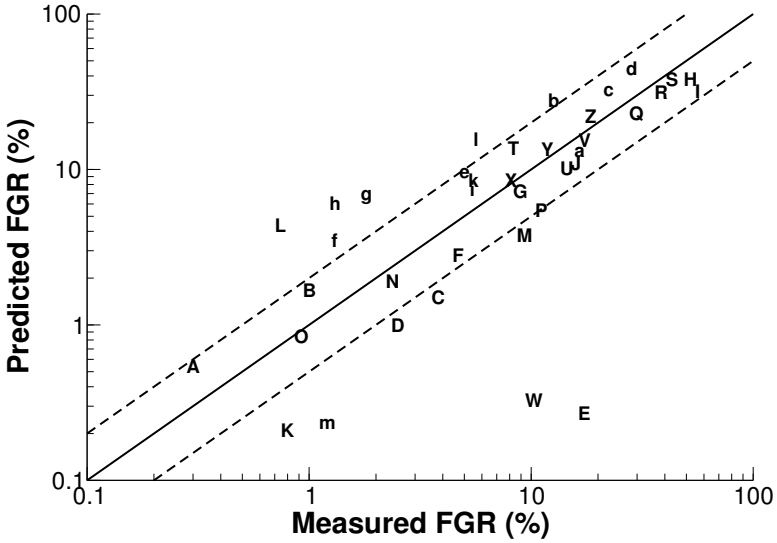

Figure 2.5: Measured vs. predicted end of life total fission gas release comparisons for normal operation/bump tested rods.

2.4.1 Fission Gas Behavior Summary

BISON predicts the total FGR well at low burnup, however, at high burnup, BISON under predicts the total FGR. To date, the Sifgrs model provides a basis for integrating increasingly accurate descriptions of the fission gas swelling and release mechanisms. Development of the more advanced description of

Table 2.3: Legend for Figure 2.5

Experiment	Designator	Experiment	Designator
HBEP A1/8-4	A	Riso 3 II3	V
HBEP A3/6-4	B	Riso 3 II5	W
HBEP BK363	C	Super Ramp PK1-1	X
HBEP BK365	D	Super Ramp PK1-2	Y
HBEP H8/36-4	E	Super Ramp PK1-3	Z
IFA-534 rod 18	F	Super Ramp PK1-4	a
IFA-534 rod 19	G	Super Ramp PK2-1	b
IFA-535 rod 809	H	Super Ramp PK2-2	c
IFA-535 rod 810	I	Super Ramp PK2-3	d
IFA-597.3 rod 8	J	Super Ramp PK2-4	e
OSIRIS H09	K	Super Ramp PK6-2	f
OSIRIS J12	L	Super Ramp PK6-3	g
Regate	M	Super Ramp PK6-S	h
R.E. Ginna rod 2	N	Tribulation BN1/3	i
R.E. Ginna rod 4	O	Tribulation BN1/4	k
Riso 2 GEm	P	Tribulation BN3/15	l
Riso 3 AN2	Q	USPWR 16x16 TSQ002	m
Riso 3 AN3	R	USPWR 16x16 TSQ022	n
Riso 3 AN4	S		
Riso 3 AN8	T		
Riso 3 GE7	U		

the intra-granular gas behavior, including consideration of the fuel swelling contribution due to intra-granular gas bubbles is currently underway.

2.5 Mechanical Behavior

Accurately representing the mechanical behavior of the fuel and clad is also essential when simulating fully-coupled thermomechanics problems like LWR fuel pins. Together with the thermal solution, the mechanical models determine the fuel-clad gap size, which may be the single most important characteristic to quantify in LWR simulations. Simulating realistic mechanical behavior is also critical when attempting to make predictions about clad structural integrity during pellet clad mechanical interaction (PCMI).

The following sections summarize BISON simulations of experiments where the fuel pellets have come into contact with the clad. Measurements of final clad length and diameter are compared to BISON calculations. These comparisons showcase the fuel and clad mechanical behavior models such as thermal expansion, clad irradiation growth, clad creep, fuel relocation, fuel swelling, fuel densification, and, perhaps most importantly, the mechanical interaction of fuel and clad as the two come into contact.

2.5.1 Clad Elongation

One way to quantify the mechanical behavior of LWR fuel rods is clad elongation. The point in time at which fuel and clad interact mechanically itself depends on several factors including pellet fracturing and relocation. It is also important to recognize that the eccentric placement of fuel pellets in the clad allows mechanical interaction from very early times.

Once the mechanical interaction begins, the relative motion of the fuel and clad depends on the friction between them. The value of the friction coefficient is understood to come with a large amount of

uncertainty.

One clad elongation case has been included to date: IFA-597. This case has been run with frictionless and glued (infinite friction) contact conditions to bound the solution. A plot of elongation vs. time is shown in Figure 2.6.

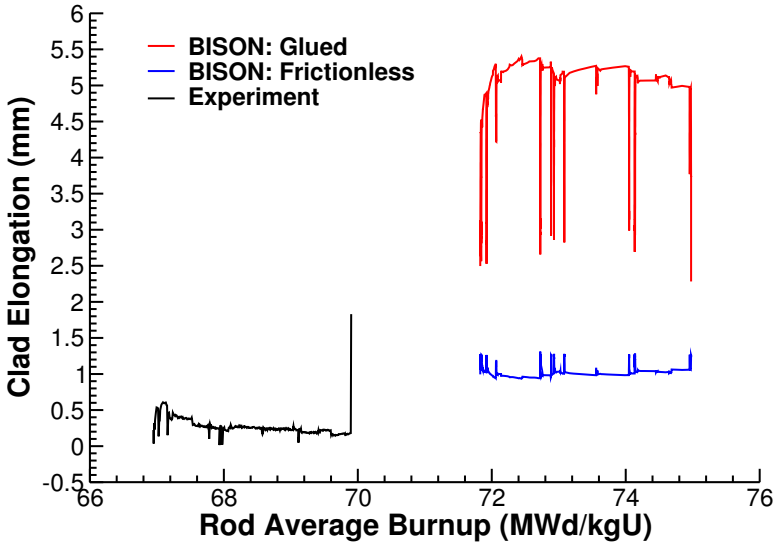

Figure 2.6: IFA-597 elongation comparison.

There is data available for eight of the cases listed to compare fuel rod elongation, however, without frictional contact, it is not feasible to make these comparisons at this time.

2.5.2 Clad Final Diameter

Clad final diameter simulations and measurements are another way to quantify mechanical behavior models. The multiple experiments considered to date where final rod diameter measurements were made. Figure 2.7 is a summary plot of the measured minus predicted clad outer diameter after base irradiation and Figure 2.8 is a summary plot of the difference of the clad diameter change during the ramp. These experiments all consisted of a base irradiation followed by application of a power ramp before the end of the experiment.

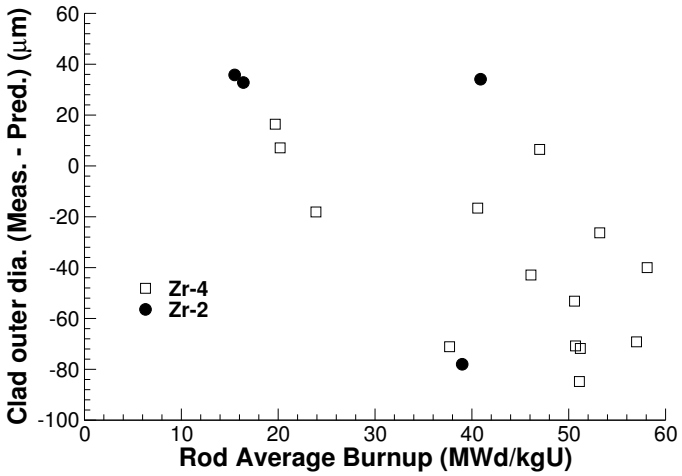

Figure 2.7: The difference between measured and predicted cladding outer diameter as a function of burnup.

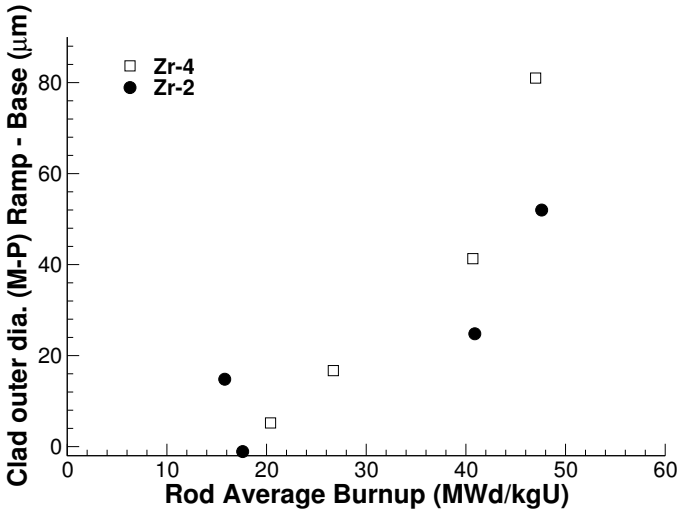

Figure 2.8: The difference between measured and predicted difference between cladding outer diameter after and before the ramp as a function of burnup.

2.5.3 Mechanical Behavior Summary

Clad elongation and final diameter experimental measurments and BISON calculations have been presented for the purpose of quantifing the mechanical behavior and contact models in BISON. Overall, the comparisons are good but show a need for more accurate models. One possibility is to upgrade the nonlinear material models. For example the clad creep models (primary, secondary, and tertiary) and instantaneous plasticity could be coupled. Perhaps more importantly, more information regarding clad material characteristics (e.g. exact alloy specifications) and testing under realistic environments (thermal and irradiated) could be obtained via testing programs and incorporated into the material models. Further development work on nonlinear material modeling is an area of focus for next year.

2.6 Accident Analysis

Efforts have been spent to expand and validate BISON for the analysis of LWR fuel rod behavior during accident situations, including Loss-of-Coolant Accidents (LOCA) and Reactivity Insertion Accidents (RIA). To date, 58 assessment cases for accident fuel rod behavior have been completed and are summarized in Table 2.2.

BISON's capability enhancements for accident analysis include models for high-temperature creep and instantaneous plasticity, crystallographic phase transition, high-temperature steam oxidation of Zircaloy cladding, and cladding failure due to burst [22, 23, 24]. Also, BISON's model of fission gas swelling and release in UO_2 was extended to include a specific treatment of burst release effect during transients [25]. In addition, in order to improve the numerical solution in presence of non-linear material behavior (plasticity, creep) during accident situations, a new automatic time step control was developed for BISON [24].

An example of BISON validation for LOCA analysis is given in Fig. 2.9, showing the comparisons between BISON predictions and experimental data of cladding inner pressure at failure and time to failure for the simulations of the PUZRY tests. The obtained accuracy is encouraging and in line with the state of the art of fuel cladding modeling under LOCA conditions.

BISON was also validated against an integral fuel rod LOCA experiments. A first example is the Halden IFA-650.2 test, which was carried out in the Halden Reactor on a fresh PWR fuel rod segment. We present comparisons between calculated and experimental inner pin pressure and time to burst for IFA-650.2. In Figure 2.10, calculated inner pin pressure is compared to the on-line experimental measurement, with predicted and experimental time to burst being also illustrated. The comparison points

out that both quantities are reasonably well predicted by BISON. Calculated time to burst is within 7 seconds of the experimental one.

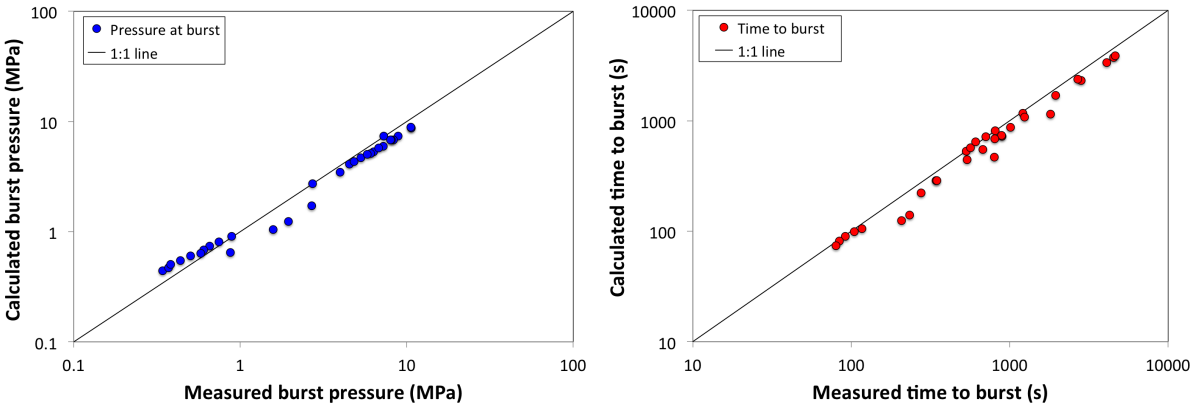

Figure 2.9: Comparison of calculated and measured cladding inner pressures at burst (left) and time to burst (right) for the PUZRY cases.

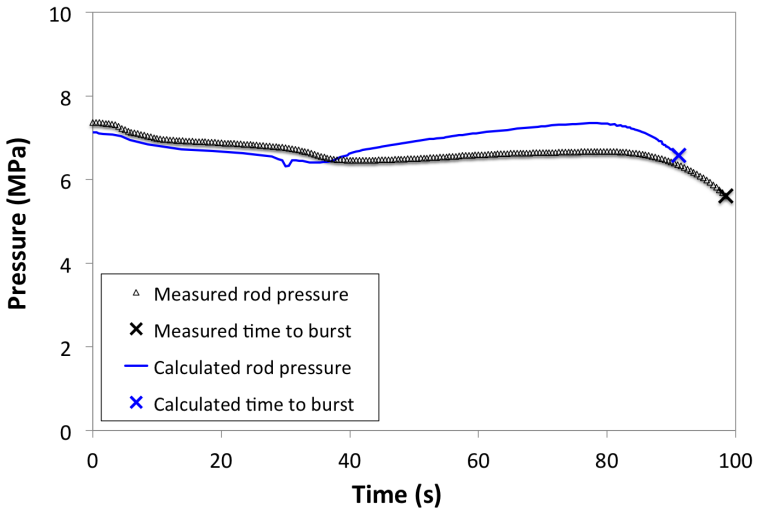

Figure 2.10: Comparison between measured and calculated fuel rod inner pressure and time to cladding bust for the Halden IFA-650.2 LOCA transient. Time zero corresponds to the beginning of the blowdown phase.

BISON LOCA validation also includes the more complex Halden test IFA-650.10, which was carried out using a segment of a PWR rod that had been irradiated in a commercial PWR (Gravelines 5, 900 MWe, EDF, France) up to a burn-up of 61 MWd/kgU. As an example of results, in Figure 2.11 the time evolution of rod inner pressure during the IFA-650.10 LOCA transient is compared to the experimental data from Halden. BISON reproduces the experimental behavior with a good accuracy. The time to burst failure is predicted to be 7 seconds before experimentally observed, which is both accurate and conservative.

In the framework of the RIA Fuel Codes Benchmark organized by the Organization for Economic Co-operation and Development (OECD)/Nuclear Energy Agency (NEA)/Working Group on Fuel Safety (WGFS) [26], results of different simulations on simplified cases were compared in order to investigate modeling of RIAs with different codes. Aside from the benchmark case 5 was selected to perform a comparison between BISON and FRAPTRAN codes [27]. This provided an opportunity for an initial assessment of BISON's ability to model RIA accidents. As an example of results from this effort,

Fig. 2.12 shows the temperature profiles at different radial locations in the rod. A good agreement is observed between BISON and FRAPTRAN calculations.

Initial validation of BISON for Reactivity-Initiated Accident cases has been performed on four cases. The four cases were base irradiated to burnup levels ranging from 33 to 64 GWd/tU and tested in the CABRI test reactor in France. The cases (CABRI REP Na 2, 3, 5, and 10) were tested under sodium coolant conditions. The BISON results are compared against experimental and calculated values reported in open literature from the IRSN and results of the FALCON fuel performance code from EPRI.

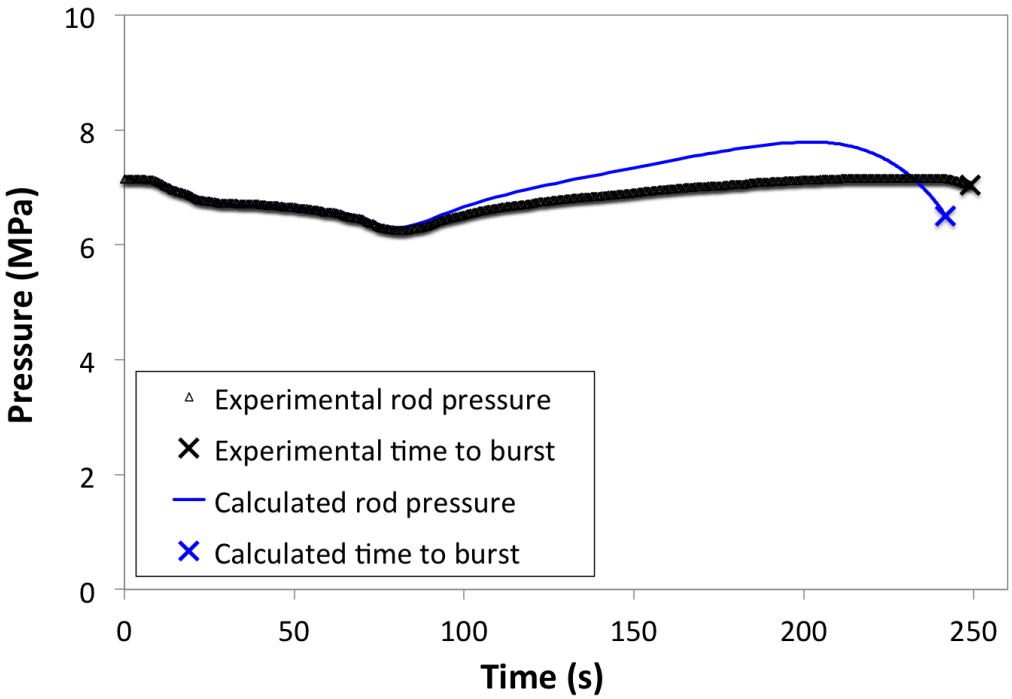

Figure 2.11: Rod inner pressure evolution during the IFA-650.10 test and time to cladding burst. BISON results are compared to the Halden experimental data.

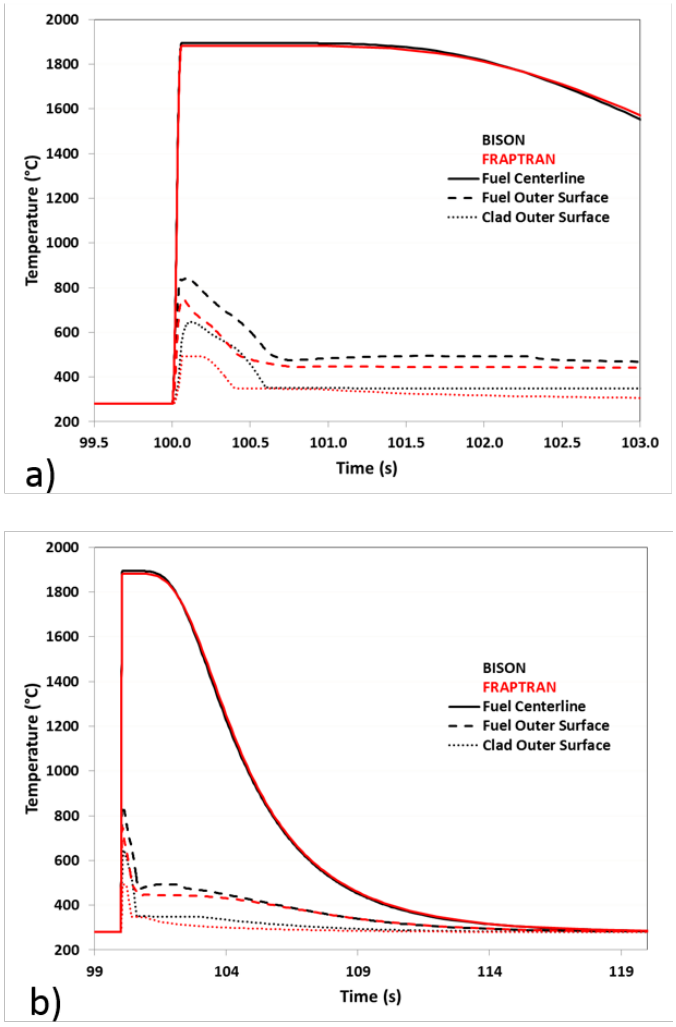

Figure 2.12: Temperature profiles at different radial locations on the rod for the WGFS RIA Fuel Codes Benchmark Case 5. a) Temperature profiles during a smaller temporal scale around the power pulse and b) larger temporal scale showing temperature profiles during the cooling of the rod.

3 TRISO-Coated Particle Fuel

3.1 Assessment Cases

As part of an International Atomic Energy Agency (IAEA) Coordinated Research Program (CRP-6) on High Temperature Gas Reactor (HTGR) reactor fuel technology, a set of benchmarking activities were developed to compare fuel performance codes under normal operation and operational transients [8]. Sixteen benchmark cases were identified, ranging in complexity from a simple fuel kernel having a single elastic coating layer, to realistic TRISO-coated particles under a variety of irradiation conditions. In each case, the particle geometry, constitutive relations, material properties, and operating conditions were carefully prescribed to minimize differences between the various code predictions; details are given in [8]. As an early code assessment exercise, BISON has been applied to 13 of the 16 benchmark cases, as summarized in Table 3.1.

Table 3.1: IAEA CRP-6 benchmark cases considered in the BISON coated-particle assessment exercise. HFR-K3 and HFR-P4 are German pebble and fuel element experiments, respectively.

Case	Geometry	Description
1	SiC layer	Elastic only
2	IPyC layer	Elastic only
3	IPyC/SiC	Elastic with no fluence
4a	IPyC/SiC	Swelling and no creep
4b	IPyC/SiC	Creep and no swelling
4c	IPyC/SiC	Creep and swelling
4d	IPyC/SiC	Creep- and fluence-dependent swelling
5	TRISO	350 μm kernel, real conditions
6	TRISO	500 μm kernel, real conditions
7	TRISO	Same as 6 with high BAF PyC
8	TRISO	Same as 6 with cyclic temperature
10	HFR-K3	10% FIMA, 5.3×10^{-25}n/m^2 fluence
11	HFR-P4	14% FIMA, 7.2×10^{-25}n/m^2 fluence

The models for all benchmark cases used either six or eight quadratic axisymmetric finite elements across the width of each coating layer. A typical mesh with eight elements per layer is shown in Figure 3.1. Note that, in addition to the axisymmetry condition, a symmetry plane is also assumed along the top of the mesh. For cases 1 and 2, numerical solutions were also obtained with twelve elements across the coating layer to determine whether the mesh was sufficiently refined. Maximum tangential stresses obtained from the refined mesh models differed at most by 0.1%, demonstrating adequate mesh convergence with the coarser meshes. Since all of the cases are spherically symmetric, identical results (within machine precision) can be obtained using either 1D spherically symmetric or 3D elements.

The BISON input and all supporting files (mesh, mesh scripts, etc.) for the thirteen TRISO benchmark cases are provided with the code distribution at bison/assessment/TRISO_benchmarks. For users who wish to run these benchmarks, additional explanation is required. Because the IAEA CRP cases involved comparison of results from a large number and variety of codes, the particle geometry, boundary conditions and material models were prescribed for each case in detail. This was done principally to avoid differences in material models, which can be substantial between the various codes. In some cases these prescribed models differed from the standard BISON TRISO material models. Rather than

implement these numerous and specific models in the code, temporary models were developed and the necessary source code to use these models was stored with the individual cases. For the benchmark cases requiring these models (all except 1-3), users must overwrite the material model source code, re-compile, run the problem, and revert back to the original source. Refer to README files, included in each directory where such modifications are required, for more detail. This cumbersome process will be elimated in the future.

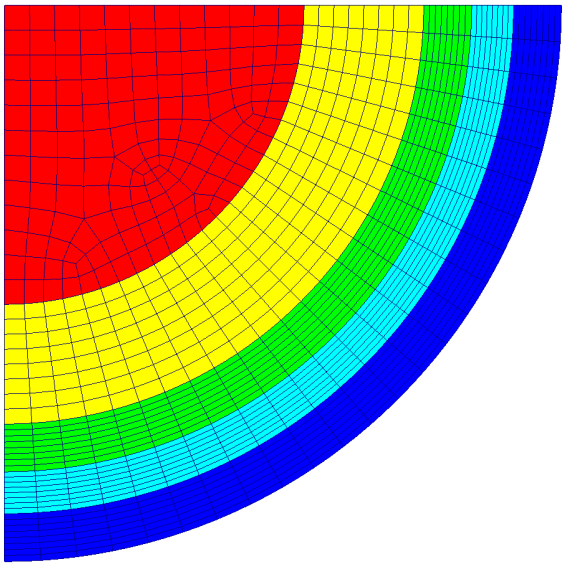

Figure 3.1: Typical computational mesh used for the IAEA CRP-6 benchmark cases.

3.2 Results

Cases 1 to 3 were limited to single and double coating layers and tested simple elastic thermomechanical behavior against analytical solutions. A comparison of the analytical and BISON numerical solutions for the maximum tangential stress, which occurs at the inner surface of the various layers, is shown in Table 3.2. Comparisons are excellent.

Table 3.2: Comparison of the BISON computed maximum tangential stress (MPa) to the analytical solution for Cases 1 to 3.

Case	Layer	Analytical	BISON	Error (%)
1	SiC	125.19	125.23	0.032
2	IPyC	50.200	50.287	0.173
3	IPyC/SiC	8.8/104.4	8.7/104.5	1.14/0.10

Cases 4a to 4d included both IPyC and SiC layers and investigated pyrolytic carbon layer behavior under a variety of conditions. Cases 5 to 8 considered a single TRISO particle with more complexity added with each subsequent case. For cases 1 to 4d, the internal gas pressure was fixed at 25 MPa while cases 5 to 8 included a linear pressure ramp. The particle temperature was held uniform at 1273 K for cases 1 to 7, but for case 8 was cycled ten times between 873 and 1273 K, characteristic of fuel in a pebble bed reactor. For cases 4 to 7, Table 3.3 compares BISON computed solutions to the range of solutions from eight coated-particle fuel codes included in the CRP-6 exercise [8]. Comparisons are of

the tangential stress at the inner surface of both the IPyC and SiC layers, at the end of irradiation. The BISON solutions are always within the range of values computed by the other codes. Note that tabulated values defining the ranges were extracted from plots in [8] and are thus not precise.

Table 3.3: Comparison of the BISON computed tangential stress (MPa) to the range of values computed by the codes included in the CRP-6 exercise. Comparisons are at the inner surface of each layer and at the end of irradiation.

Case	Layer	CRP-6 codes [range]	BISON
4a	IPyC/SiC	[925, 970]/[-775, -850]	928/-819
4b	IPyC/SiC	[-25, -25]/[138, 142]	-25.0/139
4c	IPyC/SiC	[25, 27]/[83, 92]	26.0/89.4
4d	IPyC/SiC	[25, 35]/[71, 88]	27.8/87.0
5	IPyC/SiC	[40, 58]/[-56, -28]	41.9/-32.2
6	IPyC/SiC	[27, 38]/[28, 48]	29.2/44.9
7	IPyC/SiC	[37, 50]/[10, 25]	38.0/24.6

Although code comparisons in Table 3.3 are provided only at the end of irradiation, comparisons were made at various intermediate times during the irradiation period. The BISON solutions were always within the range of solutions produced by the CRP-6 codes.

Figure 3.2 compares solutions for case 8, which involved a cyclic particle temperature, during the full irradiation history. In this figure, BISON solutions of the tangential stress at the inner wall of the IPyC and SiC layers are compared to solutions from three codes from the CRP-6 exercise, namely PARFUME [28], ATLAS [29] and STRESS3 [30]. As above, data for the code comparisons were extracted from plots in [8]. For the IPyC layer, the four solutions essentially overlay each other during the entire irradiation period. In the SiC layer, the four solutions are quite similar but some differences are evident, particularly for the first four temperature cycles. The BISON solution falls roughly midway between the PARFUME and STRESS3 solutions and is essentially identical to the ATLAS solution.

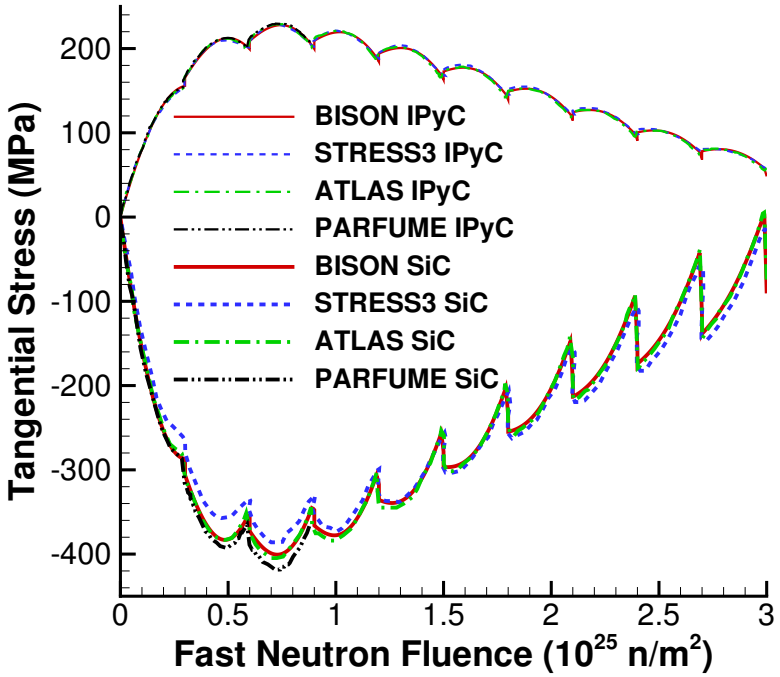

Figure 3.2: Code comparison for case 8, which included a ten cycle temperature history. Plotted is the tangential stress at the inner wall of the IPyC and SiC layers.

Cases 9 to 13 in CRP-6 were more complicated benchmarks based on past or planned experiments with TRISO-coated particles. The two cases considered here (10 and 11) were based on German fuel from pebble and fuel element experiments. Again, details are provided in [8]. Although material properties and constitutive relations were prescribed for these cases, they differed from cases 1 to 8 in two ways: (1) the internal pressure was not fixed but instead determined by fission gas release and CO production and (2) the particle size was prescribed as a population (mean value and standard deviation) rather than a single value. BISON solutions were based on the gas release and CO production models described above; however, for simplicity, only a single particle size was considered based on the mean particle diameter.

Figure 3.3 provides code comparisons of the total gas pressure (Figure 3.3(a)) and tangential stress at the inner wall of the SiC layer (Figure 3.3(b)) for benchmark cases 10 and 11. Again, BISON is compared to three codes from the CRP-6 exercise. Substantial differences exist in these solutions, particularly for the gas pressure. The BISON solution histories, however, compare well to the range of solutions given by the three well-established codes chosen for comparison.

As stated in [8], the differences between various code predictions shown in Figures 3.3(a) and 3.3(b) can be largely attributed to the models used to calculate fission gas release and CO production in the kernel. A detailed description of these models is not available in [8], limiting more detailed investigation. One obvious and significant difference is that both BISON and ATLAS employ the simple Proksch et al. [31] empirical model for CO production while PARFUME [28] uses a detailed thermochemical model.

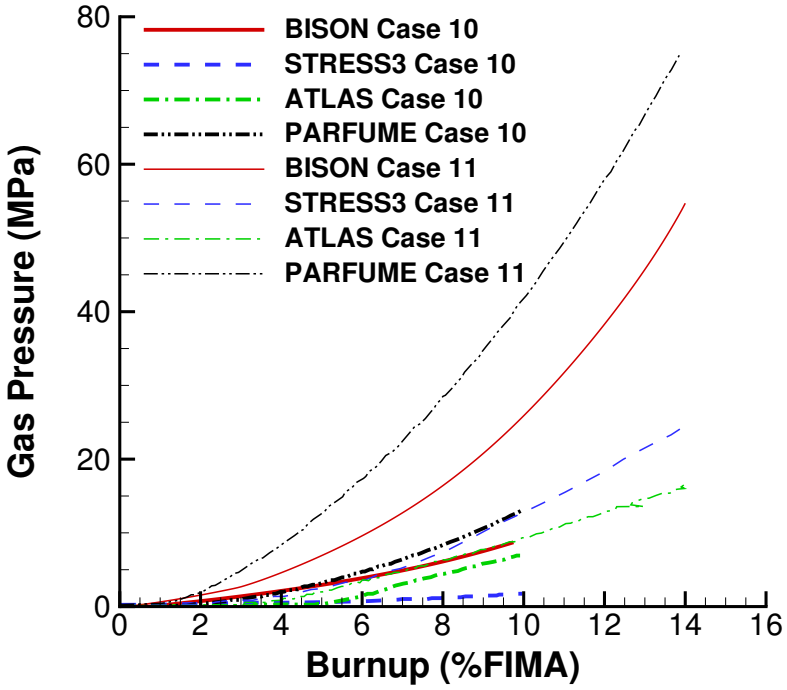

(a)

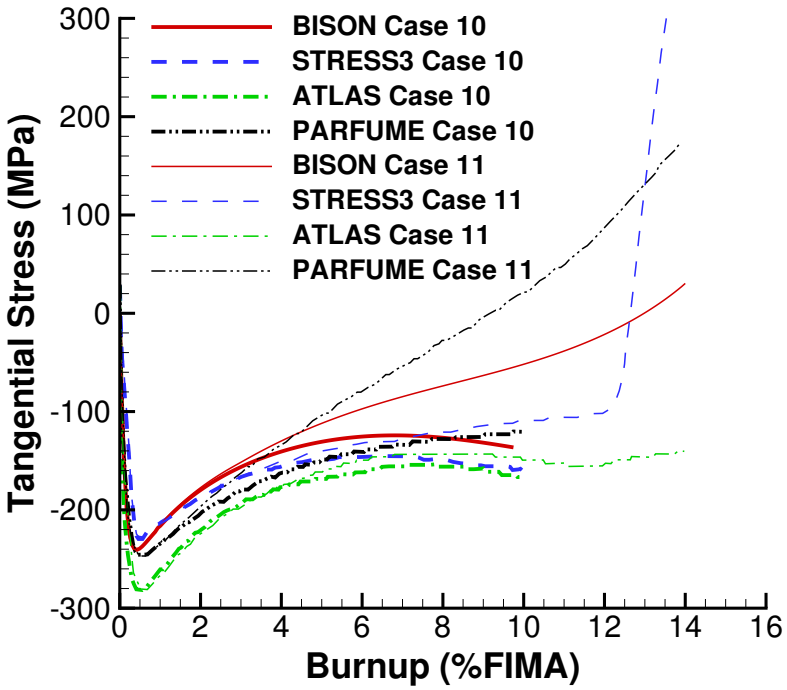

(b)

Figure 3.3: Code comparisons of the total gas pressure (a) and tangential stress at the inner wall of SiC layer (b) for benchmark cases 10 and 11.

3.3 Summary

Since the IAEA CRP cases involved comparison of results from a large number and variety of codes, the particle geometry, boundary conditions and material models were prescribed for each case in detail. This was done principally to avoid differences in material models, which can be substantial between the various codes. In some cases these prescribed models differed from the standard BISON TRISO material models. Rather than implement these numerous and specific models in the code, temporary models were developed and the necessary source code to use these models was stored with the individual cases. BISON compares well with the other codes for these benchmark cases.

It is also important to assess the TRISO material models currently within BISON against experimental results. The beginning of this assessment work is planned to occur in FY 2015.

4 1.5D Simulation Capability

4.1 Model Development and Structure

The 1.5 dimensional (1.5D) capability in BISON was developed for the simulation of LWR fuel rods in a computationally efficient manner while retaining key physics of interest. Coupling physics in a higher dimensional geometry is not always required to resolve the physics of interest, such as the modeling of radial heat transfer and radial displacement, and reducing the dimension of a fuel rod problem reduces the computational load of the simulation. The term 1.5D is used in BISON to describe a cylindrical fuel geometry model composed of several coupled 1D simulations of axial fuel and clad slices, where the slices represent specific given axial positions along the fuel rod. A 1D FEM model of the thermal and mechanical physics is solved on each axial slice. A schematic of these 1D axial slices is shown in Figure 4.1.

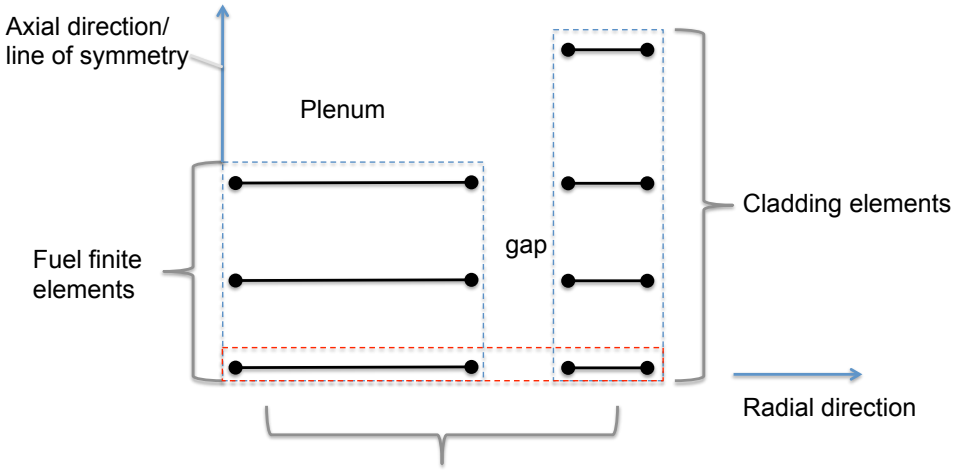

Figure 4.1: Schematic of a representative 1.5D problem and mesh

The individual 1D simulations are coupled through the use of a generalized plane strain scalar variable; these scalar plane strain variables enforce the mechanical effects of volume change, such as thermal expansion and swelling, in the axial direction. In the 1.5D simulations an individual generalized plane strain scalar variable is applied to each axial slice, for each fuel slice and each clad slice separately. The structure of the 1.5D mesh and the application of the generalized plan strain scalar variables is discussed in detail in [4].

4.2 Comparison Results

The 1.5D BISON capability is intended to be used in modeling applications involving several hundred full length fuel rods; hence, ensuring that the 1.5D capability gives reasonable results for a full length full rod is crucial in the 1.5D development process. Thus far, two full length 2D axisymmetric assessment

cases, described in Appendix A9.1, have been used for 1.5D simulation validation. The engineering scale results, including fuel centerline temperature, gap, and simulation run time, were compared for the 1.5D simulation results against the original 2D axisymmetric assessment cases, see Figures 4.2 and 4.4.

As part of the process for converting these selected LWR assessment cases into 1.5D simulations, these assessment cases were also replicated in the newer `tensor_mechanics` 2D axisymmetric system. The `tensor_mechanics` system models continuum mechanics problems with full Rank-2, Rank-3, and Rank-4 tensors; this full tensor approach is an expansion of the classical Voigt approach, which used vectors to represent stress and strain quantities. The availability of the full tensors in the `tensor_mechanics` system will enable the modeling of more general simulations in BISON, including problems involving non symmetric stress and strain Rank-2 tensors. The 1.5D capability is built on the `tensor_mechanics` system; therefore, the conversion of the 2D axisymmetric geometry models to `tensor_mechanics` is a necessary step in the implementation of these assessment cases in the 1.5D capability.

4.2.1 US PWR 16x16 TSQ002, solid pellets, full length fuel rod

The TSQ002 rod is a full length full rod with solid fuel pellets. This rod was selected because of the higher burnup value, moderately complex power history, and relatively simple fuel pin geometry.

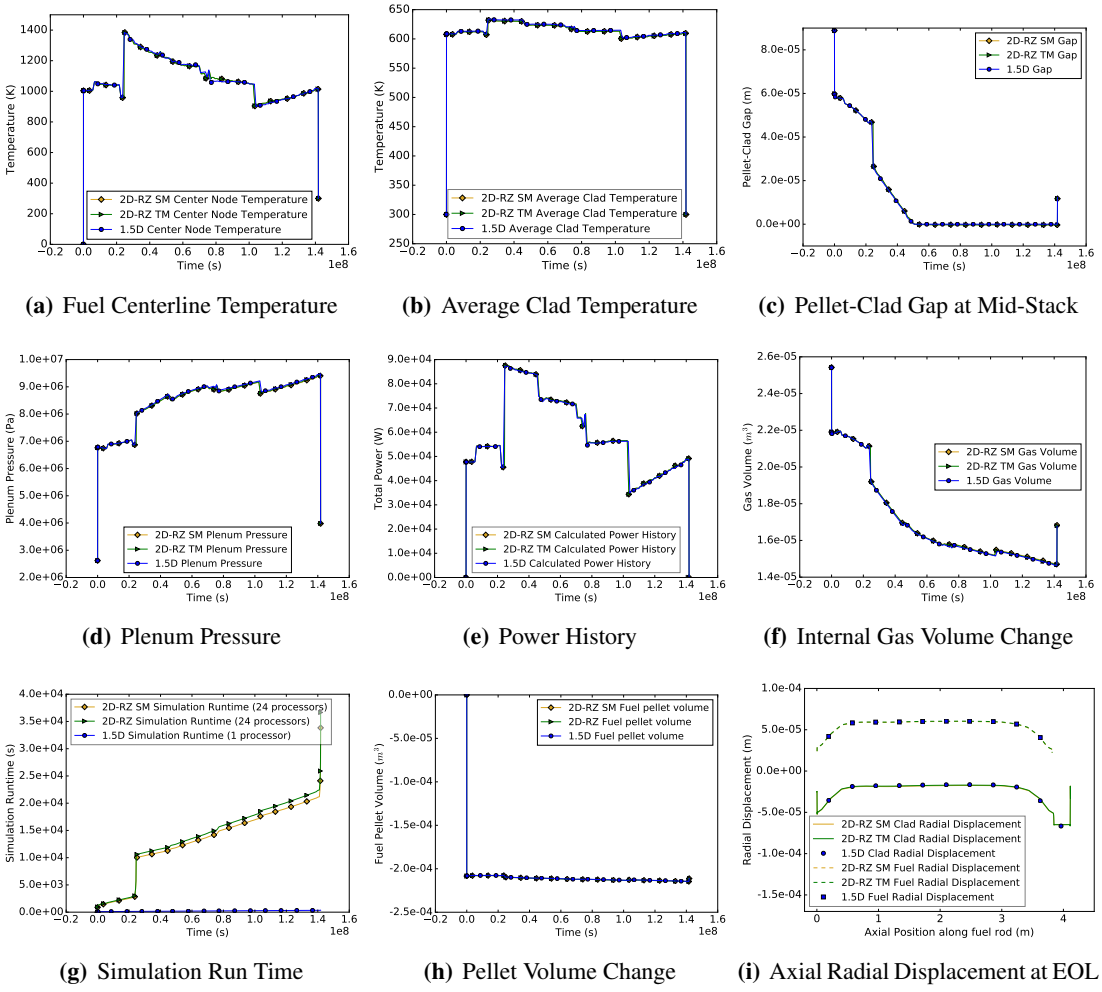

(a) Fuel Centerline Temperature **(b)** Average Clad Temperature **(c)** Pellet-Clad Gap at Mid-Stack

(d) Plenum Pressure **(e)** Power History **(f)** Internal Gas Volume Change

(g) Simulation Run Time **(h)** Pellet Volume Change **(i)** Axial Radial Displacement at EOL

Figure 4.2: US PWR 16x16 Solid Pellets: Comparison of the 1.5D BISON capability against the 2D axisymmetric simulation for the TSQ002 assessment case shows alignment among the various simulation results with a significant reduction in simulation time for the 1.5D model

In the graphs shown in Figure 4.2, the results of the comparison among the original 2D axisymmetric solid mechanics formulation, the new 2D axisymmetric tensor mechanics formulation, and the 1.5D capability are presented. Ten axial pellet slices were used in the 1.5D simulation.

The simulation comparison results demonstrate promising agreement between the two 2D axisymmetric and the 1.5D cases for the temperatures, plenum pressure, and volume change quantities. The minimal discrepancy in the pellet-clad gap size and the EOL radial displacements are anticipated consequences of the limited number of axial slices in the 1.5D simulation. The simulation run time is significantly reduced, by a factor of 140, in the 1.5D simulation compared to the full 2D axisymmetric simulations.

A parameterization study was also performed on the 1.5D TSQ002 fuel rod to examine the effect of increasing the number of axial fuel slices on the convergence of the results. Additional fuel slices reduce the computational efficiency of the 1.5D capability, yet the inclusion of a sufficient number of axial fuel slices is required to correctly capture the relevant simulation solution information. This study involved 1.5D simulation models with 10, 20, 40 and 100 axial fuel slices.

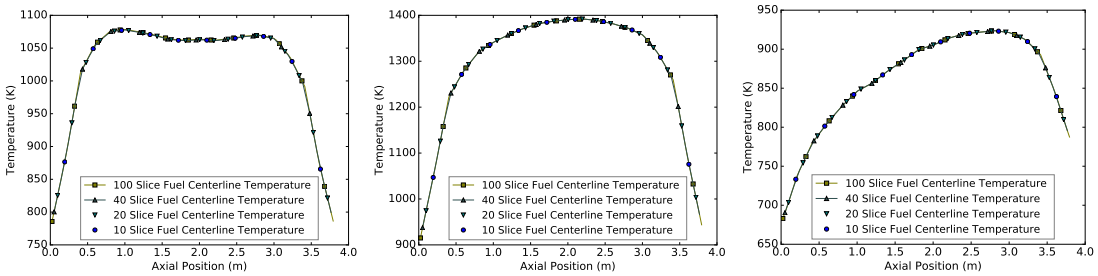

(a) Startup Power (54 kW/m) **(b)** Peak Power, Mid Life (87 kW/m) **(c)** Power Drop, Near EOL (30 kW/m)

Figure 4.3: The axial slice paremterization study using the US PWR 16x16 solid pellets rod demonstrates that fuel centerline temperature is calculated consistently despite different numbers of 1.5D axial fuel slices at significant power changes. The three power changes selected for the comparison of this fuel centerline temperature correspond to abrupt changes in the power history (see Figure 4.2 for the complete power history of the TSQ002 rod).

Temperature, fission gas release, plenum pressure, and volume change are generally insensitive to the number of axial fuel slices used in the model of the full length fuel rod while the EOL radial displacement demonstrate a slight and expected dependence on the number of axial fuel slices [4]. The parameterization study also compared the variation of the fuel centerline temperature as a function of axial position at three specific time points within the simulation: start up power, the peak power which occurs fairly early in mid-life, and a significant power drop in the later stages of the power history. In all three time points selected for the comparison of fuel temperature as function of axial position, the results from the four 1.5D slice convergence study demonstrate acceptable alignment, see Figure 4.3. The agreement in the axial temperature profile among the 10 slice, 20 slice, 40 slice, and 100 slice 1.5D simulations justifies the use of the computationally efficient 10 slice 1.5D BISON capability to model a geometrically consistent full length fuel rod.

4.2.2 US PWR 16x16 TSQ022, solid pellets, full length fuel rod

The TSQ022 rod was selected for the 1.5D validation as an natural accompaniment to the TSQ002 rod to ensure that the 1.5D BISON capability also functions with annular pellets. As in the TSQ002 solid pellets rod validation comparison, ten axial fuel slices were used in the 1.5D simulation of the TSQ022 annular pellets rod.

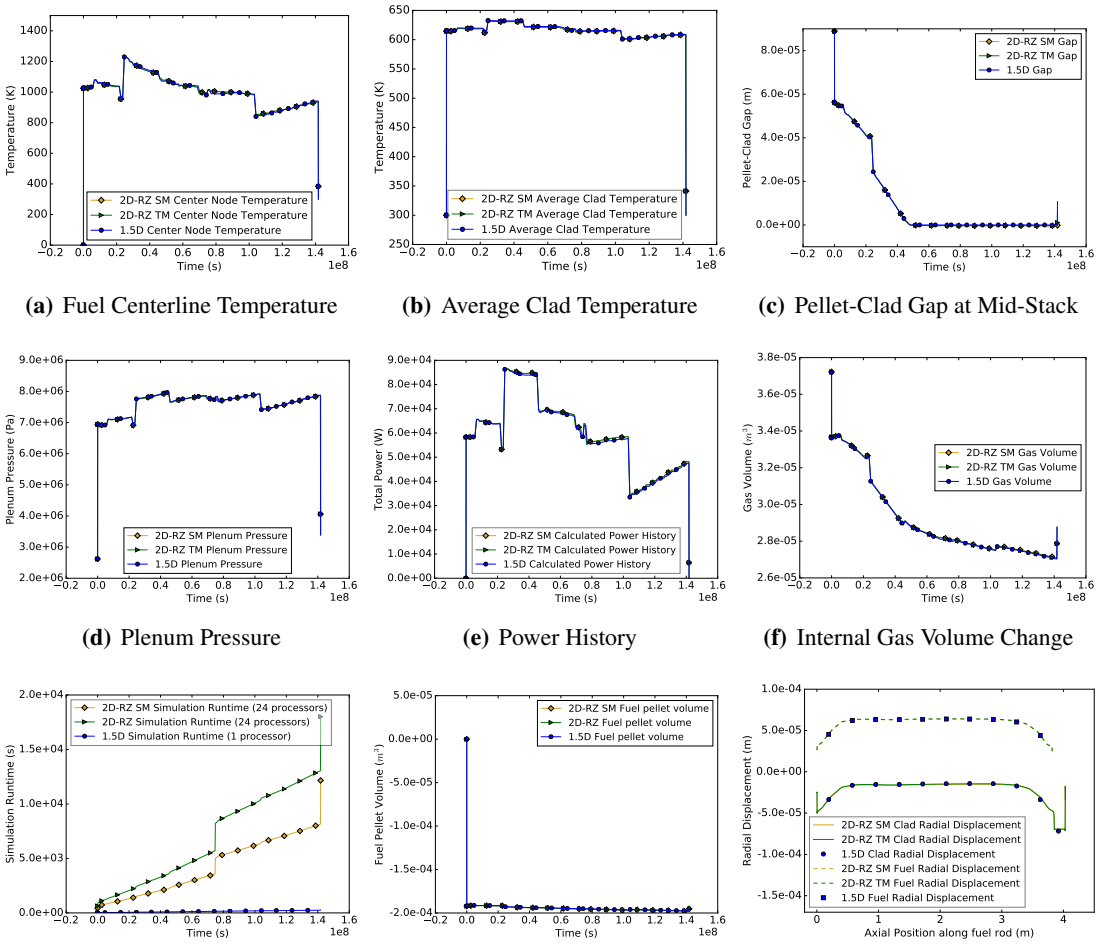

(a) Fuel Centerline Temperature **(b)** Average Clad Temperature **(c)** Pellet-Clad Gap at Mid-Stack

(d) Plenum Pressure **(e)** Power History **(f)** Internal Gas Volume Change

(g) Simulation Run Time **(h)** Pellet Volume Change **(i)** Axial Radial Displacement at EOL

Figure 4.4: US PWR 16x16 Annular Pellets: Comparison of the 1.5D BISON capability against the 2D axisymmetric simulation for the TSQ022 assessment case shows alignment among the different simulation results with a significant reduction in simulation time for the 1.5D model

As in the solid pellet TSQ002 assessment case, the comparison results of the TSQ022 annular pellet 2D axisymmetric and 1.5D cases demonstrate agreement in temperature, volume change, and plenum pressure with acceptable slight differences in the pellet-clad gap and the EOF radial displacement. The 1.5D simulation represents a simulation runtime reduction by a factor of nearly 50 compared to the runtime of the 2D axisymmetric simulations.

4.2.3 FUMEXII Simplified Fuel Pellet

The simplified FUMEX assessment case, based on the Vitanza criterion [32], was also selected for the 1.5D validation comparisons to ensure the effect of fission gas generation and release on fuel rod temperature distribution was correctly captured in the 1.5D model. The simplified case 27_1, comparison shown in Figure 4.5, consists only of a short fuel stack and with a constant power profile of 45 kW/m.

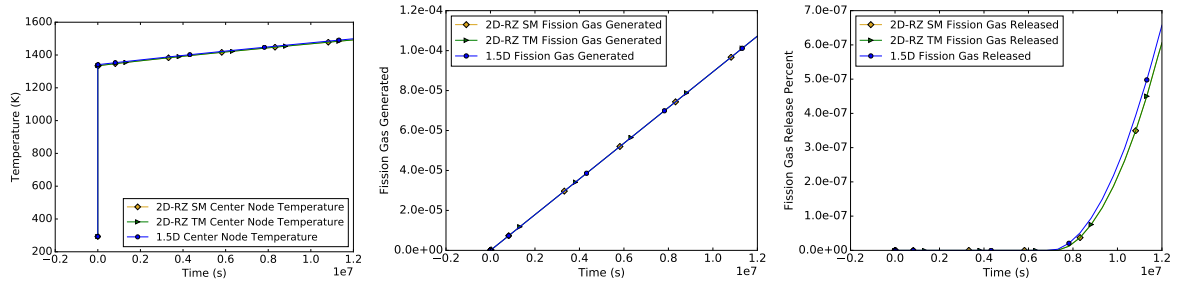

(a) Fuel Centerline Temperature **(b)** Fission Gas Generated **(c)** Fission Gas Release Percent

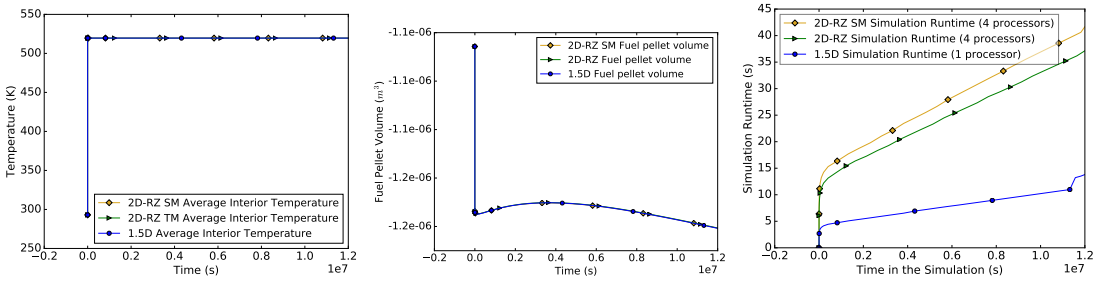

(d) Average Pellet Exterior Temperature **(e)** Fuel Pellet Volume Change **(f)** Simulation Run Time

Figure 4.5: FUMEXII Simplified Pellet Only Simulation: Comparison of the 1.5D BISON capability against the the 2D axisymmetric simulation results for the FUMEXII Simplified 27_1 pellet only assessment case demonstrates alignment among the simulations for the fuel center node temperature and fuel pellet volume change. The comparison difference between the 1.5D BISON capability and the 2D axisymmetric simulations results for the average fuel pellet exterior temperature was successfully removed by calculating the average exterior pellet temperature on only the exterior radial side of the pellet in the 2D axisymmetric simulation.

As with the full length TSQ fuel rod comparison results, the 1.5D capability matches the 2D axisymmetric results in the calculation of fuel centerline temperature, fission gas generated, and fission gas released. The shorter and wider fuel pellet geometry of the FUMEXII simplified 27_1 assessment case highlights a difference in the calculation of the average fuel pellet exterior temperature between the 2D axisymmetric and the 1.5D capability simulations [4]. The 2D axisymmetric simulations were run with a modified average pellet exterior temperature post processor that only used the exterior radial pellet surface and excluded the top and bottom of the 2D simulation pellet models. The simulation comparison results of this modified average exterior temperature post processor in the 2D axisymmetric simulation with the 1.5D simulation, shown in Figure 4.5, demonstrate agreement in the fuel pellet exterior temperature and fuel pellet volume change simulation results.

Appendices

A1 IFA 431 Rod 1, Rod 2, and Rod 3

A1.1 Overview

The IFA-431 experiment was part of an effort by the US NRC to obtain well-characterized experimental data under conditions that simulate long-term steady LWR operation [33]. IFA-431 was a heavily instrumented fuel assembly irradiated in the Halden boiling water reactor from 1975 to 1976. The test rods initially contained fresh fuel and were operated at power levels near the upper bound for full-length commercial fuel rods.

The IFA-431 assembly included six instrumented rods, each with centerline temperature instrumentation in both the top and bottom ends of the fuel column. Three of the six rods (Rods 1, 2, 3) are the focus of this assessment.

The IFA-431 assembly also contained neutron detectors, coolant thermocouples, a coolant flow meter, and a transducer to measure internal rod pressure.

A1.2 Test Description

The three test rods considered here were designed to simulate BWR-6 rod cladding material and dimensions, and included only differences in fuel-cladding gap width. The general rod specifications are summarized in Table A1.1 which contains data taken from Reference [34].

The fuel rod length was significantly shorter than full-length commercial rods to fit within the short length of the Halden reactor core. Slight differences in the pellet diameters, as defined in Table A1.1, resulted in a variation in the initial radial fuel-clad gaps of 115 μm (Rod 1), 190 μm (Rod 2), and 25.5 μm (Rod 3).

A1.2.1 Operating Conditions and Irradiation History

The reactor was operated with a coolant pressure of 3.4 MPa and an inlet temperature of 510 K. The power history was provided by experimentalists from Halden [35].

Table A1.1: IFA-431 Test Rod Specifications

Fuel Rod		
Overall length	m	0.635
Fuel stack height	m	0.5791
Nominal plenum height	mm	25.4
Number of pellets per rod		
Rod 1	mm	45
Rod 2	mm	44
Rod 3	mm	44
Fill gas composition		He
Fill gas pressure	MPa	0.1
Fuel		
Material		UO_2
Enrichment	%	10
Density	%	95
Inner diameter	mm	1.752
Outer diameter		
Rod 1	mm	10.681
Rod 2	mm	10.528
Rod 3	mm	10.858
Pellet geometry		flat end
Grain diameter	μm	22-77
Cladding		
Material		Zr-2
Outer diameter	mm	12.789
Inner diameter	mm	10.909
Wall thickness	mm	0.94

A1.3 Model Description

A1.3.1 Geometry and Mesh

All three fuels rods were meshed using 2-D axisymmetric quadratic elements. For simplicity, the pellet stack was modeled as a single continuous fuel column. The thermocouple holes were modeled as closely to the experiment as possible at the top and bottom of the fuel rod. Figure A1.1 shows a scaled view of the mesh for rod 1. Rods 2 and 3 were identical with exceptions to the thermocouple hole length and the pellet-clad gap width.

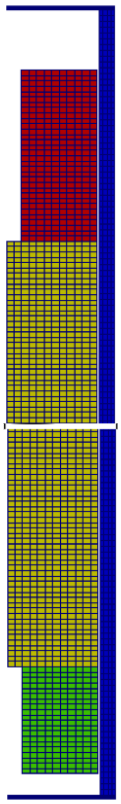

Figure A1.1: Scaled view of the finite element mesh for rod 1 (aspect ratio scaled 10x).

A1.3.2 Material and Behavioral Models

The following material and behavioral models were used for the UO_2 fuel:

- ThermalFuel - NFIR: temperature and burnup dependent thermal properties
- RelocationUO2: relocation strains, relocation activation threshold power set to 5 kW/m.
- Sifgr: Simplified fission gas release model with the combined gaseous swelling model.

For the clad material, a constant thermal conductivity of 16 W/m-K was used and both thermal and irradiation creep were considered using the Limback model [36]. The fast neutron flux used in the irradiation creep model was 1.6e12 n/m^2-s per W/m [7]. This value was multiplied by the power history (W/m) and the axial peaking factors to approximate the fast neutron flux.

A1.3.3 Boundary and Operating Conditions

The clad outer wall temperature was assumed constant at 513.3 K. The input BOL power histories for Rods 1, 2, and 3 are shown in Figure A1.2.

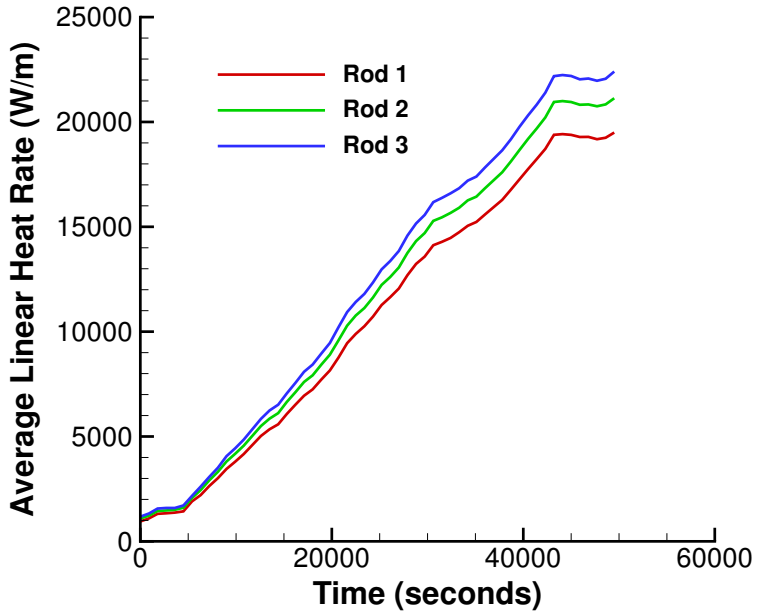

Figure A1.2: Input BOL power history for rods 1, 2, and 3.

A1.3.4 Input files

The BISON input and all supporting files (power histories, axial power profile) are provided with the code distribution at bison/assessment/IFA_431/analysis.

A1.4 Results Comparison

BISON postprocessors were used to record the power and temperature histories at nodes corresponding to the upper and lower thermocouple positions.

A1.4.1 Centerline Temperature at Beginning of Life

Initial comparisons were made to centerline fuel temperature measurements during the first rise to power, or the period referred to as the Beginning of Life (BOL). Comparisons during this period are important since they isolate several important aspects of fuel rod behavior before complexities associated with higher burnups are encountered. For example, good prediction of BOL centerline temperature requires accurate models for the unirradiated fuel thermal conductivity, gap gas conductivity, thermal expansion of both the fuel and clad materials (which set the gap width), clad conductivity, and fuel relocation.

Figures A1.3, A1.4, and A1.5 show centerline temperature comparisons at BOL for Rods 1, 2, and 3, respectively. Comparisons are excellent.

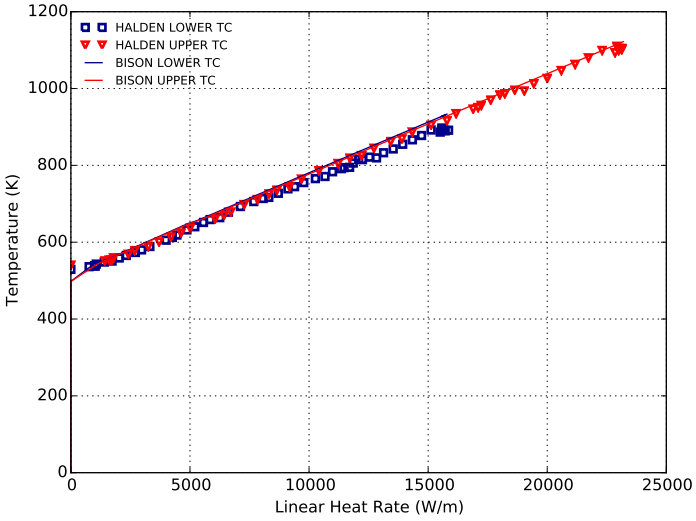

Figure A1.3: Comparison of measured and BISON predicted centerline temperatures at BOL for Rod 1.

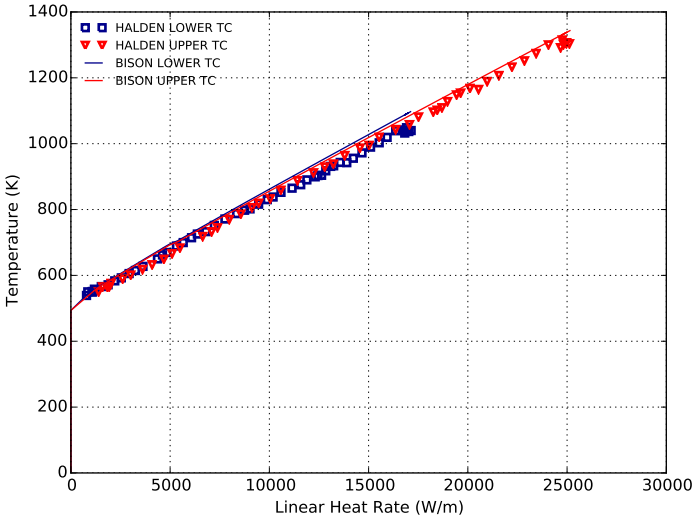

Figure A1.4: Comparison of measured and BISON predicted centerline temperatures at BOL for Rod 2.

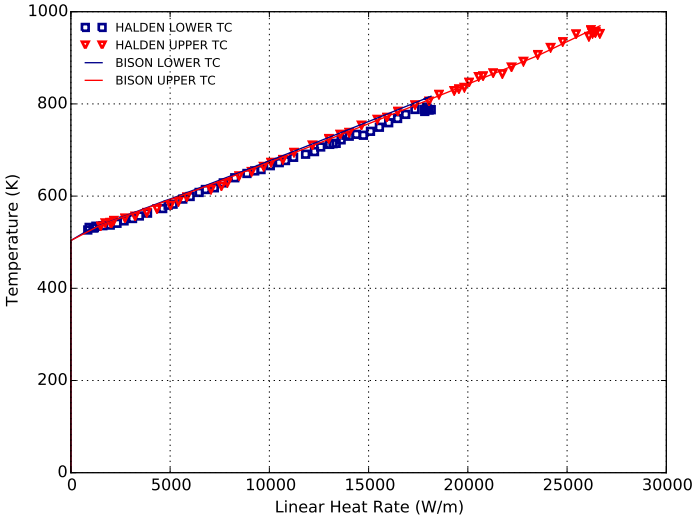

Figure A1.5: Comparison of measured and BISON predicted centerline temperatures at BOL for Rod 3.

A1.5 Discussion

The recommended activation energy for the ESCORE relocation model implemented in BISON is 19.7 kW/m [37]. Based on experimental evidence of fuel cracking as a function of rod power, Wolfgang Wiesenack from Halden recommended lowering this activation threshold power to 5 kW/m. This lower value was further confirmed through a recent relocation calibration study [38] and is now used as the default value in BISON.

A2 IFA 432 Rod 1, Rod 2, and Rod 3

A2.1 Overview

The IFA-432 experiment was part of an effort by the US NRC to obtain well-characterized experimental data under conditions that simulate long-term steady LWR operation [33]. IFA-432 was a heavily instrumented fuel assembly irradiated in the Halden boiling water reactor from 1975 to 1984. The test rods initially contained fresh fuel and were operated at power levels near the upper bound for full-length commercial fuel rods.

The IFA-432 assembly included six instrumented rods, each with centerline temperature instrumentation in both the top and bottom ends of the fuel column. Three of the six rods (Rods 1, 2, 3) are the focus of this assessment. Rod 1 achieved a burnup of approximately 30 MWd/KgU, while rods 2 and 3 achieved burnups of approximately 45 MWd/kgU. Two of the temperature measurements failed prematurely. Rod 2 contained an ultrasonic thermometer at the top of the rod, which failed very early and no data were collected. The Rod 1 upper thermocouple failed after 150 days.

The IFA-432 assembly also contained neutron detectors, coolant thermocouples, a coolant flow meter, and a transducer to measure internal rod pressure.

A2.2 Test Description

The three test rods considered here were designed to simulate BWR-6 rod cladding material and dimensions, and included only differences in fuel-cladding gap size. The general rod specifications are summarized in Table A2.1 which contains data taken from Reference [34].

The fuel rod length was significantly shorter than full-length commercial rods to fit within the short length of the Halden reactor core. Slight differences in the pellet diameters, as defined in Table A2.1, resulted in a variation in the initial radial fuel-clad gaps of 115 μm (Rod 1), 190 μm (Rod 2), and 38 μm (Rod 3).

A2.2.1 Operating Conditions and Irradiation History

The reactor was operated with a coolant pressure of 3.4 MPa and an inlet temperature of 510 K. The power history was provided by experimentalists from Halden [39].

Table A2.1: IFA-432 Test Rod Specifications

Fuel Rod		
Overall length	m	0.635
Fuel stack height	m	0.5791
Nominal plenum height	mm	25.4
Number of pellets per rod		
Rod 1	mm	45
Rod 2	mm	44
Rod 3	mm	44
Fill gas composition		He
Fill gas pressure	MPa	0.1
Fuel		
Material		UO_2
Enrichment	%	10
Density	%	95
Inner diameter	mm	1.752
Outer diameter		
Rod 1	mm	10.681
Rod 2	mm	10.528
Rod 3	mm	10.833
Pellet geometry		flat end
Grain diameter	μm	22-77
Cladding		
Material		Zr-2
Outer diameter	mm	12.789
Inner diameter	mm	10.909
Wall thickness	mm	0.94

A2.3 Model Description

A2.3.1 Geometry and Mesh

All three fuels rods were meshed using 2-D axisymmetric quadratic elements. For simplicity, the pellet stack was modeled as a single continuous fuel column. The thermocouple holes were modeled as closely to the experiment as possible at the top and bottom of the fuel rod. Figure A2.1 shows a scaled view of the mesh for rod 1. Rods 2 and 3 were identical with exceptions to the thermocouple hole length and the gap width.

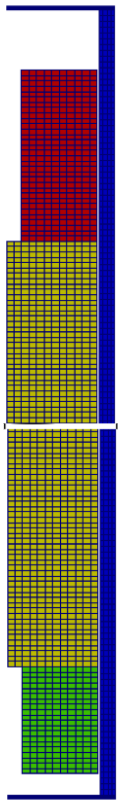

Figure A2.1: Scaled view of the finite element mesh for rod 1 (aspect ratio scaled 10x).

A2.3.2 Material and Behavioral Models

The following material and behavioral models were used for the UO_2 fuel:

- ThermalFuel - NFIR: temperature and burnup dependent thermal properties
- RelocationUO2: relocation strains, relocation activation threshold power set to 5 kW/m.
- Sifgr: Simplified fission gas release model with the combined gaseous swelling model.

For the clad material, a constant thermal conductivity of 16 W/m-K was used and both thermal and irradiation creep were considered using the Limback model [36]. The fast neutron flux used in the irradiation creep model was 1.6e12 n/m^2-s per W/m [7]. This value was multiplied by the power history (W/m) and the axial peaking factors to approximate the fast neutron flux.

A2.3.3 Boundary and Operating Conditions

The clad outer wall temperature was assumed constant at 513.3 K. The input BOL power histories for Rods 1 and 3 are shown in Figure A2.2.

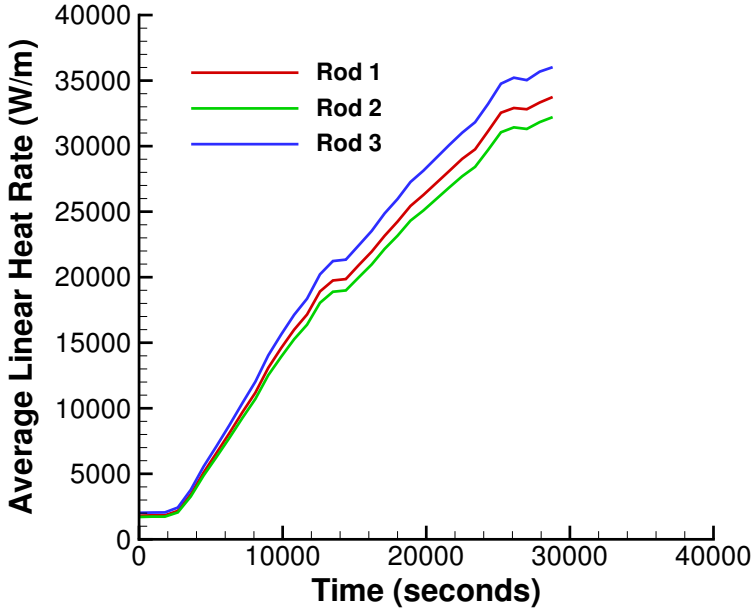

Figure A2.2: Input BOL power history for rods 1, 2, and 3

A2.3.4 Input files

The BISON input and all supporting files (power histories, axial power profile) are provided with the code distribution at bison/assessment/IFA_432/analysis.

A2.4 Results Comparison

BISON postprocessors were used to record the power and temperature histories at nodes corresponding to the upper and lower thermocouple positions.

A2.4.1 Centerline Temperature at Beginning of Life

Initial comparisons were made to centerline fuel temperature measurements during the first rise to power, or the period referred to as the Beginning of Life (BOL). Comparisons during this period are important since they isolate several important aspects of fuel rod behavior before complexities associated with higher burnups are encountered. For example, good prediction of BOL centerline temperature requires accurate models for the unirradiated fuel thermal conductivity, gap gas conductivity, thermal expansion of both the fuel and clad materials (which set the gap width), clad conductivity, and fuel relocation.

Figures A2.3, A2.4, and A2.5 show centerline temperature comparisons at BOL for Rods 1, 2, and 3, respectively. Note that for Rod 2, only lower thermocouple comparisons are possible since a gamma thermometer that failed to operate occupied this position in the rod [34]. Comparisons for all three rods are very good.

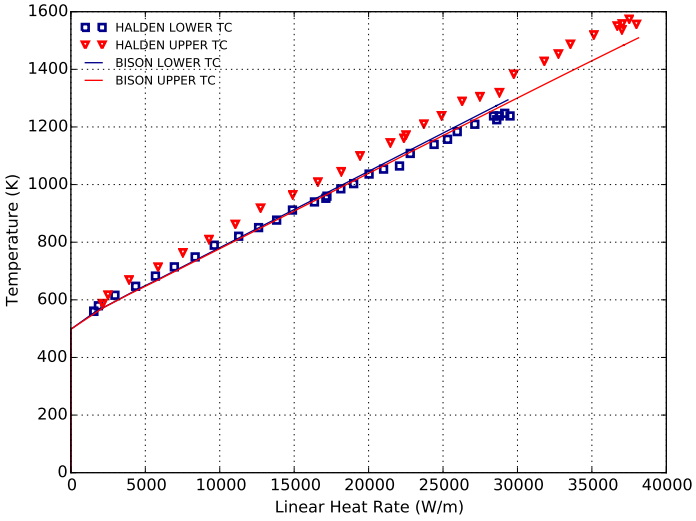

Figure A2.3: Comparison of measured and BISON predicted centerline temperatures at BOL for Rod 1.

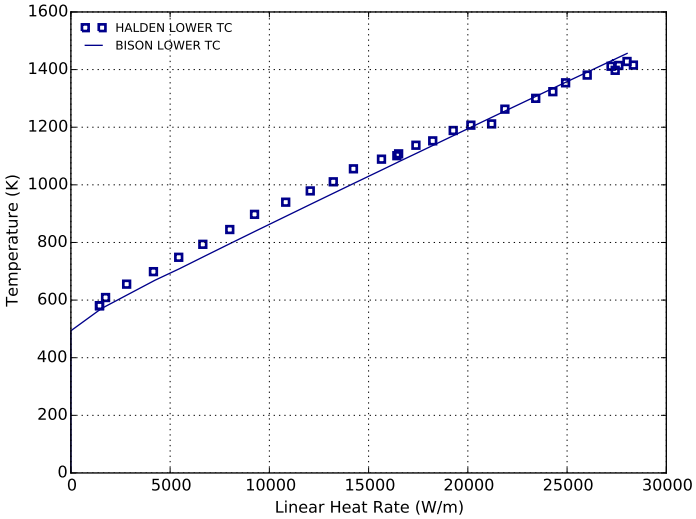

Figure A2.4: Comparison of measured and BISON predicted centerline temperatures at BOL for Rod 2.

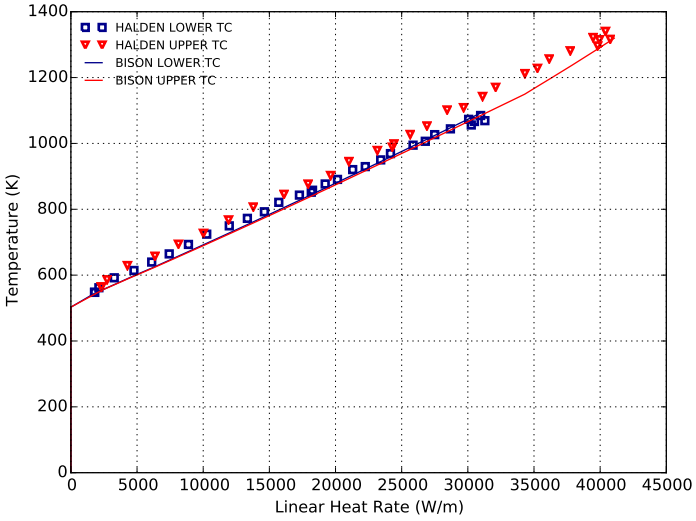

Figure A2.5: Comparison of measured and BISON predicted centerline temperatures at BOL for Rod 3.

A2.5 Discussion

The recommended activation energy for the ESCORE relocation model implemented in BISON is 19.7 kW/m [37]. Based on experimental evidence of fuel cracking as a function of rod power, Wolfgang Wiesenack from Halden recommended lowering this activation threshold power to 5 kW/m. This lower value was further confirmed through a recent relocation calibration study [38] and is now used as the default value in BISON.

A3 IFA 515.10 Rod A1

A3.1 Overview

The IFA-515.10 Rod A1 experiment was irradiated in the Halden Boiling Water Reactor (HBWR) for approximately 6 years to a discharge burnup of $\sim$76 MWd/kgUO_2. Rod A1 was fitted with a fuel centerline expansion thermometer (ET) to measure the fuel centerline temperature during irradiation [18].

A3.2 Test Description

A3.2.1 Rod Design Specifications

Rod A1 in the IFA-515.10 series was an annular short rod (0.2455 m overall length) enriched to 11.5 %. The fuel and cladding specifications are tabulated in Table A3.1.

Table A3.1: IFA-515.10 rod A1 Test Rod Specifications

Fuel Rod		
Overall length	m	0.2455
Fuel stack height	m	0.212
Nominal plenum height	mm	19.0
Fill gas composition		He
Fill gas pressure	MPa	1.0
Fuel		
Material		UO_2
Enrichment	%	11.5
Density	%	96.8
Inner diameter	mm	1.80
Outer diameter	mm	5.56
Pellet geometry		flat end
Average grain diameter	μm	15.5
Average fuel roughness	μm	0.28
Insulator Pellet		
Material		Al_2O_3
Inner diameter	mm	1.80
Outer diameter	mm	5.56
Pellet length	mm	5.0
Cladding		
Material		Zr-2
Outer diameter	mm	6.53
Inner diameter	mm	5.61
Zr-Barrier thickness	mm	0.05
Wall thickness	mm	0.46

A3.2.2 Operating Conditions and Irradiation History

The HBWR operating conditions are tabulated in Table A3.2. The reactor power history is shown in Figure A3.1. The measured reactor coolant temperature was used as the boundary temperature on the cladding outer surface.

Table A3.2: Operational input parameters.

Average coolant temperature	C	195
Coolant pressure	MPa	3.4
Fast neutron flux	n/(cm^2·s) per (kW/m)	1.6·10^{11}

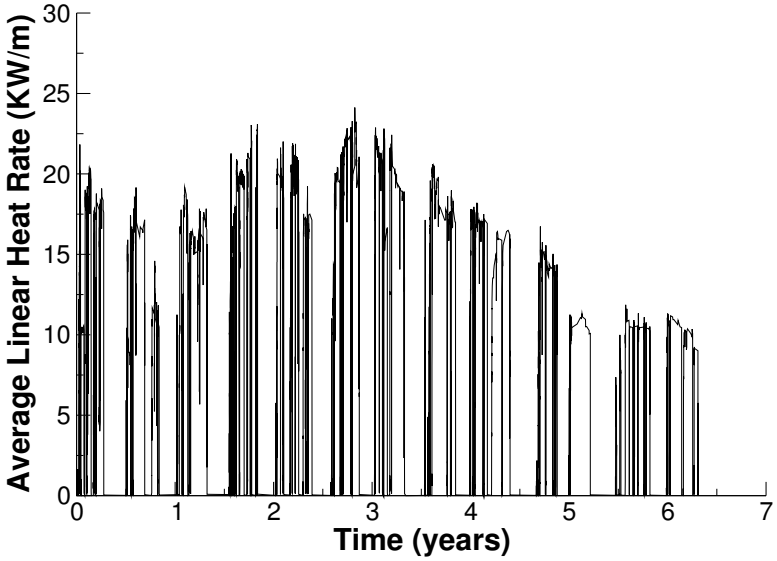

Figure A3.1: Halden irradiation through life power profile for IFA-515.10 rod A1.

A3.3 Model Description

A3.3.1 Geometry and Mesh

The assumed geometry and mesh are shown in Figure A3.2. The fuel pellet stack was modeled as a smeared column with merged insulator pellets. The insulator pellets were modeled as UO_2 (ie. the same mechanical and thermal properties) to make the simulation easier to run. The expansion thermometer was modeled as a void in the pellet/insulator stack, this was also done to ease the simulation. The BISON fuel centerline temperature was calculated as an average of the pellet interior (BISON sideset 13). The plenum length for the mesh was adjusted from the experiment length to account for the difference in volume caused by the voided expansion thermometer. The initial gas volume in the simulation was 2.3 cc, as listed in [18].

A 2-dimensional axisymmetric quadratic mesh was used. The fuel column was meshed with 111 axial and 11 radial elements (aspect ratio 11.2) and the insulator pellets with 3 axial and 11 radial elements (aspect ratio 9.75). The cladding was meshed with 150 axial and 4 radial elements (aspect ratio 16.7).

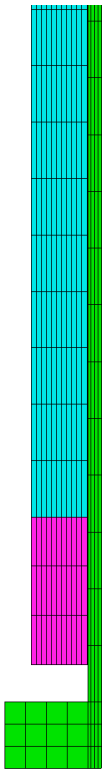

Figure A3.2: 2-D axisymmetric quadratic mesh for IFA-515.10 Rod A1 simulation. Note: This is only a cut from the bottom of the fuel rod meant to show the fuel and insulator pellet. The volume where the expansion thermometer would be in the experiment can also be seen.

A3.3.2 Material and Behavioral Models

The following material and behavioral models were used for the UO_2 fuel:

- ThermalFuel - NFIR: temperature and burnup dependent thermal properties
- VSwellingUO2: free expansion strains (swelling and densification)
- RelocationUO2: relocation strains, relocation activation threshold power set to 5 kW/m.
- Sifgrs: fission gas generation and release

For the cladding material, a constant thermal conductivity of 16 W/m-K was used and both thermal and irradiation creep were considered using the Limback model [36].

A3.3.3 Input files

The BISON input and all supporting files (power histories, axial power profile, cladding surface temperature boundary condition, fast neutron flux history, etc.) for this case are provided with the code distribution at bison/assessment/IFA_515_RodA1/analysis.

A3.3.4 Simulation Parameters and Assumptions

As mentioned in the A3.3.1 the mesh used is not an exact representation of the experiment. To make the simulation run easier the insulator pellets were modeled as UO_2 instead of Al_2O_3. Merged materials of the same type in the mesh make for easier mechanics (ie. thermal expansion and swelling). The insulator pellets were not included in the heat source term. The expansion thermometer was neglected in this mesh. This was done to alleviate troubles with thermal and mechanical properties between the thermometer and the fuel/insulator stack. The plenum length of the fuel rod was adjusted to account for the extra gas volume made from the voided thermometer. The initial gas volume is 2.3 cc as listed in [18]. The zirconium barrier on the cladding interior was not modeled, but the cladding thickness was modeled as specified in [18]. The initial fuel grain size and the fuel roughness were inputted in to BISON as averages of the numbers that were given in [18]. The test was short and located in a region were the axial flux variation average to peak is small, less than 1.03 [18]. Due to this peaking factors for power and temperature were not inputted into BISON.

A3.4 Results Comparison

A BISON postprocessor was used to extract the centerline temperature as an average of the interface of the pellet interior surface and the ET (BISON sideset 13). This provides an accurate representation of the average fuel centerline temperature since, in this case, no axial variation in fuel temperature.

A3.4.1 Temperature

The BISON results for the fuel centerline temperature show that BISON approximates the actual experimental values well. A plot of the comparison can be seen below in Figure A3.3. There are some noticeable differences between BISON and the experiment on the peaks at the beginning of the experiment. The difference between the BISON results and the experiment becomes less as the simulation progresses. This points to possible issues in the gap heat transfer model. As fuel centerline temperature was the only parameter that was measured we can only speculate on the other effects that may have contributed to this difference. Figure A3.4 shows a comparison of fuel centerline temperature and linear heat rate. This plot shows that BISON does tend to under predict through the simulation at all powers. It should be noted that the experiment low outliers are from instrument issues and should be ignored. Figure A3.5 is the same data as Figure A3.4, but the results are compartmentalized by burnup level to investigate BISON performance throughout the simulation more closely. Figure A3.5(a) shows that BISON does under predict during the early stages of the simulation. This is before the gap closes, which supports the previous hypothesis. As the simulation progresses the Figures A3.5(b), A3.5(c) and A3.5(d) show that the comparison of BISON results to experiment data improves.

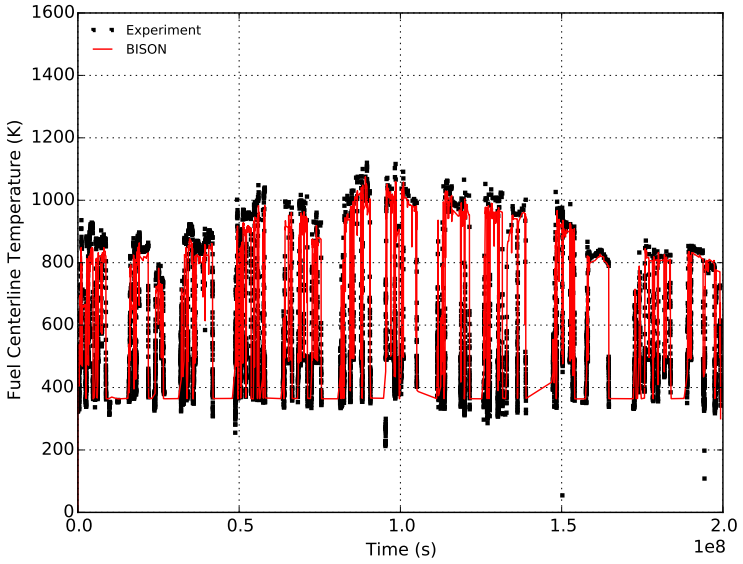

Figure A3.3: A comparison of fuel centerline temperatures from BISON calculations and experimental measurements.

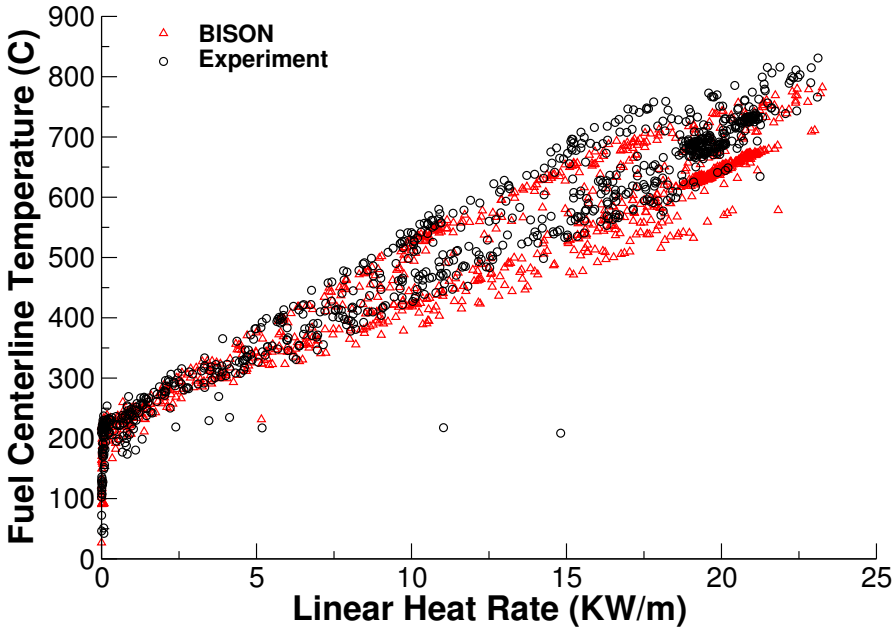

Figure A3.4: A comparison of measured and BISON predicted average fuel centerline temperature as a function of power.

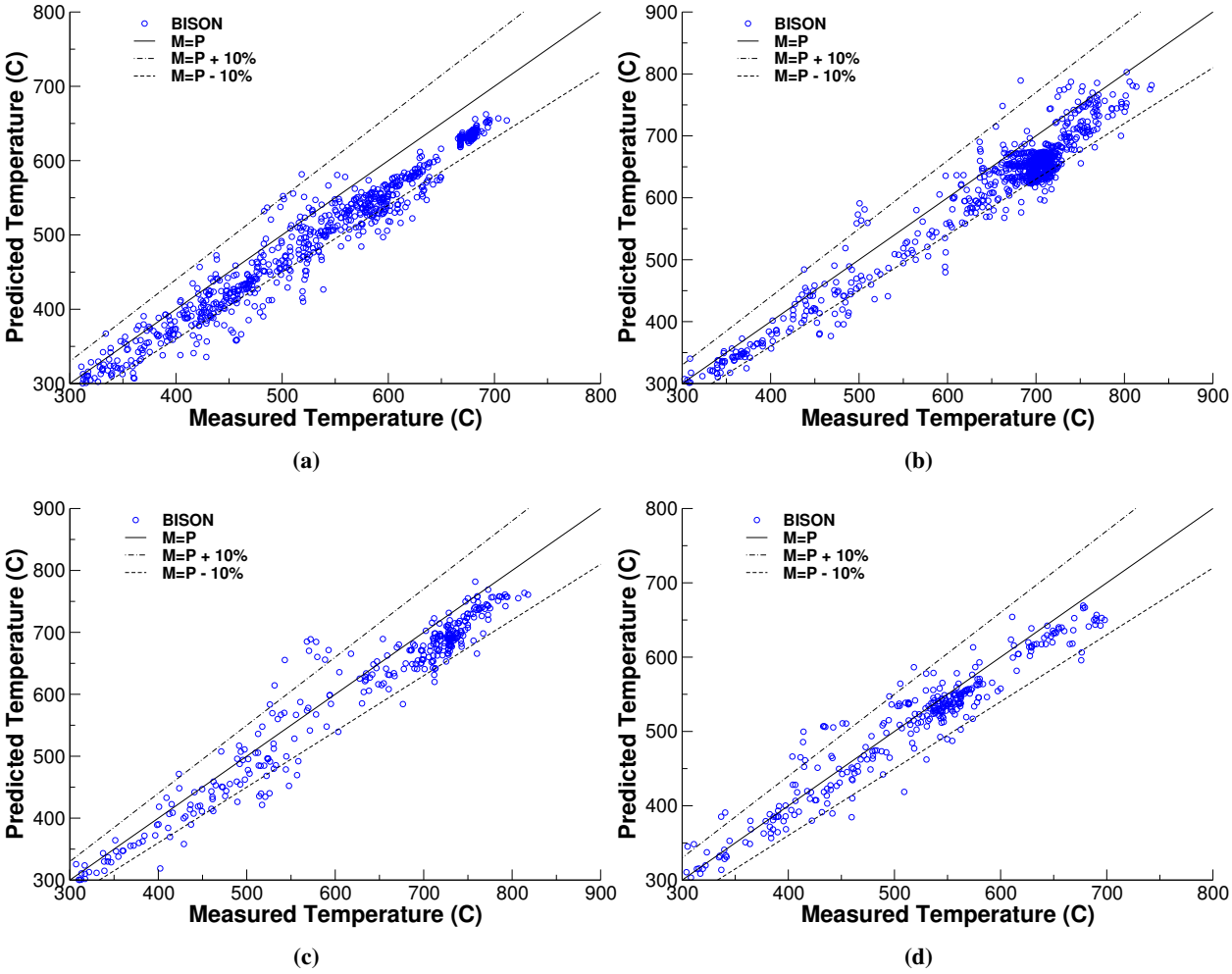

Figure A3.5: Comparison of the measured vs. predicted fuel centerline temperature for IFA-515.10 at four different burnup ranges: (a) $0 \leq Bu < 20$, (b) $20 \leq Bu < 40$, (c) $40 \leq Bu < 60$, and (d) $Bu \geq 60$ MWd/kgUO_2.

A3.5 Discussion

The results show that the fuel centerline temperature compares well between the BISON predicted and experiment measurements. Although this is true the results also show that there are possible weaknesses in the gap conductance in the early stages of the simulation. Results and information from this simulation will help to guide future BISON developments.

A4 IFA 519 Rod DH and Rod DK

A4.1 Overview

The IFA-519.9 experiment was base irradiated in the Halden Boiling Water Reactor (HBWR), experiment IFA-429, to a burnup of 26-29 MWd/kgUO_2. The three rods (rods DC, DH, and DK) were then re-fabricated to include a bellows type pressure transducer and inserted back in to the HBWR to a burnup of approximately 90 MWd/kgUO_2 [40]. The bellows transducer in rod DC failed, therefore, in-pile data is only available for rod DH and rod DK.

A4.2 Test Description

A4.2.1 Rod Design Specifications

Summary of the rod specifications for rods DH and DK are shown in Table A4.1.

Table A4.1: IFA-519 rod DH and DK Test Rod Specifications

		DH	**DK**
Fuel Rod			
Fuel stack height	m	0.244	0.245
Nominal plenum height	mm	25	24
Fill gas composition		He	He
Fill gas pressure	MPa	2.59	2.59
Fuel			
Material		UO_2	UO_2
Enrichment	%	13	13
Density	%	94.7	94.7
Outer diameter	mm	9.3	9.14
Pellet geometry		Dished both ends	Dished both ends
Dish radius	mm	16.8	16.8
Dish depth	mm	0.33	0.33
Land width	μm	1.4	1.4
Grain diameter (2D)	μm	6	17
Cladding			
Material		Zr-4	Zr-4
Outer diameter	mm	10.73	10.73
Inner diameter	mm	9.5	9.5
Wall thickness	mm	0.61	0.61

A4.2.2 Operating Conditions and Irradiation History

The HBWR operating conditions are tabulated in Table A4.2. The total reactor power history for rods DH and DK in the IFA-519.9 experiment is shown in Figure A4.1. The measured reactor coolant temperature was used as the boundary temperature on the clad outer surface.

Table A4.2: Operational input parameters.

Coolant temperature	C	227
Coolant pressure	MPa	3.4
Fast neutron flux	n/(cm^2·s) per (kW/m)	1.6·10^{11}

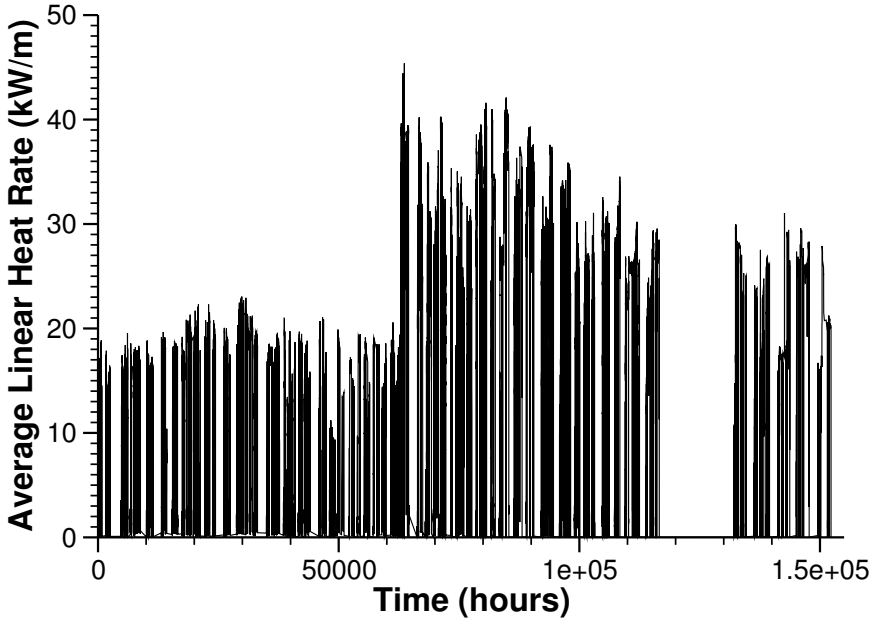

(a)

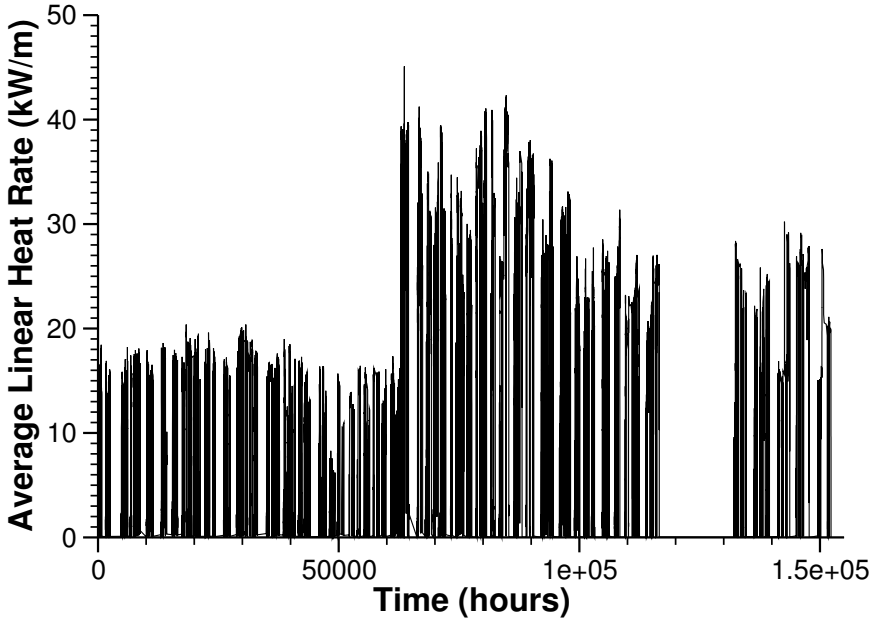

(b)

Figure A4.1: (a) Full irradiation power history for rod DH in the IFA-519.9 experiment. (b) Full irradiation power history for rod DK in the IFA-519.9 experiment.

A4.3 Model Description

A4.3.1 Geometry and Mesh

The assumed geometry and mesh for the two rods are shown in Figure A4.2. The fuel pellet stack for each rod was modeled as a smeared column. A 2-dimensional axisymmetric quadratic mesh was used for each rod. The fuel columns were meshed with 48 axial and 11 radial element and the clad were meshed with 48 axial and 4 radial elements.

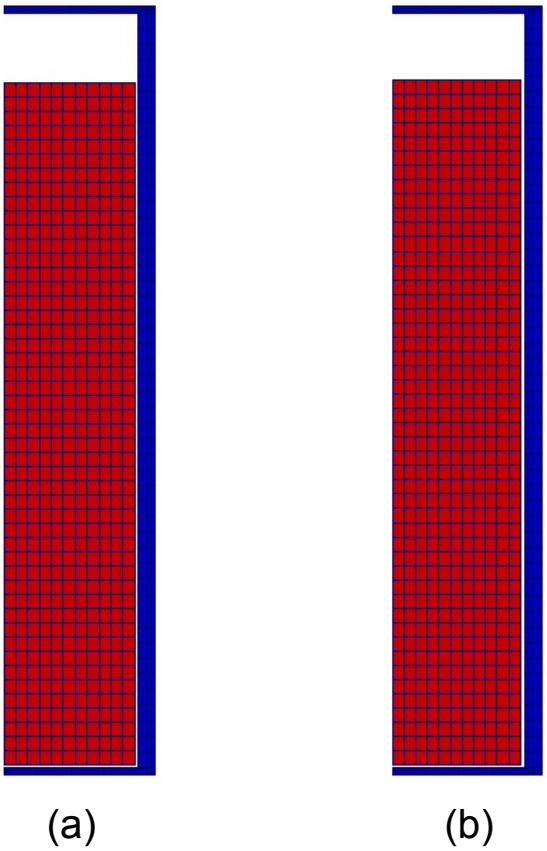

Figure A4.2: (a)2-D axisymmetric quadratic mesh for IFA-519 Rod DH simulation. (b)2-D axisymmetric quadratic mesh for IFA-519 Rod DH simulation. Note the figures above are scaled radially by a factor of 10.

A4.3.2 Material and Behavioral Models

The following material and behavioral models were used for the UO_2 fuel:

- ThermalFuel - NFIR: temperature and burnup dependent thermal properties
- VSwellingUO2: free expansion strains (swelling and densification)
- RelocationUO2: relocation strains, relocation activation threshold power set to 5 kW/m.
- Sifgrs: fission gas generation and release

For the clad material, a constant thermal conductivity of 16 W/m-K was used and both thermal and irradiation creep were considered using the Limback model [36].

A4.3.3 Input files

The BISON input and all supporting files (power histories, axial power profile, clad surface temperature boundary condition, fast neutron flux history, etc.) for this case are provided with the code distribution at bison/assessment/IFA_519/analysis/rod_DH and bison/assessment/IFA_519/analysis/rod_DK.

A4.4 Results Comparison

A BISON postprocessor was used to extract the data needed to compute the total fission gas released (FGR) from each rod. The total FGR is computed by dividing the fission gas released by the fission gas produced.

A4.4.1 Fission Gas Release

Table A4.3 summarizes the end of life (EOL) total fission gas release comparisons to the puncture results obtained durning post irradiation examination (PIE). It has been shown that the prediction of total FGR within a factor of 2 is considered acceptable [20]. Since the BISON FGR prediction is within this range, it is concluded that the FGR predictions are acceptable. As there is no fuel centerline temperature data available for comparisons, it is unknown if the underprediction of FGR is caused by a difference in the predicted and actual fuel temperature.

Table A4.3: End of Life Fission Gas Release for IFA-519.9 Rods DH and DK.

Rod	BISON Burnup ($MWd/kgUO_2$)	Halden Burnup ($MWd/kgUO_2$)	BISON FGR (%)	Halden FGR (%)	BU diff (%)	FGR diff (%)
DH	86.97	87.0	38.0	57.4	0.04	33.75
DK	83.16	88.5	33.8	52.8	6.03	36.02

A5 IFA 534 Rod 18 and Rod 19

A5.1 Overview

The purpose of the IFA-534 experiment was to investigate the effect of fuel grain size on fission gas release and pellet-clad mechanical interaction (PCMI) in high burnup fuel. [41]. IFA-534 consisted of two rods (rod 18 and rod 19) which were base irriated in the Goesgen PWR to 52-55 MWd/KgUO_2. These rods were then re-instrumented with internal pressure transducers and irradiated in the Halden Reactor. [21].

A5.2 Test Description

The two test rods considered here were designed to test the effects of fuel grain size on fission gas release and PCMI. These two rods were instrumented with pressure transducers which provided on-line data as the experiment was irradiated in the Halden Reactor. The general rod specifications are summarized in Table A5.1 which contains data taken from Reference [41] and [21].

Table A5.1: IFA-534 Test Rod Specifications

Fuel Rod		
Overall length	m	0.533
Fuel stack height	m	0.411
Nominal plenum height	mm	100
Number of pellets per rod		
Rod 18	mm	39
Rod 19	mm	39
Fill gas composition		He
Fill gas pressure	MPa	2.15
Fuel		
Material		UO_2
Enrichment		
Rod 18	%	3.84
Rod 19	%	3.79
Density	%	95
Outer diameter	mm	9.12
Pellet geometry		flat end
Grain diameter		
Rod 18	μm	22.1
Rod 19	μm	8.5
Cladding		
Material		Zr-4
Outer diameter	mm	10.75
Inner diameter	mm	9.29
Wall thickness	mm	0.73

A5.2.1 Operating Conditions and Irradiation History

Rods 18 and 19 were base irradiated at the Goesgen PWR at a coolant pressure of 15.5 MPa and coolant inlet temperature of 308 C to approximatly 52 MWd/KgUO_2. The ramp testing was done in the Halden reactor and was operated with a coolant pressure of 3.2 MPa and an inlet temperature of 232 C. The Halden power history was provided by experimentalists from Halden [42].

A5.3 Model Description

A5.3.1 Geometry and Mesh

Both fuels rods were meshed using 2-D axisymmetric quadratic elements. For simplicity, the pellet stack was modeled as a single continuous fuel column. The rods were identical so the same mesh was used for both.The fuel pellets had 111 axial elements and 11 radial elements, and the cladding consisted of 117 axial elements and 4 radial elements.

A5.3.2 Material and Behavioral Models

The following material and behavioral models were used for the UO_2 fuel:

- ThermalFuel - NFIR: temperature and burnup dependent thermal properties
- RelocationUO2: relocation strains, relocation activation threshold power set to 5 kW/m
- Sifgrs: Simplified fission gas release model with a gaseous swelling model

For the clad material, a constant thermal conductivity of 16 W/m-K was used and both thermal (primary and secondary) and irradiation creep were considered using the Limback creep model [36].

A5.3.3 Input files

The BISON input and all supporting files (power histories, axial power profile) are provided with the code distribution at bison/assessment/IFA_534/analysis.

A5.4 Results Comparison

The purpose of the IFA-534 rod 18 and rod 19 experiments were to investigate the effect of fuel grain size on fission gas release. For this purpose the only parameter that was different in the build for these two rods was the fuel grain size. There is a slight difference in the enrichment of the two rods. This difference was accounted for by making a small modification to the individual rod power based on the acutal fuel weight to get 52 MWd/KgUO_2 at the beginning of the Halden run. [43] Fission gas relase is compared against the experiment numbers and other well known fuel performance codes. Pressure data for both rods was collected with an in-situ pressure transducer. Pressure is compared between BISON and the Halden data. The data for these comparisons was digitized from plots in the FUMEX-II Final Report [21]

A5.5 IFA-534, Rod 18

A5.5.1 Fission Gas Release

The BISON end result for fission gas release compared very well the the data that Halden collected. As one may note the BISON run does not start at zero like the Halden does. After the base irradiation the rod was refabricated so that the pressure transducer could be added. At this time the rod was also

refilled with pure He gas. BISON currently misses rebasing the fission gas that was released prior to refabracation. We are currently discussing the best course of action to model this.

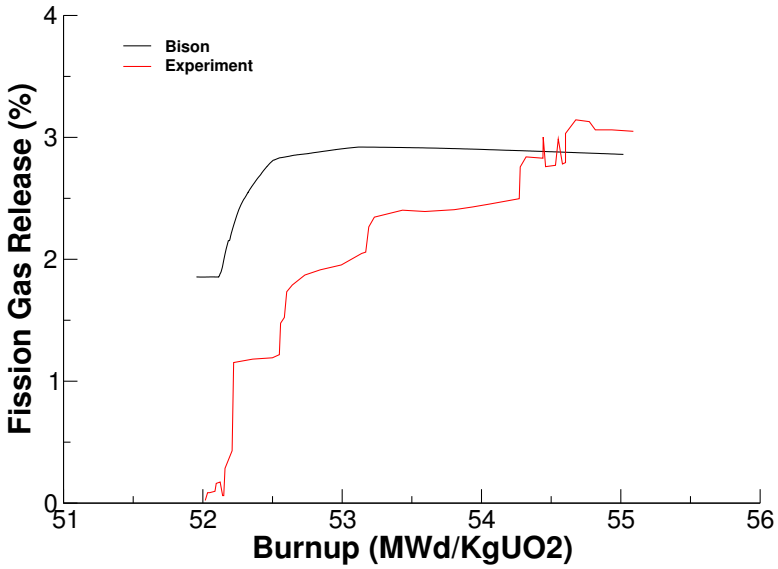

Figure A5.1: Comparison of measured and BISON predicted fission gas release during Halden irradiation for rod 18.

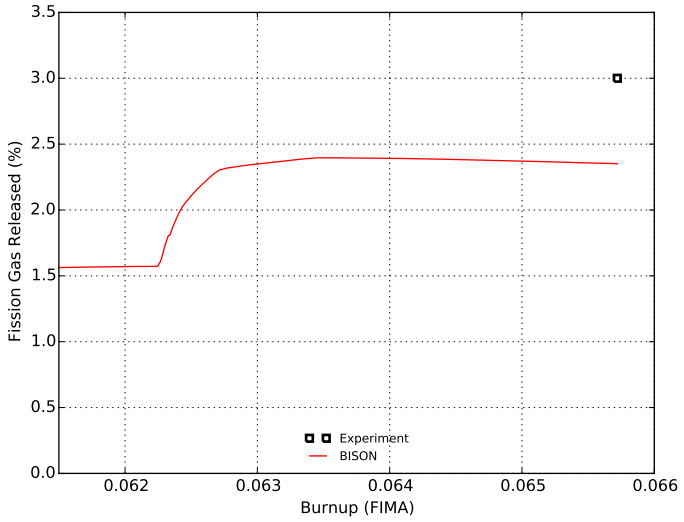

Figure A5.2: Comparison of the post irradiation examination and the BISON predicted fission gas release for rod 18.

A5.5.2 Pressure

As stated previously the rod had an in-situ pressure transmitter installed at refabraction. Due to this we have real online data of the experiment's pressure. The BISON result for the pressure is off by a bit in the start and then compares very well in the end. One possible reason for the higher pressure at the start is the extra fission gas present in the model mentioned in the discussion above. Another problem that was encountered with pressure was the model predicted gas volume. The gas volume at the start of the BISON run (base irradiation) was correct, according to the FUMEX data. At refabracation the model

underestimate gas volume leading to a much higher plenum pressure. As a temporary work around the mesh was adjusted such that the gas volume was high in the base irradiation and then was calculated by BISON to be correct in the Halden run. In this case the Fumex reported gas volume for the base irradiation and Halden run is 5.1 cm^3. A gas volume of 6.1 cm ^{3} was used for the BISON base irradiaion to achieve approximately 5.1 cm^3 for the Halden run.

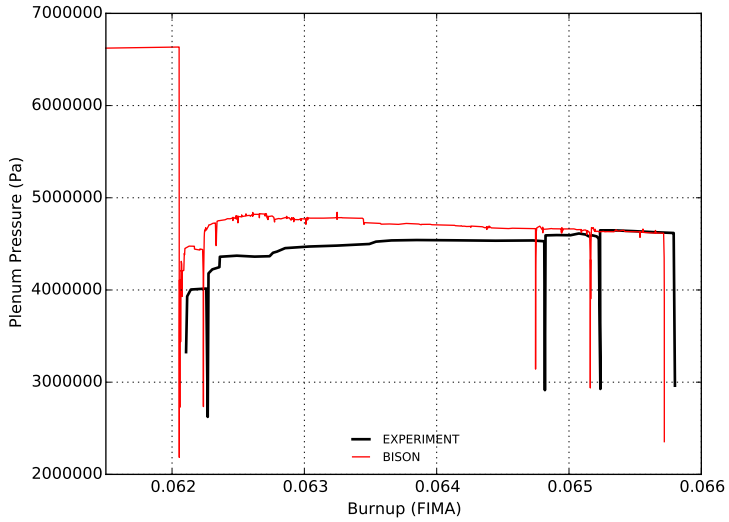

Figure A5.3: Comparison of measured and BISON predicted plenum pressure for rod 18.

A5.6 IFA-534, Rod 19

A5.6.1 Fission Gas Release

As with the the previous rod, 18, rod 19 compares well to the Halden data for fission gas release. Rod 19 does have the same issue as rod 18 in that fission gas does not start at zero. There is an added issue with the rod 19 data, there is a slight shift in the x-axis, burnup. This is common as burnup gets calculated in different manners with slightly different numbers and the shift is acceptable.

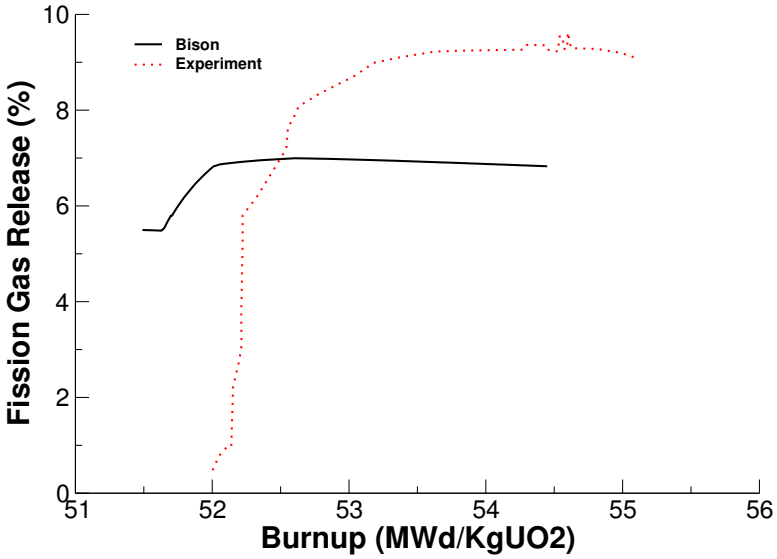

Figure A5.4: Comparison of measured and BISON predicted fission gas release during Halden irradiation for rod 19.

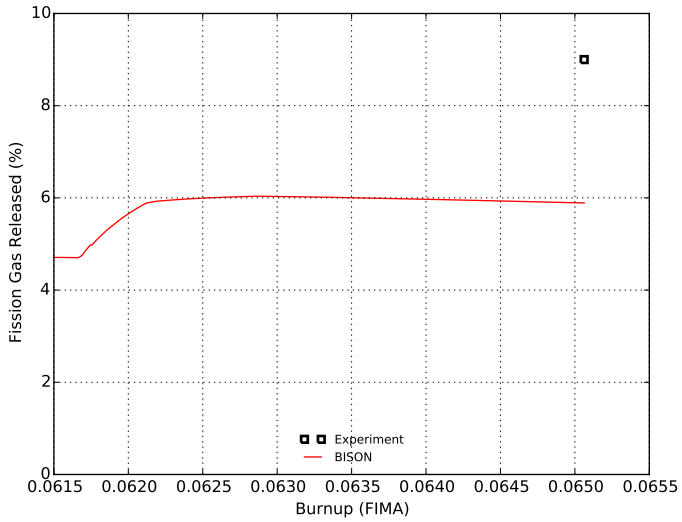

Figure A5.5: Comparison of the post irradiation examination and the BISON predicted fission gas release for rod 19.

A5.6.2 Pressure

The pressure comparision is acceptable between BISON and the experiment. Once again, rod 19 has the same issues as rod 18 so the same methods where employed. These work arounds may account for the difference in the pressure. A gas volume of 6.1 cm ^{3} was used for the BISON base irradiaion to achieve approximately 5.1 cm^3 for the Halden run.

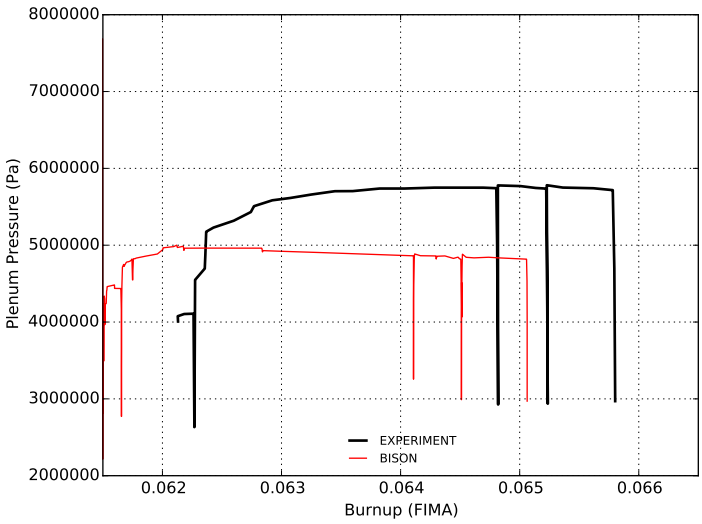

Figure A5.6: Comparison of measured and BISON predicted plenum pressure for rod 19.

A5.7 Discussion

In modeling these two rods it came to the surface that how refabracation is modeled needs to be looked at more closely. This is a good thing as it will lead to a better overall BISON. Topics such as what to do with the released fission gas at refab and the BISON calculated gas volume are being worked out. As for how refabracation works currently a user enters plenum volume, gas temperature, gas content and gas pressure. BISON uses these to calulate the number of moles of gas in the plenum. BISON then looks to the postprocessors for the previous time step to calculate the gas volume that it is going to use for the continuation of the run. This was done to attempt to capture the fuel swelling and other physics that happened in the base irradiation. As stated better approaches are being looked in to.

A6 IFA 535.5/6 Rod 809 and Rod 810

A6.1 Overview

The IFA535 test is a test that was carried out during the Halden reactor project. This particular test was conducted to examine the effect of pre-pressurisation on fission gas release in high burnup BWR-type fuel rods. In this test four rods of identical design and base irradiation history were irradiated up to a burnup of 44 MWd/kgUO_2. At the end of the base irradiation the rods were reinstrumented with pressure transducers and clad elongation sensors. Two rods at a time were installed in the IFA-535 rig and rampe with one rod of each pair pressurized with He at 32 bar at room temperature. Rod 809, presented here was part of the first IFA535 test (IFA-535.5) which consisted of a slow ramp up to 52 kW/m. The base irradiation of the rods was completed in the upper cluster of IFA-409 from May 1973 to June 1985. Upon refabrication rods 809 and 810 were repressurized to 7.0 and 32.0 bar respectively, and fission gas from the base irradiation was measured. The rods were in reactor position 4-10 from November 1985 to February 1986 for the ramp test. After reaching a burnup of 48 MWd/kg$UO_2$the rods were removed from the reactor.

A6.2 Test Description

A6.2.1 Rod Design Specifications

The rod specifications for the IFA-535 test is are summarized in Table A6.1. The clad thickness includes the 13μm niobium linear as the liner is not modeled for simplicity and is incorporated into the cladding thickness.

Table A6.1: IFA-535 Rod 809 and 810 Test Rod Specifications

Fuel Rod		
Overall length	m	0.560019
Fuel stack height	m	0.286
Nominal plenum height	mm	70.166
Base Irradiated Rod		
Fill gas composition		He
Fill gas pressure	MPa	0.1
Re-Fabricated Rod 809		
Fill gas composition		He
Fill gas pressure	MPa	7.0
Re-Fabricated Rod 810		
Fill gas composition		He
Fill gas pressure	MPa	32.0
Fuel		
Material		UO_2
Enrichment	%	9.88
Density	%	94.7
Inner diameter	mm	-
Outer diameter	mm	10.54
Pellet geometry		flat ends, chamfered
Grain diameter	μm	9.36 (not given assumed as per [44])
Pellet Dishing		
Chamfer width	cm	not given
Chamfer depth	cm	not given
Cladding		
Material		Zr-4
Outer diameter	mm	12.56
Inner diameter	mm	10.81
Wall thickness	mm	0.88

A6.2.2 Operating Conditions and Irradiation History

The base irradiation average power is shown in Figure A6.1. The average power during the bump test is shown in Figure A6.2. According to Rossiter [44] the base irradition powers were given as average powers over a timestep. Therefore following the same format as Rossiter the power was ramped to the average power of the step at a rate of 10 kw/m per hour and then remained at the average power for the duration of the timestep. The ramp test values were given as point values and the power profile was linearly interpolated between these values. There was a signifcant axial profile on the fuel through both the base irradiation and the ramp test. There were minor fluctuations of the axial profile during irradiation. To illustrate the signifcance of the axial profile a plot of the profile at the end of base irradiation (prior to refabrication) and at the end of the ramp test (prior to shut down) are provided in Figure A6.3.

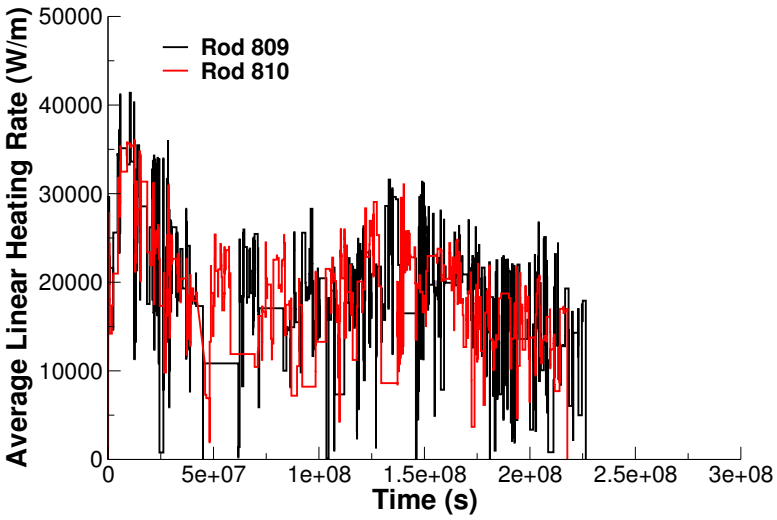

Figure A6.1: IFA-409 base irradiation used for all IFA535 tests.

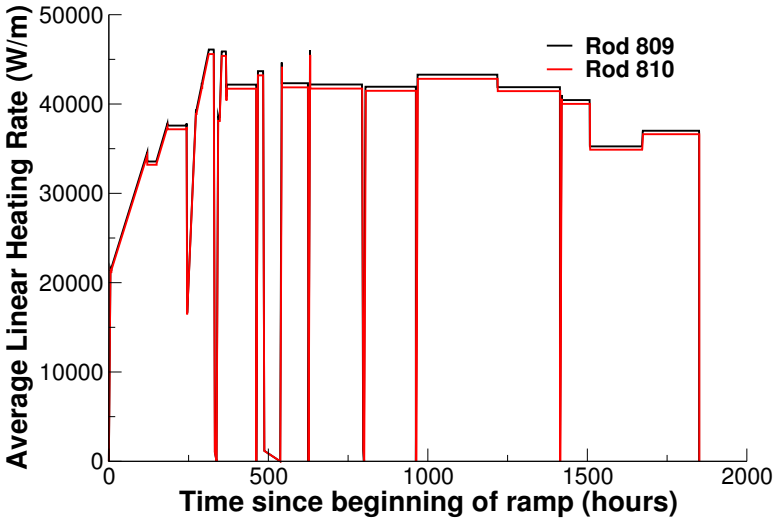

Figure A6.2: Average power history during the IFA-535.5 ramp test.

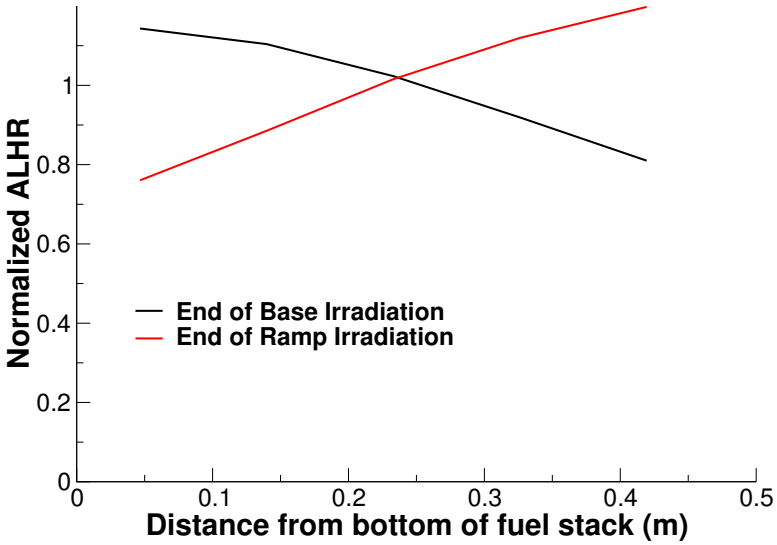

Figure A6.3: The axial power profile at the end of the base irradiation and the end of the ramp.

The clad surface temperature was input as a function, along with the fast neutron flux from data provided in the FUMEX-III data set [45]. The coolant inlet temperature and pressure for the base irradiation and power ramp is shown in Table A6.2. The clad tempature, fast flux, and axial peaking factors were modified such that the same ramp rates as the power history are applied. This ensures that the times used are consistent throughout the model.

Table A6.2: Operational input parameters.

Base Irradiation		
Coolant inlet temperature	C	Not Given
Coolant pressure	MPa	3.2
Power Ramps		
Coolant inlet temperature	C	Not Given
Coolant pressure	MPa	3.2

A6.3 Model Description

A6.3.1 Geometry and Mesh

The geometric parameters specified in Table A6.1 were used to create the mesh for this simulation. The fuel was meshed as a smeared fuel rod with 11 radial elements and 135 axial elements. The geometry was such that the refabricated rod length was modeled during the base irradiation and bump test. To account for the correct gas volume the plenum height was adjusted such that the overall voidage including radial gap, bottom plenum and top plenum were equivalent to the refabricated volume at the beginning of the ramp irradiation. The lower plenum was equal to the length of the insulator pellet that was not modeled.

A6.3.2 Material and Behavioral Models

The thermal conductivity model used for the UO_2 fuel was NFIR. The fuel was modeled as elastic and fuel swelling was coupled to the fission gas release model. In addition fuel relocation was modeled using an activation power of 5 kW/m. Fission gas release was modeled using the Sifgrs model with a transient burst release model. The cladding material, was modeled using a constant thermal conductivity of 16 W/m-K. Primary and secondary thermal, and irradiation creep were modeled.

A6.3.3 Input files

The BISON input and all supporting files (power histories, axial power profile, fast neutron flux history, etc.) for these cases are provided with the code distribution at bison/assessment/IFA_535/analysis/rod_809 and BISON/assessment/IFA_535/analysis/rod_810.

A6.4 Results Comparison

In this section the BISON simulation results are compared against the experimental data provided in the FUMEX-III data set. Measurements were provided for the rod internal pressure, fission gas release percentage and clad elongation. At the present time BISON is unable to predict clad elongation and therefore clad elongation comparisons are not included.

A6.4.1 Rod Internal Pressure

The rod internal pressure results for rods 809 and 810 are presented in Figures A6.4 and A6.5 respectively. The initial pressure at the beginning of the ramp was 0.7 MPa nad 3.2 MPa for rods 809 and 810 respectively. It is observed that BISON overpredicts the internal pressure for 809 and slightly underpredicts the pressure for rod 810. BISON predicts the correct trends in both cases and the pressure drops during power decreases are much larger in magnitude then observed in the experimental data.

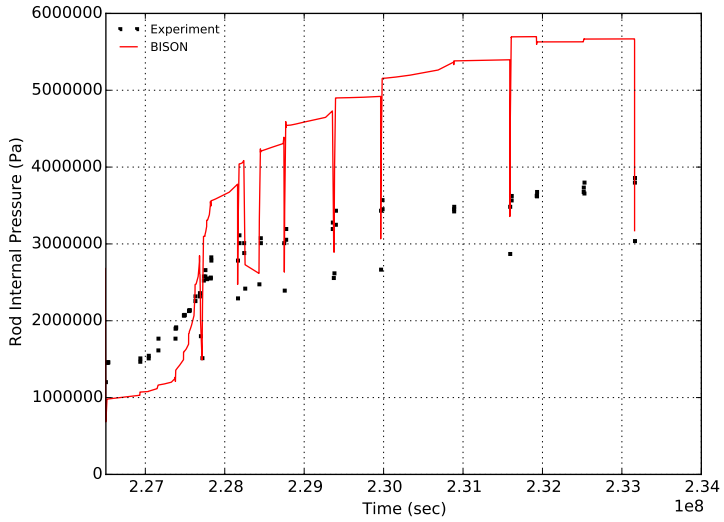

Figure A6.4: Rod internal pressure experimental comparison of IFA-535 rod 809 during the ramp test.

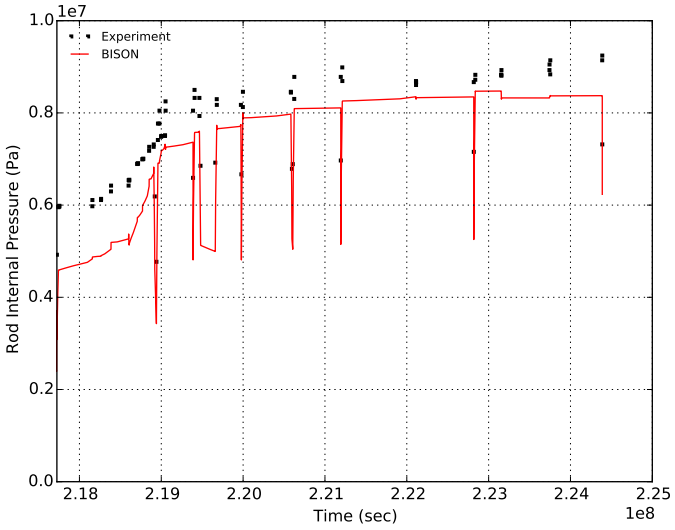

Figure A6.5: Rod internal pressure experimental comparison of IFA-535 rod 810 during the ramp test.

A6.4.2 Fission Gas Release

The fission gas release results for rods 809 and 810 are presented in Figures A6.6 and A6.7. At the end of the base irradiation the PIE measurements obtained 19.6% and 16.2% fission gas for the two rods. However, the experimental data gives values that are slightly different at the end of the base irradiation (22% and 16.9%). BISON underpredicts the fission gas released in both cases however the results are within a factor of 2 which is considered acceptable for fission gas release predicts due to the complexity and uncertainties associated with the processes.

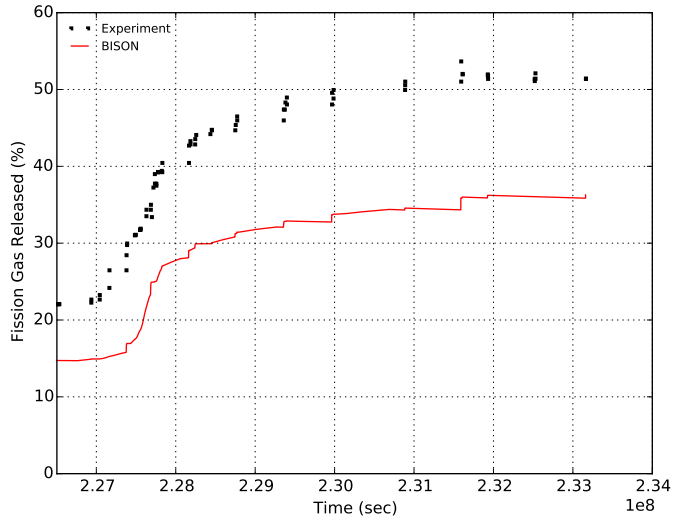

Figure A6.6: Fission gas release experimental comparison of IFA-535 rod 809 during the ramp test.

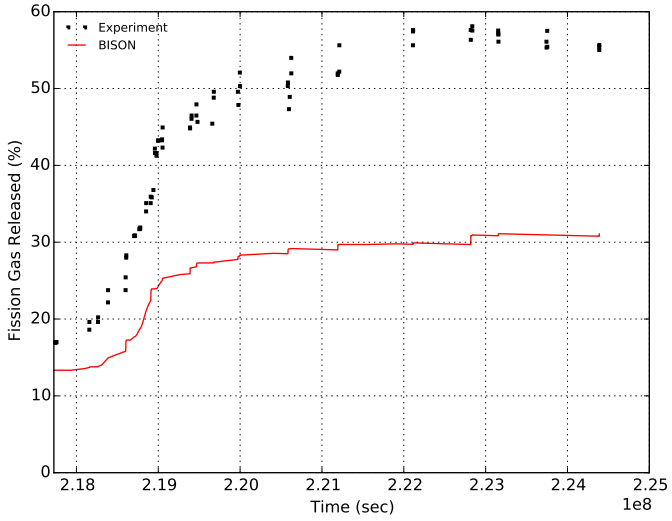

Figure A6.7: Fission gas release experimental comparison of IFA-535 rod 810 during the ramp test.

A6.4.3 Discussion

There is some significant discrepancies in the experimental data provided in the FUMEX-III data files for the IFA-409 base irradiation history. Within the data the average linear heat rate is given and the linear heating rate at 5 axial locations. The axial peaking factors used within BISON are determined by taking the axial locations and dividing by the average. Therefore the average of the axial peaking factors should equal one. Using the data given in the FUMEX-III data base this is not the case. In many cases the average linear heating rate provided is less than the lowest value reported for the axial zones, which does not make sense. Therefore to ensure the correct axial profile is applied to the fuel the average linear heat rate is recalculated by taking the average of the 5 axial values provided in the data file. Moreover at certain locations in the datat files, there are two points for a specific time. Usually one lists adt value of 0 and was therefore removed. In one case the second data point contains a negative value for power at the fifth axial location. Thus for this data point the axial peaking profile was set to completely flat and the average linear heating rate to zero to remove the unphysical negative power. The effect of this change to the base irradiation on the final results is expected to be minimal. Moreover the base irradiation given in the data files for both rods 809 and 810 were significantly different even when they were irradiated in the same IFA-409 rig. Therefore, the corresponding base irradiation provided in the data files in each case was used.

In addition to the experimental data provided in the FUMEX-III dataset, numerous well known codes also completed the simulation of rod 809. Figure A6.8 presents the rod internal pressure of BISON, TRANSURANUS, FRAPCON and ENIGMA-B alongside the experimental comparison. It can be seen that BISON's predictions are within the range predicted by other codes.

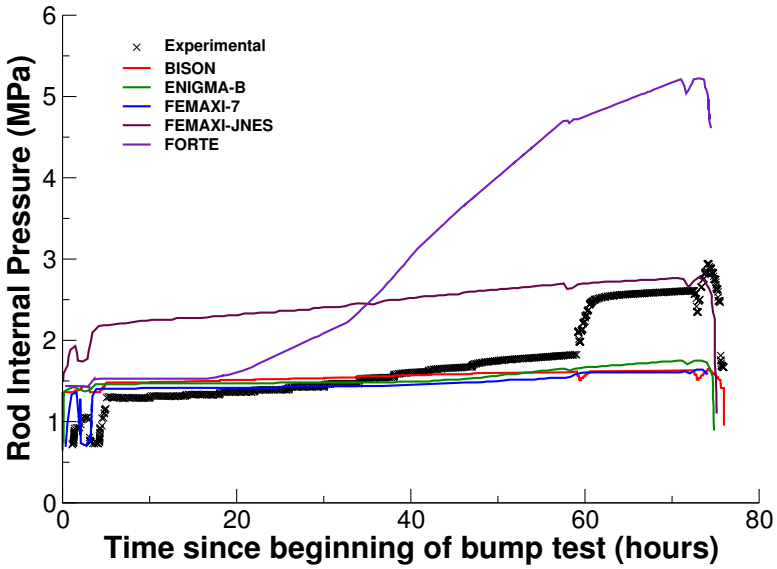

Figure A6.8: Rod internal pressure comparison of IFA-535 rod 809 during the ramp test.

A7 IFA 562 Rod 15, Rod 16, and Rod 17

A7.1 Overview

The IFA-562.2 experiments centered on through life fuel centerline temperature and were part of the Ultra High Burnup (UHB) program. They were irradiated in the Halden Boiling Water Reactor (HBWR) for 2.68 years to a average burnup of approximately 50 MWd/kgUO_2. The rods were fitted with a fuel centerline expansion thermometer (ET) to measure the fuel centerline temperature during irradiation [19].

A7.2 Test Description

A7.2.1 Rod Design Specifications

The IFA-562.2 rods were short rods of annular fuel and were enriched to 13% U-235. The fuel and cladding specifications are tabulated in Table A7.1.

Table A7.1: IFA-562.2 Test Rod Specifications

Fuel Rod		
Fuel stack height	mm	442.5
Nominal plenum height	mm	31.0
Fuel pellet height	mm	7.5
Fill gas composition		He
Fill gas pressure	MPa	1.0
Fuel		
Material		UO_2
Enrichment	%	13
Density	%	94
Inner diameter	mm	2
Outer diameter	mm	5.915
Pellet geometry		flat end
Insulator Pellet		
Material		natural UO_2
Inner diameter	mm	1.80
Outer diameter	mm	5.56
Pellet length	mm	7.5
Cladding		
Material		Zr-2
Outer diameter	mm	7.015
Inner diameter	mm	6.015
Wall thickness	mm	0.5

A7.2.2 Operating Conditions and Irradiation History

The HBWR operating conditions are tabulated in Table A7.2. The reactor power history is shown in Figure A7.1. The measured reactor coolant temperature was used as the boundary temperature on the cladding outer surface.

Table A7.2: Operational input parameters.

Average coolant temperature	C	230
Coolant pressure	MPa	3.4

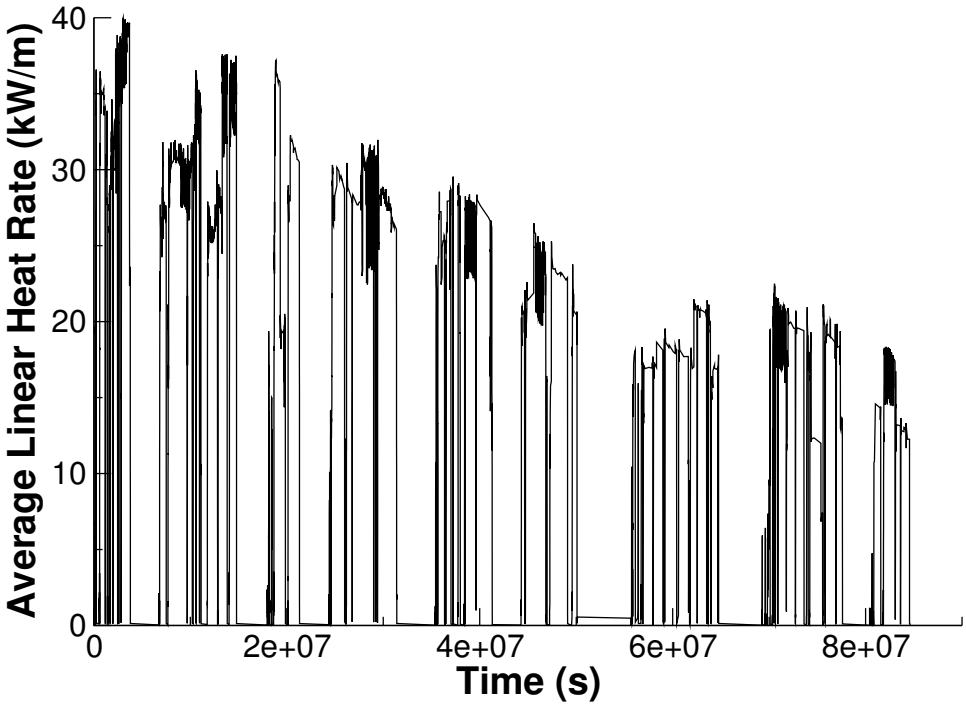

Figure A7.1: Through life power profile for IFA-562.2 rod 15. Note: Rods 15-17 power histories were very similar.

A7.3 Model Description

A7.3.1 Geometry and Mesh

The assumed geometry and mesh are shown in Figures A7.2 and A7.3. The fuel pellet stack was modeled as a smeared column with merged insulator pellets. The insulator pellets were modeled as UO_2, meaning they the same mechanical and thermal properties of the rest of the column. The expansion thermometer was modeled as a void in the pellet/insulator stack; this was done to ease the simulation. The BISON fuel centerline temperature was calculated as an average of the pellet interior (BISON sideset 13). The plenum length for the mesh was adjusted from the experiment length to account for the difference in volume caused by the voided expansion thermometer. The initial gas volumes for the simulations were as listed in [19]. A 2-dimensional axisymmetric quadratic mesh was used. The fuel column was meshed with 177 axial and 11 radial elements (aspect ratio 14) and the insulator pellets with 3 axial and 11 radial elements (aspect ratio 14). The cladding was meshed with 183 axial and 4 radial elements (aspect ratio 23.3).

Figure A7.2: 2-D axisymmetric quadratic mesh for IFA-562.2 rod 15. Note: magnified radially 10x.

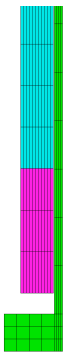

Figure A7.3: Close-up view of the IFA-562.2 rod 15. Note: This is only a cut from the bottom of the fuel rod meant to show the fuel and insulator pellet. The volume where the expansion thermometer would be in the experiment can also be seen.

A7.3.2 Material and Behavioral Models

The following material and behavioral models were used for the UO_2 fuel:

- ThermalFuel - NFIR: temperature and burnup dependent thermal properties
- VSwellingUO2: free expansion strains (swelling and densification)
- RelocationUO2: relocation strains, relocation activation threshold power set to 5 kW/m.
- Sifgrs: fission gas generation and release

For the cladding material, a constant thermal conductivity of 16 W/m-K was used and both thermal and irradiation creep were considered using the Limback model [19].

A7.3.3 Input files

The BISON input and all supporting files (power histories, axial power profile, cladding surface temperature boundary condition, fast neutron flux history, etc.) for this case are provided with the code distribution at bison/assessment/IFA_515_RodA1/analysis.

A7.3.4 Simulation Parameters and Assumptions

As mentioned in the A7.3.1 the mesh used is not an exact representation of the experiment. The insulator pellets were not included in the heat source term. The expansion thermometer was physically neglected in this mesh. This was done to alleviate troubles with thermal and mechanical properties between the thermometer and the fuel/insulator stack. The plenum length of the fuel rod was adjusted to account for the extra gas volume made from the voided thermometer. The simulation initial gas volumes were as listed in [19]. The initial fuel grain size and the fuel roughness were not given in [19]. The value of 7.75e-6 m was used for the initial grain size. This value was taken from IFA-515A1. The BISON default value of 2e-6 was used for the fuel roughness. Peaking factors were not given for this experiment. It is assumed that the rod were short enough that they did not experience much power tilting.

A7.4 Results Comparison

A BISON postprocessor was used to extract the centerline temperature as an average of the interface of the pellet interior surface and the ET (BISON sideset 13). This provides an accurate representation of the average fuel centerline temperature since, in this case, no axial variation in fuel temperature.

A7.4.1 Temperature

The BISON results for the fuel centerline temperature show that BISON over predicts the actual experimental. Plots of the comparisons can be seen below in Figures A7.4, A7.5 and A7.6. The peak fuel centerline temperatures are over estimated by 40-100 degrees C. One possible reason for the higher predicted temperature is that the fuel and cladding roughnesses were not reported. While running the initial simulations it was noticed that a smaller roughness affects the peak FCT greatly, improving the result comparisons. Fission gas release is another possible player with the FCT results. Initial fuel grain radius was not reported either and due to this 7.75e-6 m was taken from another simulation. The end of life FGR was reported by BISON to be about 3.5% for all three rods. This small amount would not affect the temperature much. The difference in the BISON results and the experiment measured can be seen as soon as the simulation starts. Meaning that the FGR is not the reason for the FCT difference. FCT were the only data measured from this experiment. Figures A7.7, A7.8 and A7.9 show a comparison of measured and predicted fuel centerline temperatures. These plots show that BISON does tend to over predict through the simulation at all powers. Included in these plots are the results from the test simulation that was run with a smaller fuel roughness. The rod 17 R_f=0.2μm results show a significant improvement in the comparison of measured and predicted. As mentioned before the fuel roughness was not reported so these results are purely academic.

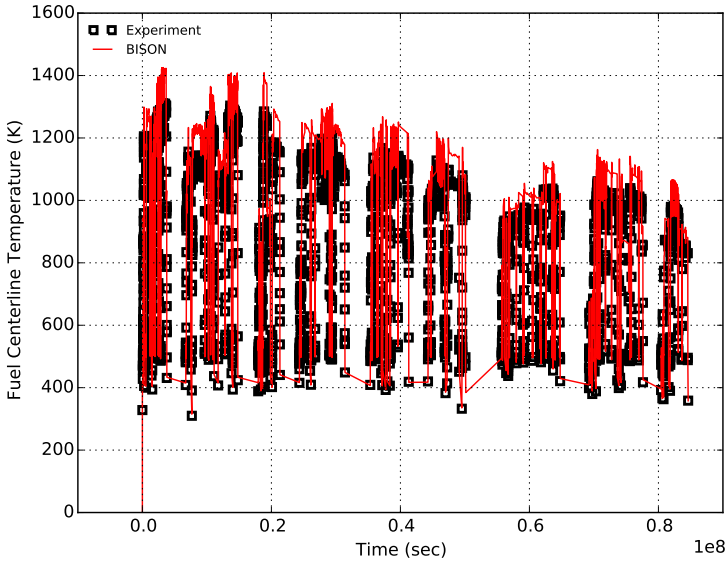

Figure A7.4: A comparison of fuel centerline temperatures for IFA-562.2 rod 15 from BISON calculations and experimental measurements.

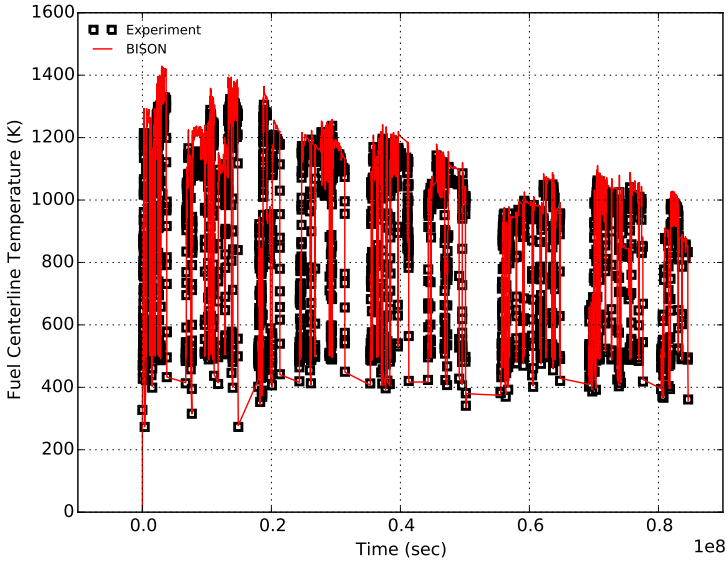

Figure A7.5: A comparison of fuel centerline temperatures for IFA-562.2 rod 16 from BISON calculations and experimental measurements.

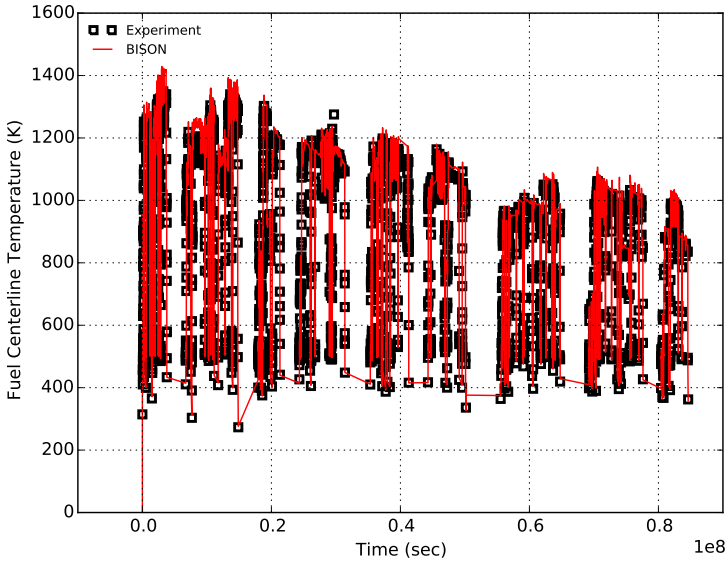

Figure A7.6: A comparison of fuel centerline temperatures for IFA-562.2 rod 17 from BISON calculations and experimental measurements.

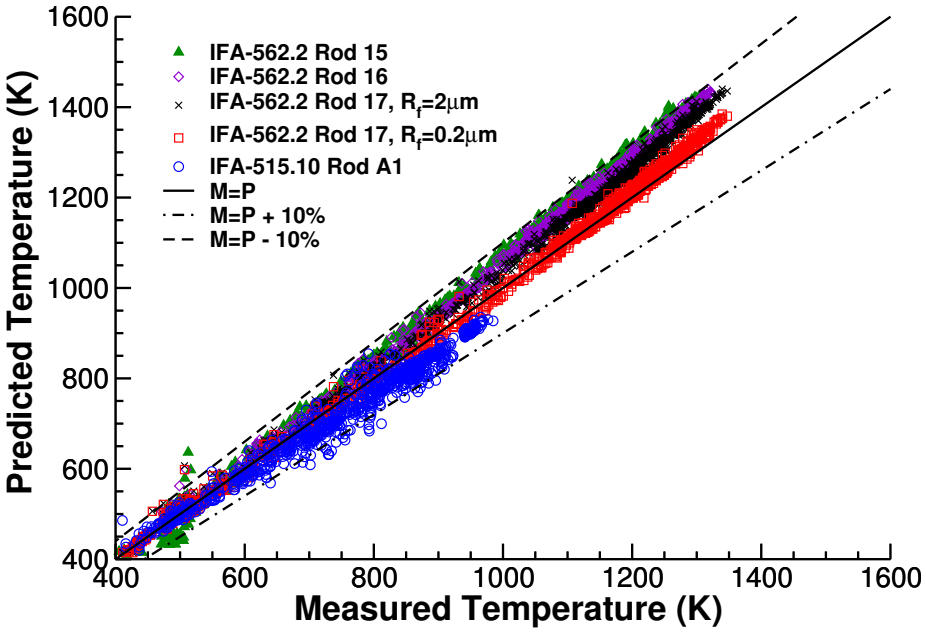

Figure A7.7: Comparison of measured vs. predicted fuel centerline temperature for IFA-562.2 at burnup 0-19 MWd/kgUO_2.

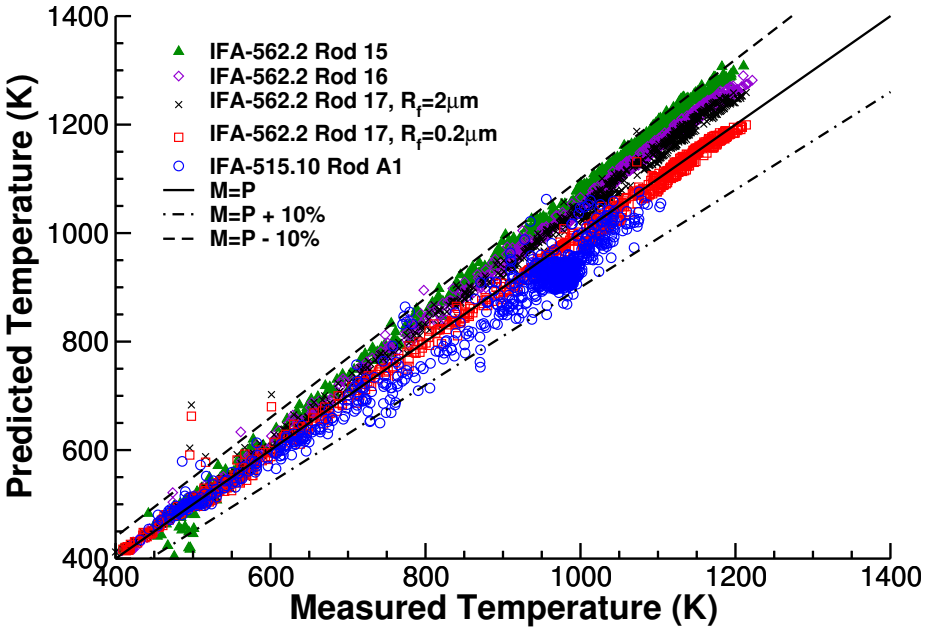

Figure A7.8: Comparison of measured vs. predicted fuel centerline temperature for IFA-562.2 at burnup 20-39 MWd/kgUO_2.

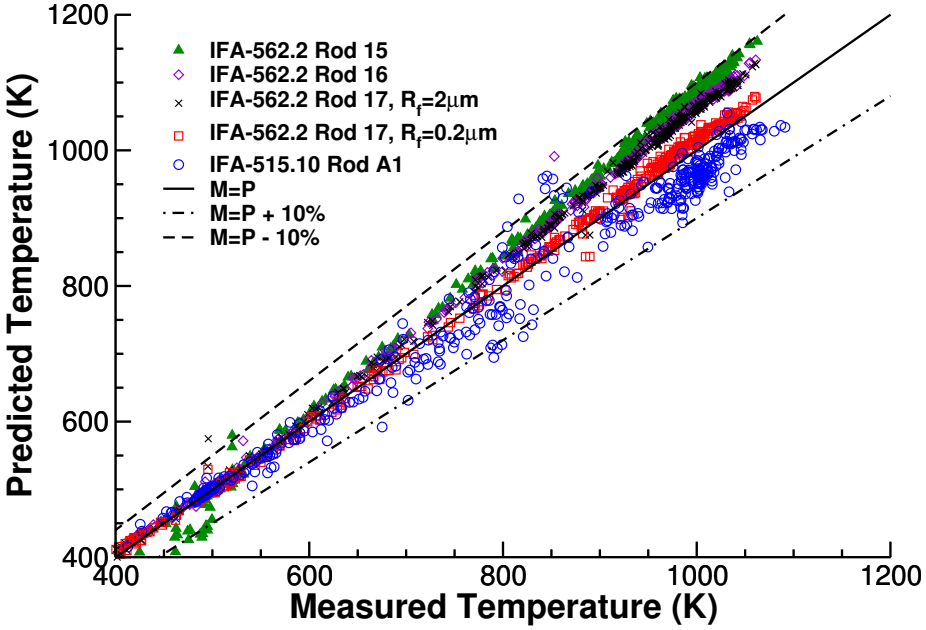

Figure A7.9: Comparison of measured vs. predicted fuel centerline temperature for IFA-562.2 at burnup 40-59 MWd/kgUO_2.

A7.5 Discussion

Fuel centerline temperature comparisons between BISON and the measured results show obvious differences, although the BISON results are within 10% of the experiment measured data. Fuel roughness was shown to be a sensitive parameter and one that we are stuck using a default value for. As mentioned previously FCT was the only data recorded from this experiment leaving us with only speculation as to what may be causing the result differences.

A8 IFA 636 Rod 5

A8.1 Overview

The IFA-636 fuel performance test was an experiment completed in the Halden reactor as part of the OECD Halden Reactor Project. The main objective of this experiment was to extend the database on the performance of UO_2-Gd_2O_3 fuel compared with commerical UO_2. The rod of interest investigated in this report is rod 5 which contained standard UO_2 fuel pellets and had online measurements of fuel elongation. Fuel elongation prior to contact can provide information on whether or not the thermal expansion, densification, solid fuel swelling and gaseous fuel swelling models are behaving as expected. Upon contact with the cladding the fuel elongation behavior becomes dependent upon the friction between the fuel stack and cladding. In the experiment it was observed that densification only occured in the UO_2 fuel whereas fuel elongation measurements in the Gd-doped fuel rods indicated essentially constant swelling with burnup. At burnups above 5 MWd/kgUO_2 the swelling rate was observed to be about 0.5 - 0.6 % ΔV/V per 10 MWd/kgUO_2 for both fuel types. The total burnup in rod 5 is approximately 34 MWd/kgUO_2.

A8.2 Test Description

A8.2.1 Rod Design Specifications

The specifications for IFA-636 rod 5 are summarized in Table A8.1.

Table A8.1: IFA-636 Rod 5 Rod Specifications

Fuel Rod		
Overall length	m	0.7288
Fuel stack height	m	0.393
Nominal plenum height	mm	20.2
Fill gas composition		He
Fill gas pressure	MPa	0.1
Fuel		
Material		UO_2
Enrichment	%	4.25
Density	%	96.1
Inner diameter	mm	-
Outer diameter	mm	8.195
Pellet geometry		dished, chamfered
Grain diameter	μm	9.36
Pellet Dishing		
Chamfer width	mm	0.51
Chamfer depth	mm	0.13
Dish diameter	mm	4.95
Dish depth	mm	0.24
Cladding		
Material		Zr-4
Outer diameter	mm	9.5
Inner diameter	mm	8.357
Wall thickness	mm	0.5715

A8.2.2 Operating Conditions and Irradiation History

The power history of the IFA-636 experiment was provided by Halden as part of the Halden Research Project (HRP). Throughout the duration of the experiment there was an axial profile that resulted in higher power to the fuel at the top of the rod. A history of the average linear heating rate applied to the fuel is presented in Figure A8.1.

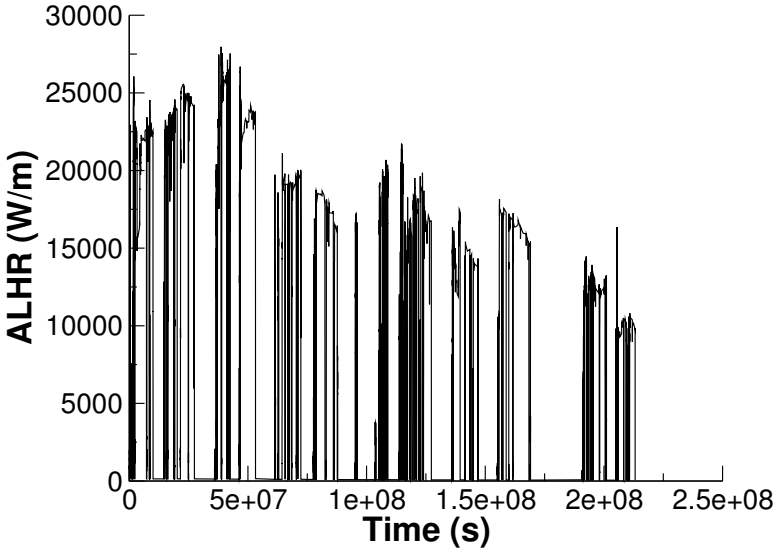

Figure A8.1: History of the average linear heating rate to the fuel for the IFA-636 rod 5 test.

The outer clad surface temperature was given in the Halden data and prescribed as a function Dirichlet boundary condition. For the fast flux to the cladding a factor of 1.6 $\times 10^{12}$ n m^{-2} s^{-1} per W/m was multiplied by the power profile. This factor is a typical value for the Halden Boiling Water Reactor. The coolant pressure for the duration of the experiment was set to 3.33 MPa.

A8.3 Model Description

A8.3.1 Geometry and Mesh

The geometric parameters specified in Table A8.1 were used to create the mesh for this simulation. The fuel was meshed as a smeared fuel rod with 11 radial and 40 axial quadratic elements. The plenum length was adjusted such that the initial void volume within the fuel element is equal to 5.4 cubic centimeters as given in the Halden report [46]. A segment of the mesh is illustrated in Figure A8.2.

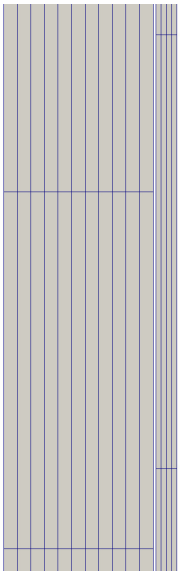

Figure A8.2: Segment of the mesh used for the fuel and cladding for the IFA-636 rod 5 simulation.

A8.3.2 Material and Behavioral Models

The NFIR thermal conductivity model was used for the UO_2 fuel. The fuel was modeled as elastic and fuel swelling was coupled to the fission gas release model. In addition fuel relocation was modeled using an activation power of 5 kW/m. Fission gas release was modeled using the Sifgrs model with a transient burst release model. The cladding material was modeled using a constant thermal conductivity of 16 W/m-K, and primary and secondary thermal, and irradiation creep were modeled.

A8.3.3 Input files

The BISON input and all supporting files (power histories, axial power profile, fast neutron flux history, etc.) for this case are provided with the code distribution at bison/assessment/IFA_636/analysis/

A8.4 Results Comparison

In this section the BISON simulation results are compared against the experimental data and information provided by Halden. Measurements were provided for fuel elongation for rod 5. From the fuel elongation measurements a calculation of the volumetric strain in the fuel was determined. Halden

takes experimental measurements every 15 minutes during the irradiation. To make the amount of data points manageable the program PowerCondense4 was used to condense the power history, axial profile, cladding temperature and cladding elongation. All condensed measurements were synchronized in time. Halden noted that the fuel elongation sensor present in rod 5 failed during irradiation. This failure is observed when the experimental data falls close to zero at an irradiation time of approximately 45 000 hours as illustrated in Figure A8.3. BISON underpredicts the fuel elongation early in life and overpredicts the fuel elongation late in life. To gain a better understanding of the behavior early in the irradiation a zoomed in version on the first 500 hours of irradiation is provided in Figure A8.4. The sharp increase in the BISON results immediately after the simulation starts is due to the fact that BISON assumes a reference temperature of 297 K for the thermal expansion.

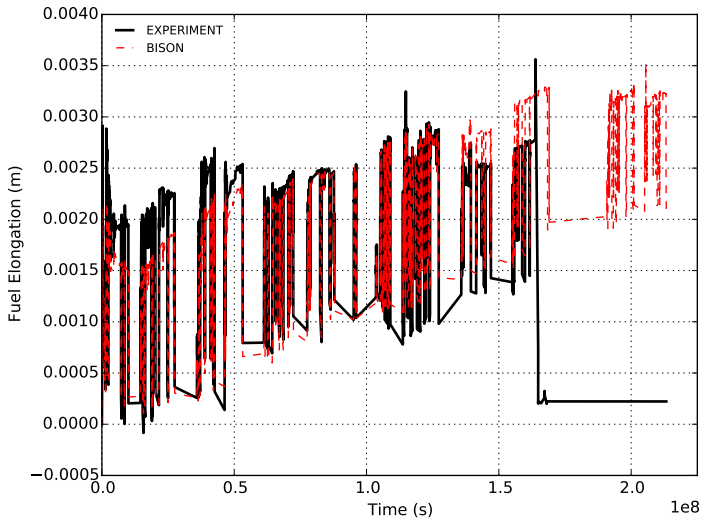

Figure A8.3: Comparison of BISON simulation results to the experimental measurements for fuel elongation for IFA-636 rod 5.

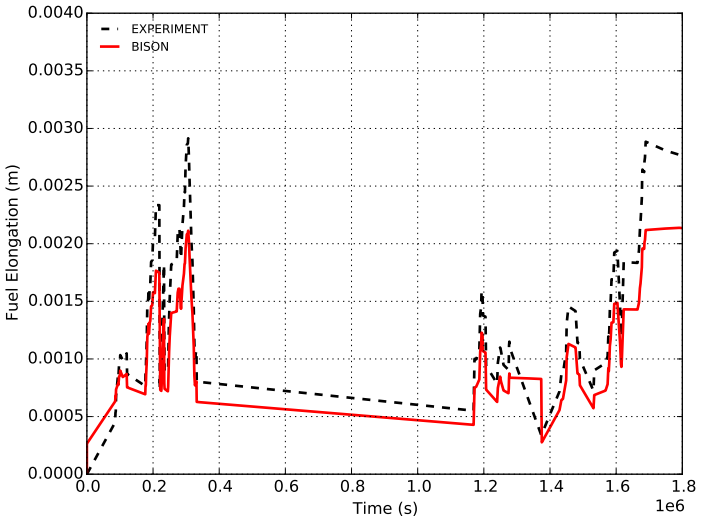

Figure A8.4: Comparison of BISON simulation results to the experimental measurements for fuel elongation for IFA-636 rod 5 for the first 500 hours of irradiation.

Halden stated in the report that the volumetric swelling rate was between 0.5% and 0.6% per 10 MWd/kgUO2 after a burnup of 5 MWd/kgUO2 as presented in Figure A8.5. A parametric study was completed comparing a BISON simulation using the total solid swelling and by assuming a solid swelling of 90% the calculated value because other fuel performance codes such as FALCON have indicated that prior to contact they automatically take 10% off the calculated value for solid swelling as it provided more accurate comparisons to experiments. The results indicate that the currently implemented solid swelling model within BISON results in an overprediction of the volumetric strain of approximately 10%.

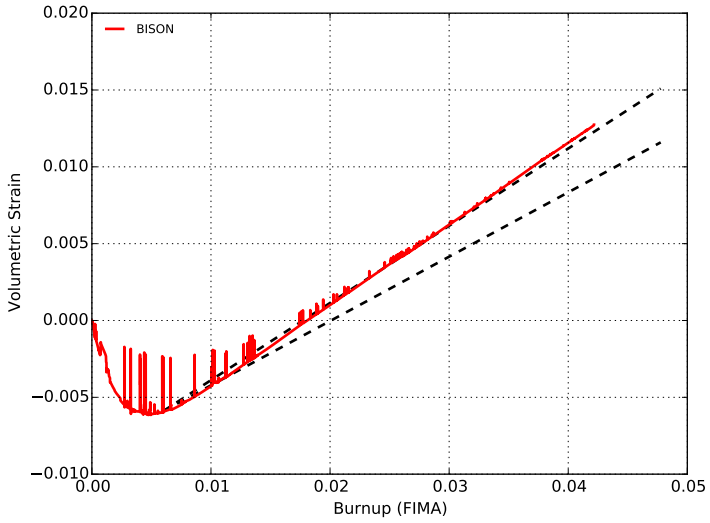

Figure A8.5: Volumetric strain predicted by BISON assuming total solid swelling and 90% solid swelling. The minimum and maximum swelling rates (0.5% and 0.6% per 10 MWd/kgUO2) given by Halden are superimposed. BISON appears to overpredict the volumetric strain.

A9 US PWR 16x16

A9.1 Overview

The US PWR 16x16 lead test assembly (LTA) extended burnup demonstration (referred to as US PWR 16x16 from here on out) was conducted during the 1980's in a US commercial pressurized water reactor (PWR) [45]. The purpose of this series of experiments was to increase final discharge burnup and to demonstrate improved fuel utilization through more efficient fuel management. Two rods out of this series, TSQ002 and TSQ022, were discharged at a burnup of approximately 58 MWd/kgU and are the subjects of this report. TSQ002 is a full length fuel rod with standard (solid) fuel pellets, whereas TSQ022 is a full length fuel rod with annular fuel pellets.

A9.2 Test Description

A9.2.1 Rod Design Specifications

As mentioned in the previous section, both rods considered in the US PWR16x16 experiment were full length rods. TSQ002 was a standard fuel rod with solid fuel pellets whereas TSQ022 had annular fuel pellets. Both fuel rods were clad with Zr-4. The rod specifications are tabulated in Table A9.1.

A9.2.2 Operating Conditions and Irradiation History

The power history for rod TSQ002 is shown in Figure A9.1. The power history for rod TSQ022 is shown in Figure A9.2. A prescribed axial profile for this experiment was provided in the FUMEX-III data [45]. The measured clad surface temperature, as a function of time, was also provided in the FUMEX-III data [45] and used as a boundary condition for this simulation. The fast neutron flux was provided in the FUMEX-III data [45] as well, and is input in to the code as a function of time. The other reactor operation parameters are tabulated in Table A9.2.

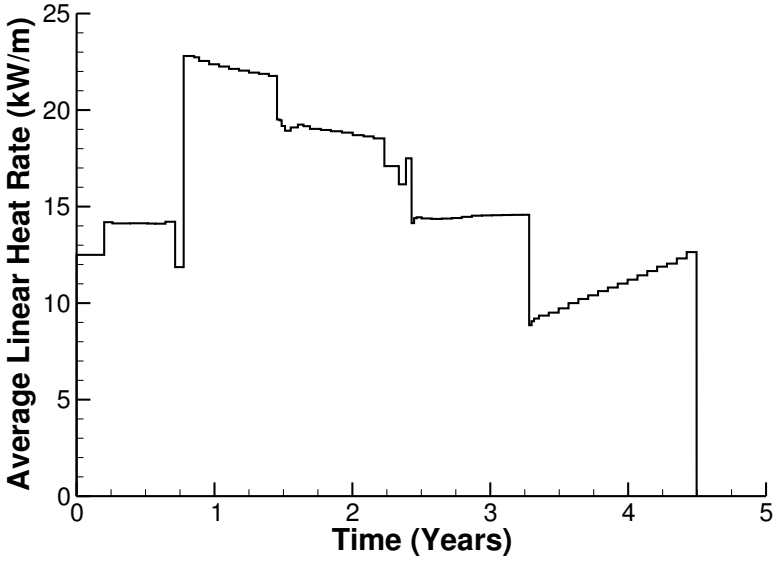

Figure A9.1: Power history for the TSQ002 fuel rod.

Table A9.1: Rod Specifications for US PWR 16x16 rods TSQ002 and TSQ022.

Fuel Rod		
Overall length	m	4.094
Fuel stack height	m	3.81
Nominal plenum height	mm	284
Number of pellets per rod		385
Fill gas composition		He
Fill gas pressure	MPa	2.62
Fuel		
Material		UO_2
Enrichment	%	3.48
Density	%	95
Inner diameter (TSQ022 only)	mm	2.337
Outer diameter	mm	8.255
Pellet geometry		dished both ends
Grain diameter	μm	7-12
Pellet Dishing		
Dish diameter	cm	0.5
Dish depth	cm	0.03
Chamfer width	cm	0.05
Chamfer depth	cm	0.016
Cladding		
Material		Zr-4
Outer diameter	mm	9.7028
Inner diameter	mm	8.4328
Wall thickness	mm	0.635

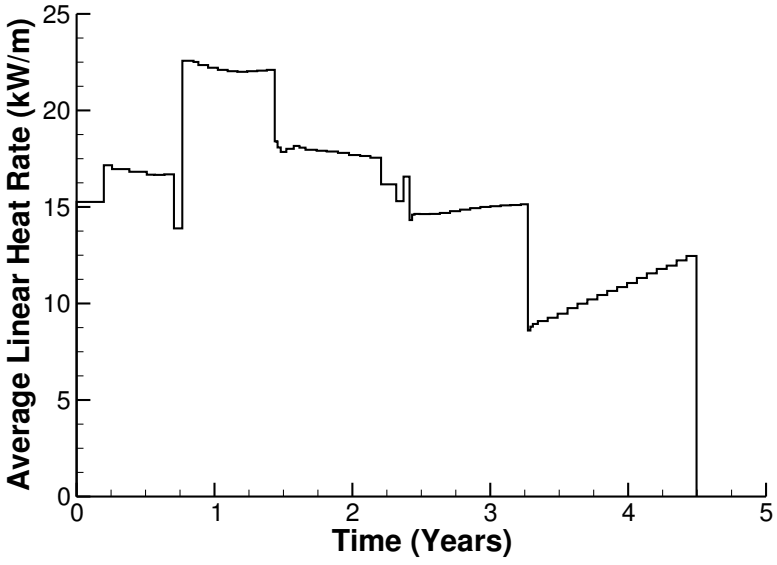

Figure A9.2: Power history for the TSQ022 fuel rod.

Table A9.2: Operational input parameters for the US commercial PWR.

Coolant inlet temperature	C	290
Coolant pressure	MPa	15.517
Fast neutron flux	n/(cm^2∗s) per (kW/m)	5.41∗10^{12}

A9.3 Model Description

A9.3.1 Geometry and Mesh

A 2-dimensional axi-symmetric quadratic mesh was used to model the geometry for both rods. The fuel pellets were modeled using a single cylindrical fuel column, refered to as a smeared pellet mesh. Both meshes consisted of 1925 axial elements and 11 radial elements. The clad mesh for both rods consisted of 1931 axial elements and 4 radial elements.

A9.3.2 Material and Behavioral Models

The following material and behavioral models were used for the UO_2 fuel:

- ThermalFuel - NFIR: temperature and burnup dependent thermal properties
- RelocationUO2: relocation strains, relocation activation threshold power set to 5 kW/m.
- Sifgrs: fission gas release model with a couple gaseous swelling model

For the clad material, a constant thermal conductivity of 16 W/m-K was used and both thermal (primary and secondary) and irradiation creep were considered using the Limback creep model [36].

A9.3.3 Input files

The BISON input and all supporting files (power histories, axial power profile, fast neutron flux history, etc.) for this case are provided with the code distribution at ..bison/assessment/US_PWR_16x16/analysis.

A9.4 Results Comparison

The purpose of this series of experiments was to increase final fuel discharge burnup and to demonstrate improved fuel utilization through more effcient fuel management. The two rods of interest, for this study, are TSQ002 and TSQ022, which compare the difference between annular and solid pellets with the standard PWR fuel design [45]. Experimental data is sparse as these are commercial rods irradiated in a commercial plant. The through life fuel centerline temperature and the through life rod internal pressure results were compared to other well know fuel performance codes. The data for these comparisons were digitized from the plots in the FUMEX-III Summary Report [45]. The total fission gas release and the end of life final rod diameter calculations were compared to experimental data.

A9.4.1 TSQ002

Temperature

As there is no experimental data to compare the fuel centerline temperature to, BISON results were compared to other well know fuel performance codes [45]. As show in Figure A9.3, the BISON predictions for fuel centerline temperature compare well with the other codes. Note: The fuel centerline temperature was taken at a node near the axial mid-plane of the rod.

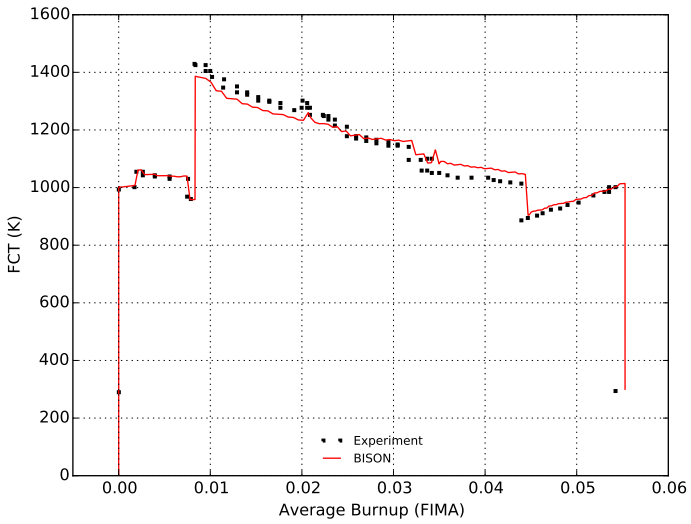

Figure A9.3: Fuel centerline temperature comparisons for rod TSQ002.

Fission Gas Release

The only fission gas release data available for this experiment is from post irradiation examination (PIE) puncture tests at the end of the fuel life. Figure A9.4 shows BISON's comparisons with the end of life experimental data.

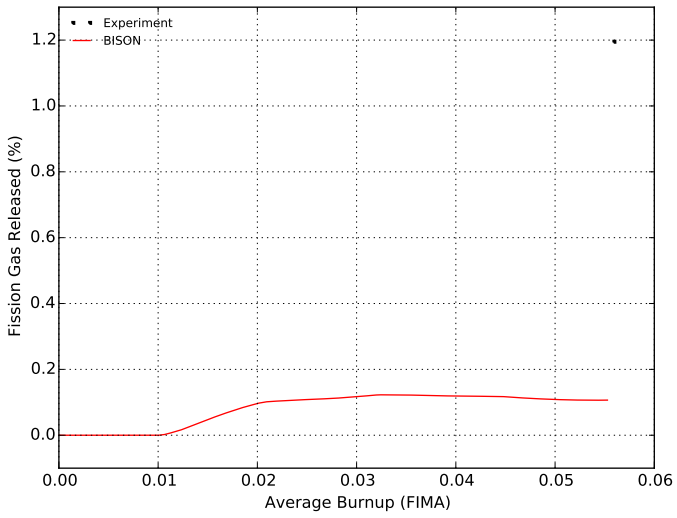

Figure A9.4: Fission gas release comparisons for rod TSQ002.

Internal Rod Pressure

As there is no rod internal pressure data to compare to, BISON calculations are compared to other well known fuel performance codes [45]. As shown in Figure A9.5, the BISON predictions of rod internal pressure compare well with the other codes.

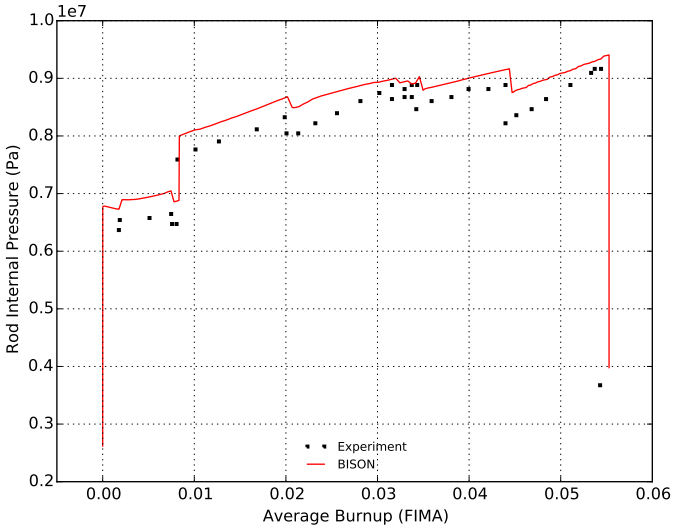

Figure A9.5: Through life code comparisons for the rod internal pressure for fuel rod TSQ002.

Rod Diameter

The final rod diameter is an indication of how well the solid mechinics featured in BISON are predicting fuel swelling and clad creep. Figure A9.6 has the BISON to experimental comparisons for the end of life final rod diamter. The BISON predictions over estimate the end of life rod diameter, with a difference of appoximatly 0.02 mm. Results of the other fuel performance codes can be found in reference [45].

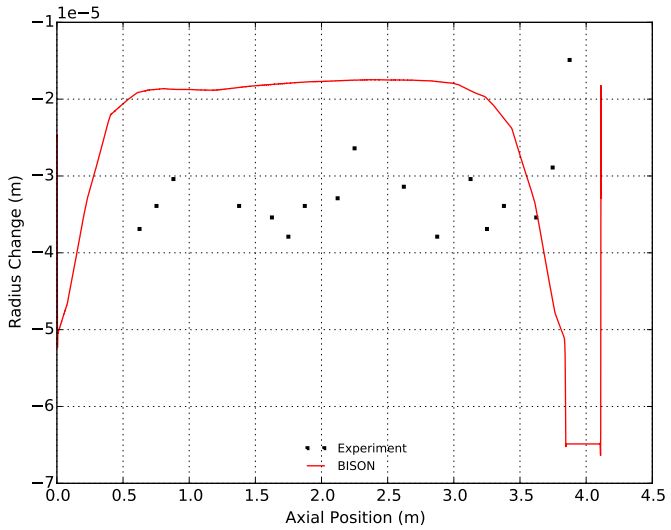

Figure A9.6: Final rod diameter comparisons for fuel rod TSQ002.

A9.4.2 TSQ022

Temperature

As there is no experimental data to compare the fuel centerline temperature to, BISON results were compared to other well known fuel performance codes [45]. As show in Figure A9.7, the BISON

predictions for fuel centerline temperature compare well with the other codes. Note: The fuel centerline temperature was take at a node near the axial mid-plane of the rod.

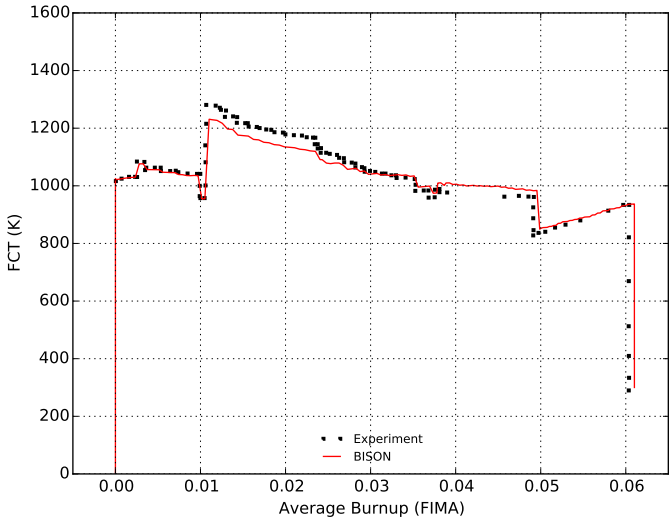

Figure A9.7: Fuel centerline temperature comparisons for rod TSQ022.

Fission Gas Release

The measured fission gas released was 0.85%, BISON did not predict any fission gas release for this experiment.

Rod Internal Pressure

As there is no rod internal pressure data to compare to, BISON calculations are compared to other well known fuel performance codes [45]. As shown in Figure A9.8, the BISON predictions for the rod internal pressure are lower than the other codes plotted. The lack of fission gas release in the BISON simulation could account for the lower pressure calculated.

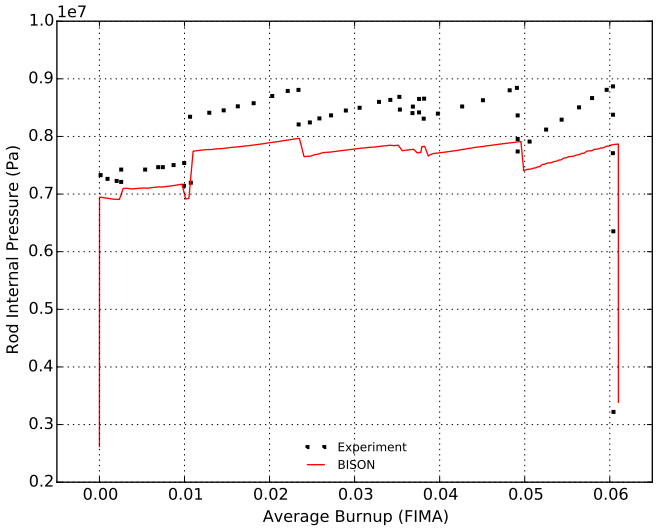

Figure A9.8: Through life code comparisons for the rod internal pressure for fuel rod TSQ022.

Rod Diameter

The final rod diameter is an indication of how well the solid mechanics featured in BISON are predicting fuel swelling and clad creep. Figure A9.9 shows the BISON to experimental comparisons for the end of life final rod diamter. The BISON predictions over estimate the end of life rod diameter, with a difference of appoximatly 0.03 mm. Results of the other fuel performance codes can be found in reference [45].

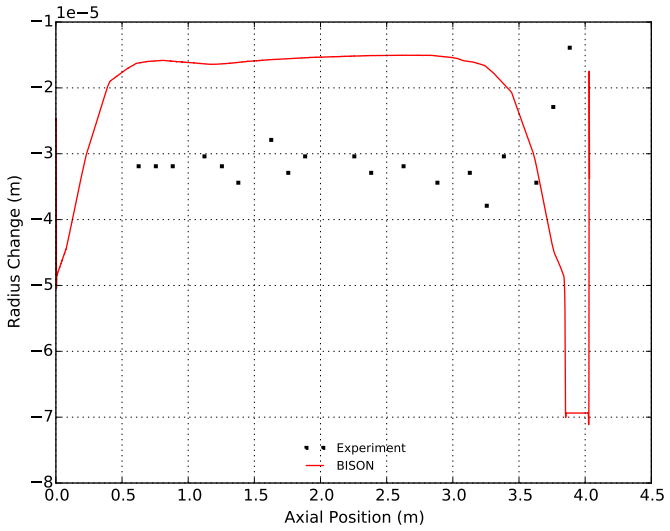

Figure A9.9: Final rod diameter comparisons for fuel rod TSQ022.

A9.5 Discussion

Data for these two simulations, TSQ002 and TSQ022, where provided in a histogram format from the FUMEX-III database. A script was written at Idaho National Laboratory to convert this histogram style formatting in to a linear style format for BISON's PiecewiseLinear function call. This script can be found with the code distribution at ..bison/assessment/US_PWR_16x16/analysis. From the results shown above it is plain to see that BISON results differ from the other codes mainly in the end of life rod diameter. Pellet-cladding interactions are extremely complex and modeling them is not a trivial matter. The BISON code is constantly undergoing changes and revisions to rectify weaknesses and results will be revisited as new and improved features are made available.

A10 IFA 597.3 Rods 7 and 8

A10.1 Overview

The IFA-597.3 rod 8 experiment conducted at Halden utilized a re-fabricated rod from the Ringhals boiling water reactor (BWR) [21]. The mother rod was irradiated at a low average power of around 16 kW/m for approximately 12 years. The mother rod was then re-fabricated to a shorter length and fitted with a fuel centerline thermocouple and an internal pressure sensor [47], [48].

The IFA-597.3 rod 7 experiment is similiar to the IFA-597.3 rod 8 experiment with the exception that it was instrumented with an elongation detector. The two experiments saw similarl powers (differed by approximately 2 kW/m). However, since the maximum power is approximately 30 kW/m this 2 kW/m difference is a significant percentage of the total power and the two simulations were run as separate rods with only the power history being changed. The fuel temperature and fission gas release results were obtained from the rod 8 simulation and the cladding elongation was obtained from the rod 7 simulation.

A10.2 Test Description

A10.2.1 Rod Design Specifications

As stated in the previous section, both rods were nearly identical and comparisons for both experiments were modeled with one simulation. The specifications for rod 8 were used for the simulation. Rod 8 was a re-fabricated rod extracted from a full length rod. The hole for the thermocouple was at the top of the fuel stack and did not penetrate the entire fuel stack. The re-fabricated rod geometry is tabulated in Table A10.1.

Table A10.1: IFA-597.3 Rod 8 Test Rod Specifications

Fuel Rod		
Overall length	m	0.3539
Fuel stack height	m	0.4098
Nominal plenum height	mm	0.0513
Mother Rod		
Fill gas composition		He
Fill gas pressure	MPa	0.1
Re-Fabricated Rod		
Fill gas composition		He
Fill gas pressure	MPa	0.5
Fuel		
Material		UO_2
Enrichment	%	3.347
Density	%	95.5
Inner diameter	mm	2.5
Outer diameter	mm	10.439
TC hole length	mm	34.0
Pellet geometry		dishing one end
Grain diameter	μm	7.83
Pellet Dishing		
Dish diameter	cm	0.5
Dish depth	cm	0.01
Chamfer width	cm	0.07
Chamfer depth	cm	0.02
Cladding		
Material		Zr-2
Outer diameter	mm	12.25
Inner diameter	mm	10.65
Wall thickness	mm	0.8

A10.2.2 Operating Conditions and Irradiation History

The power history for the base irradiation carried out at the Ringhals BWR is the same for both rods 7 and 8 and is shown in Figure A10.1. The experiment power history carried out at the Halden boiling water reactor (HBWR) is shown in Figure A10.2. The measured clad surface temperature as a function of time is shown in Figure A10.3. The other reactor operational parameters are tabulated in Table A10.2.

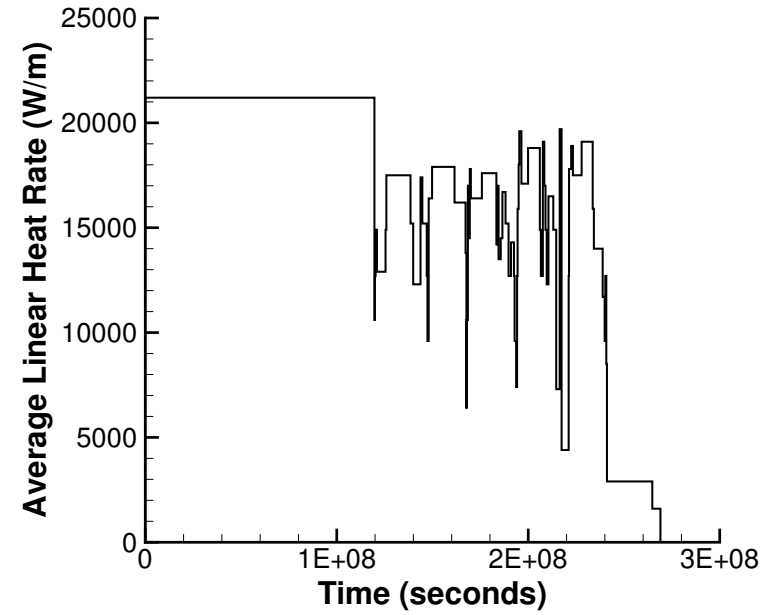

Figure A10.1: Base irradiation history for IFA-597.3, carried out at Ringhals BWR.

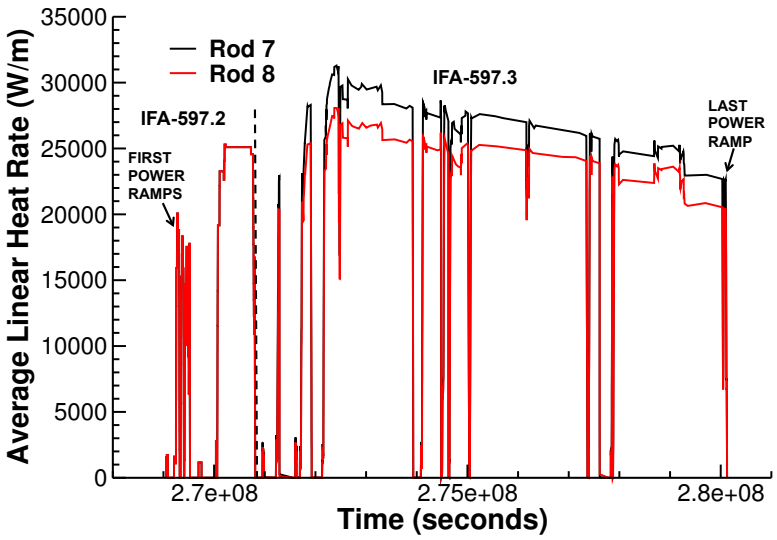

Figure A10.2: Halden irradiation periods for rods 7 and 8. The irradiations include IFA-597.2 and IFA-597.3.

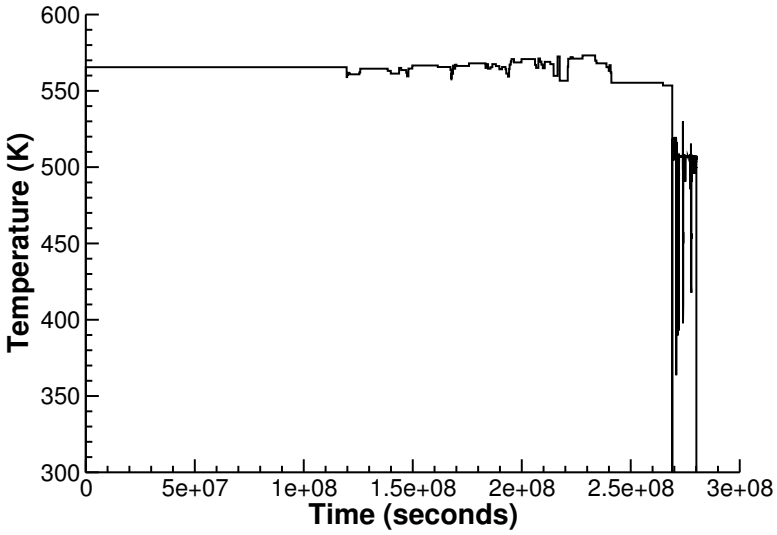

Figure A10.3: Temperature on the outside surface of the cladding for both the base irradiation and Halden irradiations for Rods 7 and 8.

Table A10.2: Operational input parameters.

Base Irradiation		
Coolant inlet temperature	C	286
Coolant pressure	MPa	7.0
Fast neutron flux	n/(cm^2·s) per (kW/m)	2.3·10^{12}
Power Ramps		
Coolant inlet temperature	C	232
Coolant pressure	MPa	3.2
Fast neutron flux	n/(cm^2·s) per (kW/m)	1.6·10^{11}

A10.3 Model Description

A10.3.1 Geometry and Mesh

The re-fabricated rod geometry was modeled for the entire simulation. The rod was modeled with two smeared pellet blocks, one annular and one solid, to account for the thermocouple at the top of the fuel rod.

A 2D-RZ axisymmetric quadratic mesh was used to model the geometry of rod 8. The fuel mesh consisted of 128 axial nodes and 14 radial nodes (11 radial elements for the annular section) and the clad was meshed with 4 radial elements through the thickness. A section of the meshed fuel rod at the thermocouple location is shown in Figure A10.4.

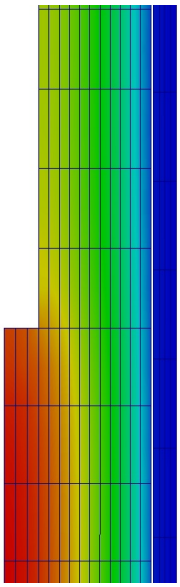

Figure A10.4: 2D-RZ axisymmetric mesh for IFA-597.3 Rod 8 simulation with temperature contour plot at thermocouple location.

A10.3.2 Material and Behavioral Models

The following material and behavioral models were used for the UO_2 fuel:

- ThermalFuel - NFIR: temperature and burnup dependent thermal properties
- RelocationUO2: relocation strains
- Sifgrs: Simplified fission gas release model with a combined solid/gaseous swelling model based on fission gas release.

Material models for Zr-4 were used as a replacement for the Zr-2 clad. For the clad material, a constant thermal conductivity of 16 W/m-K was used and both thermal (primary and secondary) and irradiation creep were considered using the Limback model [36].

A10.3.3 Input files

The BISON input and all supporting files (power histories, axial power profile, fast neutron flux history, etc.) for this case are provided with the code distribution at bison/assessment/IFA_597_3/analysis.

A10.4 Results Comparison

The IFA-597.3 Rod 8 experiment irradiated at Halden is used to demonstrate the code's capability to capture the fuel centerline temperature and the total fission gas released. The IFA-597.3 Rod 7 experiment is used to assess the code's capability to predict clad elongation during irradiation.

A10.4.1 Temperature

Comparison of the measured and predicted fuel centerline temperature during the first four and final power ramps are shown in Figure A10.5. Although BISON tends to under predict the temperature, considering uncertainties in the power and temperature measurements the comparisons are reasonable.

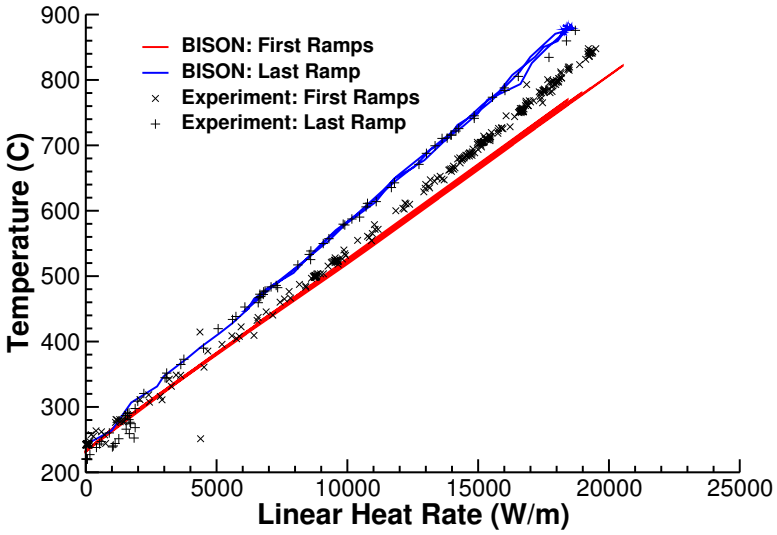

Figure A10.5: BISON fuel centerline temperature comparison to Halden experimental data.

A comparison of the predicted (P) and measured (M) fuel centerline temperatures for the entire IFA-597.3 ramp section is shown in Figure A10.6. Superimposed on the graph are a M=P, M=P+10%, and M=P−10% lines to illustrate how well BISON is predicting the fuel centerline temperature. Given the uncertainty in thermal conductivity and measurements of linear power, predictions within ±10% are considered acceptable.

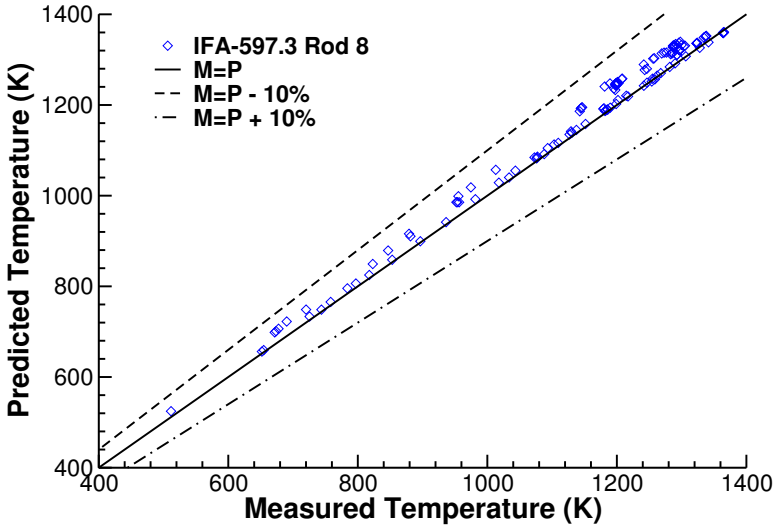

Figure A10.6: Predicted versus measured temperature throughout the IFA-597.3 Halden ramp.

A10.4.2 Fission Gas Release

BISON under predicts the total FGR at the end of base irradiation and at the end of the power ramps. The pressure transducer that was used to measure the FGR reached its maximum operating limit at 68 MWd/kgU. The total fission gas release measured during the PIE puncture test was 15.8%. BISON predicts 1.8%. The BISON results compared to experimental data is shown in Figure A10.7.

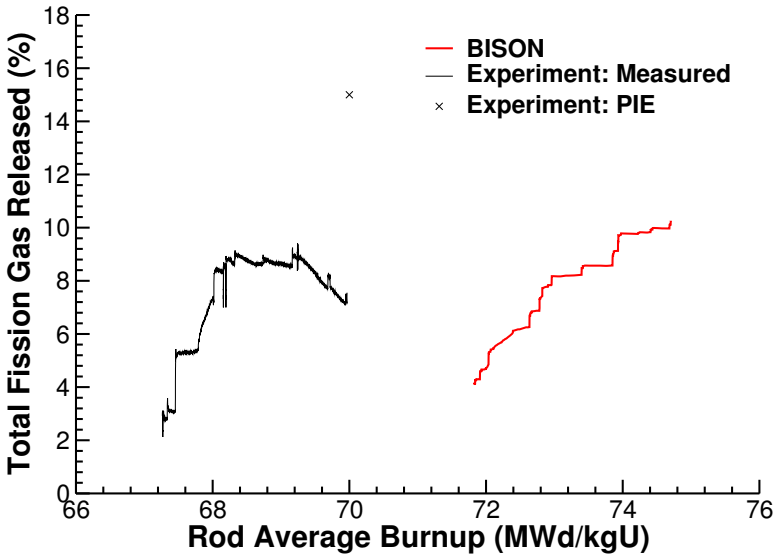

Figure A10.7: BISON fuel centerline temperature comparison to Halden experimental data.

A10.4.3 Clad Elongation

The clad elongation was predicted with both frictionless contact between the fuel and clad and with glued contact between the fuel and clad, with the actual clad elongation lying between the two predictions.

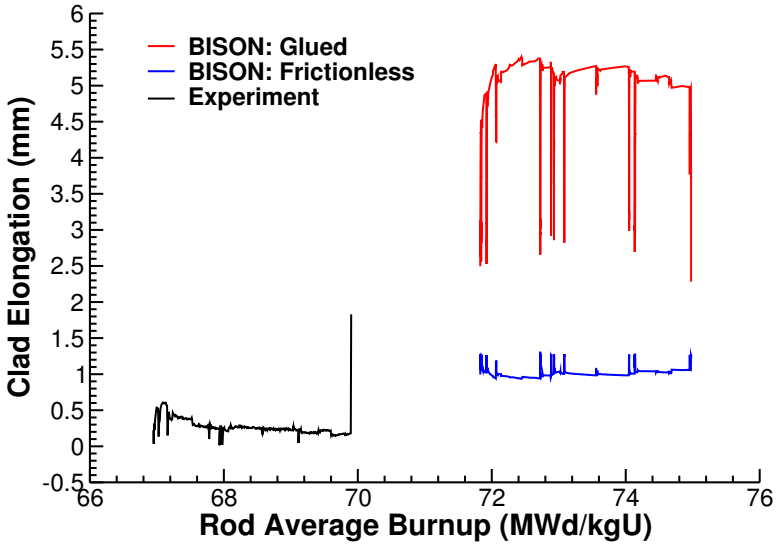

Figure A10.8: BISON fuel centerline temperature comparison to Halden experimental data.

A10.5 Discussion

BISON over predicts the burnup which leads to a shift in the comparisons; this is currently being investigated.

It is recommended that this problem be revisited when frictional contact is ready for use in order to better predict the clad elongation during the power ramps.

A11 R. E. Ginna Rod 2 and Rod 4

A11.1 Overview

The objective of the Siemens Power Corporation (SPC)- R. E. Ginna fuel irradiation program was to test proposed fuel designs with increased margin to PCI failure and potential for higher burnup. The lead fuel assemblies were fabricated by Exxon Nuclear Company (ENC, later acquired as SPC) under a cooperative program jointly sponsored by Empire State Electric Energy Research Corporation (ESEERCo), Rochester Gas and Electric Corporation (RG&E), and ENC [49]. The irradiation program conducted at the R. E. Ginna nuclear power plant evaluated 14x14 fuel rod designs with both full length and segmented test rods featuring annular or solid pellets combined with standard (CWSRA Zr-4) or Zr-barrier (Zr-lined, CWSRA Zr-4) cladding. For the purposes of this fuel analysis problem, two rodlets from a segmented fuel rod in lead fuel assembly XT03 were evaluated: one with solid pellets and one with annular pellets. Both rods used standard cladding without a Zr-barrier. This experiment was chosen for analysis because of the availability of measured data for evaluation of several fuel rod performance characteristics including fission gas release, cladding hydrogen pick-up fraction, fuel column length changes, and end-of-life internal free volume and rod internal pressure.

A11.2 Test Description

A11.2.1 Rod Design Specifications

Two segmented rodlets from lead test assembly XT03 were chosen for analysis: Rodlet-2 type SSN5 and Rodlet-4 type ASN5. The fuel rodlet cross reference identification data is shown below in Table A11.1 [50]. The geometric input parameters for the R.E. Ginna Rodlet-2 and Rodlet-4 test are summarized in Table A11.2.

Table A11.1: R.E. Ginna Fuel Rodlet Cross Reference

Rodlet Number	Assembly	Rod Position	Rod Serial Number	Segment Number	Segment Serial No.	Rodlet Type
2	XT03	M07	XV00-2604	3	S003L	SSN5
4	XT03	L02	XU10-2303	2	S015U	ASN5

Table A11.2: R. E. Ginna Rodlet-2 and Rodlet-4 Test Rod Specifications.

Fuel Rod		
Overall length	m	0.653
Fuel stack height	m	0.5418
Nominal plenum height	mm	70.8
Fill gas composition		He
Fill gas pressure	MPa	2.1
Fuel		
Material		UO_2
Enrichment (Rodlet-2)	%	3.52
Enrichment (Rodlet-4)	%	3.7
Density	%	94
Inner diameter (Rodlet-4 only)	mm	2.814
Outer diameter	mm	8.903
Nominal diametral gap	μm	190
Average grain size (Rodlet-2)	μm	22
Average grain size (Rodlet-4)	μm	20
Cladding		
Material		Zr-4
Outer diameter	mm	10.592
Inner diameter	mm	9.093
Wall thickness	mm	0.749

A11.2.2 Operating Conditions and Irradiation History

The XT03 segmented rod was irradiated for 5 cycles in the R.E Ginna reactor to a final discharge average assembly burnup of 52.07 MWd/kgU. The reactor operated at or near full power throughout the five cycles of irradiation. The power mode selected is PiecewiseLinear. The power histories for Rodlet-2 and Rodlet-4 are shown in Figures A11.1 and A11.2, respectively. These two power histories assumed a 24 hour startup time to reach full power, and a ramp rate of 0.33 kW/m/hr for large power increases. The ramp rate of 0.33 kW/m/hr was applied for Rodlet-2 at time step 18 to increase linear power from 21700 W/m to 33200 W/m in 125454.4 seconds and at time step 74 to increase linear power from 8200 W/m to 21300 W/m in 142909.1 seconds. The ramp rate was also applied for Rodlet-4 at time step 16 to go from LHGR of 16200 W/m to 33200 W/m in 185454.5 seconds and at time step 97 to go from 12600 W/m to 21400 W/m in 96000 seconds.

The startup times and ramp rates selected are based on ANATECH's experience with fuel rod modeling for steady state operation and are intended to minimize the introduction of computational artifacts from unrealistic power changes and ramp rates into the analyses . The ramp rate guidelines for typical power maneuvers are shown in Table A11.3. The axial profile was calculated from the SPC-RE-Ginna data package [51]. The measured cladding outer surface temperature as a function of time was also provided in the SPC- RE-Ginna data package [51] and was used as a boundary condition for these simulations. The cladding outer surface temperature ranged from 568 K to 601.2 K. The initial fill-gas (Helium) pressure was 2.1 MPa, and the coolant system pressure was corrected to be 15.51 MPa instead of 155.1 MPa as shown in the QA report for SPC Irradiation in RE Ginna Reactor data [52]. The fast neutron flux as a function time was calculated from the fluence data provided in the SPC-RE- Ginna data package [51]. The fast neutron flux profile was scaled to 4.8e17. Operational input parameters are summarized in Table A11.4.

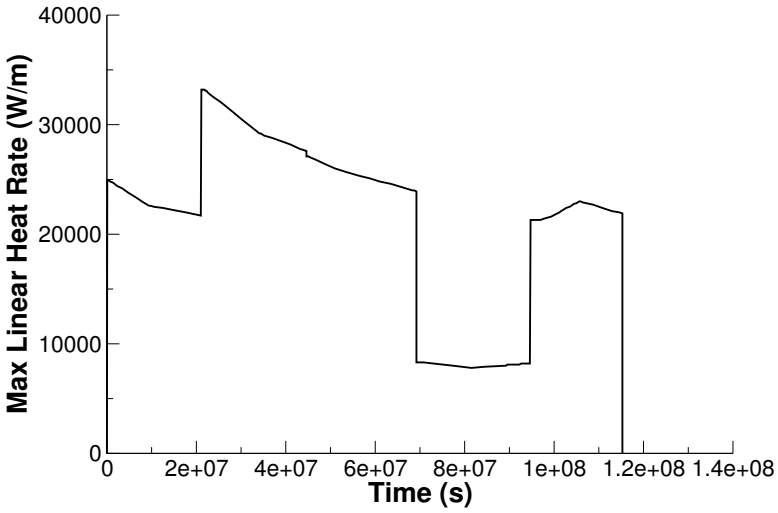

Figure A11.1: Rodlet-2 power history with 24 hours startup and ramp rate of 0.33 kW/m/hr

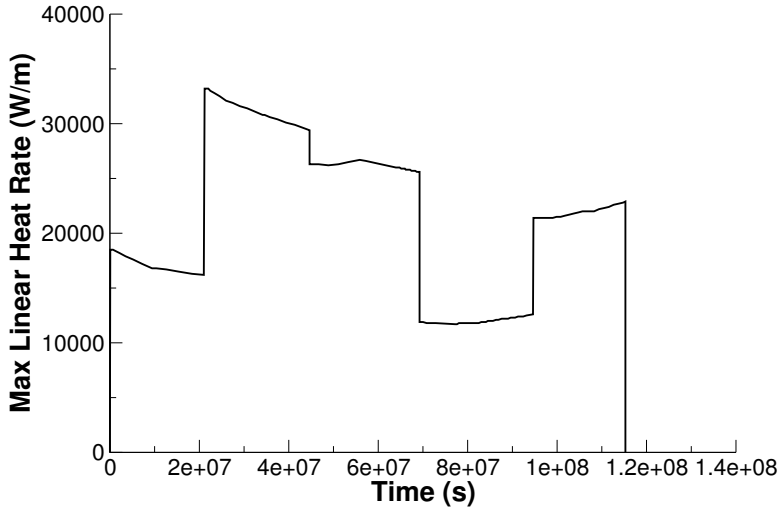

Figure A11.2: Rodlet-4 power history with 24 hours startup and ramp rate of 0.33 kW/m/hr

Table A11.3: Ramp Rate Guidelines for typical power maneuvers

Steady State Operation	**kW/ft/hr**	**kW/m/hr**
Typical operating maneuvers	0.1	0.33
Start-Ups	0.3 - 1.0	1.0 - 3.3
Fast Transients		
LOCA tests	2.2E3	7.2E3

Table A11.4: Operational input parameters

Base Irradiation		
Coolant inlet temperature	K	550.15
Coolant pressure	MPa	15.51

A11.3 Model Description

A11.3.1 Geometry and Mesh

The rod specifications in Table A11.2 were used to define the geometry for these simulations. Each rodlet was modeled as a 2-dimensional axi-symmetric linear mesh with quadratic elements. The Rodlet-2 fuel mesh consisted of 102 axial elements and 11 radial elements, whereas the Rodlet-4 fuel mesh consisted of 102 axial elements and 8 radial elements due to the presence of the fuel pellet annulus. The cladding mesh for both rodlets consisted of 4 radial elements.

In order to accurately model the fuel rod initial free volume, the overall fuel rod length and upper plenum height were adjusted during the mesh generation to account for the volume of the plenum spring which is not explicitly modeled. The overall fuel rod lengths for Rodlet-2 and Rodlet-4 were reduced from 653 mm to 600.853 mm and 593.578 mm, respectively. The plenum heights for Rodlet-2 and Rodlet-4 were reduced from 70.8 mm to 53.59 mm and 46.316 mm, respectively. The meshes for each rodlet are shown in Figures A11.3 and A11.4.

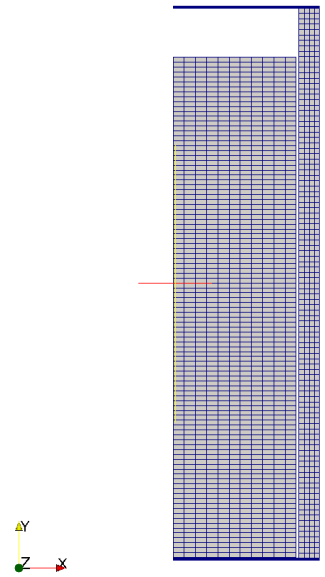

Figure A11.3: Rodlet-2 mesh

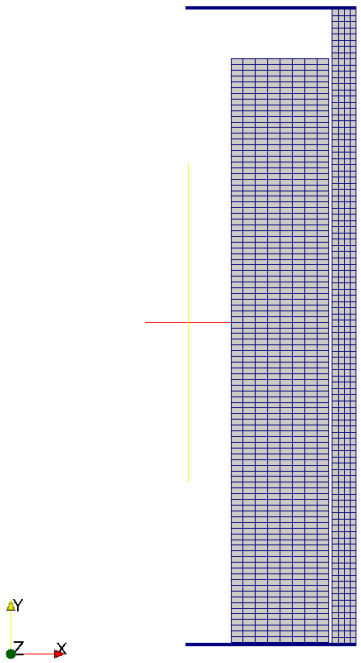

Figure A11.4: Rodlet-4 mesh

A11.3.2 Material and Behavioral Models

The following material and behavioral models were used for the UO_2 fuel:

- ThermalFuel - NFIR: temperature and burnup dependent thermal properties.

- RelocationUO2: relocation strains, relocation activation threshold power set to 5 kW/m.
- Sifgrs: fission gas release model with the combined gaseous swelling model.
- MechZry: model irradiation growth.

For the cladding material, a constant thermal conductivity of 16 W/m-K was used and both thermal and irradiation creep were considered using the Limback model [36].

A11.3.3 Input files

The BISON input and all supporting files (power histories, axial power profile, etc.) for Rodlet-2 and Rodlet-4 are provided with the code distribution at bison/assessment/RE_Ginna_Rodlets/analysis/RE_Ginna_Rodlet-2 and bison/assessment/RE_Ginna_Rodlets/analysis/RE_Ginna_Rodlet-4, respectively.

A11.4 Results Comparison

Data from the SPC-R. E. Ginna fuel irradiation program was used to assess the codes capability to capture the integral fuel rod fission gas release, rod internal pressure, fuel column length changes and cladding hydrogen pick-up fraction. A comparison of the predicted values from BISON calculations versus measured values from experimental data are shown in Table A11.5 and Table A11.6 for Rodlet-2 and Rodlet-4 respectively. Because the feature to calculate oxide thickness, cladding hydrogen concentration and pick-up fraction are not currently available in BISON, these comparisons will be performed in the future. The final burnup calculated for Rodlet-2 and Rodlet-4 were 51.508 MWd/kgU and 57.57 MWd/kgU compared to 51.6 MWd/kgU and 57.04 MWd/kgU burnup, respectively in the test documentation.

Table A11.5: Bison prediction versus measured data for Rodlet-2.

	BISON prediction	Measured Data
Burnup (MWd/kgU)	51.508	51.69
Fission Gas Release (%)	1.903	2.36
EOL Rod Internal Pressure (MPa)	4.25	2.88
Column changes (mm)	3.578	7.3 (Length Increase)
Initial free volume (cc)	5.0	5.0
Final free volume (cc)	3.599	3.7
Rod average diametral creepdown (%)	0.1944	0.793

Table A11.6: Bison prediction versus measured data for Rodlet-4.

	BISON prediction	Measured Data
Burnup (MWd/kgU)	57.57	57.04
Fission Gas Release %	0.843	0.92
EOL Rod Internal Pressure (MPa)	3.604	2.32
Column changes (mm)	4.75	4.7 (Length Increase)
Initial free volume (cc)	7.897	7.9
Final free volume (cc)	6.565	7.0
Rod average diametral creepdown (%)	0.19	0.769

A11.4.1 Fission Gas Release

The only fission gas release (FGR) data available for this experiment is from post irradiation examination (PIE) puncture tests at the end of the fuel life. Figure A11.5 and Figure A11.6 show BISONs comparisons with the end-of-life experimental data for Rodlet-2 and Rodlet-4, respectively. BISON computes a reasonable FGR value that only slightly under predicts the measured result for both rodlets.

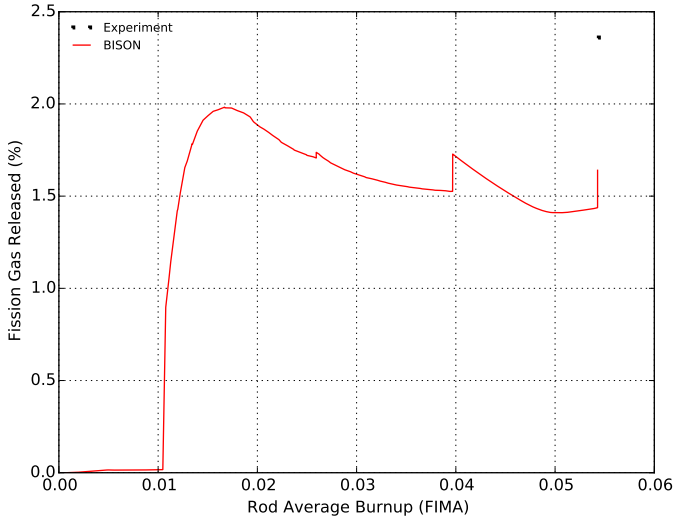

Figure A11.5: Fission gas release comparisons for Rodlet-2

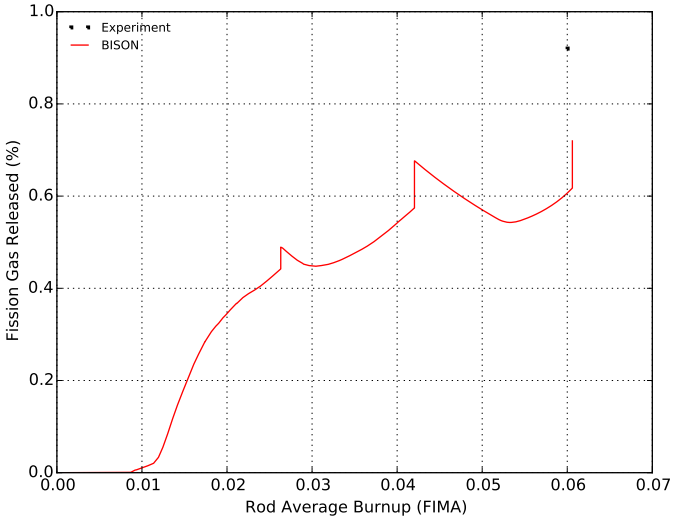

Figure A11.6: Fission gas release comparisons for Rodlet-4

A11.4.2 Rod Internal Pressure

The only rod internal pressure data available for this experiment is from PIE puncture tests at the end-of-life. Figure A11.7 and Figure A11.8 show BISONs comparisons with the experimental data for Rodlet-2 and Rodlet-4, respectively. Both figures show BISON over predicts the rod internal pressure at the end of life.

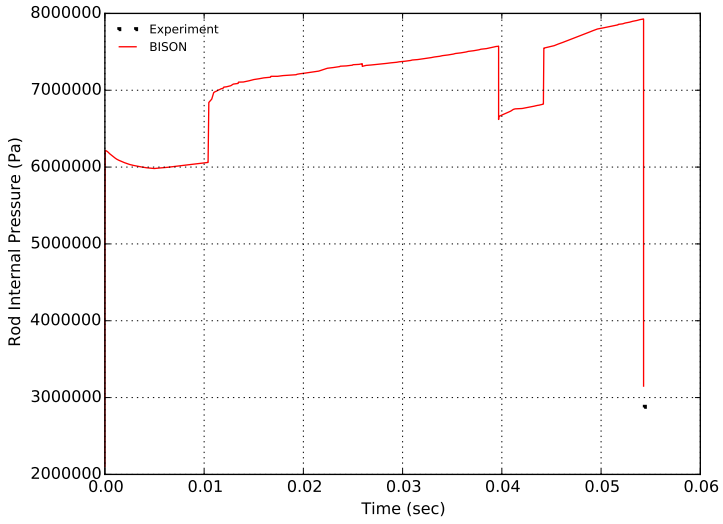

Figure A11.7: Rod internal pressure comparisons for Rodlet-2

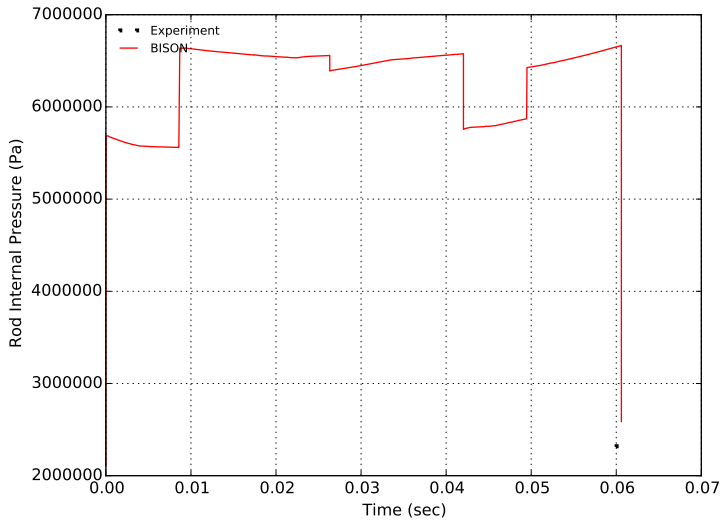

Figure A11.8: Rod internal pressure comparisons for Rodlet-4

A11.4.3 Cladding Diametral Creep

The calculated final rod diameter as a function of axial position is compared to measured data. Figure A11.9 and Figure A11.10 show BISONs comparisons with the measured end-of-life rod average diameter data for Rodlet-2 and Rodlet-4, respectively. Both figures show BISON under predicts the cladding creep down which results in larger rod computed diameters than measured.

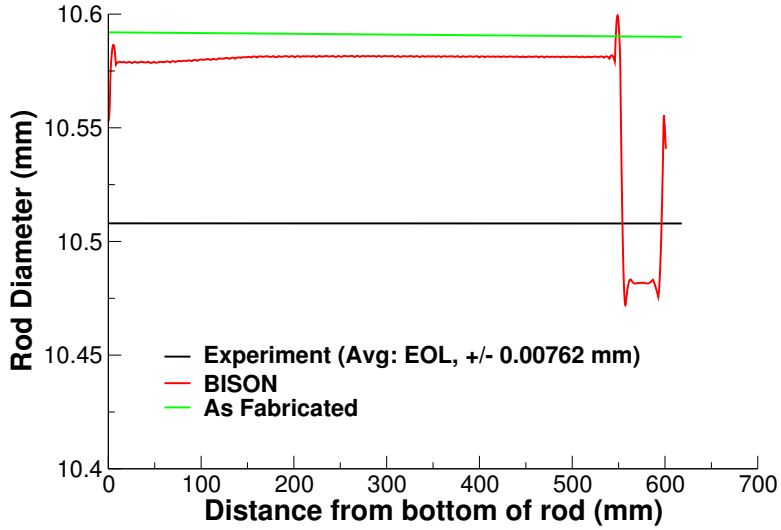

Figure A11.9: Rod diameter comparisons for Rodlet-2

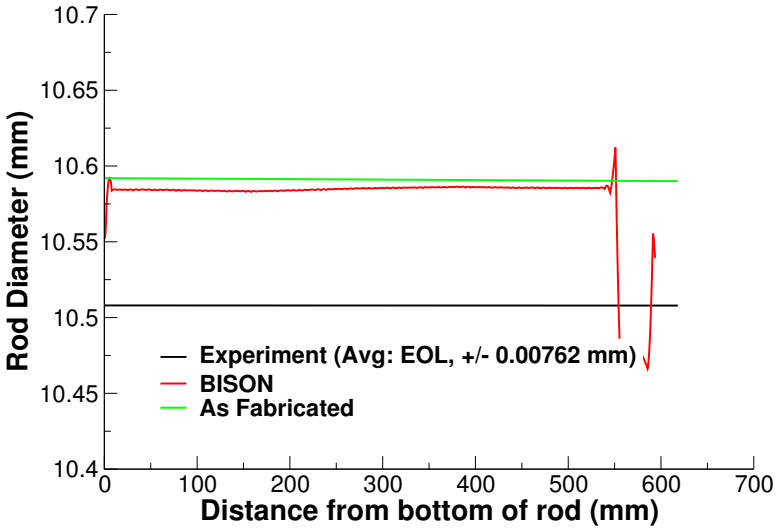

Figure A11.10: Rod diameter comparisons for Rodlet-4

A11.4.4 Discussion

Based on the data presented above, several observations can be made regarding the results obtained from BISON analyses of Rodlets 2 and 4.

- BISON predicts the EOL FGR reasonably well for both cases.
  - From Figures A11.5 and A11.6, sharp increases in FGR can be seen that correspond to large power drops. This rapid release of fission gas during power drop appears to be characteristic of the SIFGRs model implemented in BISON. This response may not be representative of FGR kinetics and warrants further review.
- BISON over predicts the measured rod internal pressure for both cases by a fairly large margin.
- BISON over predicts measured EOL cladding diameter except in the plenum region.
  - Based on evaluation of these and other assessment cases, this behavior appears to be related to fuel swelling after fuel/cladding contact. Additionally, other effects on fuel deformation including relocation, densification, fuel creep, etc. could influence the behavioral response in these analyses.

Since cladding oxide thickness and hydrogen concentration data are available for Rodlet-2 and Rodlet-4, these characteristics should be evaluated in the future once these features are available in BISON.

A12 Risø-3 AN2

A12.1 Overview

The Risø AN2 experiment conducted at the Risø DR3 water-cooled HP1 rig utilized a non re-fabricated rod from the Biblis A pressurized water reactor (PWR) [21],[53]. The rod, CB6, was irradiated over four reactor cycles up to about 41 GWd/t and inserted into the DR3 reactor without any modifications made. The rod diameter at the end of the base and experimental irradiation periods and the final fission gas release can be used for comparison.

A12.2 Test Description

A12.2.1 Rod Design Specifications

Fuel pin CB6 was the upper-middle segment of four, ~675 mm-long barrier clad segments (from top CB9, CB6, CB7, CB8) which together with a top and a bottom segment constituted a fuel rod stringer. CB6 was bump tested in the unopened condition. The CB6 rod geometry is tabulated in Table A12.1.

Table A12.1: Risø AN2 Test Rod Specifications

Fuel Rod		
Overall length	m	0.65354
Fuel stack height	m	0.5418
Nominal plenum height	mm	61.0
Mother Rod		
Fill gas composition		He
Fill gas pressure	MPa	2.31
Fuel		
Material		UO_2
Enrichment	%	2.95
Density	%	93.74
Outer diameter	mm	9.053
Pellet geometry		both ends
Grain diameter (3D)	μm	9.36
Pellet Dishing		
Dish diameter	cm	0.665
Dish depth	cm	0.013
Chamfer width	cm	0.046
Chamfer depth	cm	0.016
Cladding		
Material		Zr-4
Outer diameter	mm	10.811
Inner diameter	mm	9.261
Wall thickness	mm	0.775

A12.2.2 Operating Conditions and Irradiation History

The power history for the base irradiation carried out at the Biblis A PWR is shown in Figure A12.1. The experiment power history carried out at the Risø DR3 facility is shown in Figure A12.2. A prescribed axial profile for this experiment was provided in the FUMEX-II data [21]. The measured clad surface temperature as a function of time was also provided in the FUMEX-II data [21] and was used as a boundary condition for this simulation. The other reactor operation parameters are tabulated in Table A12.2.

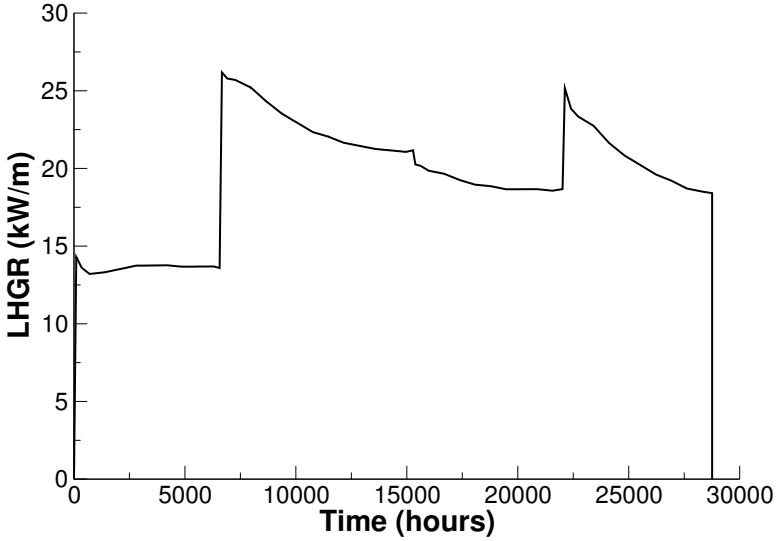

Figure A12.1: Base irradiation history for fuel segment CB6, carried out at Biblis A PWR.

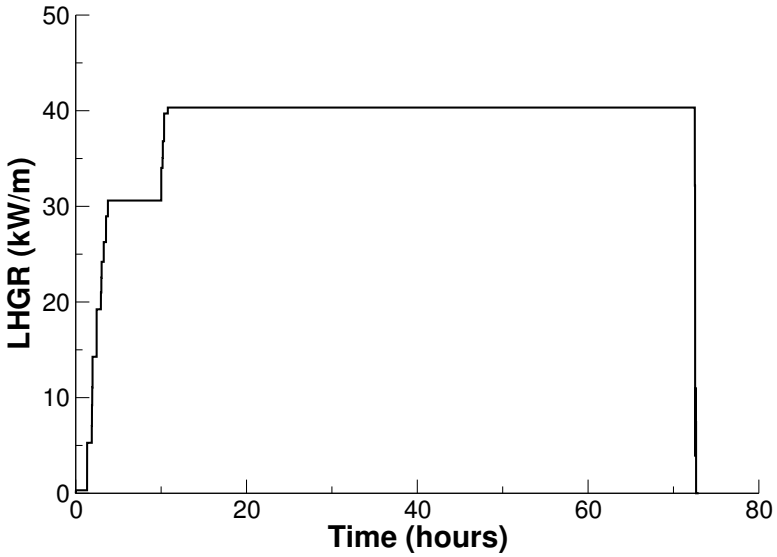

Figure A12.2: Risø DR3 irradiation period for test AN2 (CB6).

A12.3 Model Description

A12.3.1 Geometry and Mesh

The CB6 section rod geometry was modeled for the entire simulation considering a smeared column of flat ended pellets. The entire fuel stack was shifted up from the bottom of the clad by 5.1 mm, which is

Table A12.2: Operational input parameters.

Base Irradiation		
Coolant inlet temperature	C	284.7
Coolant pressure	MPa	15.52
Fast neutron flux	n/(cm^2·s) per (kW/m)	3.4·10^{12}
Power Ramps		
Coolant inlet temperature	C	NA
Coolant pressure	MPa	15.3
Fast neutron flux	n/(cm^2·s) per (kW/m)	4.0·10^{11}

the height of the insulator pellet at the bottom of the fuel rod.

A 2-dimensional axisymmetric quadratic (Quad8 elements) mesh was used to model the geometry of the rod used in the AN2 experiment. The fuel was meshed so that the total active fuel length would equal 0.54 m, leaving a total upper plenum length of 61 mm. The fuel mesh consisted of elements 2.31 mm in the axial direction and 0.4115 mm in the radial direction (for an aspect ratio of 5.613). The clad mesh consisted of elements 2.57565 mm in the axial direction and 0.19375 mm in the radial direction (for an aspect ratio of 13.29).

A12.3.2 Material and Behavioral Models

The following material and behavioral models were used for the UO_2 fuel:

- ThermalFuel - NFIR: temperature and burnup dependent thermal properties
- RelocationUO2: relocation strains, relocation activation threshold power set to 5 kW/m.
- Sifgrs: fission gas release model with coupled gaseous swelling.

For the clad material, a constant thermal conductivity of 16 W/m-K was used, and both thermal and irradiation creep were considered using the Limback creep model [36]. Thermal expansion modeling utilized the CTHEXP sub-code with its correlations for zircaloy [54].

A12.3.3 Boundary and Operating Conditions

The Risø DR3 irradiation period for the AN2 test shown in Figure A12.2 was appended to the base irradiation power history shown in Figure A12.1. It was assumed that the clad temperature during the down time between base irradiation and the Risø test was 300K. The fast neutron flux was input as a function of power and scaled to 4.9e17.

A12.3.4 Input files

The BISON input and all supporting files (power histories, axial power profile, fast neutron flux history, etc.) for this case are provided with the code distribution at bison/assessment/Riso_AN2/analysis.

A12.4 Results Comparison

The Risø AN2 experiment is used to assess the code's capability to capture the total radial displacement of the cladding surface as well as the final amount of fission gas that is released. Cladding surface displacement measurements were given with the AN2 data packet taken at ten different locations along the cladding which are used for comparison. A final fission gas release point was also taken after all testing by puncturing the rod to obtain all gasses.

A12.4.1 Cladding Displacement

BISON predicts the final cladding surface displacement with sufficient accuracy, as seen in Figure A12.3 where the sudden diameter decrease denotes the pellet-stack's edge. The cladding displacement was measured at 10 equidistant node lengths at both the pellet end and mid sections.

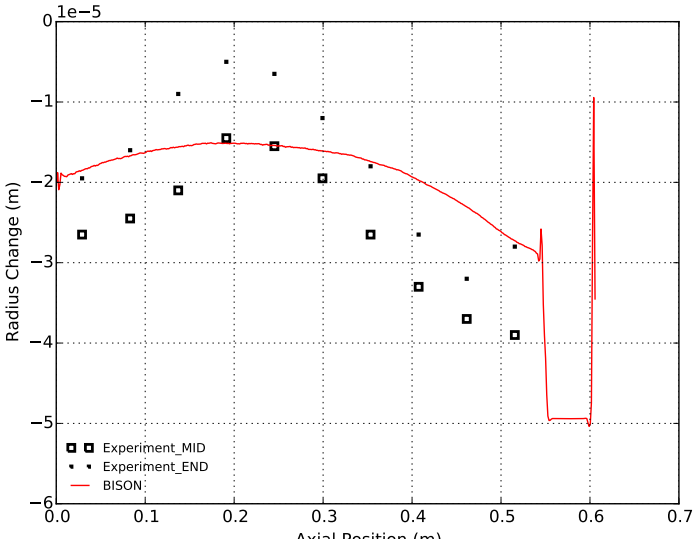

Figure A12.3: BISON fuel cladding displacement comparison to Risø experimental data.

A12.4.2 Fission Gas Release

The calculated integral fuel rod fission gas release is compared to the measured data point, in Figure A12.4. In view of the uncertainties involved in FGR modeling, the predictive accuracy is satisfactory.

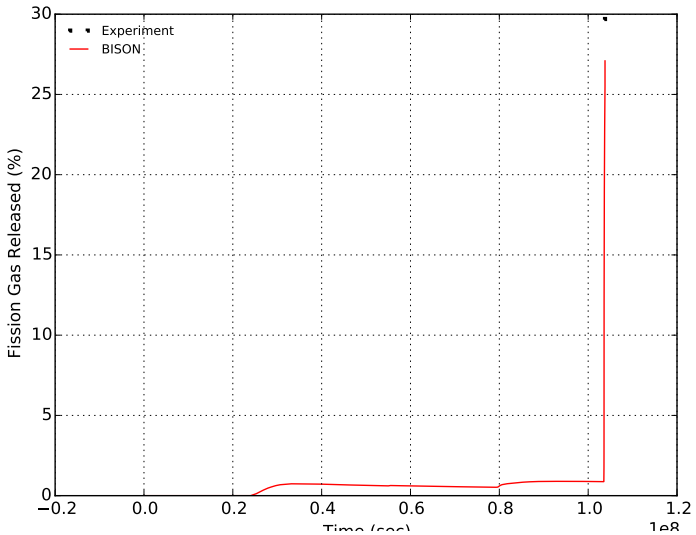

Figure A12.4: BISON total fission gas release comparison to Risø experimental data.

A13 Risø-3 AN3

A13.1 Overview

The Risø AN3 experiment conducted at the Risø DR3 water-cooled HP1 rig utilized a re-fabricated rod from the Biblis A pressurized water reactor (PWR) [21],[55]. The mother rod, CB8, was irradiated over four reactor cycles up to about 41 GWd/t, and re-fabricated to a shorter length. The re-fabricated rod, CB8-2R, was instrumented with a fuel centerline thermocouple and a pressure transducer. The fuel centerline temperature, fission gas release and rod internal pressure can be used for comparison.

A13.2 Test Description

A13.2.1 Rod Design Specifications

Rod CB8-2R was a re-fabricated rod extracted from a full length rod. The hole for the thermocouple was at the top of the fuel rod and did not penetrate the entire fuel stack. The re-fabricated rod geometry is tabulated in Table A13.1.

Table A13.1: Risø AN3 Test Rod Specifications

Fuel Rod		
Overall length	m	0.39058
Fuel stack height	m	0.286
Nominal plenum height	mm	61.0
Mother Rod		
Fill gas composition		He
Fill gas pressure	MPa	2.31
Re-Fabricated Rod		
Fill gas composition		He
Fill gas pressure	MPa	1.57
Fuel		
Material		UO_2
Enrichment	%	2.95
Density	%	93.74
Inner diameter	mm	2.5
Outer diameter	mm	9.053
Pellet geometry		both ends
Grain diameter	μm	6.0
Pellet Dishing		
Dish diameter	cm	0.665
Dish depth	cm	0.013
Chamfer width	cm	0.046
Chamfer depth	cm	0.016
Cladding		
Material		Zr-4
Outer diameter	mm	10.81
Inner diameter	mm	9.258
Wall thickness	mm	0.776

A13.2.2 Operating Conditions and Irradiation History

The power history for the base irradiation carried out at the Biblis A PWR is shown in Figure A13.1. The experiment power history carried out at the Risø DR3 facility is shown in Figure A13.2. A prescribed axial profile for this experiment was provided in the FUMEX-II data [21]. The measured clad surface temperature as a function of time was also provided in the FUMEX-II data [21] and used as a boundary condition for this simulation. The other reactor operation parameters are tabulated in Table A13.2.

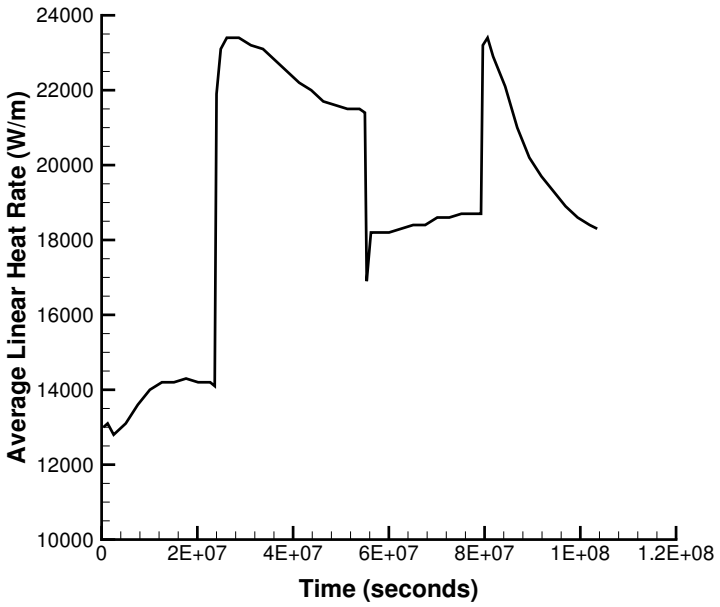

Figure A13.1: Base irradiation history for fuel segment CB8, carried out at Biblis A PWR.

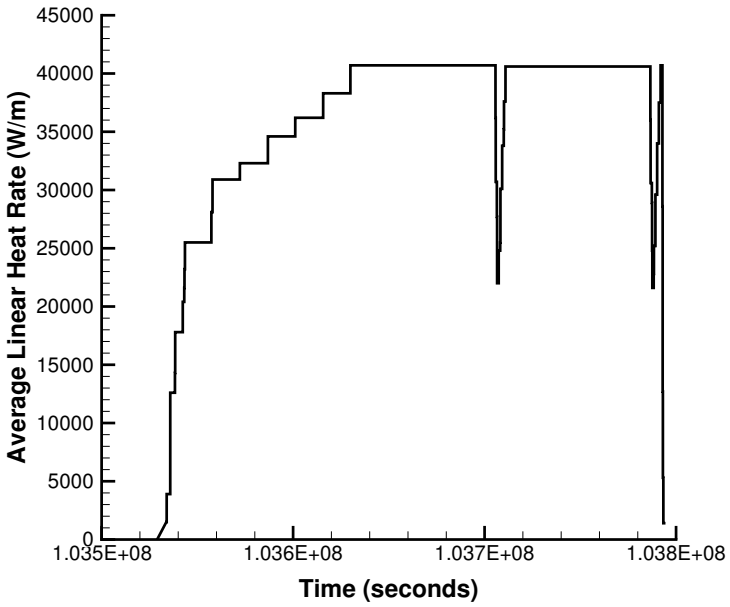

Figure A13.2: Risø DR3 irradiation period for test AN3 (CB8-2R).

Table A13.2: Operational input parameters.

Base Irradiation		
Coolant inlet temperature	C	287.7
Coolant pressure	MPa	15.52
Fast neutron flux	n/(cm^2·s) per (kW/m)	3.4·10^{12}
Power Ramps		
Coolant inlet temperature	C	NA
Coolant pressure	MPa	15.3
Fast neutron flux	n/(cm^2·s) per (kW/m)	4.0·10^{11}

A13.3 Model Description

A13.3.1 Geometry and Mesh

The re-fabricated rod geometry was modeled for the entire simulation considering a smeared column of flat ended pellets, with the top pellets containing the hole for the thermocouple. The plenum height was adjusted such that the plenum volume at the beginning of the bump test was approximately 7.0 cm^3. The entire fuel stack was shifted up from the bottom of the clad by 5.1 mm, which is the height of the insulator pellet at the bottom of the fuel rod.

A 2-dimensional axi-symmetric quadratic (Quad8 elements) mesh was used to model the geometry of the rod used in the AN3 experiment. The fuel was meshed considering two fuel pellet types. The first pellet type was 4.1 cm in length with a hole down the center, the second pellet type was 24.5 cm in length with no hole down the center. The first pellet type's mesh consisted of 29 axial nodes and 10 radial nodes (for an aspect ratio of 4.07). The second pellet type's mesh consisted of 166 axial nodes and 13 radial nodes (for an aspect ratio of 3.93). The clad mesh consisted of 131 axial nodes and 3 radial nodes. Figure A13.3 shows the top section of the mesh at the thermocouple location with a temperature contour plot.

A13.3.2 Material and Behavioral Models

The following material and behavioral models were used for the UO_2 fuel:

- ThermalFuel - NFIR: temperature and burnup dependent thermal properties
- RelocationUO2: relocation strains, relocation activation threshold power set to 5 kW/m.
- Sifgrs: fission gas release model with the combined gaseous swelling model.

For the clad material, a constant thermal conductivity of 16 W/m-K was used and both thermal and irradiation creep were considered using the Limback model [36].

A13.3.3 Boundary and Operating Conditions

The Risø DR3 irradiation period for the AN3 test shown in Figure A13.2 was appended to the base irradiation power history shown in Figure A13.1. It was assumed that the clad temperature during the down time between base irradiation and the Risø test was 500K. The fast neutron flux was input as a function of power and scaled to 4.9e17.

A13.3.4 Input files

The BISON input and all supporting files (power histories, axial power profile, fast neutron flux history, etc.) for this case are provided with the code distribution at bison/assessment/Riso_AN3/analysis.

A13.4 Results Comparison

The Risø AN3 experiment is used to assess the code's capability to capture the fuel centerline temperature and the integral fuel rod fission gas release. Fuel centerline temperature and fission gas release data from the TRANSURANUS and ENIGMA codes were digitized from the FUMEX-II report [7] for comparison with the BISON predictions.

A13.4.1 Temperature

BISON predicts the fuel centerline temperature well (see Figure A13.3) and is comparable with other well known fuel performance codes. The fuel centerline temperature is taken at a node approximately 36.4 mm from the top of the fuel stack (black dot on mesh in Figure A13.3).

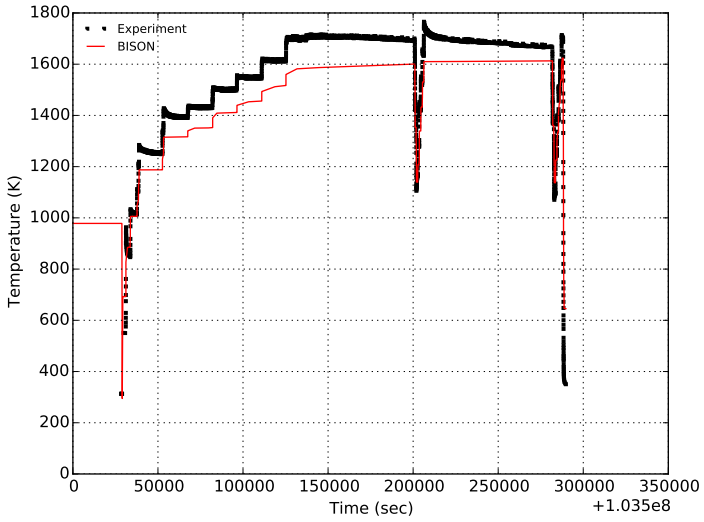

Figure A13.3: BISON fuel centerline temperature comparison to Risø experimental data.

A13.4.2 Fission Gas Release

The calculated integral fuel rod fission gas release is compared to the measured data, as well as with the TRANSURANUS and ENIGMA predictions, in Figure A13.4. In view of the uncertainties involved in FGR modeling, the predictive accuracy is satisfactory. When compared to other codes, BISON's prediction of total FGR is excellent, with many codes underpredicting the fission gas release at the end of life by more than a factor of 2 [7].

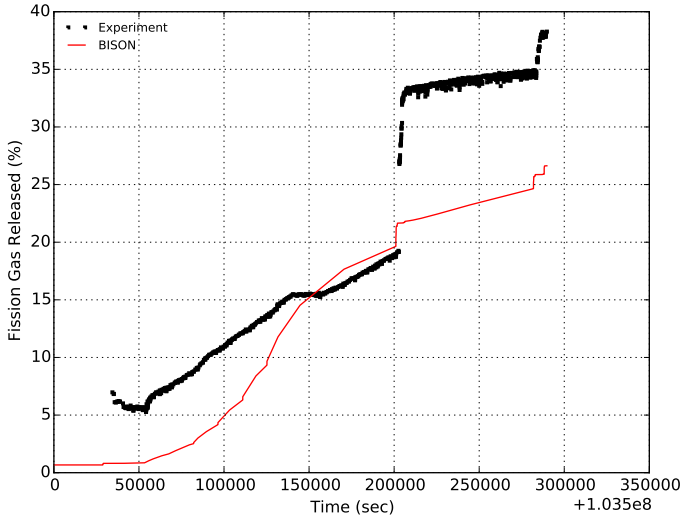

Figure A13.4: BISON total fission gas release comparison to Risø experimental data.

A13.4.3 Rod Internal Pressure

The fission gas release as a function of time during the ramp test is calculated based off the measured pressure of the rod. When compared to the measured rod internal pressure, BISON slightly over predicts the rod pressure, see Figure A13.5. This is likely due to the conditions of the rod at the refabrication time. It is reported that the fill gas is measured at room temperature, however, the temperature of the gap is higher than that of ambient temperature due to the decay heat of the already irradiated fuel.

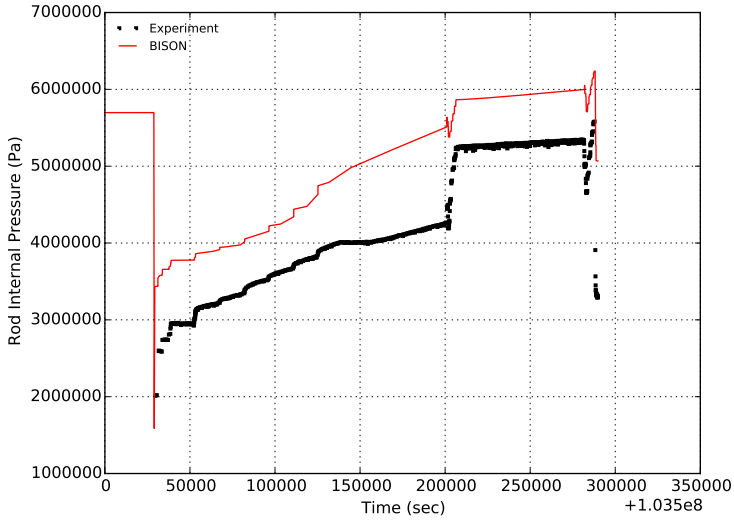

Figure A13.5: BISON rod internal pressure comparison to Risø measured data.

A14 Risø-3 AN4

A14.1 Overview

The Risø AN4 experiment conducted at the Risø DR3 water-cooled HP1 rig utilized a re-fabricated rod from the Biblis A pressurized water reactor (PWR) [56], [21]. The mother rod, CB7, was irradiated over four reactor cycles then re-fabricated to a shorter length. The re-fabricated rod, CB7-2R, was fitted with a fuel centerline thermocouple and a pressure transducer. The fuel centerline temperature, fission gas release and rod internal pressure can be used for comparison.

A14.2 Test Description

A14.2.1 Rod Design Specifications

ROB CB7-2R was a re-fabricated rod extracted from a full length rod. The hole for the thermocouple was at the top of the fuel rod and did not penetrate the entire fuel stack. The re-fabricated rod geometry is tabulated in Table A14.1.

Table A14.1: Risø AN4 Test Rod Specifications

Fuel Rod		
Overall length	m	0.330483
Fuel stack height	m	0.292
Nominal plenum height	mm	34.0
Mother Rod		
Fill gas composition		He
Fill gas pressure	MPa	2.31
Re-Fabricated Rod		
Fill gas composition		Xe
Fill gas pressure	MPa	0.1
Fuel		
Material		UO_2
Enrichment	%	2.97
Density	%	93.74
Inner diameter	mm	2.5
Outer diameter	mm	9.053
Pellet geometry		both ends
Grain diameter	μm	6.0
Pellet Dishing		
Dish diameter	cm	0.665
Dish depth	cm	0.013
Chamfer width	cm	0.046
Chamfer depth	cm	0.016
Cladding		
Material		Zr-4
Outer diameter	mm	10.81
Inner diameter	mm	9.258
Wall thickness	mm	0.776

A14.2.2 Operating Conditions and Irradiation History

The power history for the base irradiation carried out at the Biblis A PWR is shown in Figure A14.1. The experiment power history carried out at the Risø DR3 facility is shown in Figure A14.2. The axial profile for this experiment is shown in Figure A14.3. The measured clad surface temperature as a function of time is shown in Figure A14.4. The other reactor operation parameters are tabulated in Table A14.2.

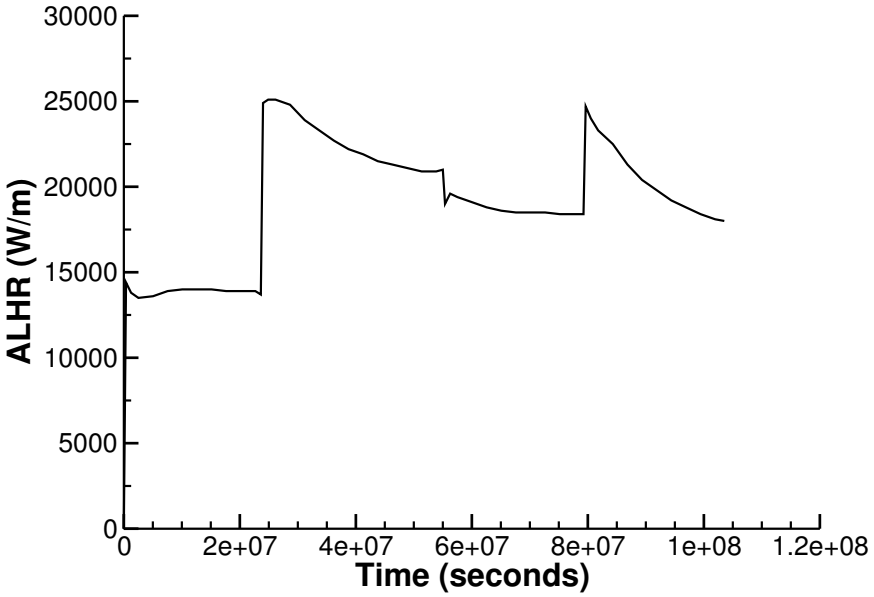

Figure A14.1: Base irradiation history for fuel segment CB7, carried out at Biblis A PWR.

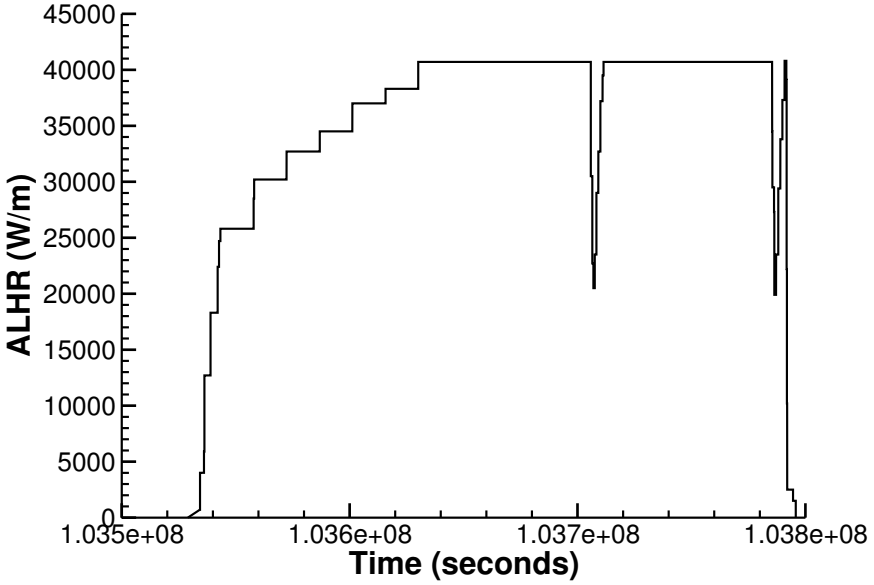

Figure A14.2: Risø DR3 irradiation period for test AN4 (CB7-2R).

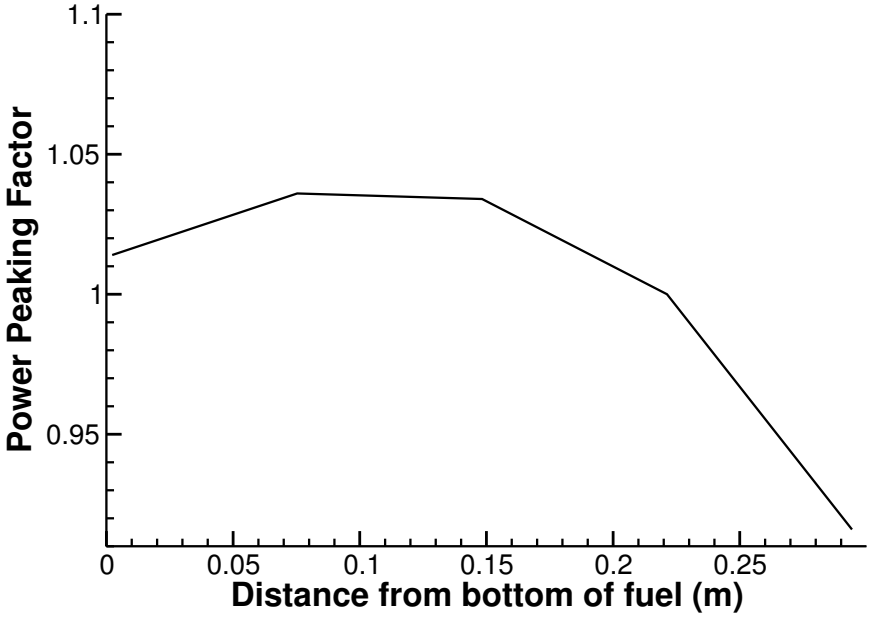

Figure A14.3: Axial power profile for Risø AN4.

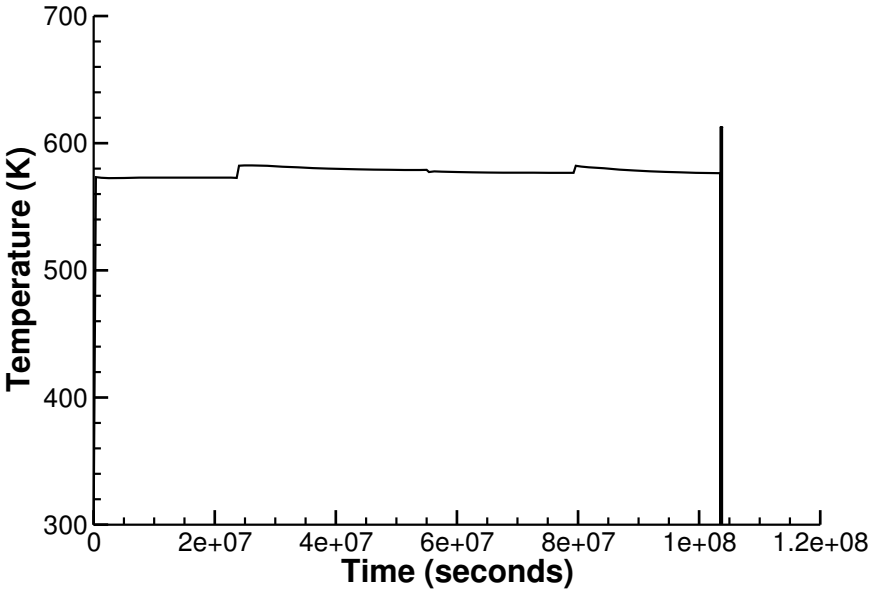

Figure A14.4: Measured clad surface temperature as a function of time.

Table A14.2: Operational input parameters.

Base Irradiation		
Coolant inlet temperature	C	287.7
Coolant pressure	MPa	15.52
Fast neutron flux	n/(cm^2$*$s) per (kW/m)	3.4$*10^{12}$
Power Ramps		
Coolant inlet temperature	C	NA
Coolant pressure	MPa	15.3
Fast neutron flux	n/(cm^2$*$s) per (kW/m)	4.0$*10^{11}$

A14.3 Model Description

A14.3.1 Geometry and Mesh

The re-fabricated rod geometry was modeled for the entire simulation as a single dished pellet. The entire fuel stack was shifted up from the bottom of the clad by 5.1 mm, which is the height of the insulator pellet at the bottom of the fuel rod.

A 2-dimensional axi-symmetric linear mesh was used to model the geometry of the rod used in the AN4 experiment. The fuel mesh consisted of 141 axial nodes and 9 radial nodes (for an aspect ratio of 5.1), the clad mesh consisted of 113 axial nodes and 5 radial nodes, see Figure A14.5.

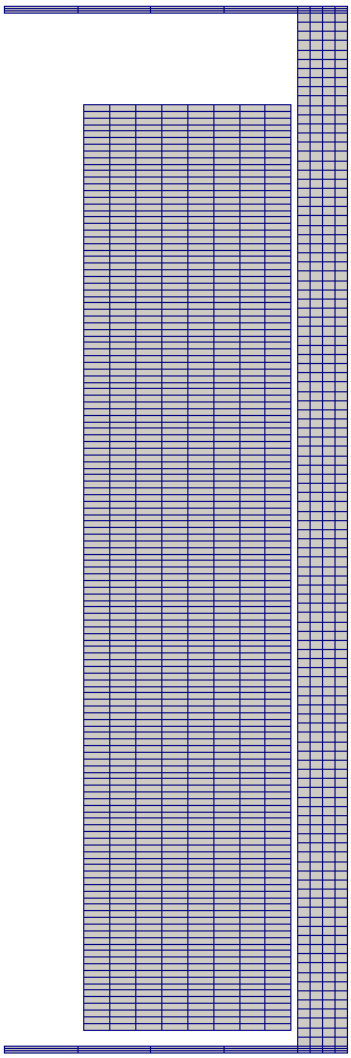

Figure A14.5: 2-D axi-symmetric mesh for Risø AN4 simulation. Note: Mesh plot is scaled axially by 0.05

A14.3.2 Material and Behavioral Models

The following material and behavioral models were used for the UO_2 fuel:

- ThermalFuel - NFIR: temperature and burnup dependent thermal properties
- RelocationUO2: relocation strains, relocation activation threshold power set to 5 kW/m.
- Sifgrs: fission gas release model with the combined gaseous swelling model.

For the clad material, a constant thermal conductivity of 16 W/m-K was used and both thermal and irradiation creep were considered using the Limback model [36].

It has been observed during late in life that the interaction layer between the fuel and clad has some contribution to the heat transfer in the gap. The effect of an interaction layer is not as obvious with helium in the gap. However, the presence of this interaction layer is magnified with xenon in the gap. The gap heat transfer model for this problem included the presence of an interaction layer between the fuel and clad. The fuel centerline temperature comparisons were extremely off when this interaction layer was not taken into consideration for this problem.

A14.3.3 Boundary and Operating Conditions

The Risø DR3 irradiation period for the AN4 test shown in Figure A14.2 was appended to the base irradiation power history shown in Figure A14.1. The power history used as an input parameter for this particular simulation is shown in Figure A14.6. The clad temperature as a function of time shown in Figure A14.4 was used as the clad boundary condition for this simulation. The fast neutron flux was input as a function of power and scaled to 4.9e17.

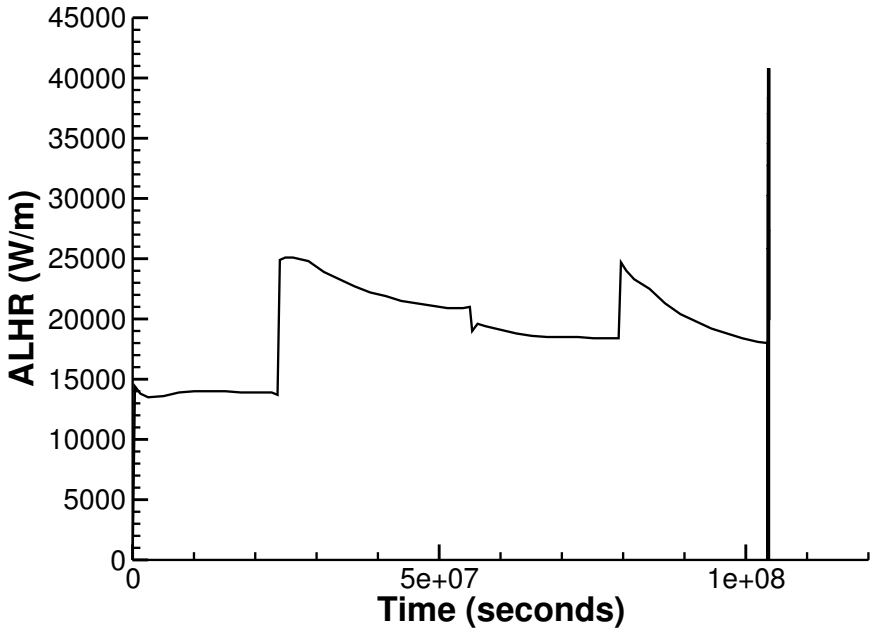

Figure A14.6: BISON input power history for Risø AN4.

A14.3.4 Input files

The BISON input and all supporting files (power histories, axial power profile, fast neutron flux history, etc.) for this case are provided with the code distribution at bison/assessment/Riso_An4/analysis.

A14.4 Results Comparison

The Risø AN4 experiment is used to assess the codes' capability to capture the fuel centerline temperature, plenum pressure and the total fission gas released. At this time BISON is not capable of capturing the total fission gas release during transient analysis, therefore, the only comparisons made were the fuel centerline temperature and plenum pressure.

A14.4.1 Temperature

The fuel centerline temperature predicted with BISON compared extremely well with the experimental data. The maximum difference between measured temperature and predicted temperature was approximately 72 degress C at the top of the ramp. (see Figure A14.7).

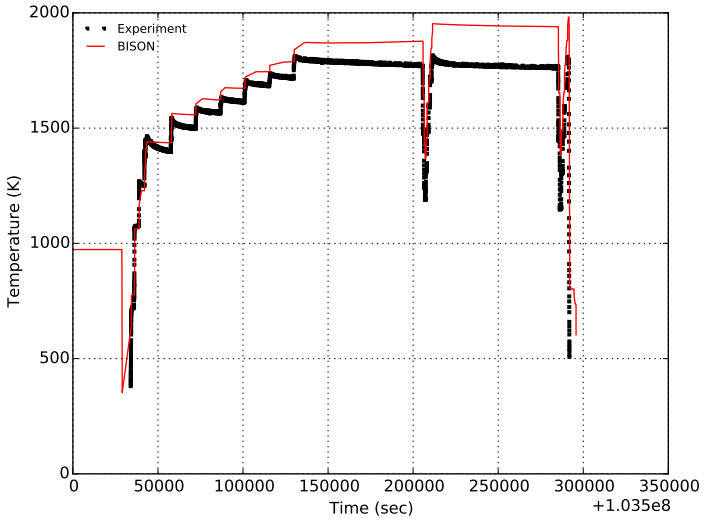

Figure A14.7: BISON fuel centerline temperature comparison to Risø experimental data.

A14.4.2 Fission Gas Release

BISON predicts the total fission gas released well with some over prediction during the first flat power section of the ramp test (see Figure A14.8).

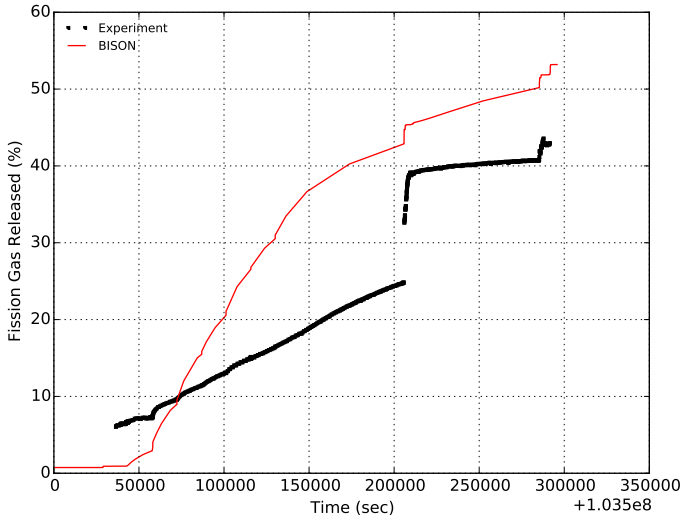

Figure A14.8: BISON total fission gas release comparison to Risø experimental data.

A14.4.3 Plenum Pressure

The calculated plenum pressure increases throughout the entire ramp test (see Figure A14.9). The pressure prediction follows the fission gas release behavior which could be the reason for the constant increase in plenum pressure during the ramp test.

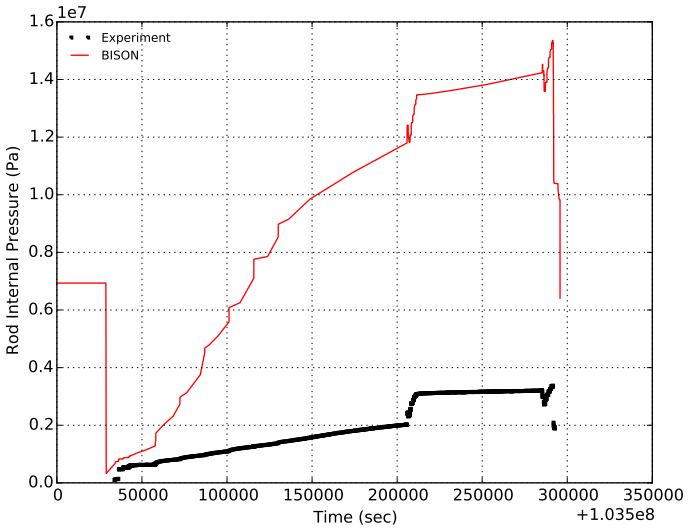

Figure A14.9: BISON plenum pressure comparison to Risø experimental data.

A15 Risø-3 AN8

A15.1 Overview

The Risø AN8 experiment was conducted at the Risø DR3 water-cooled HP1 rig and utilized an unopened rod from the Biblis A pressurized water reactor (PWR). The original fuel rod, named CB10, was irradiated over four reactor cycles up to about 44 GWd t^{-1}, then underwent ramp testing in unopened conditions, hence didn't experience any re-fabrication process.

A15.2 Test Description

A15.2.1 Rod Design Specifications

The CB10 rod geometry is tabulated in Table A15.1, in which details regarding fuel characteristics are also reported.

Table A15.1: Risø AN8 Test Rod Specifications

Fuel Rod		
Overall length	m	0.5418
Fuel stack height	m	0.514
Nominal plenum height	mm	61.0
Fill gas composition		He
Fill gas pressure	MPa	2.31
Fuel		
Material		UO_2
Enrichment	%	2.95
Density	%	93.74
Outer diameter	mm	9.053
Grain diameter	μm	6.0
Cladding		
Material		Zr-4
Outer diameter	mm	10.81
Inner diameter	mm	9.261
Wall thickness	mm	0.772

A15.2.2 Operating Conditions and Irradiation History

The power history for the base irradiation carried out at the Biblis A PWR is shown in Figure A15.1. The experiment power history carried out at the Risø DR3 facility is shown in Figure A15.2.The rod axial power profile, clad surface temperature, coolant pressure and fast flux during experiments have been prescribed coherently with the data available in the International Fuel Performance Experiments database [57] and in the Bump Test AN8 final report [58]. Details on reactor operation parameters are tabulated in Table A15.2.

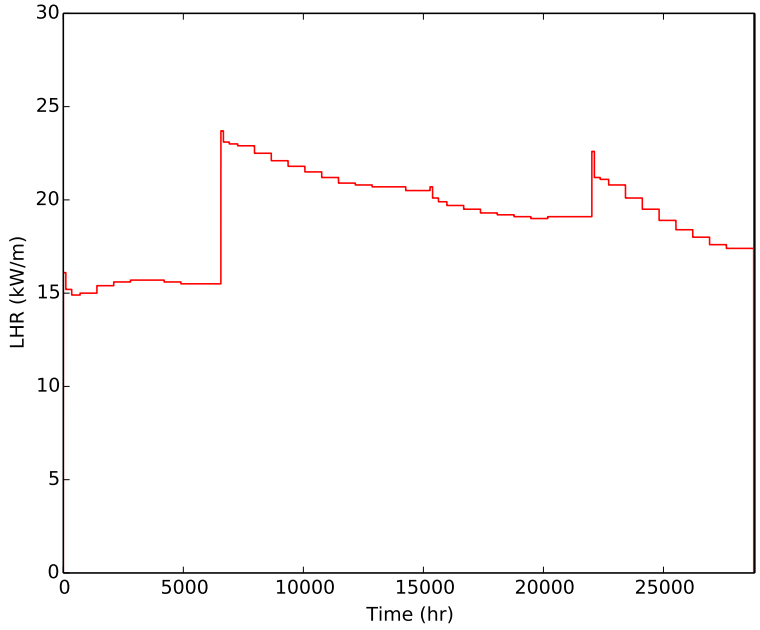

Figure A15.1: Base irradiation history for fuel segment CB10, carried out at Biblis A PWR.

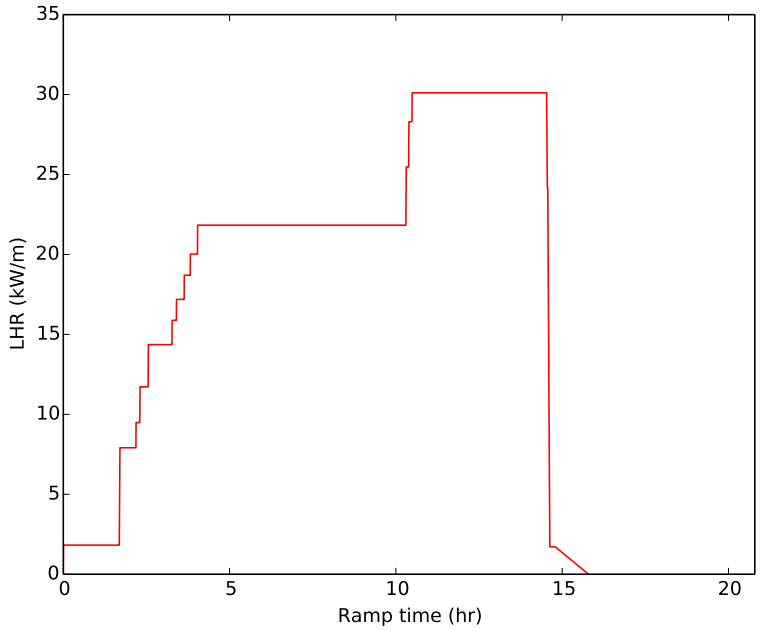

Figure A15.2: Risø DR3 irradiation period for test AN8 (CB10).

Table A15.2: Operational input parameters.

Base Irradiation		
Coolant inlet temperature	°C	284.7
Coolant pressure	MPa	15.52
Fast neutron flux	n cm^{-2} s^{-1} per (kW m^{-1})	$3.4{\cdot}10^{12}$
Power Ramps		
Coolant pressure	MPa	15.3
Fast neutron flux	n cm^{-2} s^{-1} per (kW m^{-1})	$4.0{\cdot}10^{11}$

A15.3 Model Description

A15.3.1 Geometry and Mesh

The fuel rod geometry was modeled for the entire simulation considering a smeared column of flat ended pellets.

A 2-dimensional axi-symmetric quadratic (Quad8 elements) mesh was used to model the geometry of the rod used in the AN8 experiment. The mesh scprit files employed to generate the mesh of the considered rod is included in the rod analysis subfolder.

A15.3.2 Material and Behavioral Models

The following material and behavioral models were used for the UO_2 fuel:

- ThermalFuel - NFIR: temperature and burnup dependent thermal properties.
- RelocationUO2: relocation strains, relocation activation threshold power set to 5 kW m^{-1}.
- Sifgrs: fission gas release model with coupled gaseous swelling. The transient capability is considered, and the effective diffusion coefficient is calculated according to Turnbull et al. [59].

For the clad material, a constant thermal conductivity of 16 W $m^{-1}K^{-1}$ was used, and both thermal and irradiation creep were considered. Thermal expansion modeling utilized the CTHEXP sub-code with its correlations for zircaloy [54].

A15.3.3 Boundary and Operating Conditions

The power history considered comprehends the base irradiation, shown in Figure A15.1, and the subsequent ramp test, reported in Figure A15.2. The temperature boundary conditions as a function of time was prescribed according to the files available in the IFPE databae [57].

A15.3.4 Input files

The BISON input and all supporting files (power histories, axial power profile, fast neutron flux history, etc.) for this case are provided with the code distribution at bison/assessment/Riso_AN8/analysis.

A15.4 Results Comparison

The Risø AN8 experiment is used to assess the code's capability to predict integral fission gas release (FGR) at EOL, as well as to predict cladding deformation after the ramp test.

A15.4.1 Fission Gas Release

The calculated integral fuel rod FGR is compared to the final, measured data in Figure A15.3. BISON results show a good agreement with the experimental data, in line with the intrinsic modelling uncertainties [20].

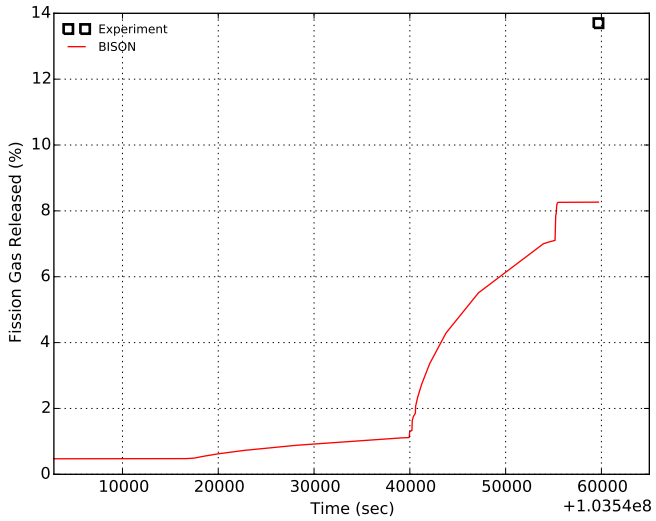

Figure A15.3: BISON total fission gas release comparison to Risø experimental data.

A15.4.2 EOL Cladding Diameter

The BISON results of cladding outer diameter at the end of irradiation as a function of axial position are presented in Figure A15.4 and compared to the experimental measurements. The figure shows an acceptable agreement between simulated and measured cladding diameter at EOL. The deviation of BISON calculations appear to be in line with state-of-the-art fuel performance codes accuracy [45]. The systematic over-estimation of the cladding diameter may be reduced if fuel creep is considered in the simulations. This issue will be further investigated in future work.

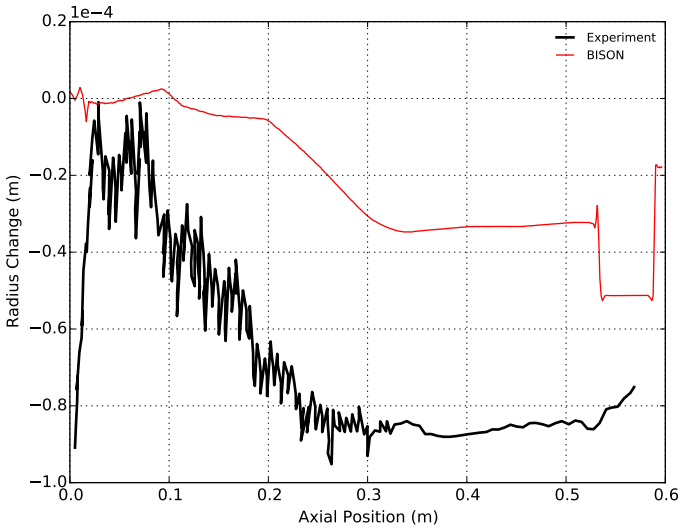

Figure A15.4: BISON cladding diameter results compared to measured data.

A16 HBEP Rod BK363, Rod BK365, and Rod BK370

A16.1 Overview

The purpose of the High Burnup Effects Programme (HBEP) task 3 rods BK363, BK365 and BK370 was to provide high burnup data on fission gas release (FGR) and fission product distributiions [21]. Rods BK363,BK365 and BK370 were irratiated to 66.7 MWd/KgU, 69.4 MWd/KgU and 50.9 MWd/KgU, respectivly, in the BR-3 pressurized water reactor (PWR) [21]. Only end of life FGR predictions were requested from the modellers.

A16.2 Test Description

The three rods in this series were manufactured by CEA and are identical. The fuel stack consisted of annular pellets and was one meter long. The only difference in experiment build was the initial plenum fill gas pressure (See Table A16.1). This portion of the HBEP experiments was designed to study the effects of fill gas pressure on FGR. It also provided data on FGR of annualar pellets for use against the solid pellets in the HBEP series [21].

A16.2.1 Operating Conditions and Irradiation History

Rods BK363, BK365 and BK370 were irratited in the BR-3 pressurized water reactor (PWR) in Belgium [60] at a coolant pressure of 13.73 MPa and coolant inlet temperature of 255 C [21]. Rods BK363 and BK365 were irratiated four cycles to burnups of 66.7 MWd/KgU and 69.4 MWd/KgU, respectively. Rod BK370 was irratiated three cycles to a burnup of 50.9 MWd/KgU. Clad temperatures and local power histories were taken at 10 axial locations and obtained from the FUMEX II data. The plot below, Figure A16.1, shows the power histories for the BK363, BK365 and BK370 rods. The power histories are similar with BK365 seeing more power in the middle stage. BK370 had a shorter irradiation time than the other 2 rods.

Table A16.1: HBEP Test Rod Specifications

Fuel Rod		
Overall length	m	1.0895
Fuel stack height	m	1.017
Nominal plenum height	mm	72.5
Number of pellets per rod		102
Pellet Height		
BK363	mm	9.98
BK365	mm	9.98
BK370	mm	9.98
Fill gas composition		He
Fill gas pressure		
BK363	MPa	1.40
BK365	MPa	2.88
BK370	MPa	2.88
Fuel		
Material		UO_2
Enrichment		
BK363	%	7.07
BK365	%	7.07
BK370	%	7.07
Density	%	93.2
Outer diameter	mm	8.188
Inner diameter	mm	2.475
Grain diameter		
All Rods	μm	13.5
Cladding		
Material		Zr-4
Outer diameter	mm	9.515
Inner diameter	mm	8.3536

A16.3 Model Description

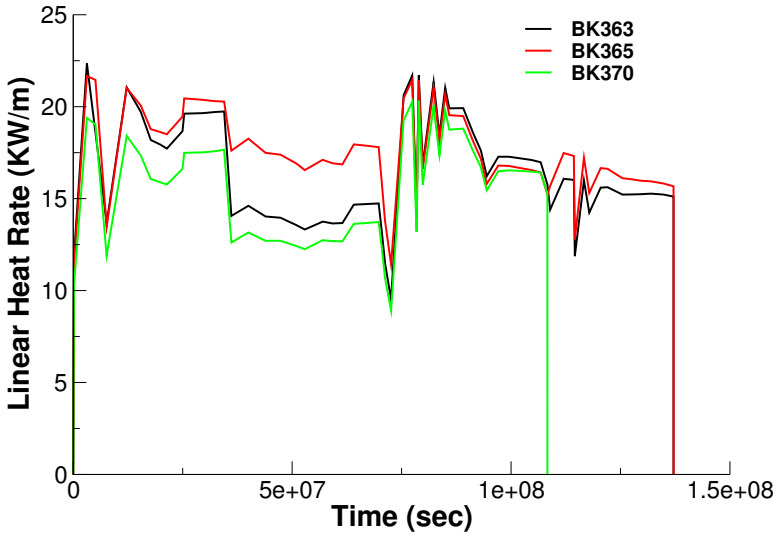

Figure A16.1: The linear heat rates for BK363, BK365 and BK370.

A16.3.1 Geometry and Mesh

All three fuel rods were meshed using 2-D axisymmetric models with quadratic elements. For simplicity, the pellet stack was modeled as a single continuous fuel column (smeared mesh). The rods were identical so the same mesh was used for all runs. The fuel pellets had 306 axial elements and 11 radial elements, and the cladding consisted of 312 axial elements and 4 radial elements.

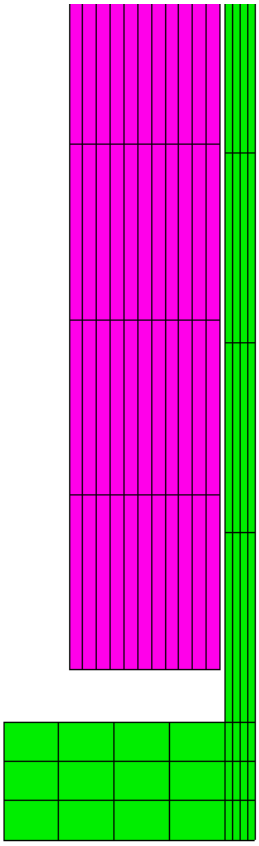

Figure A16.2: A segment of the fuel and cladding mesh used.

A16.3.2 Material and Behavioral Models

The following material and behavioral models were used for the UO_2 fuel:

- ThermalFuel - NFIR: For temperature and burnup dependent thermal properties.
- RelocationUO2: For relocation strains, the relocation activation threshold power is set to 5 kW/m.
- Sifgrs: A simplified fission gas release model (model 2) with a gaseous swelling model. The transient fission gas release model within Sifgrs was also utilized.

For the clad material, a constant thermal conductivity of 16 W/m-K was used and both thermal (primary and secondary) and irradiation creep were considered using the Limbäck creep model [36].

A16.3.3 Input files

The BISON input and all supporting files (power histories, axial power profile) are provided with the code distribution at bison/assessment/HBEP/analysis.

A16.4 Results Comparison

HBEP rods BK363, BK365 and BK370 were designed and built to investigate the effects of initial fill gas pressure on fission gas release. To achieve this the rods were built identically with only the fill gas

pressure being changed for BK363 and BK365. These 2 rods were then irradiated to approximately the same burnup. Rod BK370 was filled to the same pressure as BK365, but was only irradiated 3 cycles as opposed to 4 cycles. The following subsections discuss each test individually.

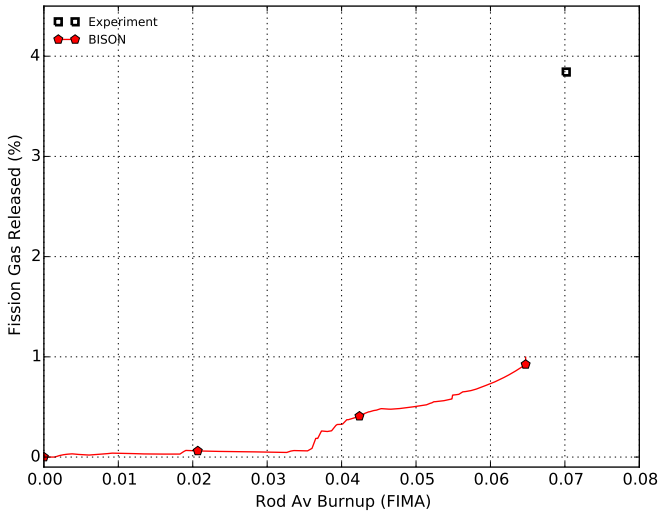

Figure A16.3: Comparison of measured fission gas release and the BISON prediction

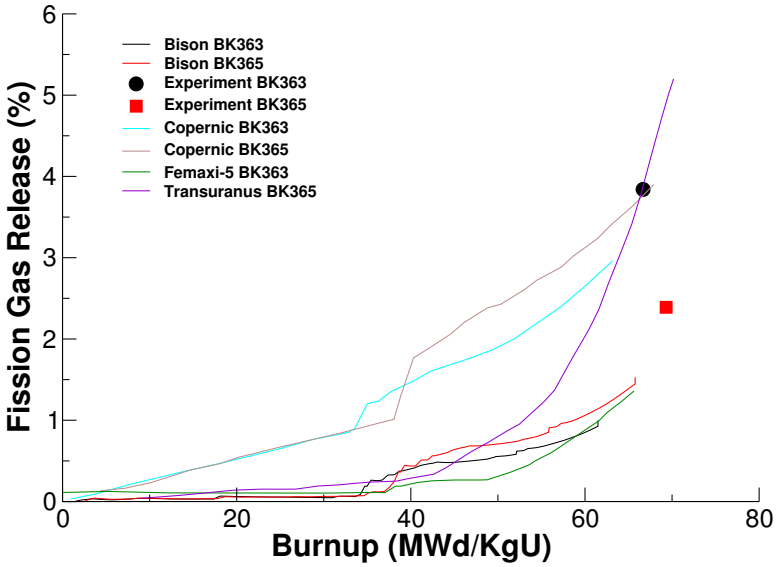

Figure A16.4: Comparison of measured fission gas release and the predictions of other codes

A16.4.1 HBEP, BK363

As can be seen above in Figures A16.3 and A16.4 the BISON calculated fission gas release is less than the experiment measured amount, about 1% and 4%, respectively. As mentioned above the Sifgrs fission gas release model with the transient release model was used in this case. This rod was held at a lower power at the phase that included 5e7 sec (see Figure A16.1). It is possible that the model did not produce enough fission gas during this phase and thus was not released in the transient phase. Evidence for this theory may be supported by BK365's performance.

A16.4.2 HBEP, BK365

As mentioned in the previous subsection, the BISON performance of the BK365 rod against the experiment was better than the BK363 rod. Shown in Figures A16.5, A16.3 and A16.4 the experiment measured amount was about 2.5% and the BISON calculation was about 1.5%. Figure A16.5 shows a comparison of the linear heat rate to the calculated fission gas release over the time of the experiment.

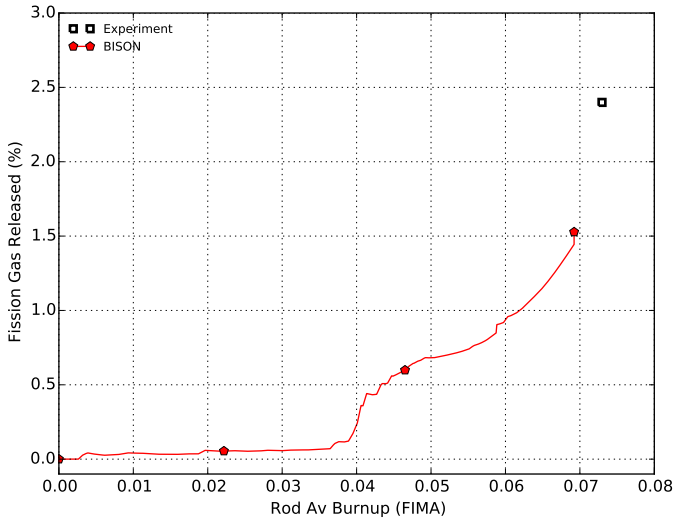

Figure A16.5: Comparison of Linear Heat Rate and Fission Gas Release for BK365

A16.4.3 HBEP, BK370

There was no experimental data collected from this rod. Other codes did simulate this rod, as did BISON, but since there are no experimental results there will be no discussion about this rod.

A16.5 Discussion

Modeling these three rods was useful to the BISON development as it shows that there is possible work needed in the high burnup structure. In comparing with other codes BISON is on the lower end of the estimates. It needs to be pointed out that for BK363 the difference between the measured and the calculated was about 3% and for BK365 it was about 1%. The amount of fission gas released overall was not much and BISON is within acceptable estimation tolerances.

A17 AREVA Idealized Case

A17.1 Overview

The AREVA Idealized Case is an optimal case designed to simulate idealized commercial power plant operation. This case was based on measurements for three rods operatedf or 3, 4, and 7 cycles in a commercial French pressurized water reactor (PWR). The three rods chosen experienced similar power histories, allowing for three fission gas release measurements for a single power history. The maximum fuel rod burnup is approximately 81.5 MWd/kgU with a total fission gas release of approximately 9% [45].

A17.2 Test Description

A17.2.1 Rod Design Specifications

The rod simulated for this particular case was based on an idealized commercial reactor fuel rod. Details of the rod geometry and specifications are summarized in Table A17.1.

Table A17.1: AREVA Idealized Case Test Rod Specifications

Fuel Rod		
Fuel stack length	m	3.65
Nominal plenum volume	cm^3	8.04
Number of pellets per rod		275
Fill gas composition		He
Fill gas pressure	MPa	1.6
Fuel		
Material		UO_2
Enrichment	%	4.5
Density	%	95
Outer diameter	mm	8.085
Pellet geometry		dished
Grain diameter	μm	15.6
Pellet Dishing (if applicable)		
Dish diameter	mm	6.0
Dish depth	mm	0.31
Chamfer width	mm	0.5425
Chamfer depth	mm	0.27
Cladding		
Material		Zr-4 (stress-relieved)
Outer diameter	mm	9.5
Inner diameter	mm	8.25
Wall thickness	mm	0.625

A17.2.2 Operating Conditions and Irradiation History

The operating conditions for this simulation were based on power cycles in a commercial French PWR. The operating conditions used are shown in Table A17.2.

Table A17.2: Operational input parameters.

Coolant inlet temperature	C	282
Coolant pressure	MPa	15.5
Coolant mass flow rate	kg/m^2-sec	3700

A17.3 Model Description

A17.3.1 Geometry and Mesh

The fuel rod geometry specified in Table A17.1 was used as a basis for the mesh used in this simulation. The fuel pellets were meshed as a single smeared fuel column. The mesh consists of 1375 axial elements and 12 radial elements in the fuel, and 1375 axial elements and 4 radial elements in the clad, see Figure A17.1. This simulation was meshed as a 2D-RZ axisymmetric geometry with quadratic elements.

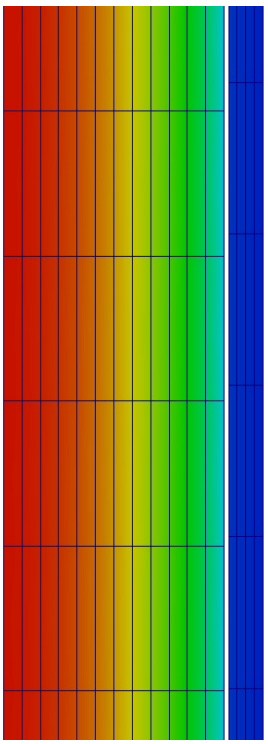

Figure A17.1: Section of BISON mesh with temperature contour.

A17.3.2 Material and Behavioral Models

The following material and behavioral models were used for the UO_2 fuel:

- ThermalFuel - NFIR: temperature and burnup dependent thermal properties
- RelocationUO2: relocation strains, relocation activation threshold power set to 5 kW/m.
- Sifgrs: coupled fission gas release and swelling model

For the clad material, a constant thermal conductivity of 16 W/m-K was used and both thermal and irradiation creep were considered using the Limback model [36].

A17.3.3 Boundary and Operating Conditions

The power history used for this simulation is shown in Figure A17.2, with axial peaking factors shown in Figure A17.3. The average fast neutron flux was input as a function as well and is shown in Figure A17.4 with axial peaking factors shown in Figure A17.5. The clad temperature was calculated using the coolant channel model.

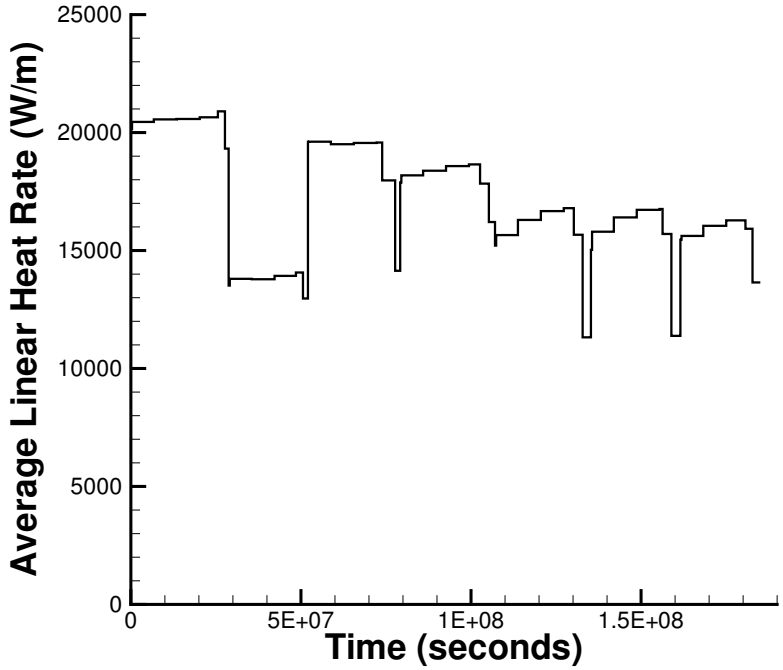

Figure A17.2: BISON input power history for the AREVA Idealized Case.

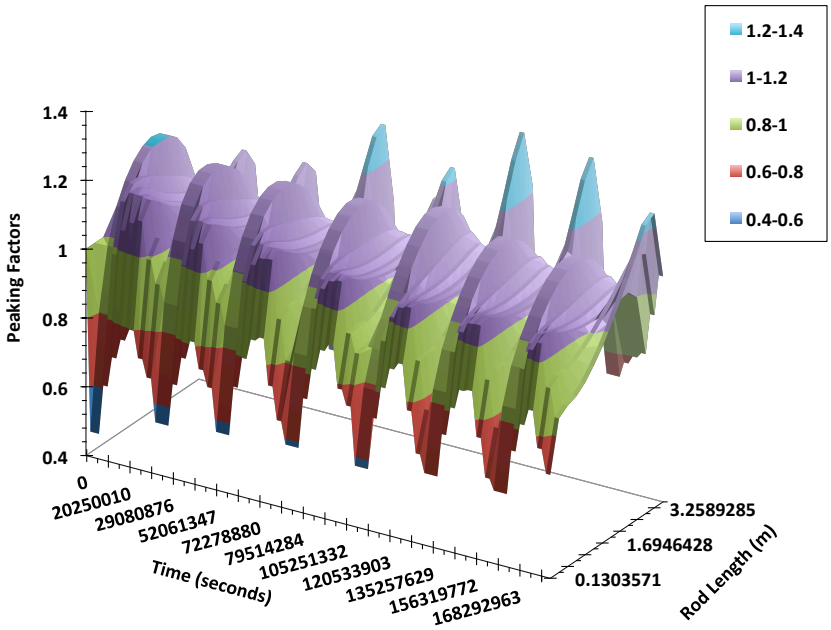

Figure A17.3: BISON input power axial peaking factors for the AREVA Idealized Case.

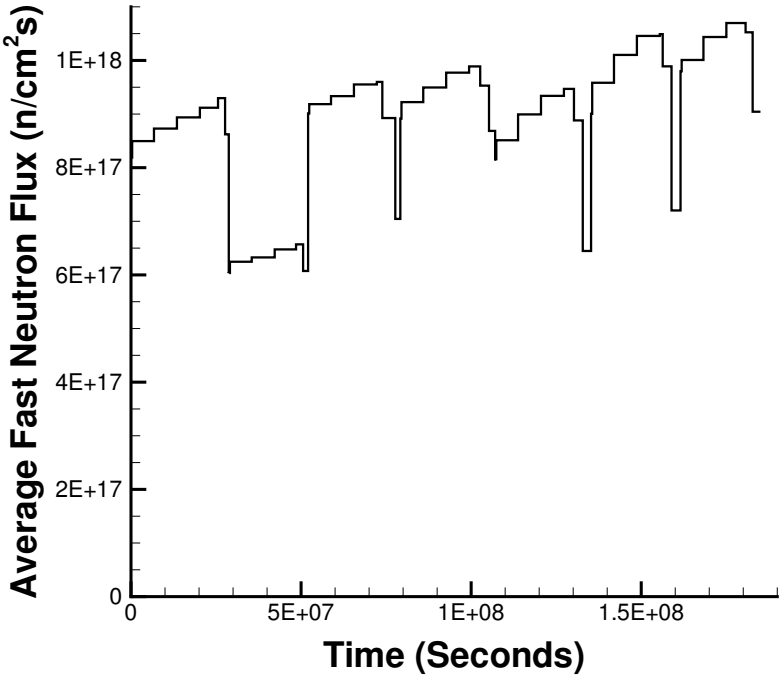

Figure A17.4: BISON input average fast neutron flux for the AREVA Idealized Case.

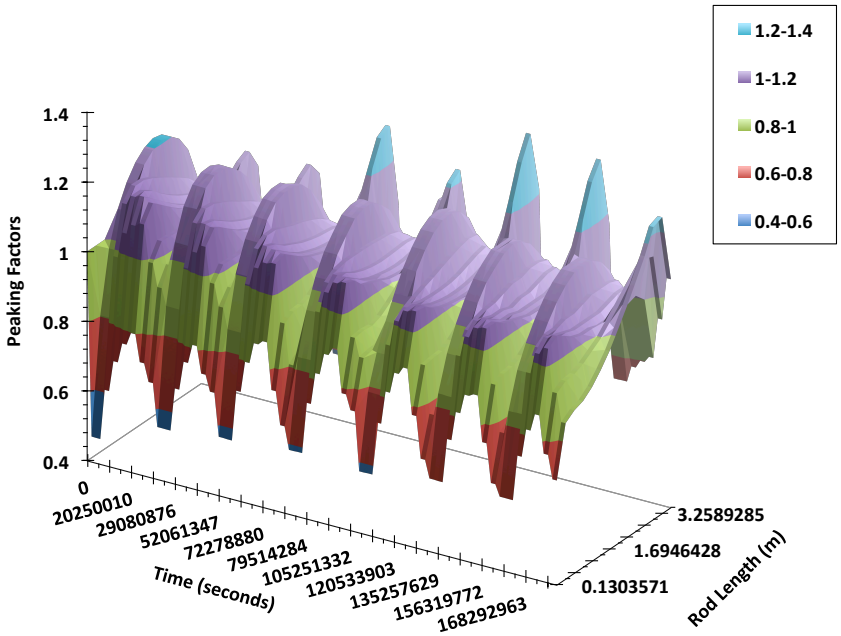

Figure A17.5: BISON input fast neutron flux axial peaking factors for the AREVA Idealized Case.

A17.3.4 Input files

The BISON input and all supporting files (power histories, axial power profile, fast neutron flux history, etc.) for this case are provided with the code distribution at bison/assessment/AREVA_idealized_case/analysis.

A17.4 Results Comparison

A17.4.1 Fission Gas Release

The expected fission gas release values are shown in Table A17.3 [45].

Table A17.3: Expected FGR values.

End of cycle	Insertion time (d)	Burnup (MWd/kg(HM))	Expected FGR value (%)
3	916.4	36.6	0.5+0.5/-0.2
4	1239.1	49.7	1.9+1.0/-0.7
7	2141.9	81.5	9.0+2.5/-2.0

BISON predicts the total fission gas release reasonably well during the early and mid-burnup regimes, however FGR is under predicted at high burnup. BISON also compares well with other well known fuel performance codes, see Figure A17.6.

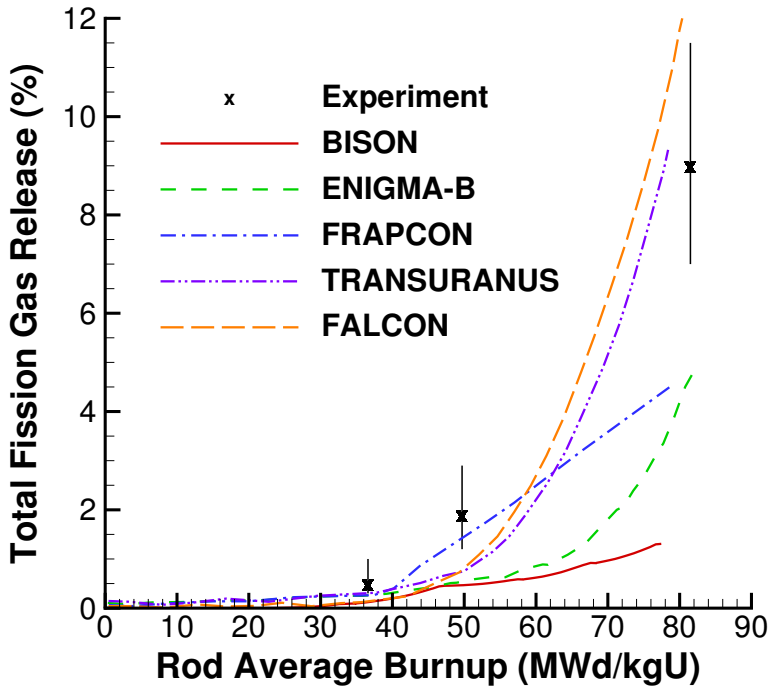

Figure A17.6: BISON predicted fission gas release in comparison to measured data and multiple fuel performance codes (code data digitized from FUMEX-III report [45]).

A17.5 Discussion

Fuel creep was not modeled at this time. Fuel creep will be considered upon availablitly of some type of fuel cracking model.

A18 FUMEX-II Simplified Cases

A18.1 Overview

Over the last few decades, the International Atomic Energy Agency (IAEA) has supported several programs related to nuclear power reactor fuel behavior and fuel behavior modeling. These efforts have collected fuel behavior experimental data, fuel irradiation experiment and hardware descriptions, and fuel modeling code results to develop a useful database of information for code assessment and to determine the maturity of currently existing fuel performance codes. One such program was the Fuel Modeling at Extended Burnup (FUMEXII [21]) program. This program, conducted from 1999-2007, outlined relevant collections of analytical exercises and appropriate experiments and encouraged participants to submit calculation results for a wide variety of fuel performance experiments in a format that readily allowed comparisons between specific codes and to experiment data when available. Given the success of this approach and ready access to the results, we chose to use some test cases from the FUMEXII program for initial assessment of certain BISON code elements. In particular, FUMEXII participants devoted significant effort to fission gas release (FGR) and an impressive compilation of experiment data and code results is given in Ref. [21].

FGR is of particular interest for the present BISON assessment since calculation of fuel centerline temperature and radial and axial temperature distribution depends heavily on fission gas generation in the pellets, migration of the gas to grain boundaries, and eventual release to the fuel pin gap and plenum. FUMEXII Case No. 27, so-called 'Simplified cases', provide an ideal basis for examining the BISON FGR model(s) performance and comparison of BISON results with results from other fuel performance codes that participated in the FUMEXII exercises. The first of the simplified cases, 27(1) focused on the Vitanza criterion [32], which is the comparison of fuel centerline temperature versus burnup at onset of FGR (e.g. 1% release). The second case was to assess the codes' ability to predict total FGR as a function of burnup up to 100 MWd/kgU. Four separate simulations were used for this case:

- 27(2a) a constant power of 15 kW/m from BOL to 100 MWd/kgU,
- 27(2b) a linearly decreasing power from 20 kW/m at BOL to 10 kW/m at 100 MWd/kgU,
- 27(2c) more realistic power history supplied by G Rossiter of BNFL,
- 27(2d) idealized 'real' history supplied by F Sontheimer of FANP.

A18.2 Test Description

A18.2.1 Rod Design Specifications

For Case 27(1), 27(2a), and 27(2b), a standard fuel description representative of a boiling water reactor (BWR) fuel rod typically irradiated in the Halden reactor was specified. The rod plenum was specified as being large as to avoid thermal feedback, the rod plenum fill gas was helium at 0.5 MPa (5 bar). The fuel pellet was solid and flat ended (no chamfer, no dish) UO_2 with 13% ^{235}U enrichment and a grain diameter of 15 microns. Cladding consisted of standard Zr-2. In the Halden reactor, fast neutron flux is typically assumed negligible and thus irradiation induced cladding creep is negligible. Also, the axial power profile in Halden is flat. The detailed specification of the pellet, cladding, and other information relevant to the exercise is shown in Table A18.1.

Table A18.1: FUMEX-II 27(1), 27(2a), and 27(2b) Fuel Rod/Pellet Specifiactions.

Fuel Rod		
Fuel stack length	m	0.0127
Number of pellets per rod		1
Fill gas composition		He
Fill gas pressure	MPa	0.5
Fuel		
Material		UO_2
Enrichment	%	13
Density	%	95
Outer diameter	mm	10.61
Pellet geometry		Flat Ended
Grain diameter	μm	15
Cladding		
Material		Zr-2
Outer diameter	mm	12.7
Inner diameter	mm	10.8
Wall thickness	mm	0.95

Table A18.2: FUMEX-II 27(2c) Fuel Rod/Pellet Specifications.

Fuel Rod		
Fuel stack length	m	3.658
Nominal plenum length	mm	162
Number of pellets per rod		275
Fill gas composition		He
Fill gas pressure	MPa	2.5
Fuel		
Material		UO_2
Enrichment	%	8
Density	%	95
Outer diameter	mm	8.2
Pellet length	mm	9.8
Pellet geometry		dished
Grain diameter	μm	75
Pellet Dishing (no chamfers)		
Dish diameter	mm	5.24
Dish depth	mm	0.3
Cladding		
Material		Zr-4
Outer diameter	mm	9.5
Inner diameter	mm	8.36
Wall thickness	mm	0.57

For case 27(2c) and 27(2d) the fuel rod specifications were provided by BNFL (Table A18.2) and FANP (Table A18.3), respectively.

Table A18.3: FUMEX-II 27(2d) Fuel Rod/Pellet Specifications.

Fuel Rod		
Fuel stack length	m	3.5
Total free volume	cm^3	30
Number of pellets per rod		318
Fill gas composition		He
Fill gas pressure	MPa	2.2
Fuel		
Material		UO_2
Enrichment	%	4
Density	%	95.5
Outer diameter	mm	9.12
Pellet length	mm	11.0
Pellet geometry		standard UO_2
Grain diameter	μm	10
Cladding		
Material		Zr-4
Outer diameter	mm	10.75
Inner diameter	mm	9.29
Wall thickness	mm	0.73

A18.2.2 Operating Conditions and Irradiation History

To match the Vitanza Threshold (described above) multiple simulations are ran at multiple powers until 1% FGR is reached. This was done for 20, 25, 30, 35, 40, and 45 kW/m. For case 27(2a) a constant power of 15 kW/m was used up to a burnup of 100 MWd/kgU. The power for case 27(2b) linearly decreased from 20 kW/m at BOL to 10 kW/m at a burnup of 100 MWd/kgU. Typical Halden BWR (HBWR) conditions were used for the operating conditions (fast neutron flux of 1.6E11 n/cm^2-sec per kW/m, coolant temperature of 232 C, and a coolant pressure of 3.2 MPa) for cases 27(1), 27(2a), and 27(2b).

The power history used for case 27(2c) is shown in Figure A18.1(a), the power is provided as a thermal power in the fuel. The ratio of thermal heat to total heat for the rod is 0.975, thus the input power is scaled by a factor of 1.025641 as BISON requires the total fission power as input. The fast neutron flux was specified as a function and is shown in Figure A18.1(b). The coolant pressure was specified as 15.5 MPa with an average clad temperature of 325 C.

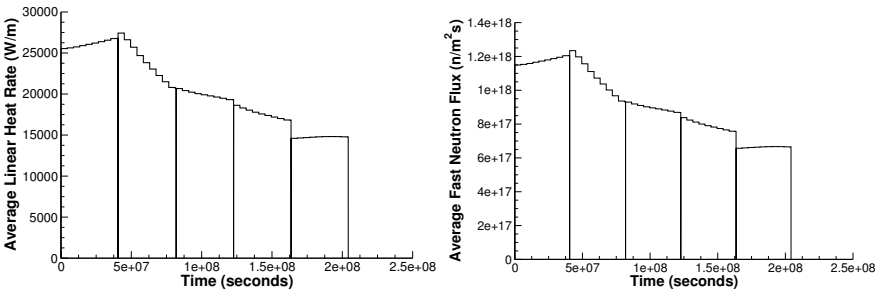

Figure A18.1: (a) Case 27(2c) average linear heat rate (b) Case 27(2c) average fast neutron flux.

The power history used for case 27(2d) is shown in Figure A18.2. The fast neutron flux had a suggested value of 4E16 n/m^2-sec per kW/m. The coolant pressure was 15.5 MPa, with a coolant temperature of 290 C and a mass flow rate of 0.4 kg/s.

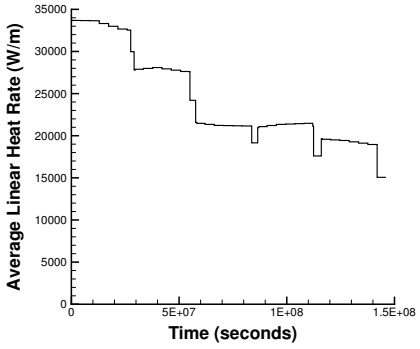

Figure A18.2: Case 27(2d) average linear heat rate.

A18.3 Model Description

A18.3.1 Geometry and Mesh

Case 27(1)

For this exercise, the main interest was interaction between the fission gas generation and release and the thermal behavior of the fuel. As such, several simplifications could be made. First, since fractional fission gas release was of prime interest, only a single fuel pellet reflecting the parameters given in Table A18.1 was modeled. Second, since fuel-cladding interaction was not of interest, the cladding was removed and only the fuel pellet was modeled. A convective boundary condition representative of Halden operating conditions was applied directly to the pellet outer radius and the top and bottom of the pellet were insulated.

Figure A18.3 shows the mesh used for BISON calculation of the Vitanza criteria. This mesh represents a 2D-RZ axi-symmetric geometry and with 12 radial and 8 axial quadratic elements.

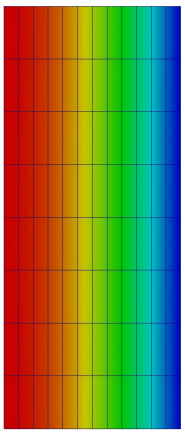

Figure A18.3: BISON single pellet mesh used for Vitanza Criteria calculation. Fuel temperature profile shown at 1% FGR for LHR of 45 kW/m.

Cases 27(2a) and 27(2b)

A similar mesh was used for cases 27(2a) and 27(2b), except the clad was modeled in these two cases. This mesh consisted of 12 radial and 8 axial quadratic elements in the fuel and 4 radial elements in the clad (see Figure A18.4).

Case 27(2c)

Fuel rod specifications in Table A18.2 were used to generate the mesh for case 27(2c). The fuel rod was meshed as a 2D-RZ axi-symmetric geometry, with 11 radial and 5 axial quadratic elements per fuel pellet. The clad thickness was meshed with 4 radial quadratic elements. A section of the fuel rod is shown in Figure A18.5.

Case 27(2d)

Fuel rod specifications in Table A18.3 were used to generate the mesh for case 27(2d). The fuel rod was meshed as a 2D-RZ axi-symmetric geometry, with 11 radial and 4 axial quadratic elements per fuel pellet. The clad thickness was meshed with 4 radial quadratic elements. A section of the fuel rod is shown in Figure A18.6.

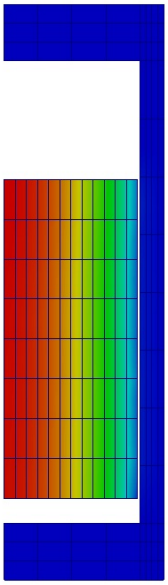

Figure A18.4: BISON mesh used for cases 27(2a) and 27(2b). Temperature contour of 27(2a) at a burnup of 100 MWd/kgU.

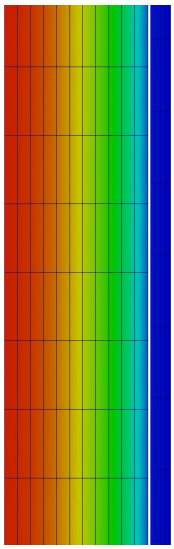

Figure A18.5: BISON mesh used for cases 27(2c). Temperature contour at a burnup of approximately 100 MWd/kgU.

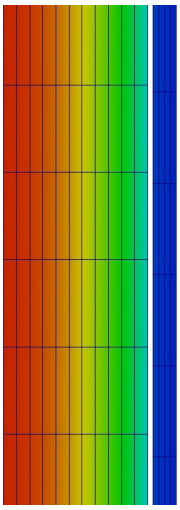

Figure A18.6: BISON mesh used for cases 27(2d). Temperature contour at a burnup of approximately 67.5 MWd/kgU.

A18.3.2 Material and Behavioral Models

The following material and behavioral models were used for the UO_2 fuel:

- ThermalFuel - NFIR: temperature and burnup dependent thermal properties
- RelocationUO2: provides burnup dependent relocation, with a relocation activation power of 5 kW/m
- Sifgrs: provides mechanistic fission gas release calculation with coupled gaseous swelling

Since the case 1 model did not include cladding, no cladding irradiation growth, cladding thermal, or cladding solid mechanics material models were included. For the case 2 series, the clad material had a constant thermal conductivity of 16 W/m-K was used and both thermal (primary and secondary) and irradiation creep were considered using the Limback model [36].

A18.3.3 Input files

The BISON input and all supporting files (power histories, axial power profile, mesh input, etc.) for this case are provided with the code distribution at bison/assessment/FUMEXII_simplified_cases/analysis.

A18.4 Results Comparison

A18.4.1 Fission Gas Release

As mentioned above, the Vitanza criteria is an empirical relationship derived from operational data at the Halden reactor. The empirical relationship has the form

$$T_{CL} = \frac{9800}{ln(\frac{Bu}{0.005})} \tag{A18.1}$$

where T_{CL} is the fuel pellet centerline temperature in C and Bu is the burnup in MWd/kgUO_2. Equation A18.1 provides the locus of centerline temperature-Bu pairs at the onset of fission gas release (onset taken to be approximately 1% FGR) for Halden operational history (e.g. various LHR with standard BWR flow, pressure, and fluid temperature values). The computational process described above was implemented with BISON to determine the onset of 1% FGR for several different LHR. Table A18.4 shows BISON numerical results for linear heat rates ranging from 15 to 45 kW/m.

Table A18.4: BISON fuel centerline temperature versus burnup at onset of FGR (various linear heat rates) for the simplified case FUMEXII 27(1).

Burnup (MWd/kgU)	FCT (C)	LHR (kW/m)
80.0	956.5	20.0
49.6	1033.0	25.0
32.9	1093.3	30.0
22.0	1147.3	35.0
14.1	1198.9	40.0
7.8	1248.0	45.0

The BISON predictions and other code comparisons (data digitized from FUMEX-II report [21] are shown with the Vitanza Criteria in Figure A18.7.

The Vitanza criteria was derived from pressure, burnup, and centerline temperature data gathered during Halden reactor operations. Most of the experimental data base for the threshold development was for maximum Bu of about 40 MWd/kgU. Reference [21] suggests that the threshold may be somewhat

conservative at higher burnups as recent high burnup data shows enhancement of FGR due to rim effect (enhanced porosity) development at the pellet surface. Several of the codes shown in Figure A18.7 have FGR models that predict gas release to be independent of fuel temperature above some burnup limit. Predictions that become vertical are indicative of this feature. BISON results are generally in good agreement with the other code results though it is clear that considerable scatter exists among the predictions.

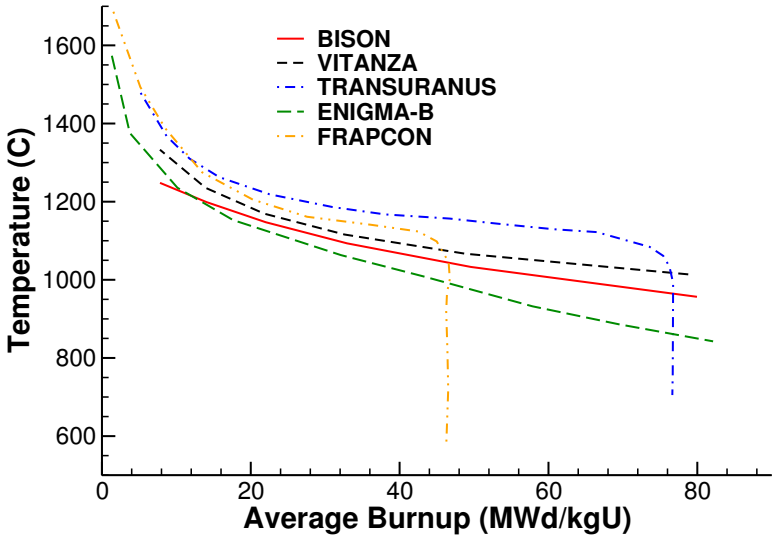

Figure A18.7: 27(1) BISON and other code results compared to Vitanza criteria [21].

BISON compares well with other well known fuel performance codes. All of the data for the other codes were digitized from plots in the FUMEX-II report [21]. Code comparisons for cases 27(2a) and 27(2b) are shown in Figure A18.8 and Figure A18.9, respectively.

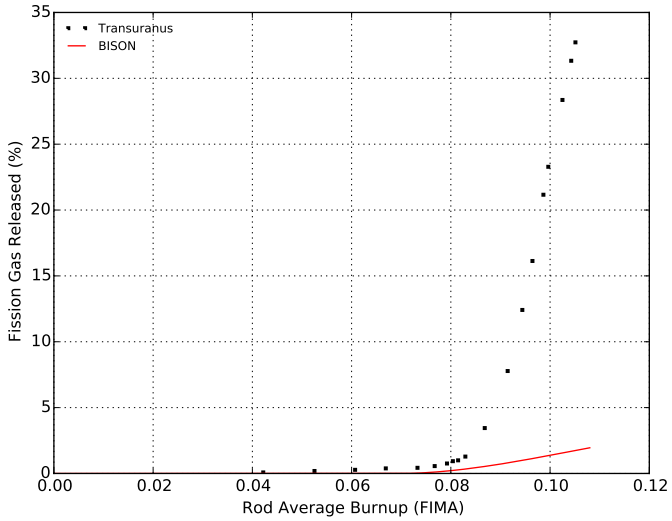

Figure A18.8: Case 27(2a) BISON comparisons with other well known fuel performance codes [21].

BISON under predicts the total FGR at high burnup, but is within an acceptable range at low and moderate burnup. The BISON comparisons to other fuel performance codes for case 27(2c) are shown

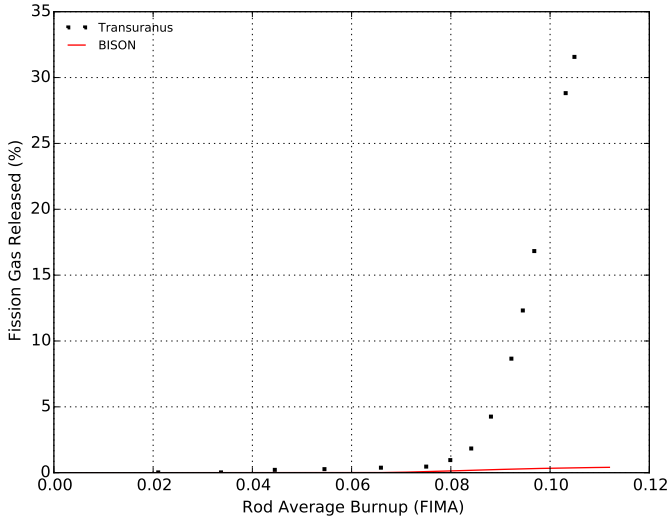

Figure A18.9: Case 27(2b) BISON comparisons with other well known fuel performance codes [21].

in Figure A18.10. The BISON comparisons to expected FGR values and other fuel performance codes for case 27(2d) are shown in Figure A18.11.

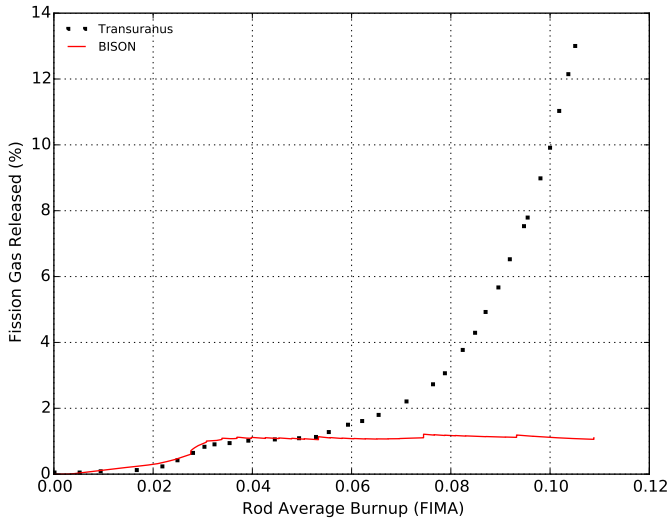

Figure A18.10: Case 27(2c) BISON comparisons with other well known fuel performance codes [21].

A18.5 Discussion

As discussed above, the mesh shown in Figure A18.3 includes only the fuel pellet. Specifications for FUMEXII 27(1) problem suggested that modelers use a large fuel rod plenum to preclude thermal feedback effects from the plenum and gap on FGR. After some experimentation with this concept, it became apparent that in BISON it was computationally more efficient to eliminate the cladding and plenum altogether since unrestricted fission gas release was the matter of interest.

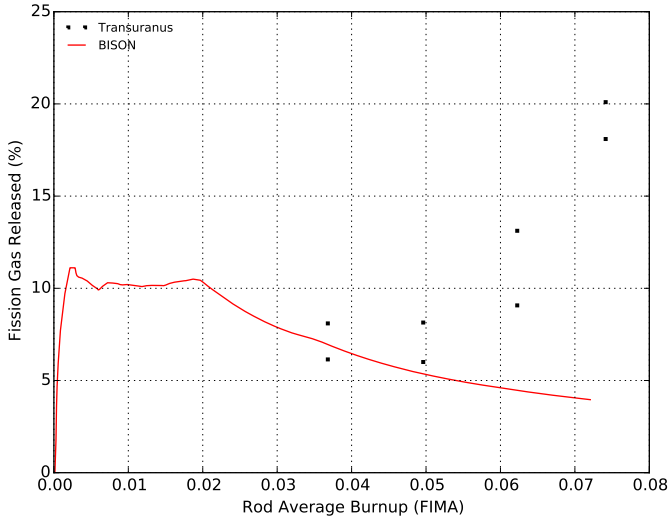

Figure A18.11: Case 27(2d) BISON comparisons with other well known fuel performance codes [21].

The overall results from the FUMEX-II simplified cases study indicate that a more accurate high burnup release model is needed in BISON. At low and moderate burnup, BISON does an adequate job predicting total fission gas release.

A19 Risø-2 GEm

A19.1 Overview

The Risø-2 GE-m test is a bump test that was carried out during the second Risø Transient Fission Gas Release Project in 1985 [61]. The fuel pin STR013 was supplied by General Electric Company and was punctured and refabricated prior to the bump test. The STR013 fuel element measured 973.50 mm long tip-to-tip. The length of fuel irradiated during the bump test was 271 mm long. The fuel segment was base irradiated in the Millstone reactor at low powers ranging from 10-15 kW/m to a burnup of approximately 14 MWd/kgUO_2. A unique feature of the GE fuel used for this test is that it has a Niobium liner buried 0.075 mm from the clad inner diameter to resist failure due to Pellet-to-Cladding Interaction (PCI). For simplicity this liner was ignored in the simulation. The bump test was performed in the water-cooled HP-1 rig under BWR conditions in the DR3 test reactor.

A19.2 Test Description

A19.2.1 Rod Design Specifications

The rod specifications for the Risø-2 GE-m test is are summarized in Table A19.1.

A19.2.2 Operating Conditions and Irradiation History

The base irradiation average power is shown in Figure A19.1. The average power during the bump test is shown in Figure A19.2. The axial power profile is nearly linear for the duration of the base irradiation and bump test. During the base irradiation there are small fluctuations in the axial power profile as a function of time. The axial profile for the duraction of the bump test is shown in Figure A19.3.
Since the data was provided in a histogram form the input power profile used by BISON was modified to add additional points that are 10 s later than the supplied points to provide a short ramp time between plateaus in the histogram. The small duration of the ramp results in the use of a power profile that is very close to a histogram which permits the use of a piecewise linear algorithm. Moreover the first ramp in power has been broken down into 24 short ramps as per recommendations by ANATECH.

The clad surface temperature was input as a function, along with the fast neutron flux from data provided in the FUMEX-III data set [45]. The coolant inlet temperature and pressure for the base irradiation and power ramp is shown in Table A19.2. The clad tempature, fast flux, and axial peaking factors were modified such that the 10 s ramps are also applied. This ensures that the times used are consistent throughout the model.

Table A19.1: Rod specifications of rods STR013 and Risø-2 GE-m

Base Fuel Rod (STR013)		
Tip-to-tip length	m	0.9735
Fuel Length	m	0.778
Active Fuel Length	m	0.7557
Nominal plenum height	mm	0.1444
Number of pellets in rod		63
Fill gas composition		He
Fill gas pressure (0 C)	MPa	1.7
Fuel		
Material		UO_2
Enrichment	%	2.89
Density	%	95.73
Outer diameter	mm	10.89
Pellet geometry		Chamfered
Grain diameter	μm	19.0
Pellet Chamfer (both ends)		
Dish diameter	cm	–
Dish depth	cm	–
Chamfer width	mm	0.25
Chamfer depth	mm	0.38
Cladding		
Material		Zr-2
Outer diameter	mm	12.54
Inner diameter	mm	11.11
Wall thickness	mm	0.71
Refabricated Fuel Rod (GE-m)		
Fuel stack height	m	0.271
Number of pellets in rod		23
Fill gas composition		He
Fill gas pressure (0 C)	MPa	0.49

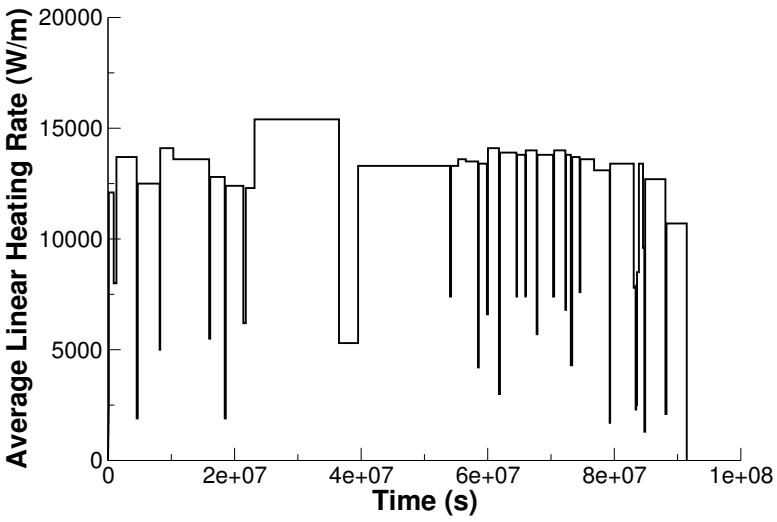

Figure A19.1: Base irradiation average power history for test pin STR013.

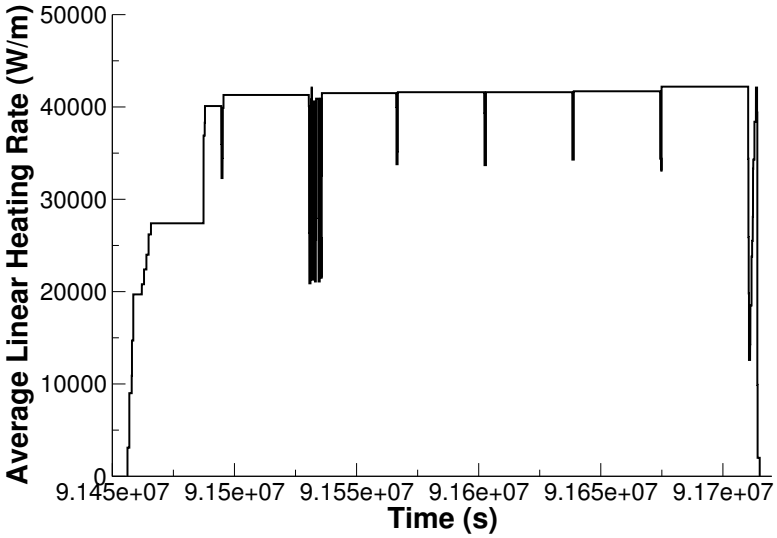

Figure A19.2: Average power history during the bump test.

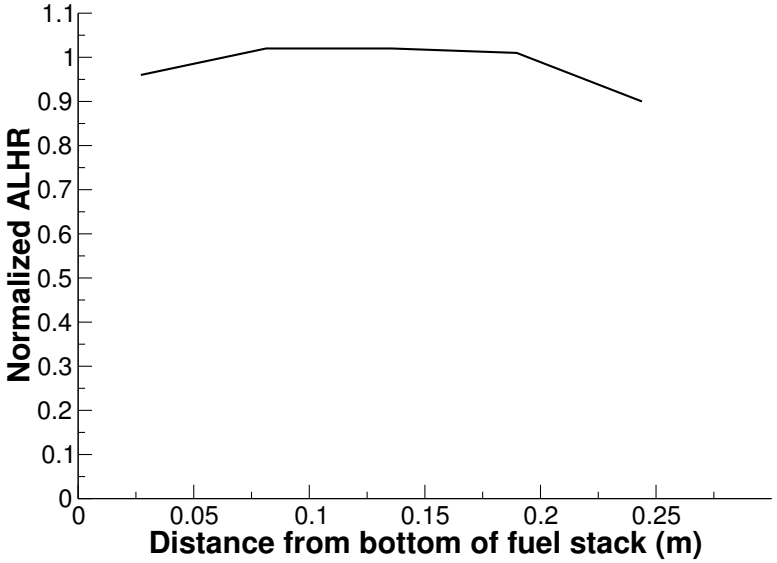

Figure A19.3: The axial power profile during the bump test

Table A19.2: Operational input parameters.

Base Irradiation		
Coolant inlet temperature	C	287.8
Coolant pressure	MPa	7.24
Power Ramps		
Coolant inlet temperature	C	289
Coolant pressure	MPa	7.2

A19.3 Model Description

A19.3.1 Geometry and Mesh

The geometric parameters specified in Table A19.1 were used to create the mesh for this simulation. The fuel was meshed as a smeared fuel rod with 11 radial elements and 184 axial elements. Figure A19.4 shows a section of the mesh with a temperature contour plot. The geometry was such that the refabricated rod length was modeled during the base irradiation and bump test. To account for the correct gas volume the plenum height was adjusted such that the overall voidage including chamfers, radial gap, bottom plenum and top plenum were equivalent to the refabricated volume at the base irradiation. The lower plenum was equal to the length of the Hafnium Oxide insulator pellet that was not modeled. Due to fuel swelling and cladding creep down the initial volume at the beginning of the bump test is slightly lower than the refabrication.

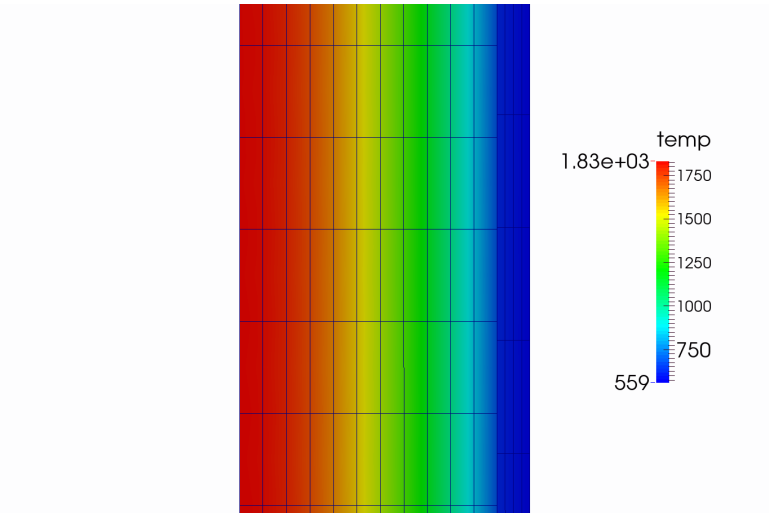

Figure A19.4: A section of the mesh with a temperature contour at t = 9.15662×10^7s.

A19.3.2 Material and Behavioral Models

The thermal conductivity model used for the UO_2 fuel was NFIR. The fuel was modeled as elastic and fuel swelling was coupled to the fission gas release model. In addition fuel relocation was modeled using an activation power of 5 kW/m. Fission gas release was modeled using the Sifgrs model with a transient burst release model. The cladding material, was modeled using a constant thermal conductivity of 16 W/m-K. Primary and secondary thermal, and irradiation creep were modeled.

A19.3.3 Input files

The BISON input and all supporting files (power histories, axial power profile, fast neutron flux history, etc.) for this case are provided with the code distribution at bison/assessment/Riso_GEM_STR013/analysis.

A19.4 Results Comparison

A19.4.1 Clad Diameter

A comparison of the predicted and measured rod outer diameter is shown in Table A19.3. The comparisons include the average rod diameter prior to the bump test, and the maximum and average changes in diameter during the test. No ridging was observed before the bump test and there is little to unclear evidence at the conclusion of the bump test.

Table A19.3: Clad diameter comparisions before and after the bump test.

	Average Diameter before Ramp (mm)	Maximum Diameter Increase (μm)	Average Diameter Increase (μm)
Experimental	12.536	8	5
Refab T=273 K Smeared	12.500	2.169	-5.434
Refab T=273 K Discrete	12.500	2.740	2.120
Refab T=373 K Smeared	12.506	0.406	-7.219
Refab T=373 K Discrete	12.506	0.470	-7.216

A19.4.2 Fission Gas Release

A comparison of the predicted and measured total fission gas release is shown in Figure A19.5. Since the base irradiation is a low power and low burnup irradiation BISON accurately predicts FGR of approximately zero percent. However, at the end of the ramp test, BISON under predicts the total FGR. Although the end of life percentage of FGR was underpredicted by the BISON simulation it is an acceptable result as it is within a factor of two of the experimental data.

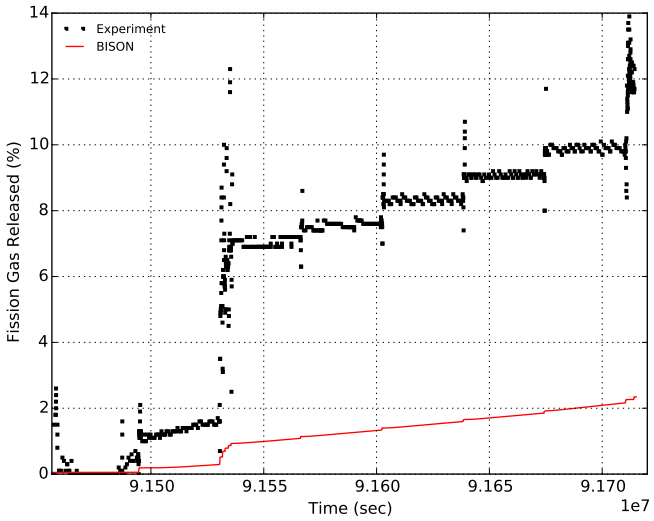

Figure A19.5: Fission gas release comparison of GE-m during the bump test.

A19.4.3 Rod Internal Pressure

A comparison of the predicted and measured internal rod pressure is shown in Figure A19.6. BISON overpredicts the rod internal pressure from the beginning of the bump test. This is likely due with the refabrication calculation. The trend observed is encouraging as it is exactly the same as the experimental data. However, there appears to be an systematic offset in the internal pressure from the beginning of the bump test. Further investigation is required to determine the cause of this offset.

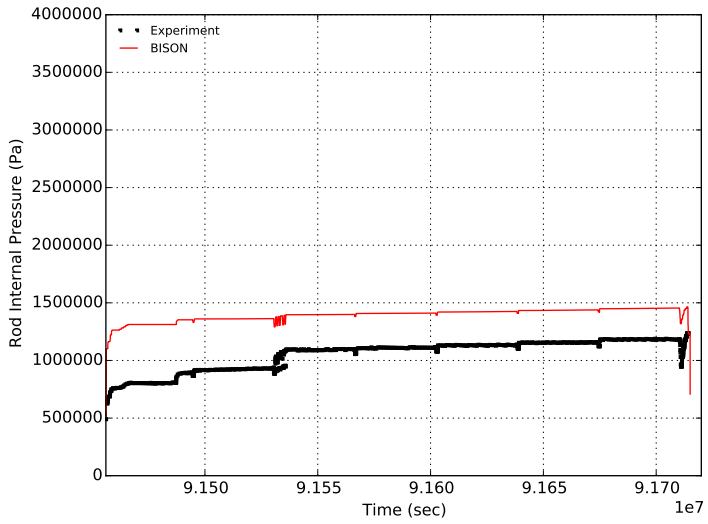

Figure A19.6: Rod internal pressure comparison of GE-m during the bump test.

A19.4.4 Discussion

The comparisons of the results against the experimental data for the refabrication supplied in the FUMEX-III data were examined in the previous two subsections. It appears that the rod internal pressure strongly depends upon the refabrication temperature. Therefore a sensitivity analysis of the plenum pressure behavior as a function of the refabrication temperature was completed. By keeping the refabrication temperature and volume constant and varying the refabrication temperature the amount of initial moles after refabrication can be varied. BISON uses the refabrication data provided in the input file to calculate the initial moles after refabrication. Then the calculated moles and the postprocessor values for the average gas temperature and the gas volume are used to determine the internal gas pressure. To ensure the calculated pressure is close to the refabrication pressure the cladding temperature during the refabrication process must be set equal to the refabrication temperature. The sensitivity analysis was completed for refabrication temperatures of 273 K (given in the experimental data), 373 K, 473 K and 546 K. The rod internal pressure results of the analysis are presented in Figure A19.7 and the fission gas release results are presented in Figure A19.8.

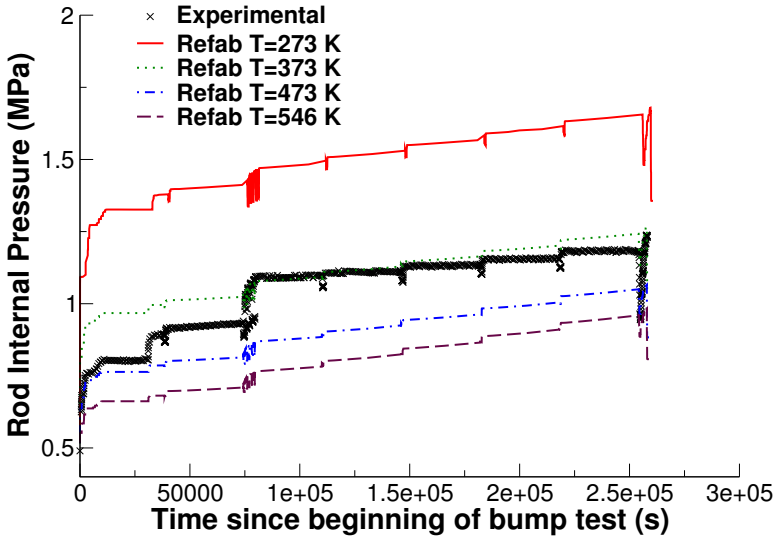

Figure A19.7: Sensitivity analysis of the rod internal pressure as a function of the refabrication temperature.

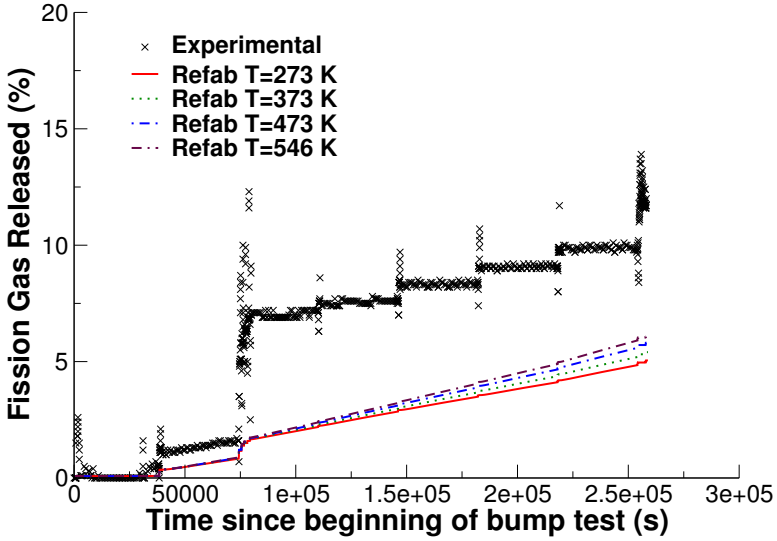

Figure A19.8: Sensitivity analysis of the fission gas release as a function of the refabrication temperature

Based upon the sensitivity analysis it is observed that as the refabrication temperature increases from 273 K to 546 K the internal rod pressure decreases and the fission gas released increases. This is expected because by changing the refabrication time the number of moles decreases. Less initial moles results in a lower internal rod pressure. The increasing temperature contributes to the increase fission gas release that is observed. The key takeaway of the sensitivity analysis is that the internal rod pressure for the duration of irradiation is strongly influenced by the refabrication temperature, or more importantly the difference between the refabrication temperature and the cladding temperature after refabrication. For example if the cladding temperature is brought down to 273 K during the refabrication process to be equal to the internal gas temperature. Once refabrication is complete the cladding surface temperature is increased to 562 K (the supplied boundary condition). This change in temperature is more than double the refabrication temperature and by the ideal gas law when the volume and initial moles remain relatively constant, the pressure more than doubles. Therefore, the largest contributing factor to the rod internal pressure discrepancy is the difference between the reported refabrication temperature and the cladding boundary condition.

The refabrication data is provided to calculate the initial moles in the void volume within the rod. Then using the gas volume and temperature postprocessors the plenum pressure is calculated using the determined initial moles. By examining the ideal gas law it should not matter what temperature the refabrication pressure is reported at because the refabrication volume remains constant. However, to correctly model the evolution of the rod internal pressure, the temperature at which the refabrication was completed at is required to ensure the temperature change from refabrication to bump test operation is correct.

A20 Risø-3 II3

A20.1 Overview

The Risø II3 experiment conducted at the Risø DR3 water-cooled HP1 rig utilized a re-fabricated rod from the Millstone-1 BWR [45],[62]. The mother rod, STR014, was irradiated over three reactor cyclers up to about 14.5 GWd/t, and re-fabricated to a shorter length. The re-fabricated rod, II3 (STR014-3R), was instrumented with a fuel centerline thermocouple and a pressure transducer. The fuel centerline temperature, fission gas release, rod internal pressure, and rod outer diameter can be used for comparison.

A20.2 Test Description

A20.2.1 Rod Design Specifications

Rod II3 was a re-fabricated rod extracted from a full length rod. The hole for the thermocouple was at the top of the fuel rod and did not penetrate the entire fuel stack. The re-fabricated rod geometry is tabulated in Table A20.1.

Table A20.1: Risø II3 Test Rod Specifications

Fuel Rod		
Overall length	m	0.3616
Fuel stack height	m	0.291
Nominal plenum height	mm	51.0
Mother Rod		
Fill gas composition		He
Fill gas pressure	MPa	1.53
Re-Fabricated Rod		
Fill gas composition		He
Fill gas pressure	MPa	0.684
Fuel		
Material		UO_2
Enrichment	%	2.89
Density	%	95.77
Inner diameter	mm	2.5
Outer diameter	mm	10.89
Pellet geometry		both ends
Grain diameter	μm	12.2
Pellet Dishing		
Dish diameter	cm	0.0
Dish depth	cm	0.0
Chamfer width	cm	0.038
Chamfer depth	cm	0.018
Cladding		
Material		Zr-2
Outer diameter	mm	12.53
Inner diameter	mm	11.11
Wall thickness	mm	0.71

A20.2.2 Operating Conditions and Irradiation History

The power history for the base irradiation carried out at the Millstone-1 BWR is shown in Figure A20.1. The experiment power history carried out at the Risø DR3 facility is shown in Figure A20.2 and run at BWR conditions by reducing the system pressure to 7.24 MPa. A prescribed axial profile for this experiment was provided in the FUMEX-III data [45]. The measured clad surface temperature as a function of time was also provided in the FUMEX-III data [45] and used as a boundary condition for this simulation. The other reactor operation parameters are tabulated in Table A20.2.

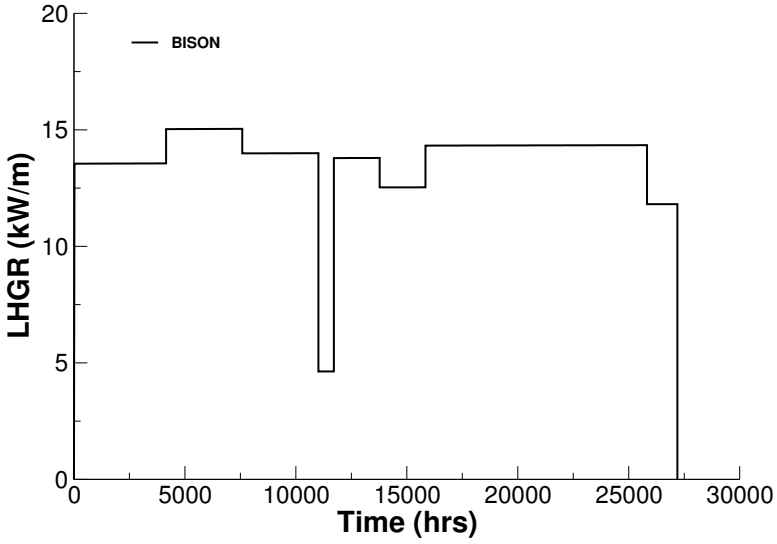

Figure A20.1: Base irradiation history for fuel segment STR014, carried out at Millstone-1 BWR.

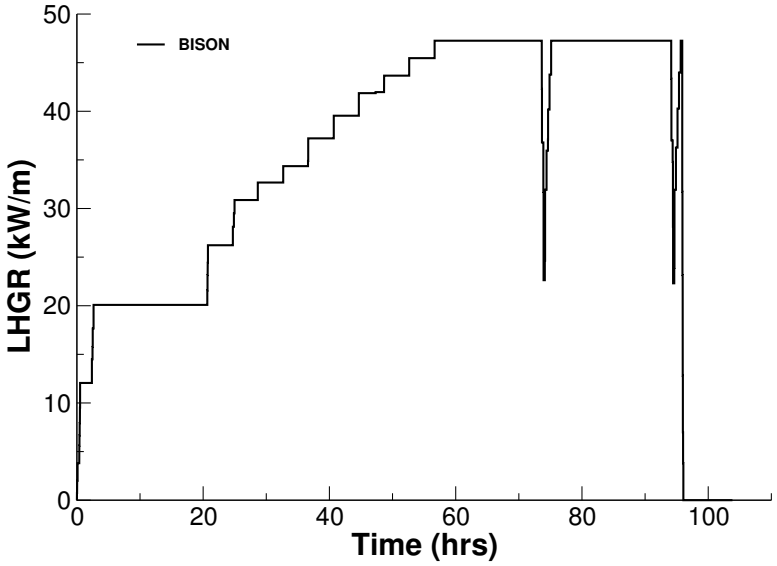

Figure A20.2: Risø DR3 irradiation period for test II3 (STR014-3R).

Table A20.2: Operational input parameters.

Base Irradiation		
Coolant inlet temperature	C	287.8
Coolant pressure	MPa	7.24
Fast neutron flux	n/(cm^2·s) per (kW/m)	1.6·10^{12}
Power Ramps		
Coolant inlet temperature	C	NA
Coolant pressure	MPa	7.24
Fast neutron flux	n/(cm^2·s) per (kW/m)	4.0·10^{11}

A20.3 Model Description

A20.3.1 Geometry and Mesh

The re-fabricated rod geometry was modeled for the entire simulation considering a smeared column of flat ended pellets, with the top pellets containing the hole for the thermocouple. The plenum height was adjusted such that the plenum volume at the beginning of the bump test was approximately 7.41 cm^3.

A 2-dimensional axi-symmetric quadratic (Quad8 elements) mesh was used to model the geometry of the rod used in the II3 experiment. The fuel was meshed considering two fuel pellet types. The first pellet type was 4.2 cm in length with a hole down the center, the second pellet type was 24.9 cm in length with no hole down the center. The first pellet type's mesh is comprised of elements 3.953 mm in the axial direction and 0.3889 mm in the radial direction (for an aspect ratio of 10.16). The second pellet type's mesh is comprised of elements 2.0 mm in the axial direction and 0.3813 mm in the radial direction (for an aspect ratio of 5.244). The clad mesh is comprised of elements 4.278 mm in the axial direction and 0.1775 mm in the radial direction (for an aspect ratio of 24.1).

A20.3.2 Material and Behavioral Models

The following material and behavioral models were used for the UO_2 fuel:

- ThermalFuel - NFIR: temperature and burnup dependent thermal properties
- RelocationUO2: relocation strains, relocation activation threshold power set to 5 kW/m.
- Sifgrs: fission gas release model with the combined gaseous swelling model.

For the clad material, a constant thermal conductivity of 16 W/m-K was used and both thermal and irradiation creep were considered using the Limback model [36].

A20.3.3 Boundary and Operating Conditions

The Risø DR3 irradiation period for the II3 test shown in Figure A20.2 was appended to the base irradiation power history shown in Figure A20.1. It was assumed that the clad temperature during the down time between base irradiation and the Risø test was 373K. The fast neutron flux was input as a function of power.

A20.3.4 Input files

The BISON input and all supporting files (power histories, axial power profile, fast neutron flux history, etc.) for this case are provided with the code distribution at bison/assessment/Riso_II3/analysis.

A20.4 Results Comparison

The Risø II3 experiment is used to assess the code's capability to capture the fuel centerline temperature, the integral fuel rod fission gas release, rod internal pressure, and rod outer diameter. All results were compared against the II3 data found in the FUMEX-III data sets [45].

A20.4.1 Temperature

BISON predicts the shape of temperature curve well, but fails to reach measured thermocouple temperatures as shown in Figure A20.3. One possible explaination for the lower predicted temperature is the underprediction of fission gas release as seen in Figure A20.4. The fuel centerline temperature is taken at a node approximately 38 mm from the top of the fuel stack.

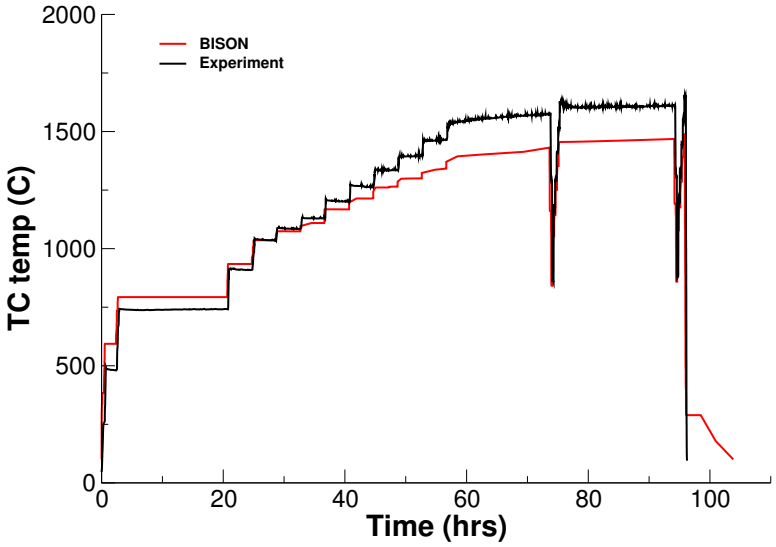

Figure A20.3: BISON fuel centerline temperature comparison to Risø experimental data

A20.4.2 Fission Gas Release

The calculated integral fuel rod fission gas release is compared to the measured data in Figure A20.4. In view of the uncertainties involved in FGR modeling, the predictive accuracy is satisfactory, falling well within the uncertainty factor of 2 [7].

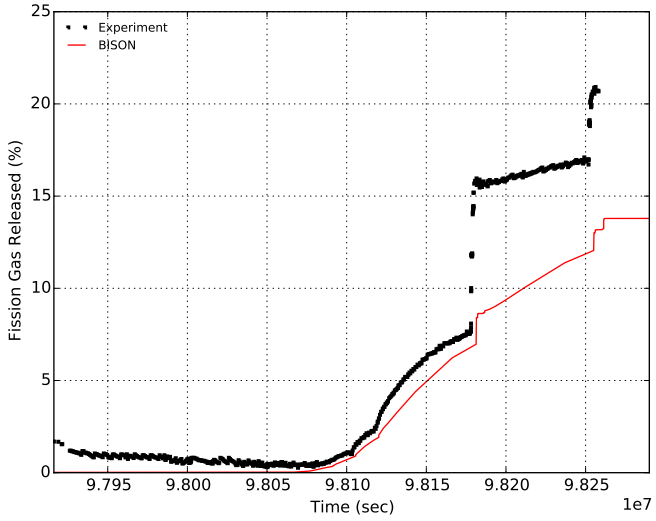

Figure A20.4: BISON ramp test fission gas release comparison to Risø experimental data.

A20.4.3 Rod Internal Pressure

The calculated rod internal pressure matches the measured data set well as seen in Figure A20.5 following the given shape of the measured cuve accurately.

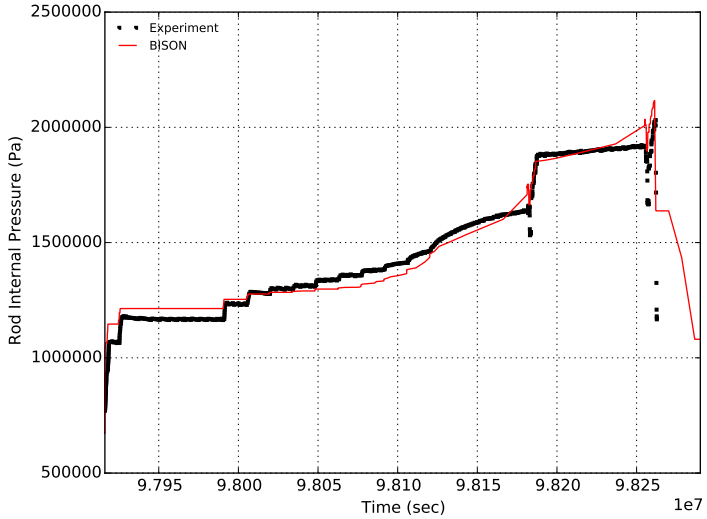

Figure A20.5: BISON rod internal pressure comparison to Risø experimental data.

A20.4.4 Rod Outer Diameter

The calculated rod diameter seems to predict more cladding creepdown than experiment results suggest as shown in Figure A20.6. Since BISON currently does not have a cladding option for cold worked Zry2, a SRA Zry4 cladding was chosen instead.

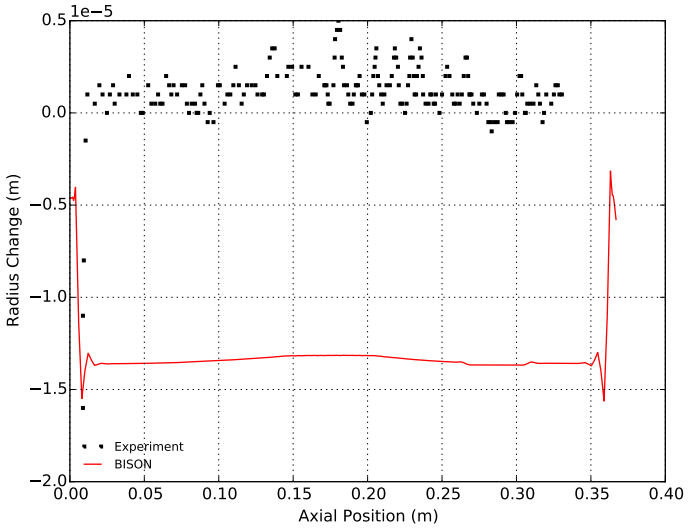

Figure A20.6: BISON rod outer diameter comparison to Risø experimental data.

A20.5 Discussion

For the grain size, a chosen diameter of 12.2 μm was used. A brief discussion of how the grain size had already been multiplied by the correction factor of 1.56 can be found in the PRECHAR.II3 file included in the FUMEX-II3 data sets [45].

A21 Risø-3 II5

A21.1 Overview

The Risø II5 experiment conducted at the Risø DR3 water-cooled HP1 rig utilized a re-fabricated rod from the Halden BWR [45]. The mother rod, M72-2, was one of the six ZR-2 clad UO_2fuel pins in the IFA161 test rig. This base irradiation was completed between July 14, 1968 and October 2, 1981. Upon compleiton of the base irradiation the mother rod was refabricated and bump tested as part of the II5 experiment. The refabricated rod II5 was instrumented with a fuel centerline thermocouple and a pressure transducer. The fuel centerline temperature, fission gas release, rod internal pressure, and rod outer diameter can be used for comparison.

A21.2 Test Description

A21.2.1 Rod Design Specifications

Rod II5 was a re-fabricated rod extracted from a full length rod. The hole for the thermocouple was at the top of the fuel rod and did not penetrate the entire fuel stack. The re-fabricated rod geometry is tabulated in Table A21.1.

Table A21.1: Risø II5 Test Rod Specifications

Fuel Rod		
Overall length	m	0.3563
Fuel stack height	m	0.2878
Nominal plenum height	mm	65.47
Mother Rod		
Fill gas composition		He
Fill gas pressure	MPa	0.09
Re-Fabricated Rod		
Fill gas composition		He
Fill gas pressure	MPa	0.641
Fuel		
Material		UO_2
Enrichment	%	5.078
Density	%	94.7
Inner diameter	mm	0
Outer diameter	mm	12.625
Pellet geometry		dished both ends
Grain diameter	μm	9.984
Pellet Dishing		
Dish diameter	mm	11.125
Dish depth	mm	0.3
Chamfer width	mm	0.0
Chamfer depth	mm	0.0
Cladding		
Material		Zr-2
Outer diameter	mm	14.00
Inner diameter	mm	12.85
Wall thickness	mm	0.56

A21.2.2 Operating Conditions and Irradiation History

The power history for the base irradiation carried out at the Halden BWR is shown in Figure A21.1. The experiment power history carried out at the Risø DR3 facility is shown in Figure A21.2 and run at BWR conditions by reducing the system pressure to 7.24 MPa. A prescribed axial profile for this experiment was provided in the FUMEX-III data [45]. The measured clad surface temperature as a function of time was also provided in the FUMEX-III data [45] and used as a boundary condition for this simulation. The other reactor operation parameters are tabulated in Table A21.2.

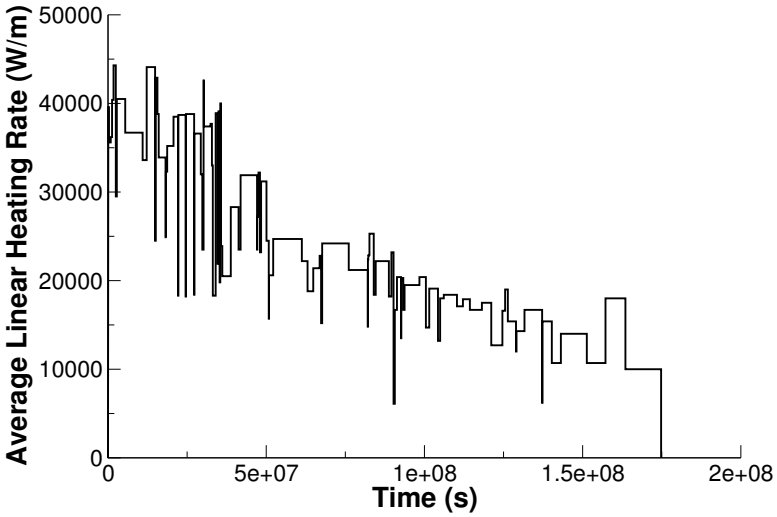

Figure A21.1: Base irradiation history for fuel segment STR014, carried out at Halden BWR.

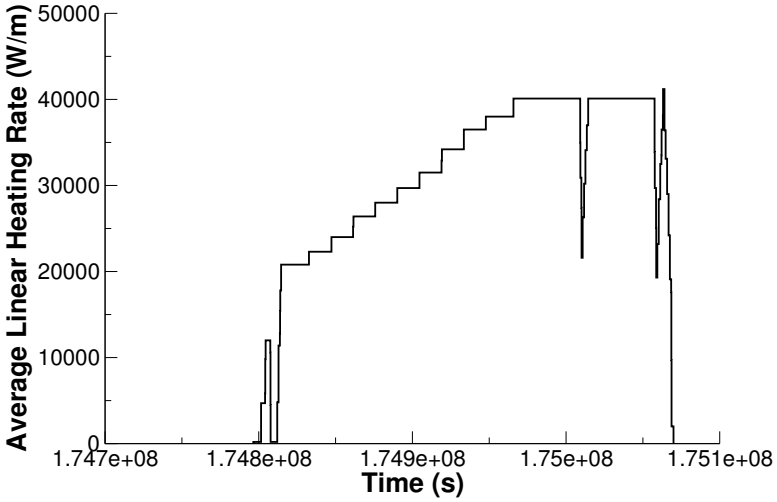

Figure A21.2: Risø DR3 irradiation period for test II5.

A21.3 Model Description

A21.3.1 Geometry and Mesh

The re-fabricated rod geometry was modeled for the entire simulation considering a smeared column of flat ended pellets, with the top pellets containing the hole for the thermocouple. The plenum height was adjusted such that the plenum volume at the beginning of the bump test was approximately 8.68 cm^3.

Table A21.2: Operational input parameters.

Base Irradiation		
Coolant inlet temperature	C	287.8
Coolant pressure	MPa	3.2
Fast neutron flux	n/(m^2·s) per (W/m)	5.5·10^{12}
Power Ramps		
Coolant inlet temperature	C	NA
Coolant pressure	MPa	7.2
Fast neutron flux	n/(m^2·s) per (W/m)	4.0·10^{12}

A 2-dimensional axi-symmetric quadratic (Quad8 elements) mesh was used to model the geometry of the rod used in the II5 experiment. The fuel was meshed considering two fuel pellet types. The first pellet type was 1.38 cm in length with a 0.125 cm diameter hole down the center, the second pellet type was 1.297 cm in length with no hole down the center. The first pellet type's mesh is comprised of elements 4.6 mm in the axial direction and 0.460227 mm in the radial direction (for an aspect ratio of 9.995). The second pellet type's mesh is comprised of elements 4.323 mm in the axial direction and 0.4602 mm in the radial direction (for an aspect ratio of 9.393). The clad mesh is comprised of elements 5.353 mm in the axial direction and 0.1438 mm in the radial direction (for an aspect ratio of 37.22).

A21.3.2 Material and Behavioral Models

The following material and behavioral models were used for the UO_2 fuel:

- ThermalFuel - NFIR: temperature and burnup dependent thermal properties
- RelocationUO2: relocation strains, relocation activation threshold power set to 5 kW/m.
- Sifgrs: fission gas release model with the combined gaseous swelling model.

For the clad material, a constant thermal conductivity of 16 W/m-K was used and both thermal and irradiation creep were considered using the Limback model [36].

A21.3.3 Boundary and Operating Conditions

The Risø DR3 irradiation period for the II5 test shown in Figure A21.2 was appended to the base irradiation power history shown in Figure A21.1. It was assumed that the clad temperature during the down time between base irradiation and the Risø test was 273K as per the experimental data. The fast neutron flux was input as a function of power.

A21.3.4 Input files

The BISON input and all supporting files (power histories, axial power profile, fast neutron flux history, etc.) for this case are provided with the code distribution at bison/assessment/Riso_II5/analysis.

A21.4 Results Comparison

The Risø II5 experiment is used to assess the code's capability to capture the fuel centerline temperature, fission gas release, rod internal pressure, and rod outer diameter. All results were compared against the II5 data found in the FUMEX-III data sets [45].

A21.4.1 Centerline Temperature

BISON predicts the shape of temperature curve well, but fails to reach measured thermocouple temperatures as shown in Figure A21.3. One possible explaination for the lower predicted temperature is the underprediction of fission gas release as seen in Figure A21.4. The fuel centerline temperature is taken at a node approximately 38 mm from the top of the fuel stack.

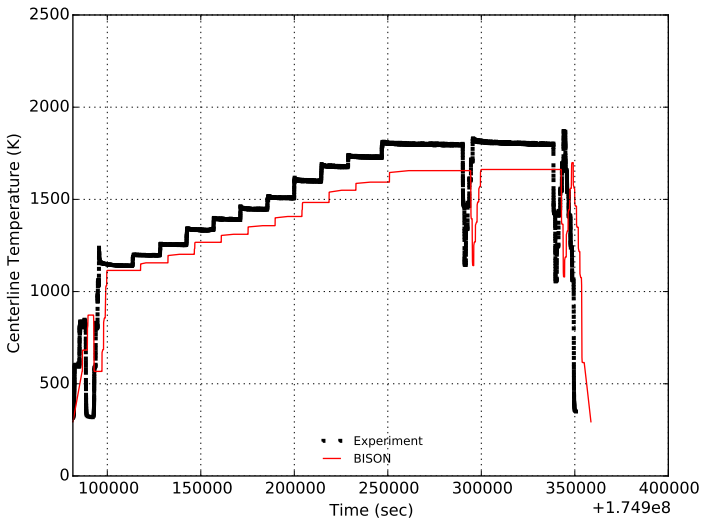

Figure A21.3: BISON fuel centerline temperature comparison to Risø experimental data

A21.4.2 Fission Gas Release

The calculated integral fuel rod fission gas release for the ramp tests is compared to the measured data in Figure A21.4. For this prediction the fission gas released during the base irradiation is not included. It is observed that BISON significantly underpredicts the fission gas release. The experiment predicts 11% and BISON predicts approximately 0.33%. This significant difference is partly due to the fact the transient burst release model in the Sifgrs fission gas release model in BISON was turned off due to convergence issues. In order to have the burst release model work the interpenteration of the fuel and clad was enormously large at about 12 microns. Therefore, to have acceptable penetration results (less then 3 microns) the transient release model was not used.

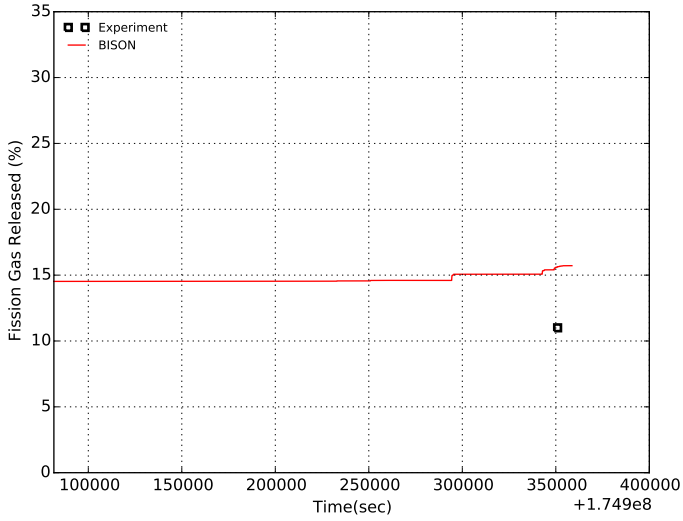

Figure A21.4: BISON ramp test fission gas release comparison to Risø experimental data.

A21.4.3 Rod Internal Pressure

Figure A21.5 illustrates the comparison between BISON and the experimental data for the rod internal pressure during the bump test. It is observed that BISON immediately rises to a larger pressure after refabrication. This is due to the difference in temperature between the cladding boundary and the refabrication temperature immediately after refabrication. A further analysis of these results is provided in the Discussion section.

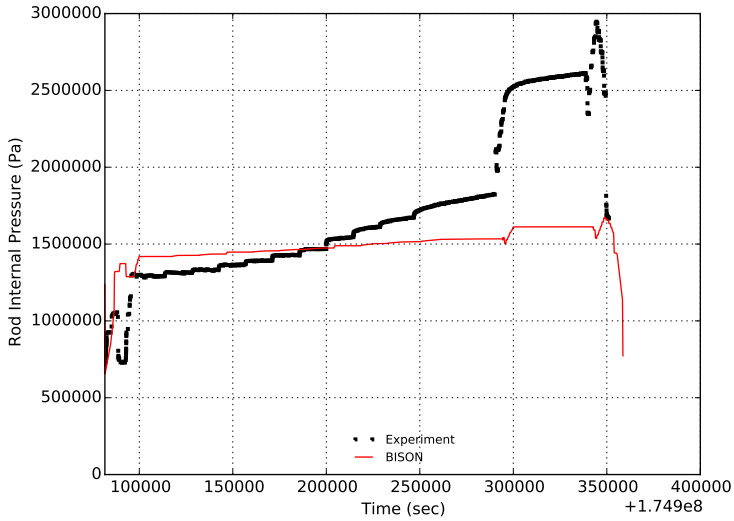

Figure A21.5: BISON rod internal pressure comparison to Risø experimental data.

A21.4.4 Clad Diameter

Figure A21.6 shows the comparison between BISON and the experimental data for the cladding diameter for two cases: pre-ramp and post-ramp. In general bison does a reasonable job at predicting the cladding diameter pre-ramp but significantly underpredicts the diameter post-ramp. For the experimental data, the 2 points above one another using the same symbols indicate the maximum and minimum diameters

observed at that location due to pellet hourglassing. Since a smeared model was used in BISON a single value was obtained. Ideally this line should fall between the 2 data points. The cause of the discrepancy between BISON and the experimental predictions is because the transient release model was not used for fission gas release. If the burst release model was used a large internal gas pressure would be observed and a higher amount of fission gas swelling would occur within the fuel pellets. A larger swelling would result in a large cladding diameter. In addition, a discrete pellet model would be ideal to capture the hourglassing effect and to predict the maximum and minimum diameter values.

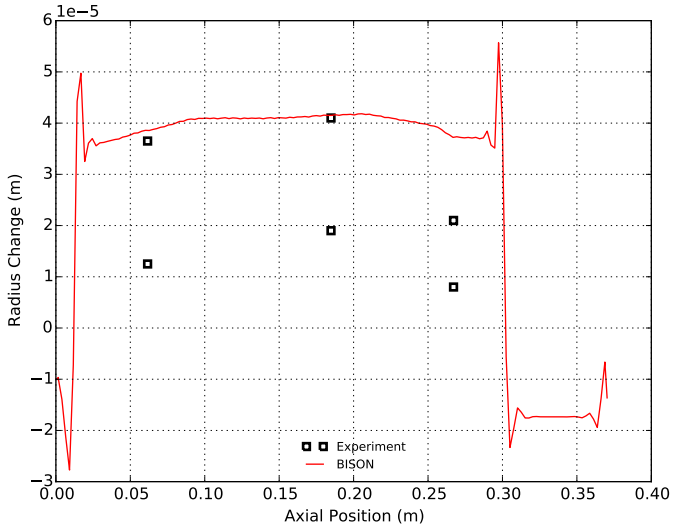

Figure A21.6: BISON clad diameter comparison to Risø experimental data pre-ramp and post-ramp

A21.5 Discussion

In this section, comparison plots of BISON against the experimental data and a variety of well known fuel performance codes is completed for rod internal pressure and fission gas release. Figure A21.7 illustrates the rod internal pressure comparison. It is observed that despite BISON not matching the experimental data that well it falls within the range of the other codes. In fact ENIGMA-B, FEMAXI-7 and BISON all predict relatively similar trends in the pressure behavior. Similar results are presented in Figure A21.8 for fission gas release. All the codes presented underpredict the fission gas release. Although BISON predicts the lowest fission gas release, if penetration can be minimized such that the burst release model could be used, BISON would fall within the spread of the fuel performance codes.

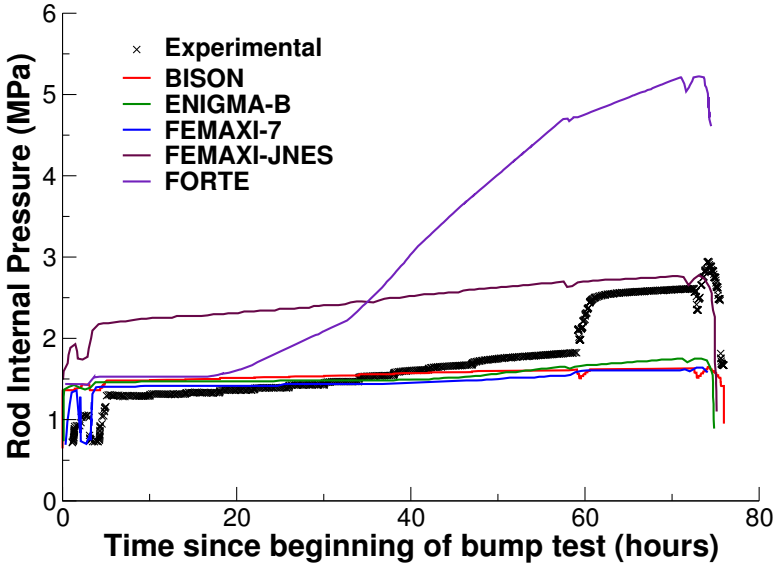

Figure A21.7: BISON rod internal pressure comparison to experimental data and other well known codes.

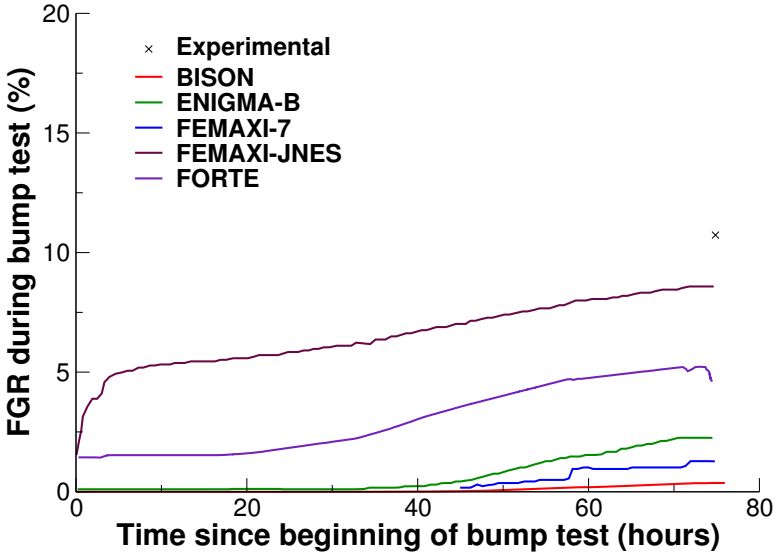

Figure A21.8: BISON ramp test fission gas release comparison experimental data and other well known codes.

A22 Risø-3 GE7

A22.1 Overview

The Risø-3 GE7 test is a bump test that was carried out during the third Risø Transient Fission Gas Release Project in 1989 [63]. The fuel pin ZX115 was supplied by General Electric Company and was neither punctured nor re-fabrication prior to the test. The test pin was the lower middle segment of four approximately 0.975 m long segments assembled to a stringer. The fuel segment was base irradiated in the Quad Cities-1 boiling water reactor (BWR) over four reactor cycles. The bump test was performed in the water-cooled HP-1 rig under BWR conditions in the Risø DR3 test reactor.

A22.2 Test Description

A22.2.1 Rod Design Specifications

The rod specifications for the Risø-3 GE7 test is are summarized in Table A22.1.

Table A22.1: Risø-3 GE7 rod specifications.

Fuel Rod		
Fuel stack height	mm	752.1
Nominal plenum height	mm	143.4
Fill gas composition		He
Fill gas pressure	MPa	0.29
Fuel		
Material		UO_2
Enrichment	%	3.0
Density	%	95.2
Outer diameter	mm	10.41
Pellet geometry		Chamfered
Grain diameter	μm	11.3-12.8
Pellet Chamfer (both ends)		
Dish diameter	cm	–
Dish depth	cm	–
Chamfer width	mm	0.18
Chamfer depth	mm	0.38
Cladding		
Material		Zr-2
Outer diameter	mm	12.26
Inner diameter	mm	10.63
Wall thickness	mm	0.815

A22.2.2 Operating Conditions and Irradiation History

The base irradiation average power is shown in Figure A22.1. The average power during the ramp test is shown in Figure A22.2. The axial power profile is nearly linear for the base irradiation, however,

during the ramp test, the power is shifted heavily to the bottom of the rod (see Figure A22.3). The clad surface temperature was input as a function, along with the fast neutron flux from data provided in the FUMEX-III data set [45]. The coolant inlet temperature and pressure for the base irradiation and power ramp is shown in Table A22.2.

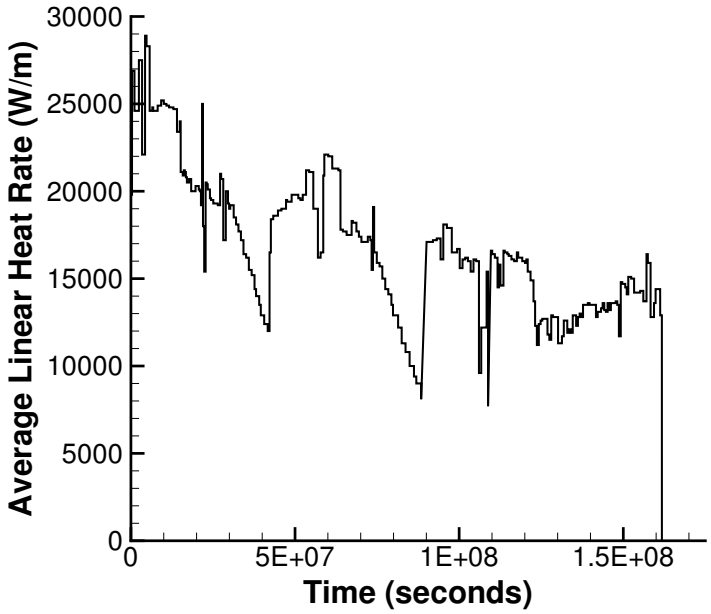

Figure A22.1: Base irradiation average power history for test pin ZX115.

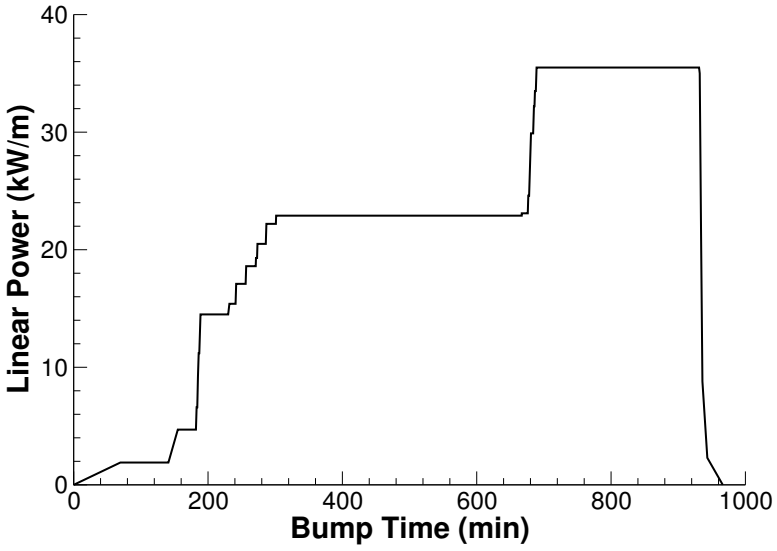

Figure A22.2: Average power history during power ramp. Note: The time has been zeroed to the start of the ramp.

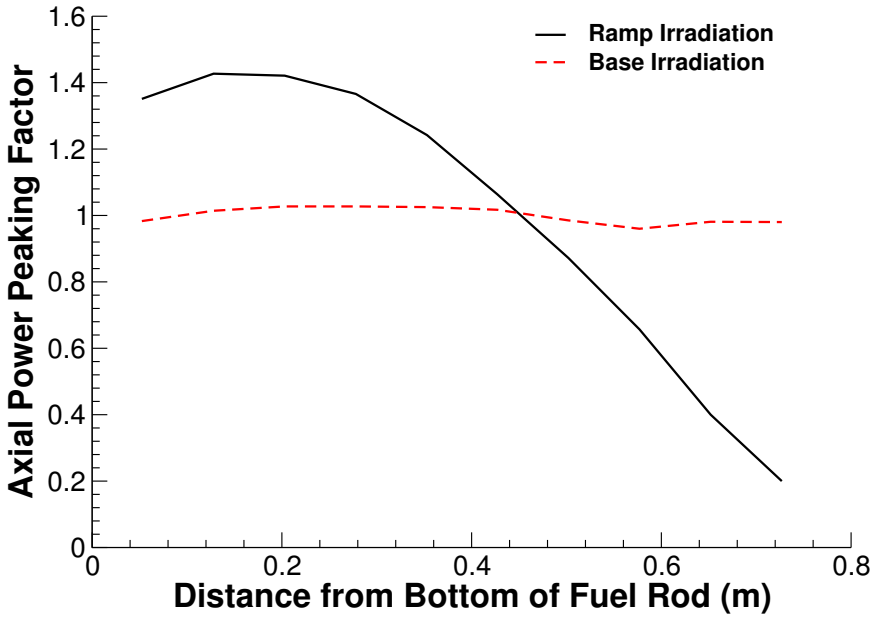

Figure A22.3: Axial power profile during base irradiation and ramp test.

Table A22.2: Operational input parameters.

Base Irradiation		
Coolant inlet temperature	C	295
Coolant pressure	MPa	7.24
Power Ramps		
Coolant inlet temperature	C	289
Coolant pressure	MPa	7.24

A22.3 Model Description

A22.3.1 Geometry and Mesh

The Risø GE7 ZX115 rod was modeled both as a smeared fuel pellet stack and as a discrete fuel pellet stack. The geometric parameters specified in Table A22.1 were used to create the meshes for these simulations. The smeared fuel was meshed as a single smeared fuel column with 11 radial elements and 432 axial elements. The discrete fuel was meshed as 72 individual pellets, each with 8 axial and 11 radial elements. Figure A22.4 shows a section of the mesh with a stress contour plot. This contour plot was made near the end of the run. Actual numbers are irrelevant in this case as this plot is only meant to show the discretization.

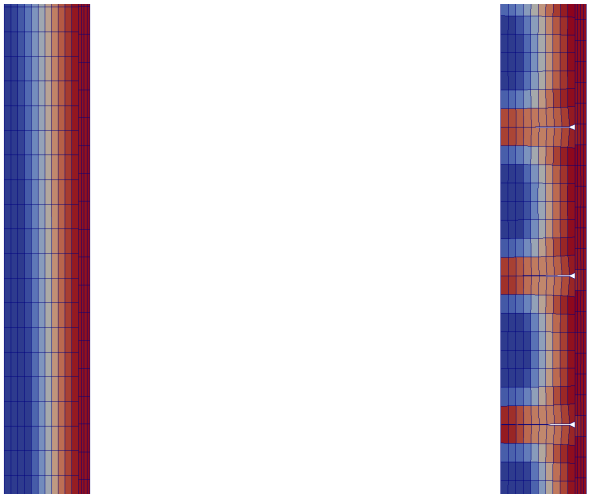

Figure A22.4: A section of the GE7 ZX115 fuel rod mesh with a temperature contour plot.

A22.3.2 Material and Behavioral Models

The following material and behavioral models were used for the UO_2 fuel:

- ThermalFuel - NFIR: temperature and burnup dependent thermal properties.
- RelocationUO2: relocation strains, relocation activation threshold power set to 5 kW/m.
- Sifgrs: Simplified fission gas release model with physics based gaseous swelling model.

For the clad material, a constant thermal conductivity of 16 W/m-K was used. Both thermal (primary and secondary creep) and irradiation creep were considered and combined with a J_2 plasticity model to simulate rapid cladding deformation during power ramps.

A22.3.3 Input files

The BISON input and all supporting files (power histories, axial power profile, fast neutron flux history, etc.) for this case are provided with the code distribution at bison/assessment/Riso_GE7_ZX115/analysis.

A22.4 Results Comparison

A22.4.1 Clad Diameter

A comparison of the predicted and measured rod outer diameter at post base irradiation and post ramp is shown in Figure A22.5. Starting with the post base irradiation it can be seen from Figure A22.5 that BISON over predicted the Under predicted the rod diameter for both the smeared and discrete cases. This is most likely cause by over predicting the cladding creep down. At this point in the irradiation the cladding creep is mostly a function of thermal creep. It can also be seen that the post base profile matches the base irradiation peaking factors seen in Figure A22.3. The diameter matching the axial profile so well supports the thought that the cladding creep is over predicted. As mentioned, Figure A22.5 also shows the post bump results. BISON under predicts the rod diameter for both the smeared and discrete cases here as well. The ramp test for this experiment had a strong axial profile by design. The diameter profile for both BISON cases does match the axial profile. The difference between the post ramp measured results and the discrete average diameter in the power tilted region is about 0.005 mm.

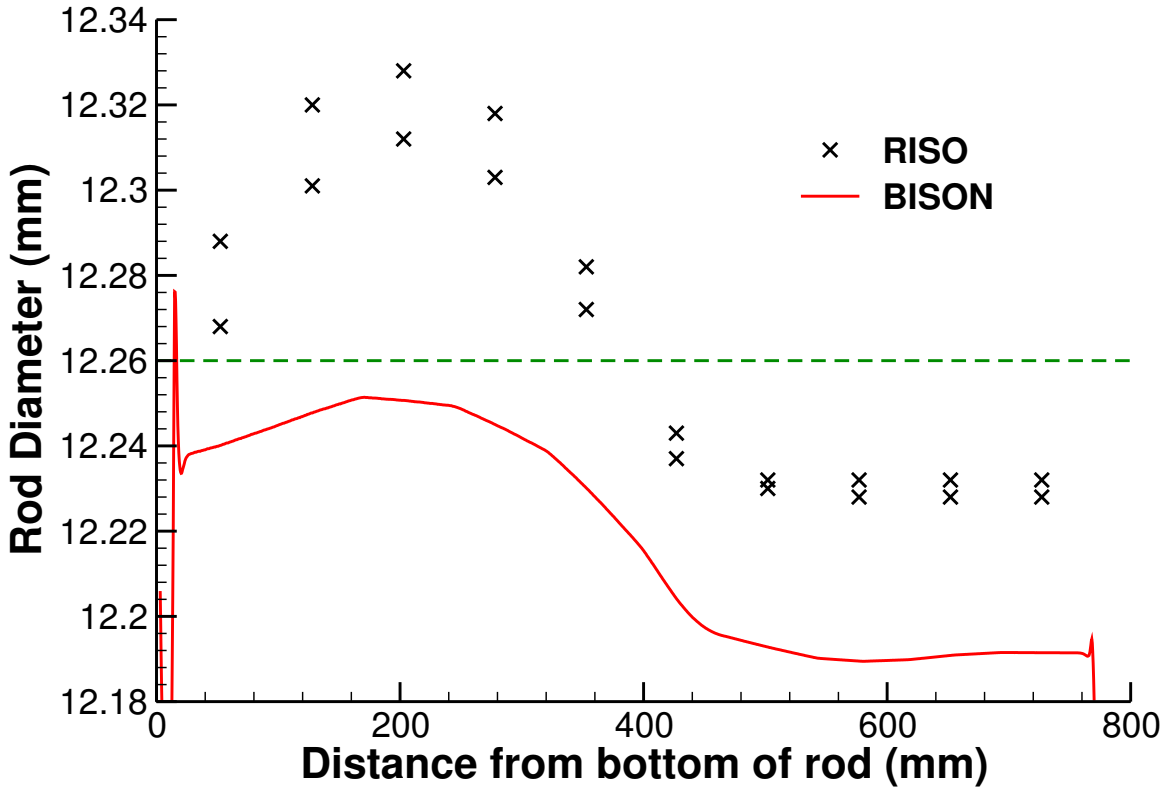

Figure A22.5: Risø GE7 experimental rod diameter comparisons before and after the power ramp.

A22.4.2 Other Results

The Risø GE7 experiment was centered around fuel rod diameter, but other parameters were measured as well. Figure A22.6 is a composite of the other parameters measured during the ramp. Figure A plots the fuel centerline temperature of the smeared pellet simulation against the discrete pellet model. The plot shows that the two models compare very closely with the discrete pellet having a slightly higher temperature in the ramp. Figure B is of the fission gas released. The measured results were taken at the end of the ramp test by puncture method. Both the smeared and the discrete models compare well to the measured results. The discrete compares better with slightly more fission gas release, this is due to the higher temperature the discrete pellets saw. Figure C plots the plenum pressure of the test. Once again the smeared and the discrete models compare well to the post ramp puncture test. The discrete model shows a higher internal pressure during the ramp caused by the combination of higher temperature and increased fission gas release. Figure D plots the internal gas volume of the rod. The smeared and discrete cases follow each other until just after the start of the high power ramp. Current thoughts on what is happening here are as follows: As the temperature increases the fuel stack volume increases due to thermal expansion and fuel swelling causing the gas volume it decrease. Shortly after the start of the ramp the smeared and discrete cased diverge and the discrete gains volume. Thoughts are that the thermal expansion takes over and opens the gap between the pellets. This also starts to cause the bamboo effect on the cladding as it creeps down. The gaps opening and possible clad lift due to bambooing could account for the gas volume increase. It should be noted that the abrupt down spike at the end of the run is from numerical error. The end results for free gas volume are under estimated.

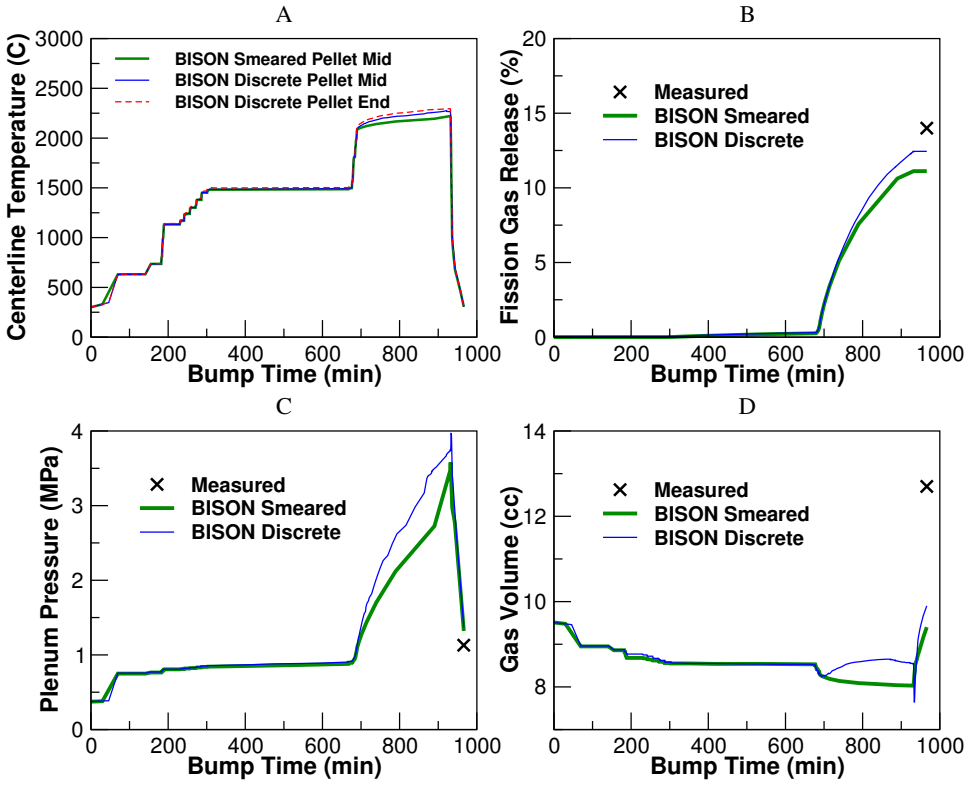

Figure A22.6: BISON and Risø GE7 results for A) BISON calculated fuel centerline temperature B) fission gas release C) plenum pressure D) free gas volume during and after the power ramp.

A22.4.3 Discussion

From the results shown above it can be seen that BISON over predicts the cladding creep in both the base irradiation and the ramp phases of this experiment. Going in to this experiment there were a couple assumptions made that will affect the outcome of the diameter. Cladding oxidation was omitted, due to this BISON should always under predict the rod diameter. The fuel was modeled as elastic and there was no frictional contact between the fuel and cladding. Both of these will change the overall results of this simulation. As mentioned in the previous section both smeared and discrete post ramp FGR, plenum pressure and gas volume all compare to each other and the measured results. As new methods are implemented in to BISON this simulation will be revisited.

A23 OSIRIS J12

A23.1 Overview

This test is of a segmented PWR rod base-irradiated in the Electricity of France (EDF) Gravline 5 PWR [45]. The segment was then re-fabricated and ramp-tested in the French Alternative Energies and Atomic Energy Commission (CEA) OSIRIS reactor to investigate PCMI resistance. This experiment was chosen because it allows for an evaluation of several aspects of the code, including fully coupled thermo-mechanics, contact, and several nonlinear material models.

A23.2 Test Description

A23.2.1 Rod Design Specifications

The geometric input parameters for the OSIRIS J12 test are summarized in Table A23.1.

Table A23.1: OSIRIS J12 Test Rod Specifications

Fuel Rod		
Overall length	m	0.5224
Fuel stack height	m	432.95
Nominal plenum height	mm	89.44
Number of pellets per rod		32
Fill gas composition		He
Fill gas pressure	MPa	2.6
Fuel		
Material		UO_2
Enrichment	%	4.5
Density	%	95.73
Outer diameter	mm	8.192
Pellet geometry		Dished
Grain diameter	μm	10
Pellet Dishing (no chamfers)		
Dish diameter	mm	6
Dish depth	mm	0.32
Cladding		
Material		Zr-2
Outer diameter	mm	9.5
Inner diameter	mm	8.36
Wall thickness	mm	0.57

A23.2.2 Operating Conditions and Irradiation History

The approximately 0.522 m segmented Zircaloy-4 clad rod was irradiated for 2 cycles in the EDF Gravline 5 PWR to a final discharge burn-up of 23.852 MWd/kgU. The average powers in the 2 cycles were approximately 16 and 23 kW/m. The rod segment designated J12-5, which was irradiated in the fifth span from the lower end of the assembly, was refabricated with new end plugs without altering either the fuel column or the internal fill gas. After a conditioning period of 762 minutes at 21 kW/m, the power was increased quickly (9 kW/m/min.) and held at 39.5 kW/m for 739 minutes. The axial profile was flat during base irradiation. The peaking factors during the bump test varied from approximately 0.75 at the ends of the segment to 1 at the center. The power history is presented in Figure A23.1, and the power ramp is shown in Figure A23.2. The initial fill-gas (Helium) pressure was 2.6 MPa, and the coolant pressure was 15.5 MPa. The external clad temperature was defined as a function of time and constant in space over the section of rod, the specified clad temperature in Figure A23.3 was used in this simulation. The clad temperature was about 585 K during base irradiation and about 615 K during the ramp. The fast neutron flux in the clad was supplied via input using experimental data supplied with the experiment. Operational input parameters are summarized in Table A23.2.

Table A23.2: Operational input parameters.

Base Irradiation		
Coolant inlet temperature	C	
Coolant pressure	MPa	15.5
Fast neutron flux	n/(m^2·s) per (W/m)	4.8·10^{13}
Power Ramp		
Coolant inlet temperature	C	
Coolant pressure	MPa	14.7
Fast neutron flux	n/(m^2·s) per (W/m)	4.8·10^{13}

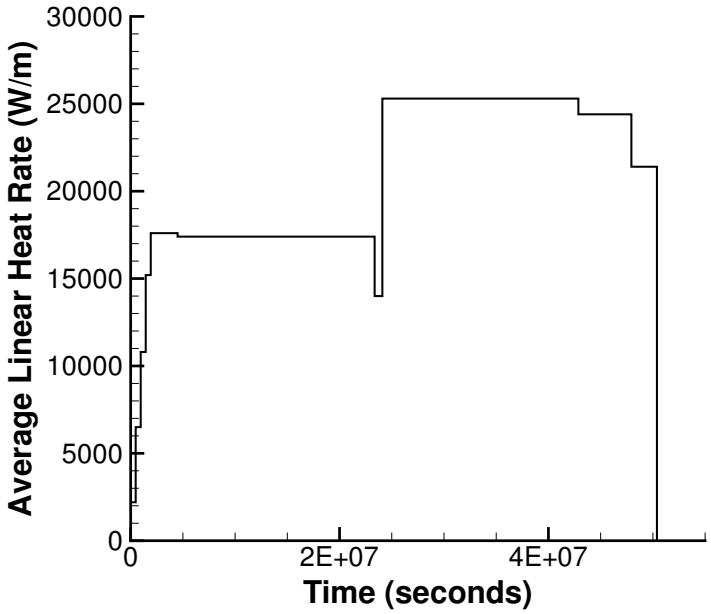

Figure A23.1: OSIRIS J12 power history in the Gravlines 5 PWR.

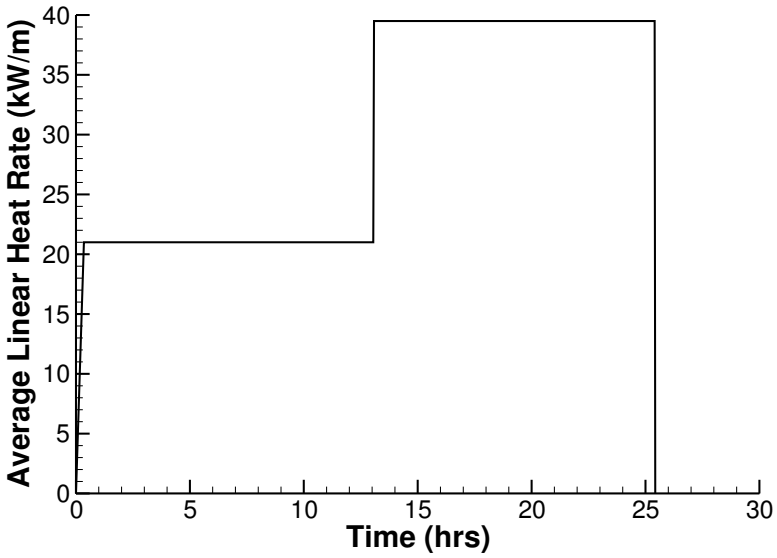

Figure A23.2: OSIRIS J12 power ramp

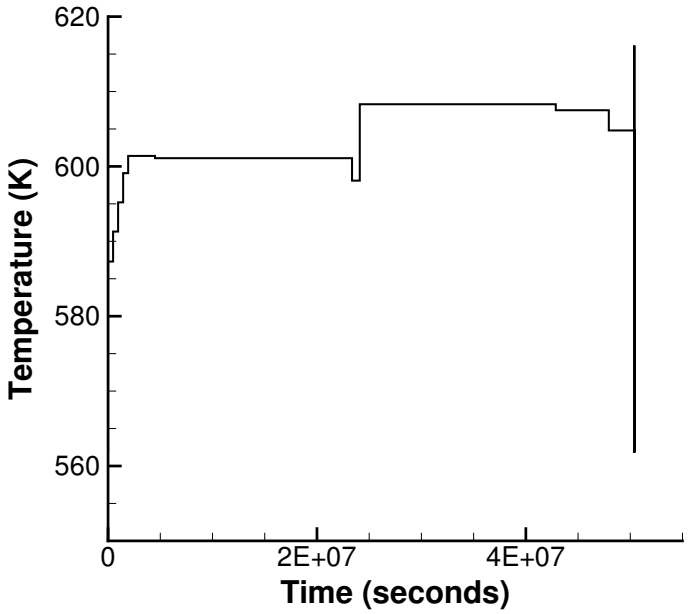

Figure A23.3: OSIRIS J12 clad temperature

A23.3 Model Description

A23.3.1 Geometry and Mesh

The rod specifications in Table A23.1 were used as input for the geometry for this simulation. The J12-5 rod was modeled as a 2D-RZ axisymmetric discrete pellet mesh with quadratic elements. Each pellet consisted of 16 axial elements and 9 radial elements. The clad was meshed with 4 elements through the thickness. Figure A23.4 is a section of the mesh with a temperature contour.

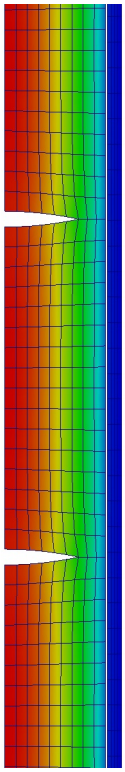

Figure A23.4: OSIRIS J12-5 mesh with temperature contour.

A23.3.2 Material and Behavioral Models

The following material and behavioral models were used for the UO_2 fuel:

- ThermalFuel - NFIR: temperature and burnup dependent thermal properties
- RelocationUO2: relocation strains, relocation activation threshold power set to 5 kW/m.
- Sifgrs: Simplified fission gas release model with a combined solid/gaseous swelling model based on fission gas release.

For the clad material, a constant thermal conductivity of 16 W/m-K was used and both thermal (primary and secondary) and irradiation creep were considered.

A23.3.3 Input files

The BISON input and all supporting files (power histories, axial power profile, fast neutron flux history, etc.) for this case are provided with the code distribution at bison/assessment/OSIRIS_J12/analysis.

A23.4 Results Comparison

A23.4.1 Clad Diameter

A comparison of the predicted and measured rod outer diameter is shown in Figure A23.5. The solid blue line is the as-manufactured rod diameter, prior to irradiation. The experimental data, shown as "+" (post-ramp) and "x" (pre-ramp) symbols, indicate the measured average rod diameter at both the end and middle fuel pellet locations, giving an indication of rod ridging due to pellet hour-glassing. The green solid line is the predicted rod diameter following the power bump and the red solid line is the predicted rod diameter prior to the ramp.

BISON under predicts clad creep down resulting in a larger than measured diameter. The overall shape of the rod after the ramp is captured well with BISON, as well as the clad ridging caused by the hour glassing (bamboo effect) of the discrete pellets.

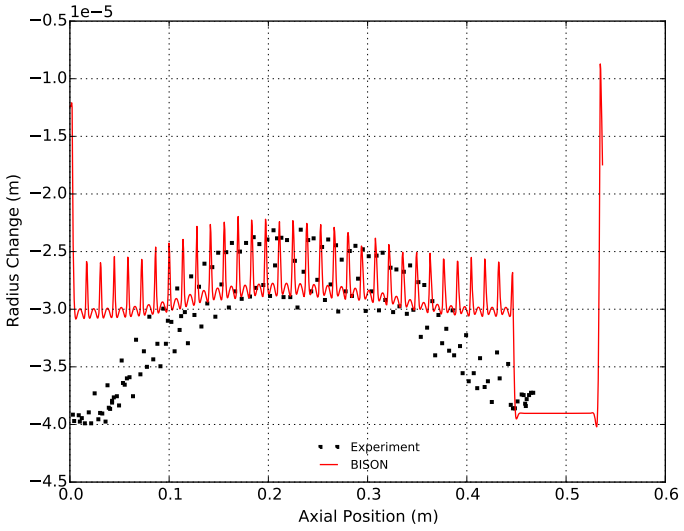

Figure A23.5: OSIRIS J12 experimental measurements and BISON calculation results from before and after the power ramp.

A24 OSIRIS H09

A24.1 Overview

The OSIRIS H09 test rod is a standard full length PWR rod that was irradiated for 4 cycles in the Electricity of France (EDF) Cruas 2 PWR to a final discharge rod average burn-up of 46.06 MWd/kgU [64]. This experiment was chosen for analysis because of the availability of measured data for evaluation of several fuel rod performance characteristics including fission gas release, cladding hydrogen content, fuel column length changes, rod growth, oxide thickness, rod internal pressure, whole pellet density, end-of-life internal free volume, and radial distribution of Cs, Nd, Pu and Xe.

A24.2 Test Description

A24.2.1 Rod Design Specifications

The geometric input parameters for the OSIRIS H09 rod are summarized in Table A24.1.

Table A24.1: OSIRIS H09 Test Rod Specifications.

Fuel Rod		
Overall length	m	3.8517
Fuel stack height	m	3.66038
Nominal plenum height	m	0.13932
Fill gas composition		He
Fill gas pressure	MPa	3.1
Fuel		
Material		UO_2
Enrichment	%	3.249
Density	%	95.31
Outer diameter	mm	8.190
Nominal diametral gap	μm	160
Average grain size	μm	9.060
Cladding		
Material		Zr-4
Outer diameter	mm	9.508
Inner diameter	mm	8.35
Wall thickness	mm	0.575

A24.2.2 Operating Conditions and Irradiation History

The H09 rod was irradiated for 4 cycles in the OSIRIS reactor to a final discharge average burnup of 46.06 MWd/kgU. The power mode selected for this simulation is PiecewiseConstant. The average linear powers in the 4 cycles were approximately 22, 20, 18, and 15 kW/m [64]. The average power history for is shown in Figure A24.1. The power history assumed a 24 hour startup time that was broken into 24 timesteps in one hour increments. Because the axial power shapes and boundary conditions are modeled as PieceswiseBilinear, a ramp time of 360 seconds (0.1 hours) was assumed at each power step for the axial power shape and boundary condition input. The startup time of 24 hours and the ramp time of 360 seconds (0.1 hours) are based on ANATECH's experience with fuel rod modeling for steady state operation and the development of Falcon Verification and Validation cases. They are intended to minimize the introduction of computational artifacts from unrealistic power changes and ramp rates into the analyses. The axial power profile was calculated from the OSIRIS data package [64] taken from the IFPE database. The cladding outer surface temperature as a function of time was also provided in the OSIRIS data package [64], and was used as a boundary condition for this simulation. The cladding outer surface temperature ranged from 562.55 K to 611.95 K. The initial fill-gas (Helium) pressure was 3.1 MPa, and the coolant system pressure was 15.5 MPa. The fast neutron flux as a function time was calculated from the data provided in the OSIRIS data package [64]. Operational input parameters are summarized in Table A24.2.

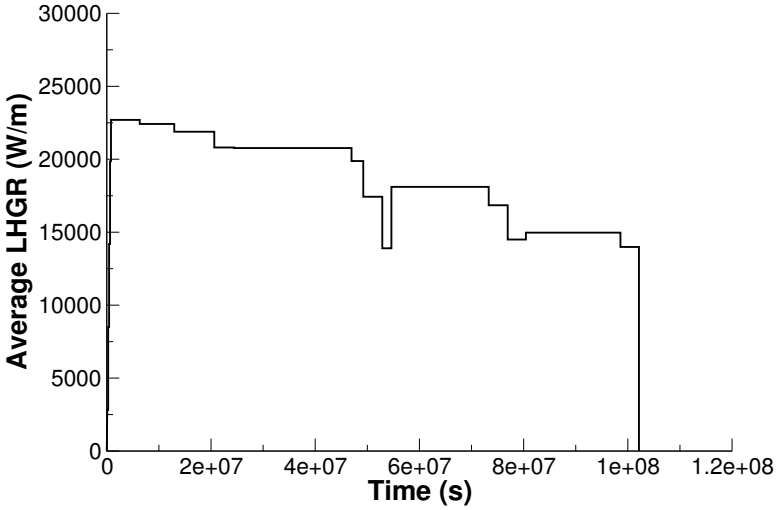

Figure A24.1: OSIRIS H09 power history with 24 hours startup

Table A24.2: Operational input parameters

Base Irradiation		
Coolant inlet temperature	K	562.55
Coolant pressure	MPa	15.5
Fast Neutron Flux		
Cycle 2	n/(m^2·s) per (W/m)	4.2·10^{13}
Cycle 3	n/(m^2·s) per (W/m)	4.6·10^{13}
Cycle 4	n/(m^2·s) per (W/m)	4.8·10^{13}
Cycle 6	n/(m^2·s) per (W/m)	4.8·10^{13}

A24.3 Model Description

A24.3.1 Geometry and Mesh

The rod specifications in Table A24.1 were used to define the geometry for this simulation. The OSIRIS H09 rod was modeled as a two-dimensional, axi-symmetric linear mesh with quadratic elements. The fuel mesh consisted of 11 radial elements and the cladding mesh consisted of four radial elements to form a clad thickness of 0.575 mm. The fuel stack length is 3.66 m and the plenum height is 0.139 m. The mesh of the top portion of the rod is shown in Figure A24.2.

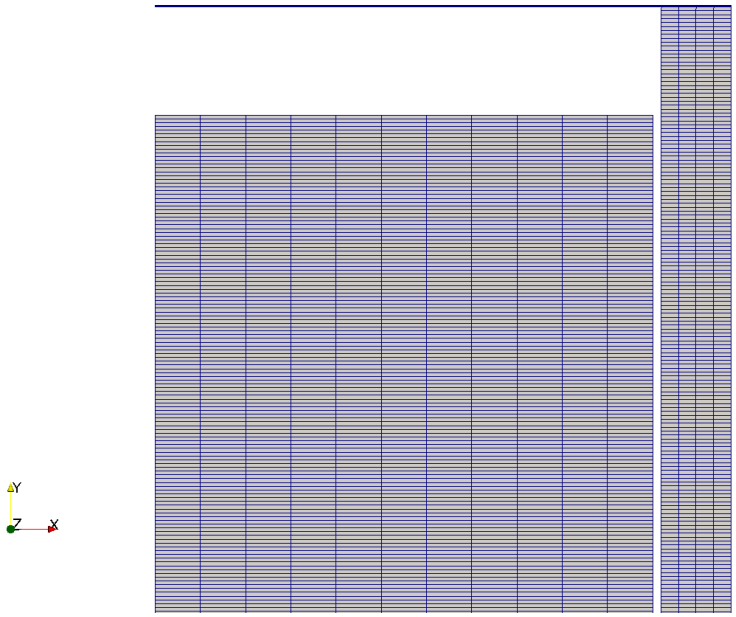

Figure A24.2: OSIRIS H09 mesh (not to scale)

A24.3.2 Material and Behavioral Models

The following material and behavioral models were used for the UO_2 fuel:

- ThermalFuel - NFIR: temperature and burnup dependent thermal properties.
- RelocationUO2: relocation strains, relocation activation threshold power set to 5 kW/m.
- Sifgrs: fission gas release model with the combined gaseous swelling model.
- MechZry: model irradiation growth for Zircaloy-4.

For the cladding material, a constant thermal conductivity of 16 W/m-K was used and both thermal and irradiation creep were considered using the Limback model [36].

A24.3.3 Input files

The BISON input and all supporting files (power histories, axial power profiles, etc.) OSIRIS H09 rod are provided with the code distribution at folder bison/assessment/OSIRIS_H09/analysis in the code repository.

A24.4 Results Comparison

Data from the OSIRIS fuel irradiation program was used to assess the code's capability to capture the integral fuel rod fission gas release, rod internal pressure, rod growth, fuel column length changes, axial cladding diameter, cladding hydrogen content and oxide thickness at the end of life. A comparison of the predicted values from BISON calculations versus measured values from experimental data are shown in Table A24.3. Because the feature to calculate cladding hydrogen concentration and oxide thickness are not currently available in BISON, these comparisons will be performed in the future. The final burnup calculated was 44.64 MWd/kgU compared to 46.06 MWd/kgU burnup in the test documentation.

Table A24.3: Bison prediction versus measured data for OSIRIS H09.

	BISON prediction	Measured Data
Burnup (MWd/kgU)	44.65	46.06
Fission Gas Release (%)	0.21	0.8
EOL Rod Internal Pressure at RT (MPa)	6.67	4.338
EOL Internal free volume (cc)	9.35	11.1
Fuel column changes (mm)	22.41	26.62
Fuel rod growth (mm)	23.08	28.8

A24.4.1 Fission Gas Release

The fission gas release data available for this experiment is from post irradiation examination (PIE) puncture tests. Figure A24.3 show BISON's comparisons with the end-of-life measurement for the OSIRIS H09 rod. BISON computes a reasonable FGR value that under predicts the measured result.

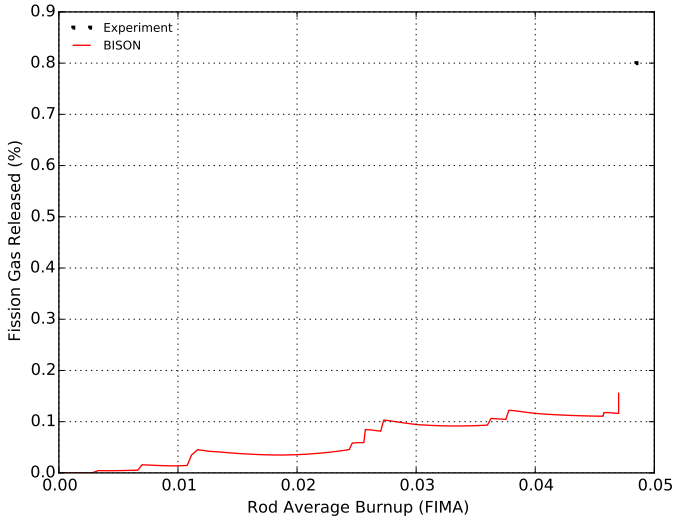

Figure A24.3: Fission gas release comparisons for OSIRIS H09

A24.4.2 Rod Internal Pressure

The only rod internal pressure data available for this experiment is from PIE puncture tests at the end-of-life. Figure A24.4 shows BISON's comparisons to the experimental data for the OSIRIS H09 rod. The figure shows BISON over predicts the rod internal pressure.

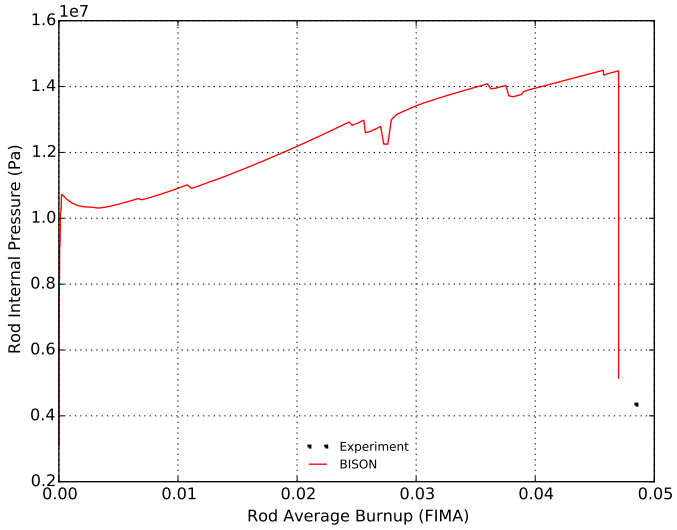

Figure A24.4: Rod internal pressure comparison for OSIRIS H09

A24.4.3 Cladding Diameter

The calculated final rod diameter as a function of axial position is compared to measured data. A comparison of the computed and measured end-of-life rod diameter data (excluding oxide thickness) is shown in Figure A24.5. The figure shows BISON over predicts the cladding diameter at the end of life which results in less cladding computed creep down than measured.

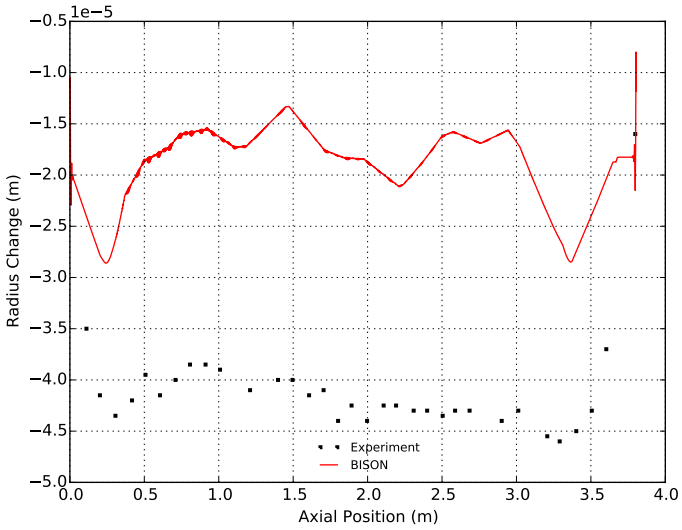

Figure A24.5: EOL average cladding diameter comparisons for OSIRIS H09

A24.4.4 Discussion

Based on the data presented above, several observations can be made regarding the results obtained from BISON analyses of the OSIRIS H09 test rod.

- BISON's prediction the EOL FGR is reasonable, but somewhat low.

- BISON over predicts the measured rod internal pressure by a fairly large margin.
- BISON over predicts measured EOL cladding diameter.
  - Based on evaluation of these and other assessment cases, this behavior appears to be related to fuel swelling after fuel/cladding contact. Additionally, other effects on fuel deformation including relocation, densification, fuel creep, etc. could influence the behavioral response in these analyses.

Since cladding oxide thickness and hydrogen concentration data are available for OSIRIS H09 rod, these characteristics should be evaluated in the future once these features are available in BISON.

A25 REGATE

A25.1 Overview

Regate is one of the experiments of the Fuel Modeling at Extended Burnup (FUMEX-II) program [21]. This experiment was carried out in order to provide data on Fission Gas Release (FGR) and clad diameter change. The rod is a short fuel segment irradiated in a commercial PWR and ramped in the french SILOE test reactor. The original segment was base irradiated in the Gravlines 5 PWR up to 47.415 MWd/kgHM.

Non-destructive post-irradiation examination (PIE) was performed on the fuel segment after discharge from the Gravlines 5 PWR with measurements on clad diameter and total fission gas release (based on Kr-85 gamma scan measurements), the total measured FGR after base irradiation was 1.5%. It is important to note that the fuel segment was not subject to any re-fabrication after base irradiation in Gravlines 5 PWR (power history shown in Figure A25.1).

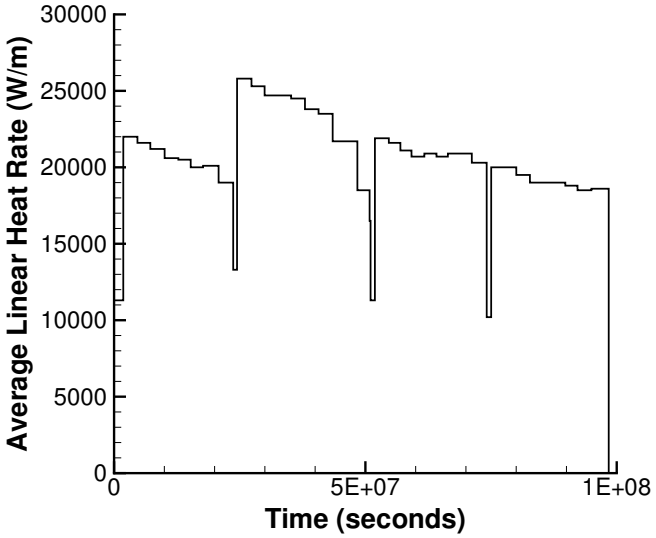

Figure A25.1: Rod average power history in the Gravlines 5 reactor.

The Kr-85 concentration was also measured with gamma scanning to measure a total of 9.3% FGR after the ramp test in the SILOE reactor. Puncturing tests were done after the power ramp in the SILOE reactor, to measure the total FGR of 10.2%. The oxide layer thickness and total clad diameter were also measured in PIE after the ramp test.

BISON comparisons to clad diameter and FGR are reported herein.

A25.2 Test Description

A25.2.1 Rod Design Specifications

The geometric input parameters for the FumexII–Regate case are summarized in Table A25.1.

Table A25.1: Regate geometric input parameters

Fuel Rod		
Overall length	m	0.522
Fuel stack height	m	0.43595
Nominal plenum height	mm	48.15
Number of pellets per rod		32
Fill gas composition		He
Fill gas pressure	MPa	2.5
Fuel		
Material		UO_2
Enrichment	%	4.487
Density	%	94.8
Outer diameter	mm	8.192
Pellet geometry		dished
Grain diameter	μm	8.7
Pellet Dishing		
Dish diameter	mm	6
Dish depth	mm	0.32
Chamfer width	mm	0.531
Chamfer depth	mm	0.16
Cladding		
Material		Zr-2
Outer diameter	mm	9.5
Inner diameter	mm	8.36
Wall thickness	mm	0.57

A25.2.2 Operating Conditions and Irradiation History

The irradiation was adjusted by varying the distance of the rig from the SILOE core. The ramp test irradiation history consisted of a pre-condition power step of 19.5 kW/m (peak power) for 48 hours, prior to ramping at 1.0 kW/m/min up to 38.5 kW/m (peak power) which was held for 1.5 hours. The rod average power history during the SILOE irradiation is shown in Figure A25.2. As the height of the SILOE reactor ($\sim$0.6 m) is comparable to the segment length ($\sim$0.44 m), the axial power is not flat during the ramp test, leading to values of $P_{average}/P_{max}$ of 0.9 and P_{min}/P_{max} of 0.65.

Table A25.2: Operational input parameters.

Base Irradiation		
Clad temperature	C	317
Coolant pressure	MPa	15.5
Fast neutron flux		Figure A25.3
Power Ramps		
Clad temperature	C	77 -338
Coolant pressure	MPa	13
Fast neutron flux	n/(cm^2·s)	2.0·10^{13}

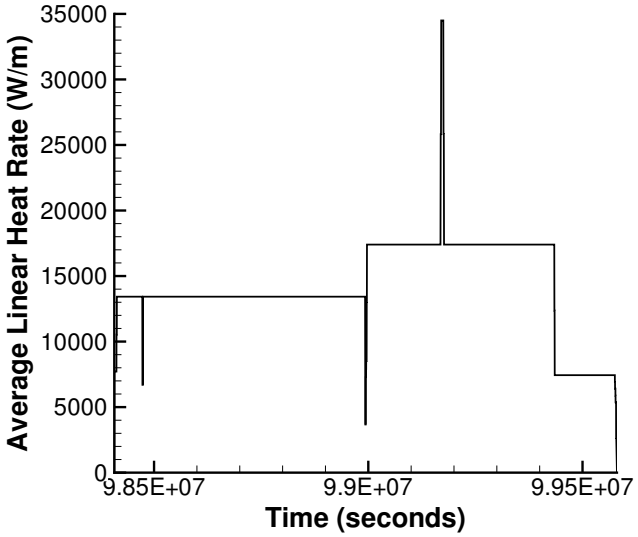

Figure A25.2: Rod average power history in the SILOE reactor.

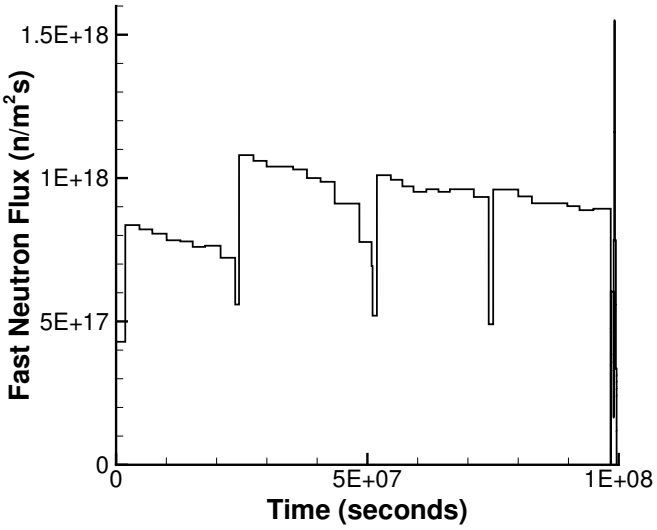

Figure A25.3: Fast neutron flux history. This history was supplied with the experimental data.

A25.3 Model Description

A25.3.1 Geometry and Mesh

A 2D-RZ axisymmetric discrete pellet mesh with quadratic elements was used to model this experiment. Each pellet was meshed with 16 axial and 9 radial elements. The clad was meshed with 4 axial elements. Figure A25.4 shows a section of the meshed with a temperature contour plot during the ramp test.

A25.3.2 Material and Behavioral Models

The following material and behavioral models were used for the UO_2 fuel:

- ThermalFuel - NFIR: temperature and burnup dependent thermal properties

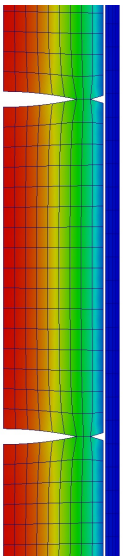

Figure A25.4: Section of mesh used for Regate simulation with temperature contour during the ramp test in the SILOE reactor.

- RelocationUO2: relocation strains, relocation activation threshold power set to 5 kW/m.
- Sifgrs: Simplified fission gas release model with a combined solid/gaseous swelling model based on fission gas release.

For the clad material, a constant thermal conductivity of 16 W/m-K was used and both thermal and irradiation creep were considered using the Limback model [36]. Due to the high mises stress in the clad, plasticity was also used to get the proper deformation during the power ramp in the Risø DR3 reactor.

A25.3.3 Input files

The BISON input and all supporting files (power histories, axial power profile, fast neutron flux history, etc.) for this case are provided with the code distribution at bison/assessment/FUMEXII_Regate/analysis.

A25.4 Results Comparison

A25.4.1 Fission Gas Release

BISON over predicts FGR after the base irradiation in the Gravlines 5 PWR and under predicts the FGR at the end of the ramp test. The comparisons are plotted in Figure A25.5.

A25.4.2 Clad Diameter

BISON over predicts clad creep down which results in a smaller diameter than measured during PIE. The BISON comparisons to experimental measurements before and after the ramp are shown in Figure A25.6.

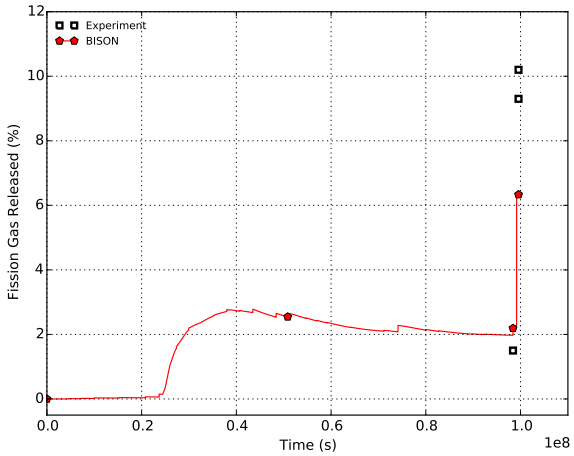

Figure A25.5: BISON FGR comparisons to experimental data.

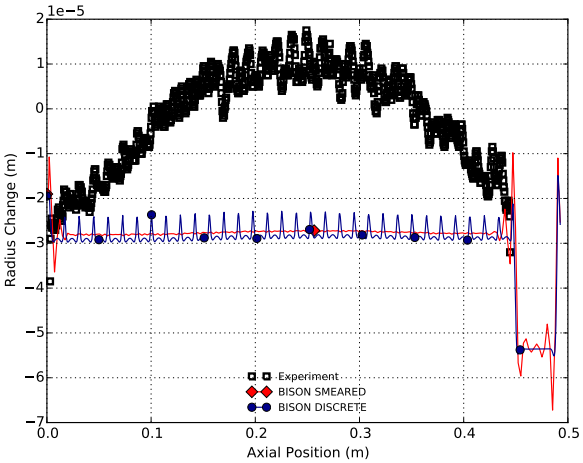

Figure A25.6: BISON rod diameter comparisons to experimental measurements before and after the power ramp.

A26 TRIBULATION Rod BN1/3, rod BN1/4, and Rod BN3/15

A26.1 Overview

The objectives of the TRIBULATION (Tests Relative to High BUrnup Limitations Arising Normally in LWR's) International Programme were to 1) assess fuel rod behaviour at high burnup with an earlier transient and 2) to investigate the behaviour of different fuel rod designs and manufacturers when subjected to a steady state irradiation history to high burn-up. The program was organized jointly by BelgoNucleaire and the Nuclear Energy Centre at Mol (CEN/SCK) with the co-sponsorship of 14 participating organizations [65]. For the purpose of this fuel analysis problem, three out of the 19 fuel rods from the TRIBULATION Database [66] were evaluated with BISON. The three fuel rods were fabricated by BelgoNucleaire (BN) and are referred to as test rods BN1/3, BN1/4 and BN3/15 in this document. All three rods used standard Zircaloy-4 cladding and were discharged at rod average burnups of approximately 51.6, 51.2, and 51.1 MWd/kgU, respectively. Non-destructive post irradiation examination (PIE) was performed at various stages throughout testing of the BN rods for cladding creep down, cladding ovalization, rod growth and fuel column length changes. Destructive PIE was performed at the end-of-life for fission gas release and internal void volume. This experiment was chosen for analysis because of the availability of measured data for evaluation of several fuel rod performance characteristics including fission gas release, cladding creep down, fuel column length changes, rod growth and end-of-life internal free volume.

A26.2 Test Description

A26.2.1 Rod Design Specifications

An overview of the test matrix and cross reference identification data for BN1/3, BN1/4 and BN3/15 are shown below in Table A26.1 [66]. The specific geometric input parameters for the test rods are summarized in Table A26.2. BN1/3 contained fuel pellets from two different batches with slightly different pellet mean densities. This simulation assumed the same pellet density of 10.408 g/cm^3 for test BN1/3 because the two densities were close to each other. The fuel pellets for BN1/3 and BN1/4 have an initial enrichment of 8.25% while BN3/15 had an initial enrichment of 5.76%. The cladding material for all three rods was Zircaloy-4. The cladding was stress relieved at 460 C for 2.5 hours. BN1/3 and BN1/4 were pressurized with helium to 1.96 MPa (20 kg/cm^2) while BN3/15 was pressurized to 0.098 MPa (1 kg/cm^2).

Table A26.1: Overview of test matrix for test rods BN1/3, BN1/4 and BN3/15

Matrix No.	Test No.	Rod No.	BR3 cycle Nos.	BR2 transient Power (kW/m)	BR3 cycle Nos.	History
3	BN1/3	3-47	4B	34.7(for 540 sec)	4C, 4D1	NDT, T, NDT, BR3(4C+4D), NDT, DT
4	BN1/4	3-342	4B		4C, 4D1	NDT, BR3(4C+4D), NDT, DT
15	BN3/15	1-610	4A, 4B		4D2	NDT, BR3(4D), NDT, DT

NDT = non destructive tests
DT = destructive tests
T = transient irradiation in BR2

Table A26.2: BN1/3, BN1/4 and BN3/15 Rod Specifications.

Fuel Rod	Unit	BN1X3	BN1X4	BN3X15
Overall length	m	1.1352	1.1360	1.1358
Fuel stack height	m	1.0019	0.9976	0.9956
Upper plenum height	mm	88.3	93.4	95.2
Fill gas composition		He	He	He
Fill gas pressure	MPa	1.96133	1.96133	0.09807
Fuel	Unit	BN1/3	BN1/4	BN3/15
Material		UO_2	UO_2	UO_2
Enrichment	%	8.25	8.25	5.76
Pellet mean density	g/cm3	10.408-10.340	10.355	10.435
Pellet mean density	$\%TD$	94.965-94.345	94.474	95.037
Outer diameter	mm	8.04	8.04	8.04
Nominal diametral gap	μm	200	200	200
Average grain size	μm	11	11	10
Cladding	Unit	BN1/3	BN1/4	BN3/15
Material		Zr-4	Zr-4	Zr-4
Outer diameter	mm	9.50 +/- 0.04	9.50 +/- 0.04	9.50 +/- 0.04
Inner diameter	mm	8.24 +/- 0.04	8.24 +/- 0.04	8.24 +/- 0.04
Wall thickness	mm	not $<$0.58	not $<$0.58	not $<$0.58

A26.2.2 Operating Conditions and Irradiation History

The irradiation of the BelgoNucleaire (BN) fuel rods chosen for the TRIBULATION programme was carried out in the BR2 and BR3 reactors of the Nuclear Energy Centre at Mol at Mol-Belgium (CEN/SCK). The base irradiation for BN1/3, BN1/4 and BN3/15 was performed in the BR3 reactor up to a specified preconditioning burnup between 20 and 40 GWd/tM peak pellet. Following the base irradiation, the rods were non-destructively examined. BN1/3 was transferred to the BR2 reactor for fast operational transient testing and then continued further irradiation in BR3. The fast operational transient for test BN1/3 consisted of a preconditioning period of at approximately 2 days 26600 W/m, followed by a rapid power increase to 35400 W/m at a ramp rate of approximately 1960 W/m/s. After a hold period of about 9 minutes, the power was then rapidly decreased to near the preconditioning level. Following the base irradiation and non-destructive exmaination, BN1/4 and BN3/15 were transferred back to the BR3 reactor for further irradiation.

The power mode selected for this simulation is PiecewiseConstant. The power histories for BN1/3, BN1/4, and BN3/15 are shown in Figures A26.1, A26.2 and A26.3, respectively. These three power histories assumed a 24 hour startup time that was broken into 24 timesteps of one hour increments. Because the axial power shapes and boundary conditions are modeled as PieceswiseBilinear, a ramp time of 360 seconds (0.1 hours) was assumed at each power step for the axial power shape and boundary condition input. The startup time of 24 hours and the ramp time of 360 seconds (0.1 hours) are based on ANATECH's experience with fuel rod modeling for steady state operation and the development of Falcon Verification and Validation cases. They are intended to minimize the introduction of computational artifacts from unrealistic power changes and ramp rates into the analyses. The axial power profile and cladding outer surface temperature profile as a function of time were calculated from the TRIBULATION data package [66]. The initial fill-gas (Helium) pressure was 1.96 MPa for BN1/3 and BN1/4 and 0.098 MPa for BN3/15. The coolant system pressure was 13.729 MPa for the BR3 irradiation and 14.0 MPa for the BR2 irradiation. The fast neutron flux profile was scaled to a factor of 4.8e17. Operational input parameters are summarized in Table A26.3.

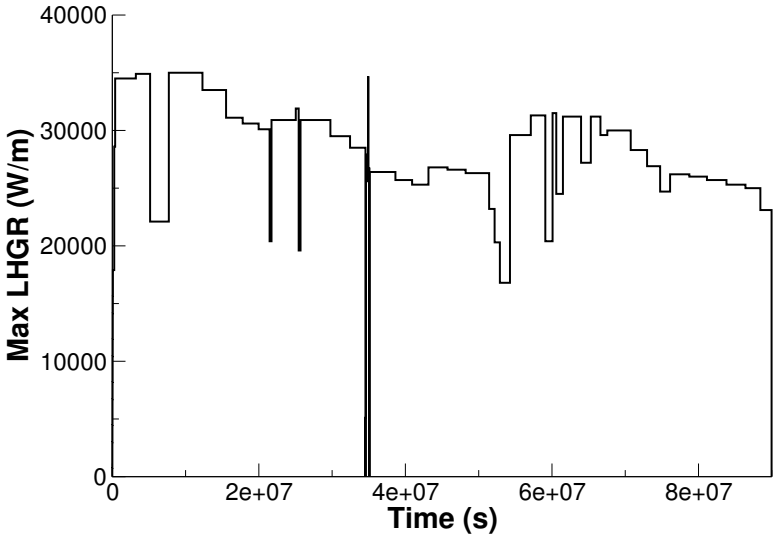

Figure A26.1: BN1/3 power history

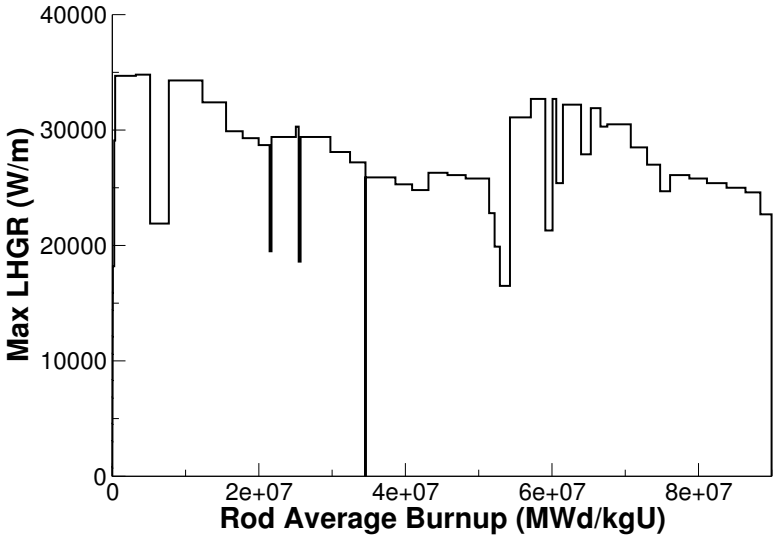

Figure A26.2: BN1/4 power history

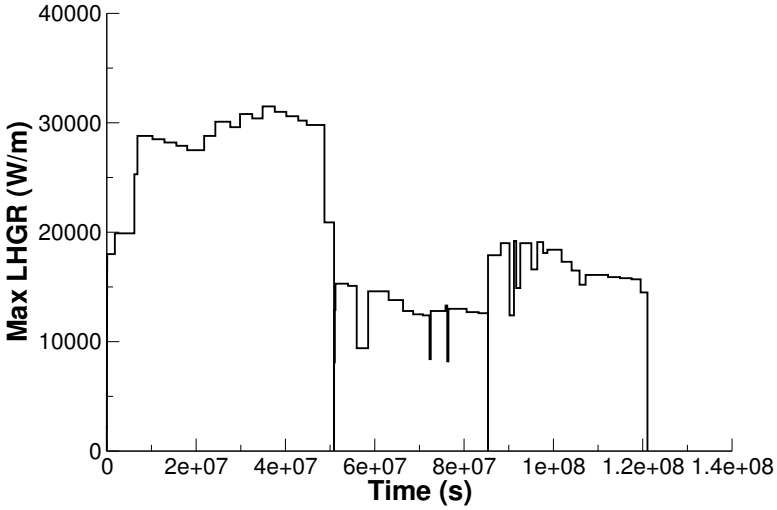

Figure A26.3: BN3/15 power history

Table A26.3: Operational input parameters

Base Irradiation		
Coolant inlet temperature	K	529.15
Coolant pressure for BR3 Irradiation	MPa	13.729
Coolant pressure for BR2 Irradiation	MPa	14.0

A26.3 Model Description

A26.3.1 Geometry and Mesh

The rod specifications in Table A26.2 were used to define the geometry for these simulations. The BN1/3, BN1/4 and BN3/15 rods were modeled as a two-dimensional, axi-symmetric linear mesh with quadratic elements. The fuel mesh for all three rods consisted of 11 radial elements and the cladding

mesh consisted of four radial elements to form a cladding thickness of 0.63 mm. In order to accurately model the fuel rod initial free volume, the overall fuel rod length and upper plenum height were adjusted during mesh generation to account for the volume of the plenum spring which is not explicitly modeled. The overall fuel rod lengths for BN1/3, BN1/4, and BN3/15 were reduced from 1135.2 mm, 1136.0 mm, and 1135.8 mm to 1081.01 mm, 1081.46 mm and 1081.34 mm, respectively. The plenum heights for BN1/3, BN1/4, and BN3/15 were reduced from 88.3 mm, 93.4 mm, and 95.2 mm to 67.5 mm, 71.3 mm, and 73.1 mm, respectively. The TRIBULATION BN1/3, BN1/4 and BN3/15 meshes are shown in Figures A26.4, A26.5 and A26.6 respectively.

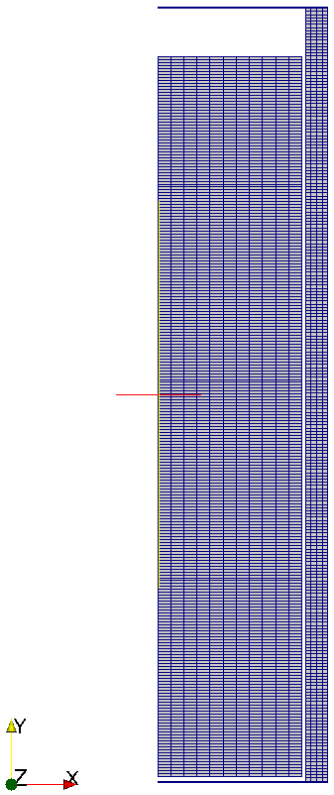

Figure A26.4: BN1/3 mesh

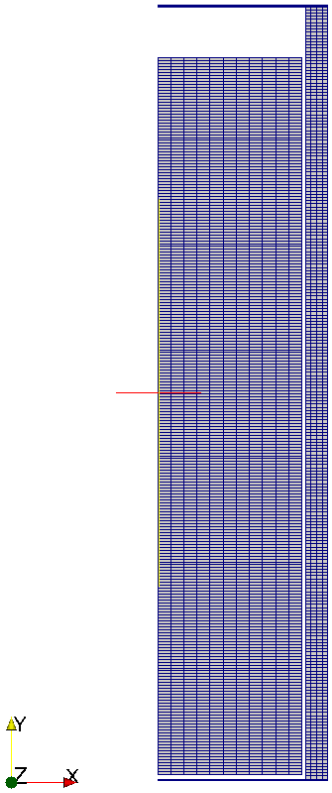

Figure A26.5: BN1/4 mesh

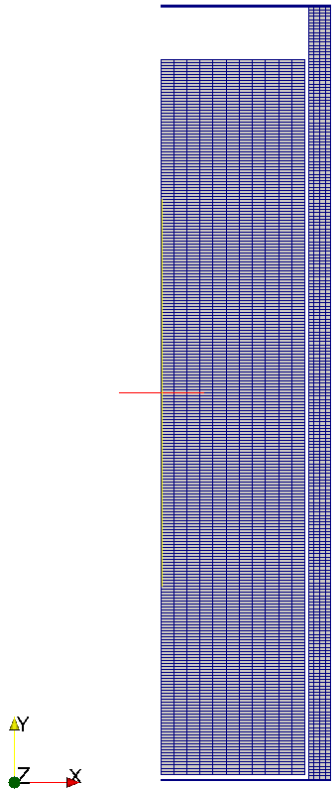

Figure A26.6: BN3/15 mesh

A26.3.2 Material and Behavioral Models

The following material and behavioral models were used for the UO_2 fuel:

- ThermalFuel - NFIR: temperature and burnup dependent thermal properties.
- RelocationUO2: relocation strains, relocation activation threshold power set to 5 kW/m.
- Sifgrs: fission gas release model with the combined gaseous swelling model.
- MechZry: model irradiation growth for Zircaloy-4.

For the cladding material, a constant thermal conductivity of 16 W/m-K was used and both thermal and irradiation creep were considered using the Limback model [36].

A26.3.3 Input files

The BISON input and all supporting files (power histories, axial power profiles, etc.) for BN1/3, BN1/4 and BN3/15 are provided with the code distribution at bison/assessment/Tribulation/analysis/BN1X3, bison/assessment/Tribulation/ analysis/BN1X4, and bison/assessment/Tribulation/analysis/BN3X15, respectively.

A26.4 Results Comparison

Data from the TRIBULATION irradiation program was used to assess the code's capability to capture the integral fuel rod fission gas release, cladding creep down strain, fuel column changes, fuel rod growth, and rod internal void volume. A comparison of the predicted values from BISON calculations versus measured values from experimental data are shown in Tables A26.4, A26.5, and A26.6 for BN1/3, BN1/4, and BN3/15 rods, respectively.

Table A26.4: Bison prediction versus measured data for BN1/3.

	BISON prediction	Measured Data
Burnup (MWd/kgU)	50.65	51.6
Fission Gas Release (%)	7.083	5.4
Fuel column changes (mm)	9.048	4.5 (Length Increase)
Final void volume (cc)	4.36	6.46
Fuel rod growth (mm)	2.877	6.03

Table A26.5: Bison prediction versus measured data for BN1/4.

	BISON prediction	Measured Data
Burnup (MWd/kgU)	50.59	51.2
Fission Gas Release %	8.335	5.5
Fuel column changes (mm)	8.915	3.9 (Length Increase)
Final void volume (cc)	4.56	6.12
Fuel rod growth (mm)	2.997	4.86

Table A26.6: Bison prediction versus measured data for BN3/15.

	BISON prediction	Measured Data
Burnup (MWd/kgU)	50.66	51.1
Fission Gas Release %	16.47	5.6
Fuel column changes (mm)	10.295	7.4 (Length Increase)
Final void volume (cc)	4.43	6.02
Fuel rod growth (mm)	2.858	1.62

A26.4.1 Fission Gas Release

The only fission gas release data available for this experiment is from destructive PIE puncture tests. Figures A26.7, A26.8, and A26.9 show BISON's comparisons with end-of-life measurement for the BN1/3, BN1/4, and BN3/15, respectively. BISON computes a reasonable FGR value that over predicts the measured results for BN1/3 and BN1/4 by a small margin. However, BISON over predicts the measured result for BN3/15 by a fairly large margin.

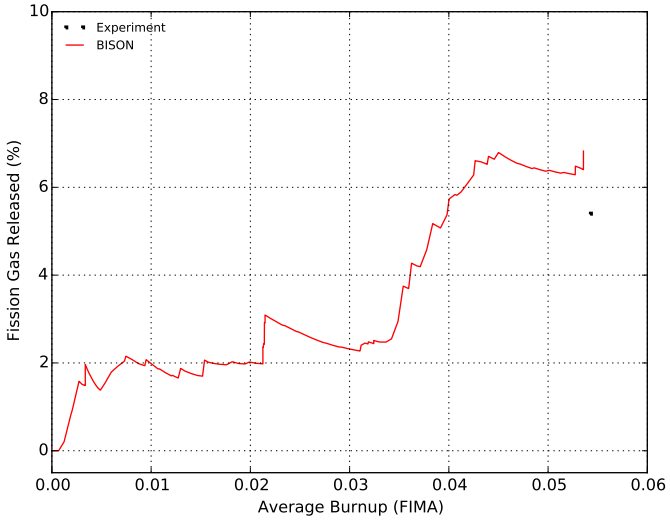

Figure A26.7: Fission gas release comparisons for BN1/3

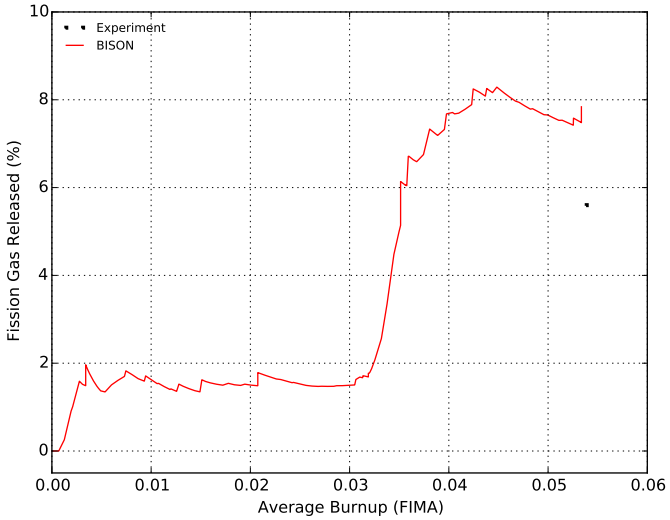

Figure A26.8: Fission gas release comparisons for BN1/4

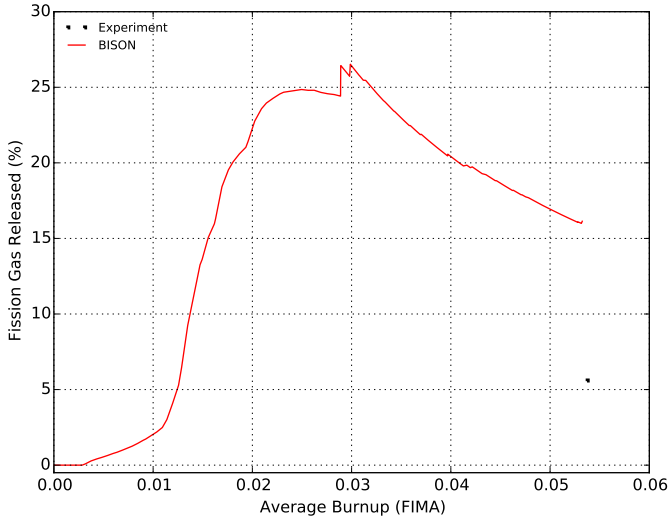

Figure A26.9: Fission gas release comparisons for BN3/15

A26.4.2 Cladding Creep Down Strain

The calculated cladding creep down strain as a function of axial position is compared to measured data. The cladding creep down strain is calculated from the computed cladding diamter. Figure A26.10 shows comparisons of BISON computed results for BN1/3 to the measured cladding creep down strain data at the end of the first BR3 irradiation, after the BR2 transient, and at the end of the second BR3 irradiation. Reasonable cladding creep down strain values are computed at the end of the first BR3 irradiation and after the BR2 transient, but not at the end of the second BR3 irradiation. BISON strongly over predicts the cladding creep down strain toward the center of the fuel stack at the end of the second BR3 irradiation. Figure A26.11 shows comparisons of BISON computed results to measured cladding creep down strain data at the end of the first and second BR3 irradiation for BN1/4. Similar to the BN1/3 results, reasonable cladding creep down values at the end of the first BR3 irradiation are computed for BN1/4, but not at the end of the second BR3 irradiation. Figure A26.12 shows comparisons of BISON computed results to measured cladding creep down strain data at the end of the second BR3 irradiation for BN3/15. For BN3/15, BISON strongly over predicts the cladding creep down strain toward the center of the fuel stack at the end of the second BR3 irradiation.

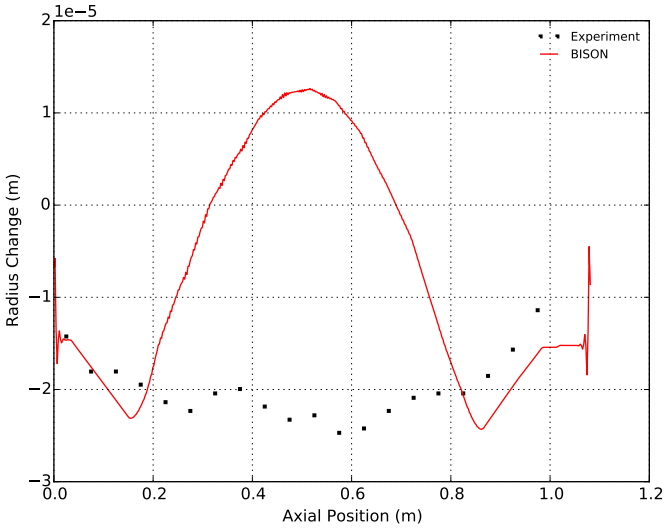

Figure A26.10: Cladding creep down strain comparisons for BN1/3

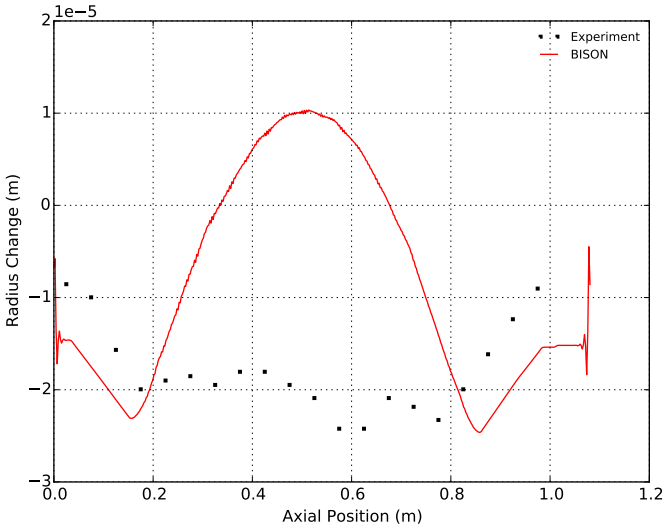

Figure A26.11: Cladding creep down strain comparisons for BN1/4

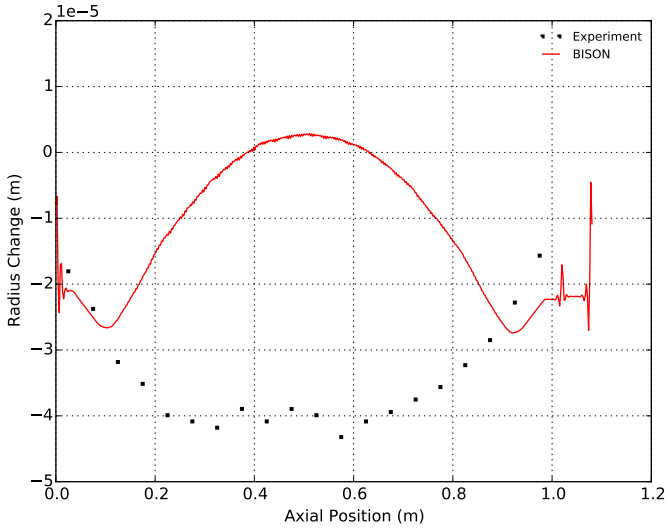

Figure A26.12: Cladding creep down strain comparisons for BN3/15

A26.4.3 Discussion

Based on the data presented above, several observations can be made regarding the code execution and the results obtained from BISON analyses of the BN1/3, BN1/4, and BN3/15 test fuel rods.

- Due to the low initial fill gas pressure for the BN3/15 rod, BISON experienced difficulty converging. The convergence issue appears to be related to fission gas release, rod internal pressure prediction and fuel/cladding contact behavior. Therefore, the PETSc option and time stepping controls were updated in the Executioner block to obtain convergence. The PETSc options selected for -pc_type and -pc_factor_mat_solver_package input is 'lu' and 'superlu_dist'. The timestep_limiting_function, max_function_change, and force_step_every_function_point options were not used. These updates resolve the convergence issues for the simulation of BN3/15 rod. However, this issue warrants further review for the analysis of rods with low initial fill gas pressure.
- BISON over predicts the EOL FGR by a large margin for BN3/15 rod.
  - From Figures A26.7, A26.8 and A26.9, sharp increases in FGR can be seen that correspond to large power drops. This rapid release of fission gas during power drop appears to be characteristic of the SIFGRs model implemented in BISON. This response may not be representative of FGR kinetics and warrants further review.
- BISON over predicts the EOL cladding creep down strain for all three rods by a very large margin.
  - Based on evaluation of these and other assessment cases, this behavior appears to be related to fuel swelling, especially affecting cladding creep down after fuel/cladding contact. Additionally, other effects on fuel deformation including relocation, densification, fuel creep, etc. The combined effect of these mechanisms could also influence the behavioral response seen in these analyses.

A27 Calvert Cliffs-1 Prototype

A27.1 Overview

To demonstrate safe and reliable methods to implement improved uranium utilization in light water reactors, the high burnup demonstration program called PROTOTYPE was jointly initiated by Baltimore Gas and Electric Co. and Combustion Engineering, Inc. [67] in 1978. The objectives of this program were to 1) extend the operating cycle length of Calvert Cliffs Units-1 and -2 from 12 to 18 months and 2) to demonstrate acceptable performance of fuel rods to peak-rod, discharge burnups of approximately 50 GWd/MTU [67]. The PROTOTYPE program included the irradiation of four Batch G assemblies and a Batch H assembly. The PROTOTYPE fuel rods in Batch G assemblies which have variations in the fuel pellet geometry underwent 4 cycles of irradiation that was extended to include a 5th cycle of irradiation while fuel rods in Batch H assembly which has higher initial enrichment than Batch G rods underwent 4 cycles of irradiation in Calvert Cliffs-1. Batch G assemblies average and peak rod burnup after five cycles is 54.4 and 63.5 GWd/MTU, respectively. Batch H assembly average and peak rod burnup after four cycles of irradiation is 50.6 and 56.0 GWd/MTU, respectively. For the purpose of this fuel analysis problem, 11 fuel rods from Batch G assemblies and two fuel rods from Batch H assembly were evaluated with BISON. All 13 fuel rods were fabricated by Combustion Engineering (CE) and are referred to as test rods BFM034, BFG092, BFL009, BFM156, BFM043, BEN013, BFL031, BFM073, BFM070, BFJ027, and BFM071 from Batch G, and UFE067 and UFE019 from Batch H in this document. These fuel rods used standard Zircaloy-4 cladding but have variations in the pellet design characteristics. Poolside examinations were performed visually after each cycle of irradiation. Destructive examination was performed in hot cell at AECL's Chalk River Laboratories for seven fuel rods from Batch G Assembly C1G003, four fuel rods from Batch G Assembly C1G006, and two fuel rods from Batch H Assembly C1H038. Destructive Post Irradiation Examination (PIE) was performed at the end-of-life (EOL) for evaluation of fission gas release, internal void volume, and oxide thickness. This experiment was chosen for analysis because they represent full size, commercial fuel rods designs, and a large inventory of measured data. The measured data from the hot cell examination are provided in the TR-103302-V2 [68] and NPSD-493-NP [69] reports to EPRI.

A27.2 Test Description

A27.2.1 Fuel Rod Design Specifications

An overview of the 13 Calvert Cliffs-1 fuel rods that were destructively examined in hot cell and chosen for BISON simulation are shown below in Table A27.1 [67]. These commercial fuel rods have variations in the pellet design characteristics which include standard length, reduced length and annular pellet. The two test rods with annular pellets are BFL031 and BFL009. The five test rods with reduced length pellets are BFM034, BFM043, BFM073, BFM070 and BFM071. The rest of the test rods have standard pellet length. Zircaloy-4 cladding material was used for all the test rods and was supplied by Sandvik Special Metals. The fuel rod characterization parameters are summarized in Tables A27.2 and A27.3 [67]. All 13 test rods have cladding outer diameter of 11.176 mm, cladding inner diameter of 9.7536 mm, and pellet outer diameter of 9.5631 mm. The nominal fuel stack height is 3.472 m. The pellet mean density varies based on the fuel design characteristics. This simulation assumed the pellet theoretical density of 10972.65 kg/m^3. Since the average grain sizes were not characterized for rods UFE067 and UFE019, they were assumed to be 8.4 microns in this simulation based on grain sizes noted for the other standard

fuel pellets in the experiment. Batch G test rods have initial enrichment of 3.67% except for rod BFJ027 which has an initial enrichment of 3.66%. Batch H test rods have initial enrichment of 3.98%.

Table A27.1: Overview of Calvert Cliffs-1 Fuel Rods Destructively Examined in Hot Cell

Assembly Serial No. and Fuel Batch	Rod Serial Number	Rod Type (pellet)	Rod Average Burnup (GWd/MTU)	Cladding Material	Number of Cycles
C1G003(Batch G)	BFM034	Reduced Length	63.451	Zircaloy-4	5
C1G003(Batch G)	BFG092	Standard	57.945	Zircaloy-4	5
C1G003(Batch G)	BFL009	Annular	58.106	Zircaloy-4	5
C1G003(Batch G)	BFM156	Standard	56.854	Zircaloy-4	5
C1G003(Batch G)	BFM043	Reduced Length	60.506	Zircaloy-4	5
C1G003(Batch G)	BEN013	Standard	59.835	Zircaloy-4	5
C1G003(Batch G)	BFL031	Annular	58.268	Zircaloy-4	5
C1G006(Batch G)	BFM073	Reduced Length	60.319	Zircaloy-4	5
C1G006(Batch G)	BFM070	Reduced Length	60.761	Zircaloy-4	5
C1G006(Batch G)	BFJ027	Standard	58.726	Zircaloy-4	5
C1G006(Batch G)	BFM071	Reduced Length	57.143	Zircaloy-4	5
C1H038(Batch H)	UFE067	Standard	54.841	Zircaloy-4	4
C1H038(Batch H)	UFE019	Standard	46.791	Zircaloy-4	4

Table A27.2: Fuel Rod Characterization Data

Rod Serial Number	Rod Length (m)	Enrich. wt % U235	Pellet Length (mm)	Open Porosity (%)	Avg. Initial Density %TD	Avg. Grain Size (micron)
BFM034	3.733	3.67	7.62	0.482	94.662	7.7
BFG092	3.733	3.67	11.43	0.142	94.882	8.4
BFL009	3.733	3.67	11.43	0.398	95.332	7.7
BFM156	3.733	3.67	11.43	0.142	94.882	8.4
BFM043	3.733	3.67	7.62	0.482	94.662	7.7
BEN013	3.733	3.67	11.43	0.142	94.882	8.4
BFL031	3.733	3.67	11.43	0.398	95.332	7.7
BFM073	3.733	3.67	7.62	0.482	94.662	7.7
BFM070	3.733	3.67	7.62	0.482	94.662	7.7
BFJ027	3.733	3.66	11.43	0.142	94.882	8.4
BFM071	3.733	3.67	7.62	0.482	94.662	7.7
UFE067	3.728	3.98	11.43	not meas.	94.750	not meas.
UFE019	3.728	3.98	11.43	not meas.	94.750	not meas.

Table A27.3: Additional Fuel Rod Characterization Data

Rod Serial Number	Nominal Fuel Stack Height (m)	Cladding OD (mm)	Cladding ID (mm)	Clad Thickness (mm)	Pellet OD (mm)	Pellet ID (mm)
BFM034	3.472	11.176	9.7536	0.7112	9.5631	0
BFG092	3.472	11.176	9.7536	0.7112	9.5631	0
BFL009	3.472	11.176	9.7536	0.7112	9.5631	2.7178
BFM156	3.472	11.176	9.7536	0.7112	9.5631	0
BFM043	3.472	11.176	9.7536	0.7112	9.5631	0
BEN013	3.472	11.176	9.7536	0.7112	9.5631	0
BFL031	3.472	11.176	9.7536	0.7112	9.5631	2.7178
BFM073	3.472	11.176	9.7536	0.7112	9.5631	0
BFM070	3.472	11.176	9.7536	0.7112	9.5631	0
BFJ027	3.472	11.176	9.7536	0.7112	9.5631	0
BFM071	3.472	11.176	9.7536	0.7112	9.5631	0
UFE067	3.472	11.176	9.7536	0.7112	9.5631	0
UFE019	3.472	11.176	9.7536	0.7112	9.5631	0

A27.2.2 Operating Conditions and Irradiation History

The irradiation of the fuel rods in Batch G assemblies chosen for the PROTOTYPE Program and fuel rods in the Batch H assembly was carried out in the Calvert Cliffs Unit 1 reactor. The test rods in the Batch G assemblies were irradiated for five cycles (Cycle 5 to 9) and were discharged with an assembly average burnup of 57.4 GWd/MTU while the test rods in the Batch H assembly were irradiated for four cycles (Cycle 6 to 9) and were discharged with an assembly average burnup of 50.6 GWd/MTU [67]. Following each irradiation cycle, the fuel assemblies underwent poolside examinations to monitor the overall assembly condition and test rod performance. For selected rods from Batch G and Batch H assemblies, the poolside examinations after the last cycle included detailed visual examinations, eddy current testing, rod length measurements, oxide film thickness measurements, and profilometry. The selected fuel rods were then shipped to AECL's Chalk River Laboratories for destructive examination.
The power mode selected in the BISON input deck for these simulations was PiecewiseConstant. The power histories for seven selected test rods in Batch G Assembly C1G003 and four selected test rods in Batch G Assembly C1G006 are shown in Figures A27.1 and A27.2, respectively. The power histories for two selected test rods in Batch H Assembly C1H038 are shown in Figure A27.3. These power histories assumed a 24 hour startup time that was broken into 24 timesteps of one hour increments. Because only cycle burnup data for each power step and rod average burnup data at the end of each cycle were available, the equations below were used to convert the power history data from a function of burnup to a function of time. These equations were derived by ANATECH to calculate time-based power histories from burnup-based power history data.

The linear mass density of Uranium is calculated as follows

$$wt = \frac{\pi}{4} \cdot f_{uo2} \cdot f_d \cdot t_d \cdot d_p^2 \tag{A27.1}$$

The time difference between each burnup increment is calculated by

$$\Delta t_i = ucf \left[\frac{\Delta bu \cdot wt}{LP} \right] \tag{A27.2}$$

where,

t_d is the fuel theoretical density (10972.65 kg/m^3),
f_{uo2} is the fractional uranium mass (0.881),
ucf is the units conversion factor (24000 kW-hr/MWd),
f_d is the fuel fractional density (unitless),
d_p is the pellet diameter (m),
Δbu is the difference in burnup increment (MWd/kgU), and
LP is the linear power (kW/m)

Because the rod average burnup data at the end of each cycle of irradiation is available in addition to the cycle burnup data, the difference in burnup increment, Δbu, is calculated as follows

$$\Delta bu = \frac{(bu_i - bu_{i-1})}{\Delta bu_{eoc}} \cdot \Delta bu_{rodavg} \tag{A27.3}$$

where,

bu_i - bu_{i-1} is the difference in cycle burnup increment (MWd/kgU),
Δbu_{eoc} is the difference in cycle burnup at the end of the cycle

and beginning of the cycle (MWd/kgU), and
Δbu_{rodavg} is the difference in rod average burnup at the
end-of-cycle and beginning of cycle (MWd/kgU)

Because the power histories are input as functions of cumulative time, the time during burnup increments must be summed to obtain cumulative time.

$$t_{ci} = t_{ci-1} + \Delta t_i \tag{A27.4}$$

Table A27.4 below provides the input and calculated linear mass density, wt, values for the 13 selected test rods. Because rods BFL009 and BFL031 have annular pellets, the pellet diameter was recalculated to be 0.0091688 m based on the area of the solid pellet. The annular pellet diameter was recalculated because the input pellet diameter, d_p, requires a solid pellet diameter in order to correctly calculate the linear mass density.

Table A27.4: Fuel Rod Parameters and Calculated Linear Mass Density

Rod Serial Number	Fractional Uranium Mass f_{uo2}	Fractional Density f_d	Pellet Diameter d_p (m)	Calculated wt
BFM034	0.881	0.94662	0.0095631	0.6573
BFG092	0.881	0.94882	0.0095631	0.6588
BFL009	0.881	0.95332	0.0091688	0.6085
BFM156	0.881	0.94882	0.0095631	0.6588
BFM043	0.881	0.94662	0.0095631	0.6573
BEN013	0.881	0.94882	0.0095631	0.6588
BFL031	0.881	0.95332	0.0091688	0.6085
BFM073	0.881	0.94662	0.0095631	0.6573
BFM070	0.881	0.94662	0.0095631	0.6573
BFJ027	0.881	0.94882	0.0095631	0.6588
BFM071	0.881	0.94662	0.0095631	0.6573
UFE067	0.881	0.94750	0.0095631	0.6579
UFE019	0.881	0.94750	0.0095631	0.6579

Because the axial power shapes and boundary conditions are modeled as PieceswiseBilinear, a ramp time of 360 seconds (0.1 hours) was assumed at each power step for the axial power shape and boundary condition input. The startup time of 24 hours, the equations for unit conversion of burnup to time, and the ramp time of 360 seconds (0.1 hours) are based on ANATECH's experience with fuel rod modelling for steady state operation and the development of Falcon Verification and Validation cases. They are intended to minimize the introduction of computational artifacts from unrealistic power changes and ramp rates into the analyses. The normalized axial power profile as a function of time was calculated from the data package. The coolant system pressure was 15.51 MPa and the initial fill-gas (Helium) pressure was 2.723 MPa. Operational and fast neutron flux input parameters are summarized in Table A27.5 and Table A27.6, respectively.

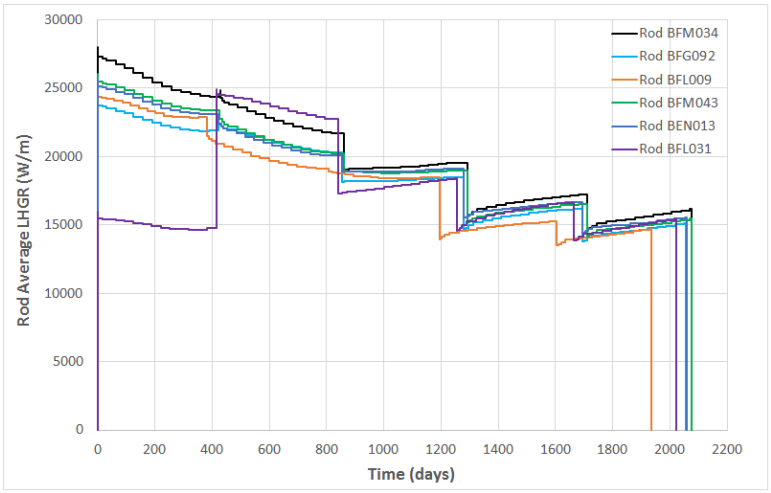

Figure A27.1: Assembly C1G003 Rods BFM034, BFG092, BFL009, BFM156, BFM043, BEN013, and BFL031 power histories

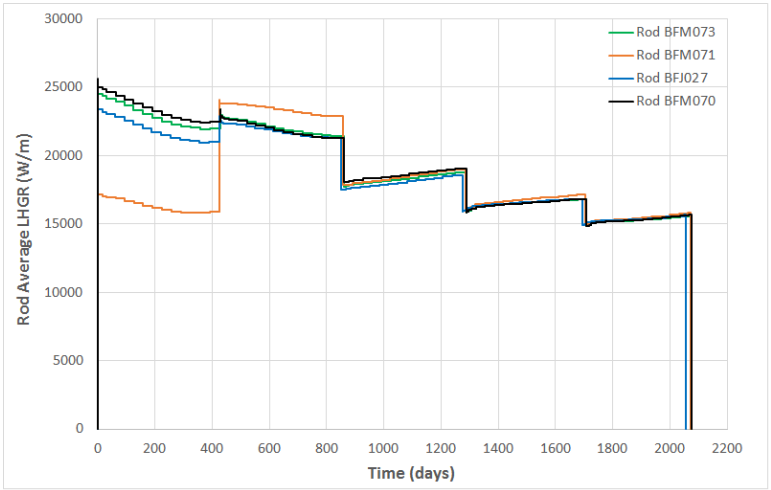

Figure A27.2: Assembly C1G006 Rods BFM073, BFM070, BFJ027, and BFM071 power histories

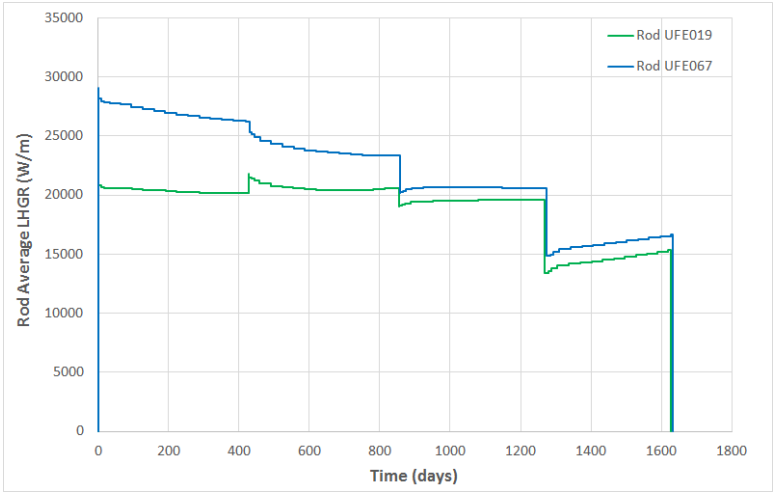

Figure A27.3: Assembly C1H038 Rods UFE067 and UFE019 power histories

Table A27.5: Operational Input Parameters

Parameter	Unit	Value
Coolant inlet temperature	K	557.15
Coolant system pressure	MPa	15.513
Coolant mass velocity	kg/m^2-s	3682.14

Table A27.6: Core Average Fast Neutron Flux Input Parameters

	BOC n/m^2-s $(\times 10^{17})$	EOC n/m^2-s $(\times 10^{17})$
Cycle 5	6.288	6.776
Cycle 6	7.663	6.736
Cycle 7	6.567	6.749
Cycle 8	6.541	6.797
Cycle 9	6.411	6.622

A27.3 Model Description

A27.3.1 Geometry and Mesh

The rod specifications in Table A27.2 were used to define the geometry for these simulations. The 13 selected rods were modeled as a two-dimensional, axi-symmetric linear mesh with quadratic elements. The fuel mesh for all 13 test rods consisted of 12 radial elements and the cladding mesh consisted of four radial elements to form a cladding thickness of 0.7112 mm. In order to accurately model the fuel rod initial free volume, the overall fuel rod length and upper plenum height were adjusted during mesh generation to account for the volume of the plenum spring which is not explicitly modeled. The adjusted fuel rod lengths and plenum heights for the 13 test cases are shown in Table A27.7. The mesh for 11 out of the 13 selected test rods that have standard or reduced length pellet types is shown in Figure A27.4. The mesh for the two fuel rods (BFL031 and BFL009) which have annular pellet types is shown in Figure A27.5.

Table A27.7: Adjusted Fuel Rod Length and Plenum Height

Rod Serial Number	Adjusted Rod Length(m)	Adjusted Plenum Height (m)
BFM034	3.79312	0.31392
BFG092	3.76274	0.28354
BFL009	3.70247	0.22327
BFM156	3.81935	0.34015
BFM043	3.79754	0.31834
BEN013	3.76501	0.28581
BFL031	3.69979	0.22059
BFM073	3.79834	0.31914
BFM070	3.80088	0.32168
BFJ027	3.76863	0.28943
BFM071	3.79647	0.31727
UFE067	3.77933	0.30013
UFE019	3.77693	0.29773

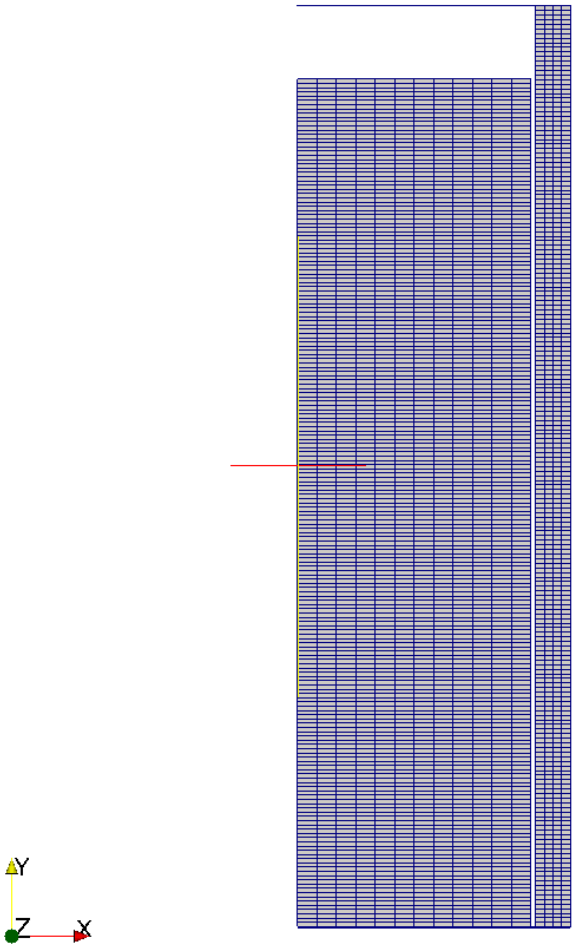

Figure A27.4: Fuel rod with standard or reduced length pellet mesh (not to scale)

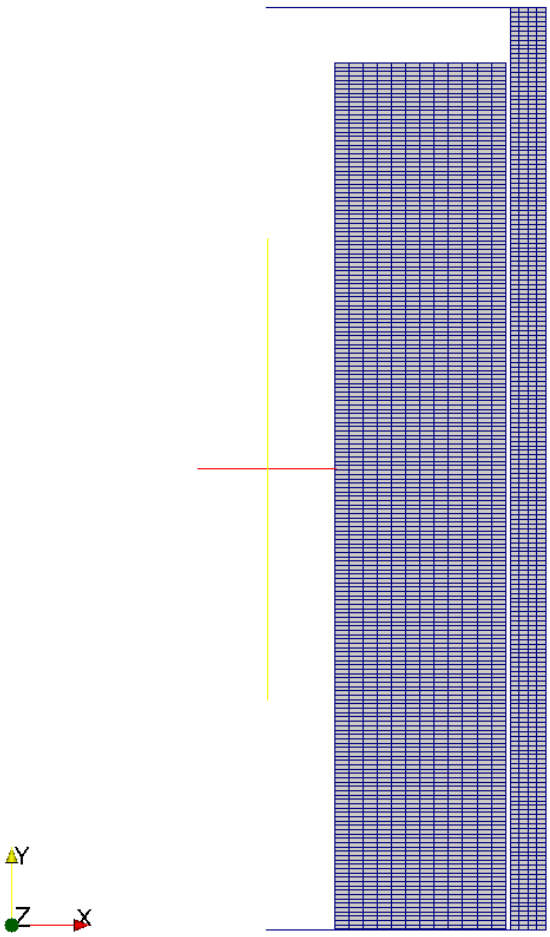

Figure A27.5: Fuel rod with annular pellet type mesh (not to scale)

A27.3.2 Material and Behavioral Models

The following material and behavioral models were used for the UO_2 fuel:

- ThermalFuel - NFIR: temperature and burnup dependent thermal properties.
- RelocationUO2: relocation strains, relocation activation threshold power set to 5 kW/m.
- Sifgrs: fission gas release model with the combined gaseous swelling model.
- MechZry: model mechanical deformation for Zircaloy-4.

For the cladding material, a constant thermal conductivity of 16 W/m-K was used and both thermal and irradiation creep were considered using the Limback model [36].

A27.3.3 Input files

The BISON input and all supporting files (power histories, axial power profiles, etc.) for all 13 selected Calvert Cliffs-1 test rods are provided with the code distribution at bison/assessment/Calvert_Cliffs-1_Prototype/analysis.

A27.4 Results Comparison

Data from the PROTOTYPE irradiation program was used to assess the code's capability to capture the integral fuel rod fission gas release, cladding creep down strain, oxide thickness, fuel rod growth, rod internal pressure, and void volume. The predicted values for all 13 selected test rods from BISON calculations are shown in Table A27.8. The measured values from experimental data are shown in Table A27.9 for comparisons. The rod axial growth measured data is not available for rod BFL031. BISON computes reasonable burnup, end-of-life (EOL) void volume, fission gas release, and EOL rod internal pressure for all 13 test rods when compared to measured data. BISON consistently over predicts fuel rod axial growth by an average of about 20% for all 13 test rods.

Table A27.8: Bison prediction for Calvert Cliffs-1 test rods

Rod Serial Number	Burnup (GWd/ MTU)	FGR (%)	Initial Void Vol. (cc)	Final Void Vol. (cc)	Rod Axial Growth (mm)	Axial Growth Strain (m/m)	Rod Int. Pressure (MPa)
BFM034	64.211	1.749	33.680	22.976	43.081	0.01136	3.939
BFG092	58.635	0.863	31.410	21.273	40.005	0.01063	3.854
BFL009	58.605	0.183	47.050	37.465	38.045	0.01028	3.296
BFM156	57.541	0.738	35.640	25.397	40.218	0.01053	3.667
BFM043	61.227	1.215	34.010	23.524	41.712	0.01098	3.822
BEN013	60.548	1.166	31.580	21.301	40.047	0.01062	3.918
BFL031	58.870	0.210	46.850	37.261	40.245	0.01088	3.283
BFM073	61.015	1.250	34.070	23.607	42.409	0.01117	3.803
BFM070	61.469	1.310	34.260	23.753	41.250	0.01085	3.828
BFJ027	59.429	1.043	31.850	21.646	41.400	0.01098	3.846
BFM071	57.904	1.200	33.930	23.675	42.520	0.01120	3.762
UFE067	55.357	2.672	32.650	22.479	36.348	0.00962	4.082
UFE019	47.246	0.817	32.470	23.036	33.280	0.00881	3.744

Table A27.9: Measured data for Calvert Cliffs-1 test rods

Rod Serial Number	Burnup (GWd/ MTU)	FGR (%)	Initial Void Vol. (cc)	Final Void Vol. (cc)	Rod Axial Growth (mm)	Axial Growth Strain (m/m)	Rod Int. Pressure (MPa)
BFM034	63.451	3.8	33.68	26.3	34.366	0.00921	4.302
BFG092	57.945	1.7	31.41	24.65	39.116	0.01048	3.634
BFL009	58.106	1.6	47.05	38.91	33.655	0.00902	3.392
BFM156	56.854	1.4	35.64	28.2	31.826	0.00853	3.558
BFM043	60.506	3.0	34.01	27.35	35.052	0.00939	4.061
BEN013	59.835	2.3	31.58	24.71	29.616	0.00793	3.806
BFL031	58.268	1.6	46.85	39.51			3.323
BFM073	60.319	2.9	34.07	27.73	35.966	0.00963	3.992
BFM070	60.761	3.1	34.26	27.14	33.579	0.00900	4.089
BFJ027	58.726	2.0	31.85	24.95	39.853	0.01068	3.689
BFM071	57.143	2.3	33.93	27.7	32.791	0.00878	3.868
UFE067	54.841	2.6	32.65	24.66	28.346	0.00760	4.020
UFE019	46.791	0.9	32.47	26.24	28.346	0.00760	3.544

A27.4.1 Fission Gas Release

The only fission gas release data available for this experiment is from destructive PIE puncture tests. Figures A27.6 to A27.18 show BISON's comparisons with EOL measurement for the 13 selected test rods in the current evaluation. BISON consistently under predicts the measured results by up to 2.1% for 12 out of the 13 selected test rods. Only rod UFE067 slightly over predicts the measured value. Both rods UFE019 and UFE067 predicts the fission gas release reasonably well compared to the measured result. Some adjustment may be needed to improve the FGR prediction since it is systemic and consistently under predicting. Currently, there's no specific model for gas release at high burnup. The next step is to investigate the high burnup gas release model.

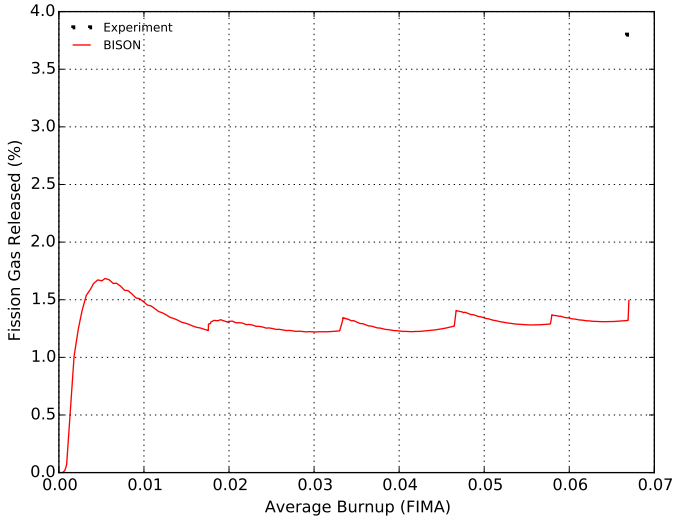

Figure A27.6: Fission gas release comparisons for BFM034

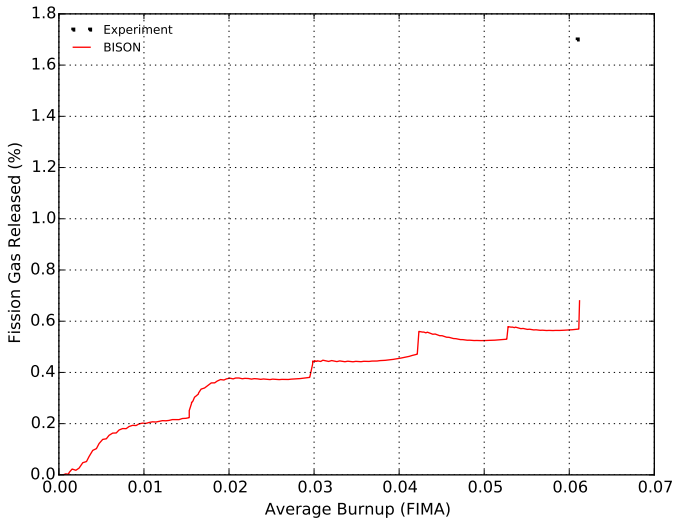

Figure A27.7: Fission gas release comparisons for BFG092

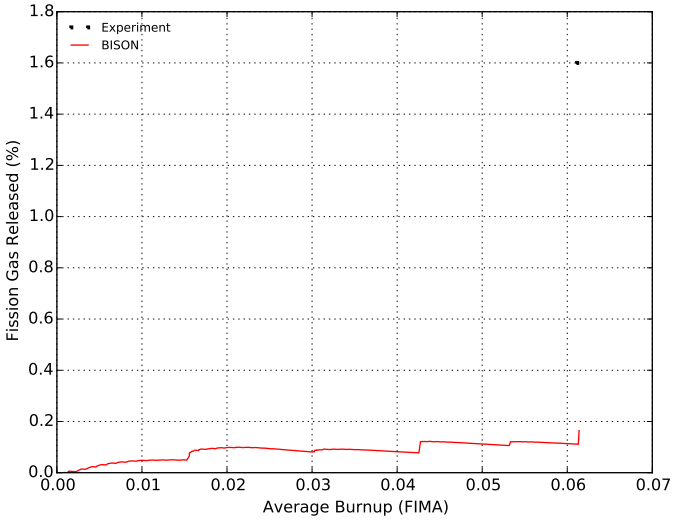

Figure A27.8: Fission gas release comparisons for BFL009

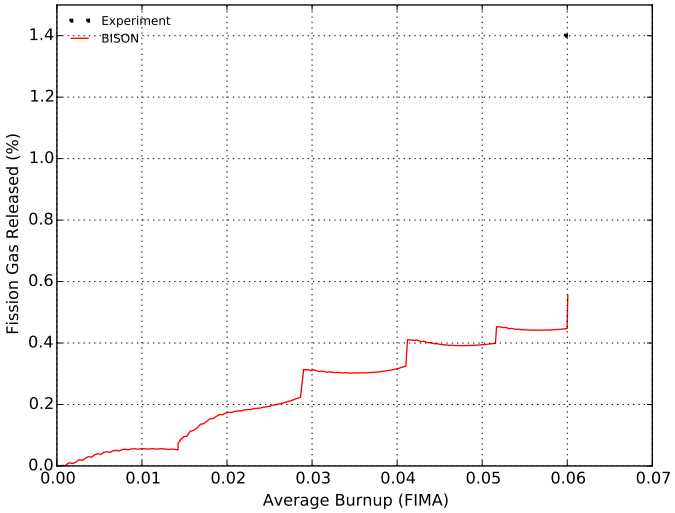

Figure A27.9: Fission gas release comparisons for BFM156

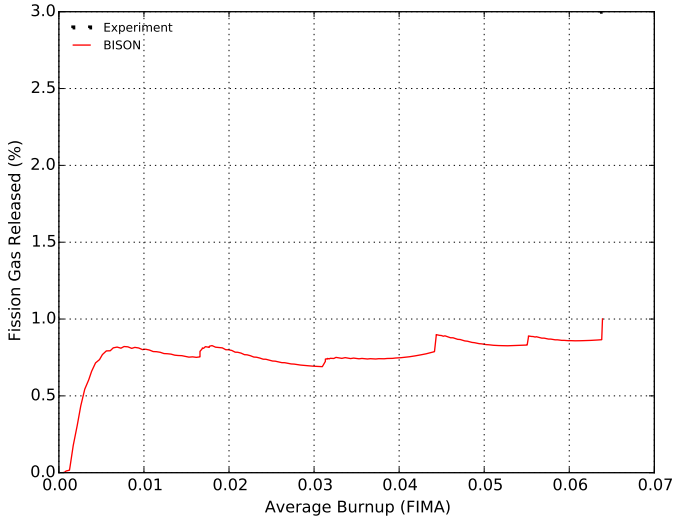

Figure A27.10: Fission gas release comparisons for BFM043

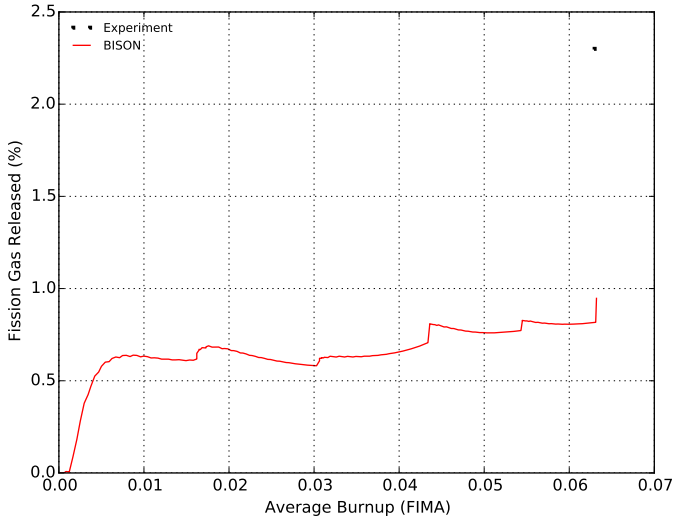

Figure A27.11: Fission gas release comparisons for BEN013

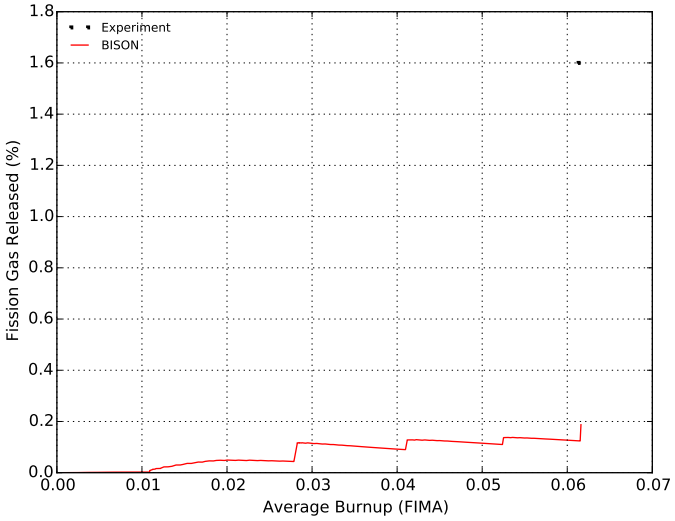

Figure A27.12: Fission gas release comparisons for BFL031

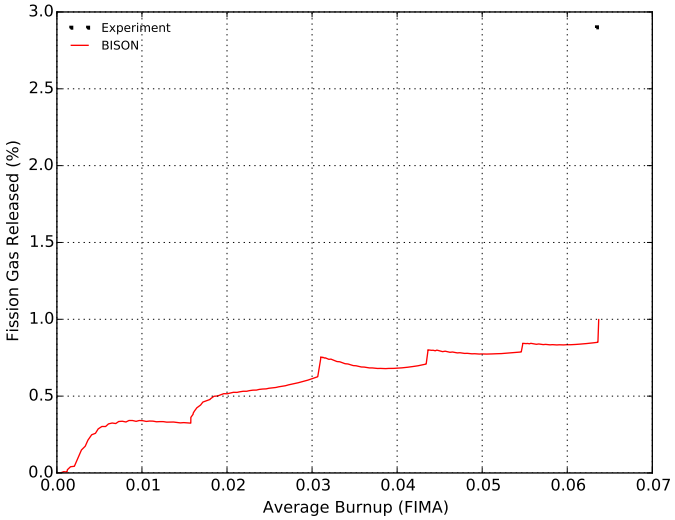

Figure A27.13: Fission gas release comparisons for BFM073

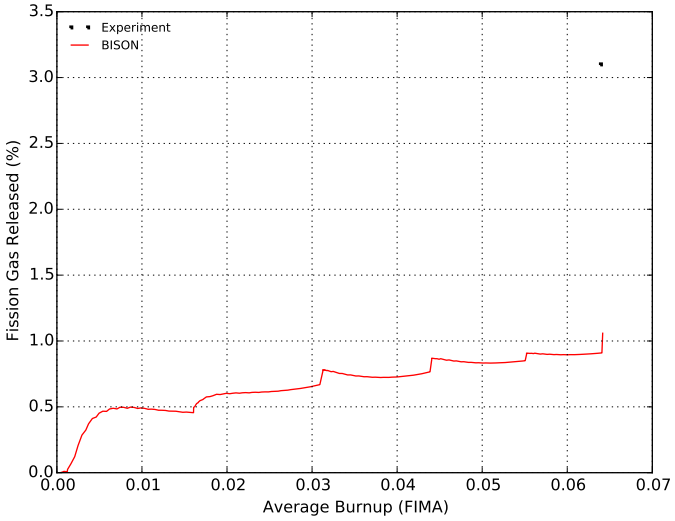

Figure A27.14: Fission gas release comparisons for BFM070

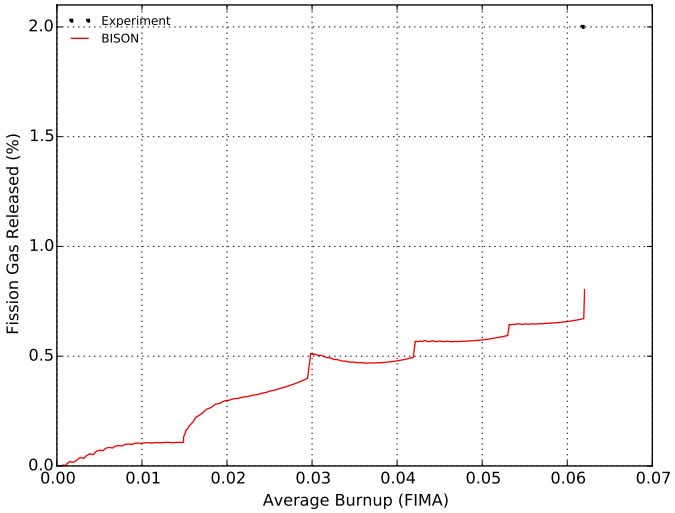

Figure A27.15: Fission gas release comparisons for BFJ027

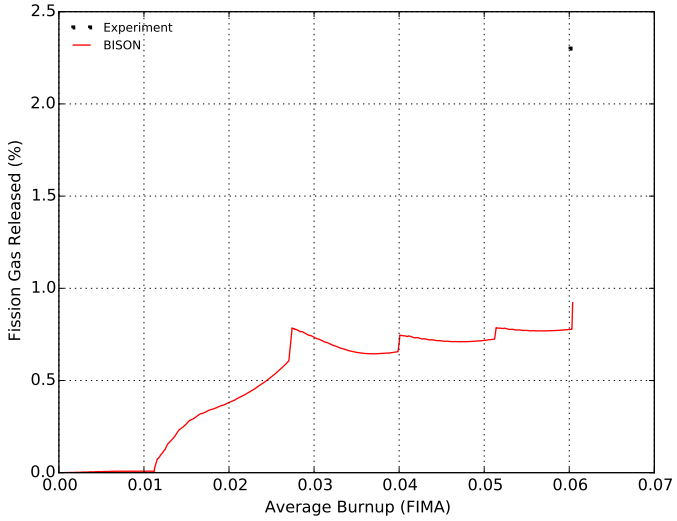

Figure A27.16: Fission gas release comparisons for BFM071

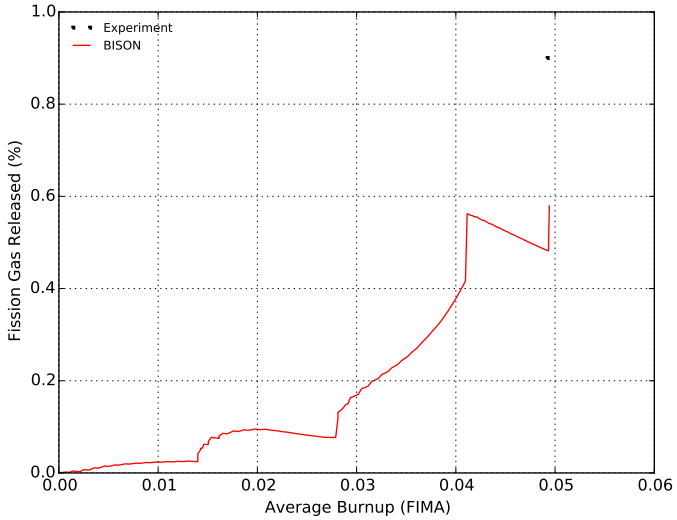

Figure A27.17: Fission gas release comparisons for UFE019

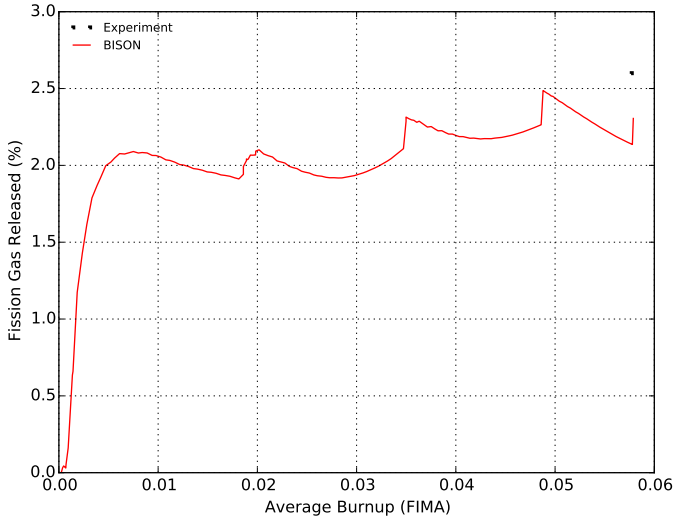

Figure A27.18: Fission gas release comparisons for UFE067

A27.4.2 Rod Internal Pressure

The only rod internal pressure data available for this experiment is from destructive PIE puncture tests. Figures A27.19 to A27.31 show BISON's comparisons with EOL measurement for the 13 selected test rods. BISON predicts the rod internal pressure reasonably well compared to the measured result for all 13 test rods.

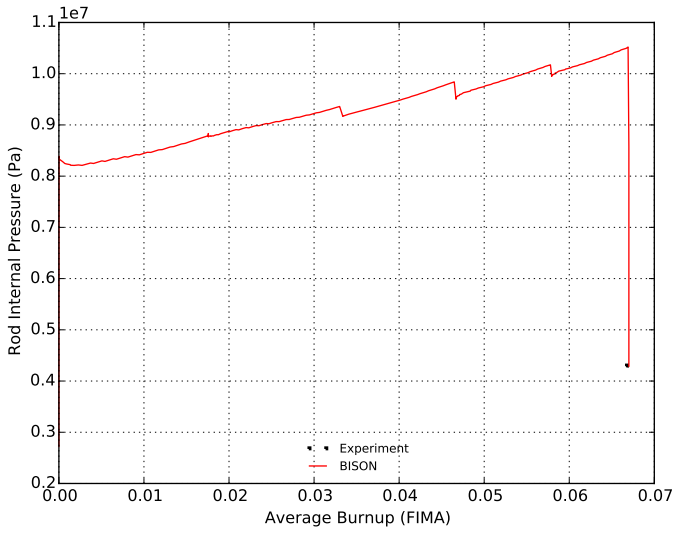

Figure A27.19: Rod internal pressure comparisons for BFM034

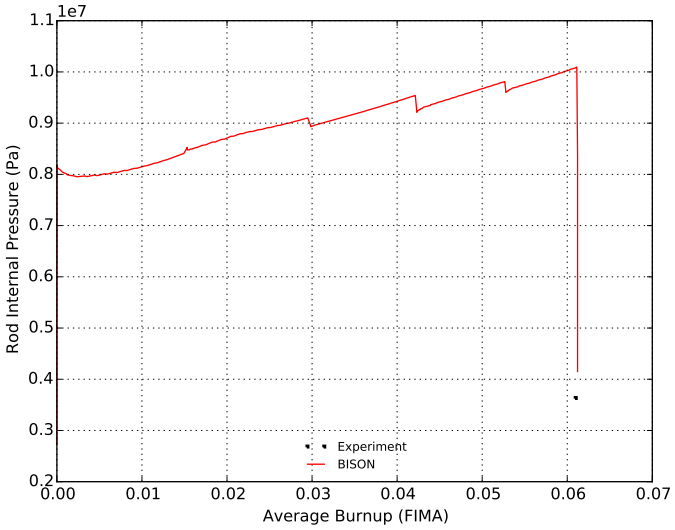

Figure A27.20: Rod internal pressure comparisons for BFG092

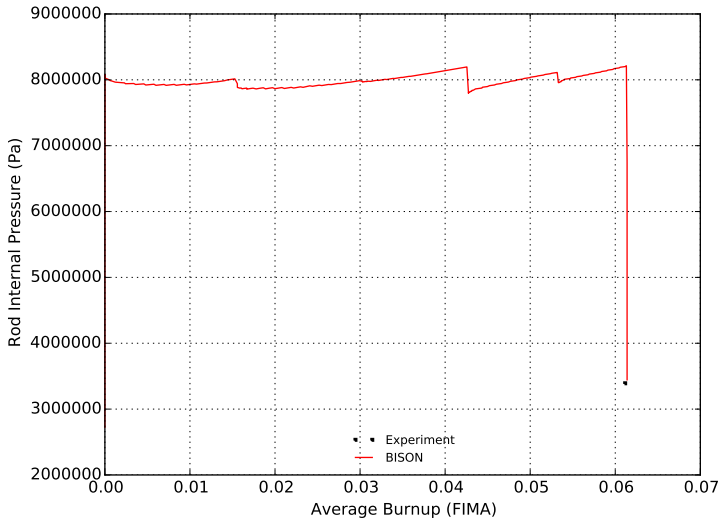

Figure A27.21: Rod internal pressure comparisons for BFL009

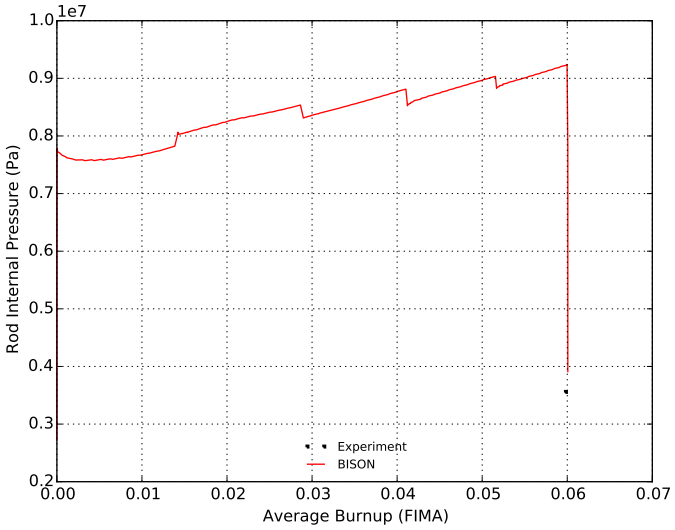

Figure A27.22: Rod internal pressure comparisons for BFM156

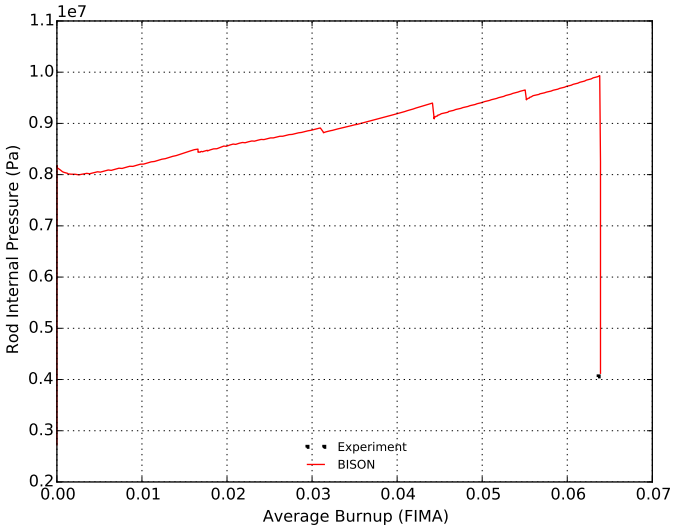

Figure A27.23: Rod internal pressure comparisons for BFM043

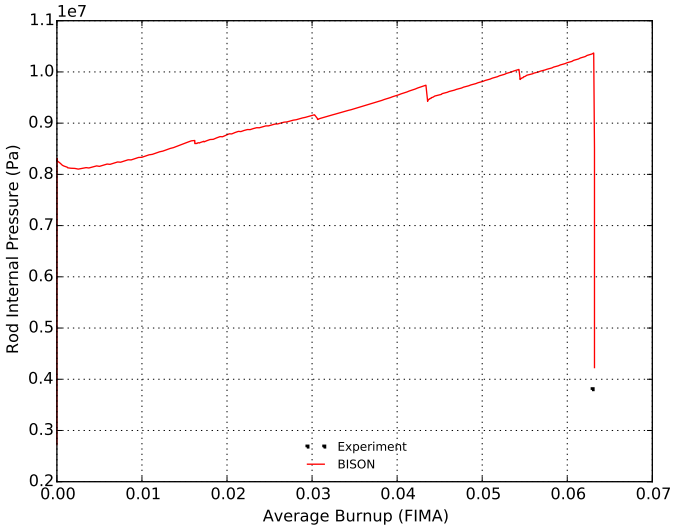

Figure A27.24: Rod internal pressure comparisons for BEN013

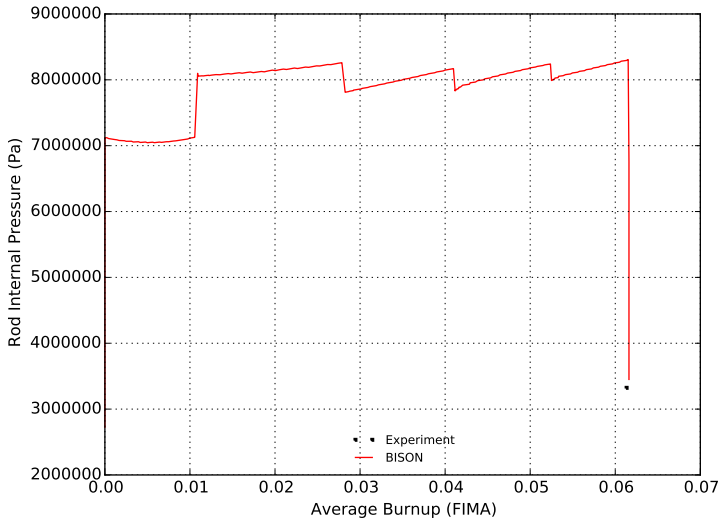

Figure A27.25: Rod internal pressure comparisons for BFL031

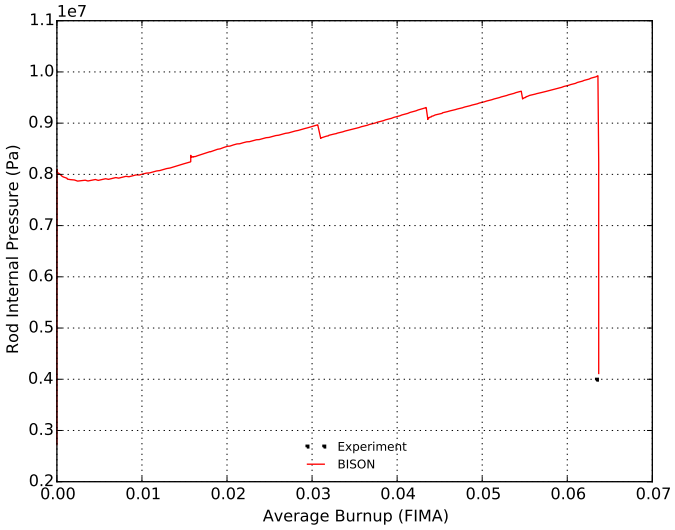

Figure A27.26: Rod internal pressure comparisons for BFM073

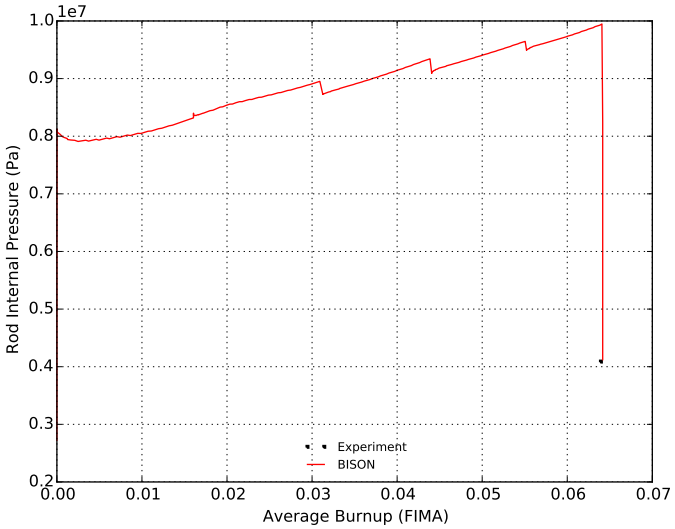

Figure A27.27: Rod internal pressure comparisons for BFM070

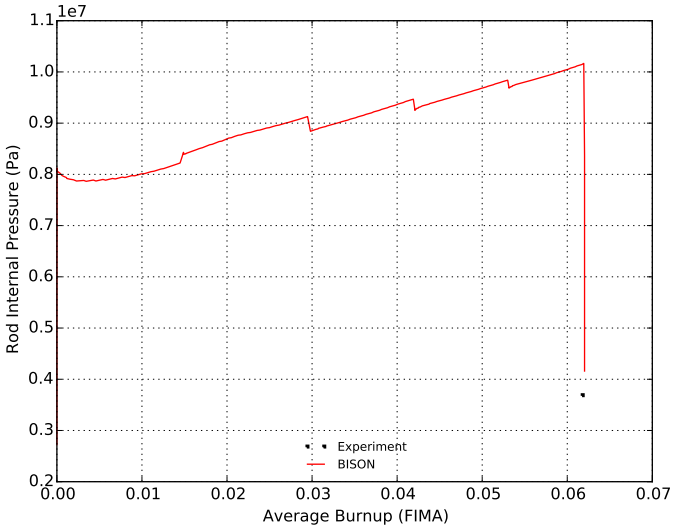

Figure A27.28: Rod internal pressure comparisons for BFJ027

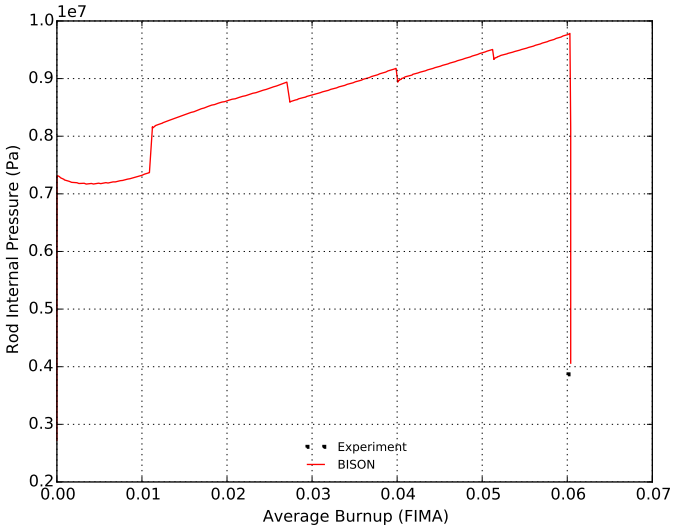

Figure A27.29: Rod internal pressure comparisons for BFM071

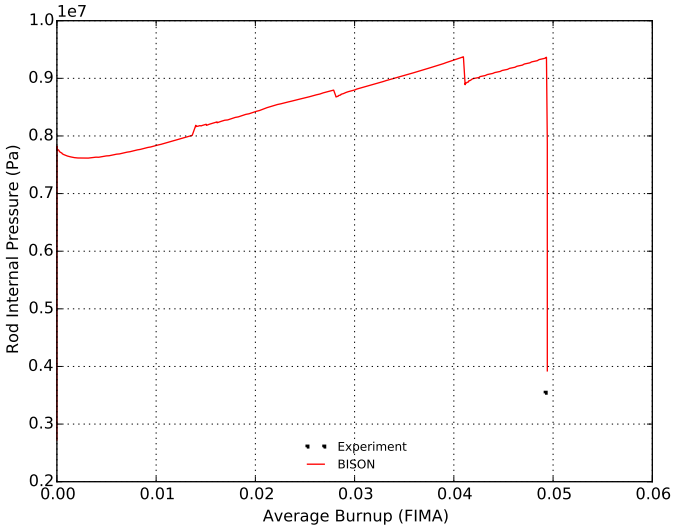

Figure A27.30: Rod internal pressure comparisons for UFE019

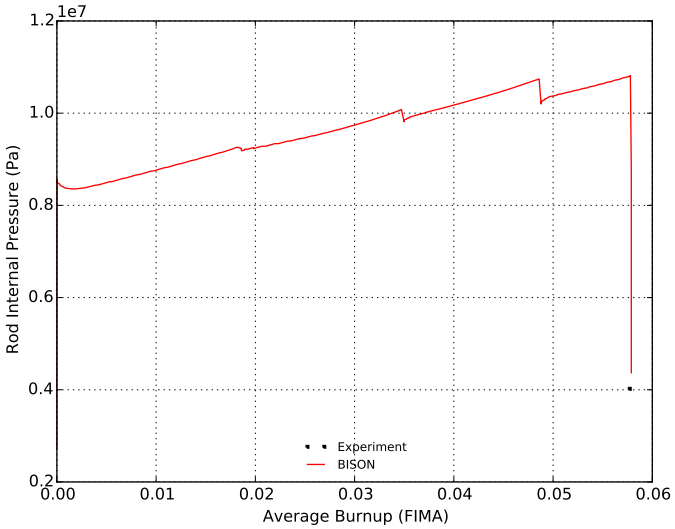

Figure A27.31: Rod internal pressure comparisons for UFE067

A27.4.3 Cladding Creep Down Strain

The calculated cladding creep down strain as a function of axial position is compared to measured data. The cladding creep down strain is calculated from the computed cladding diameter. Figures A27.32 to A27.43 show comparisons of BISON computed results to the measured cladding creep down strain data for 12 out of the 13 selected test rods. Cladding strain data were not available for rod BFL031. The results show BISON over predicts the cladding outer diameter at the EOL for all 12 test rods.

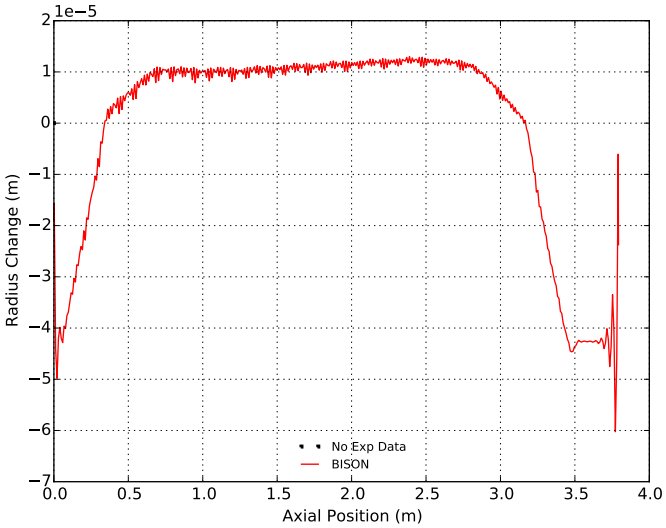

Figure A27.32: Cladding creep down strain comparisons for BFM034

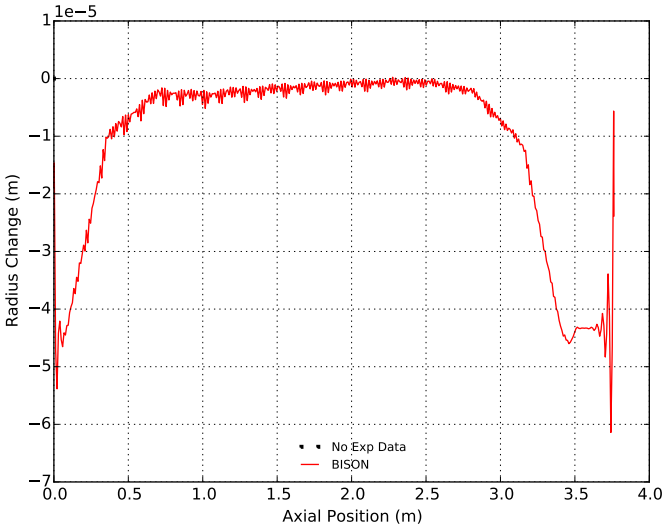

Figure A27.33: Cladding creep down strain comparisons for BFG092

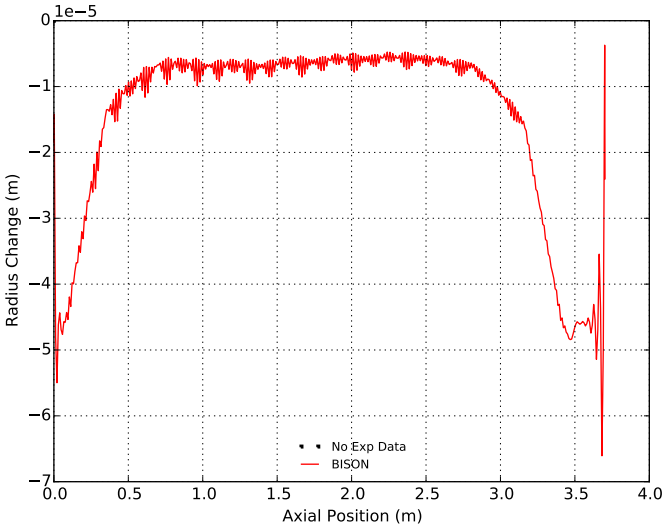

Figure A27.34: Cladding creep down strain comparisons for BFL009

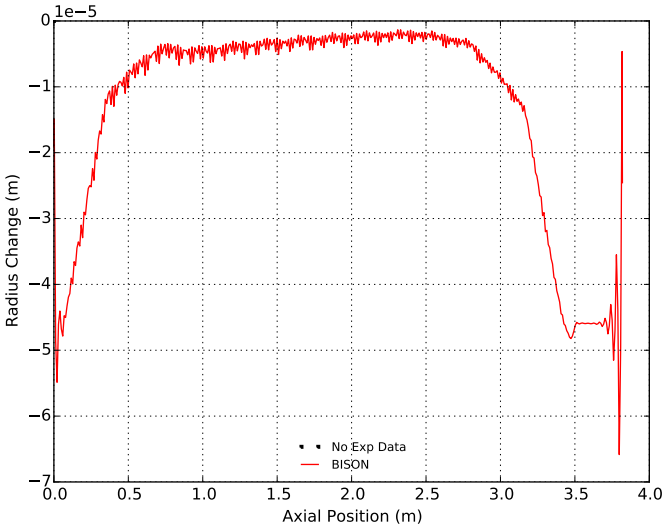

Figure A27.35: Cladding creep down strain comparisons for BFM156

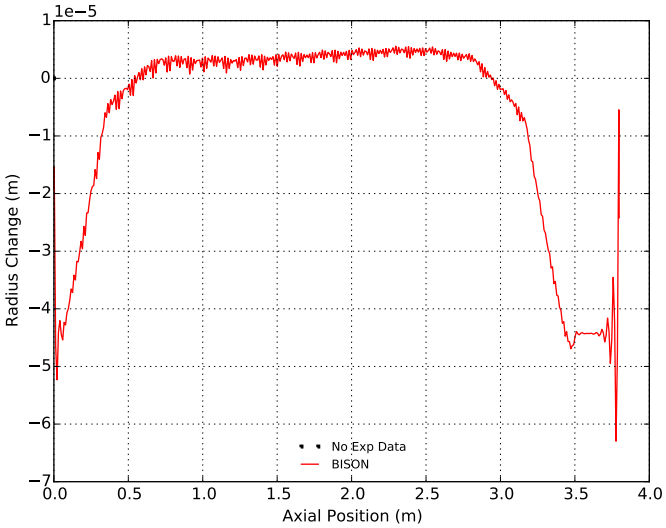

Figure A27.36: Cladding creep down strain comparisons for BFM043

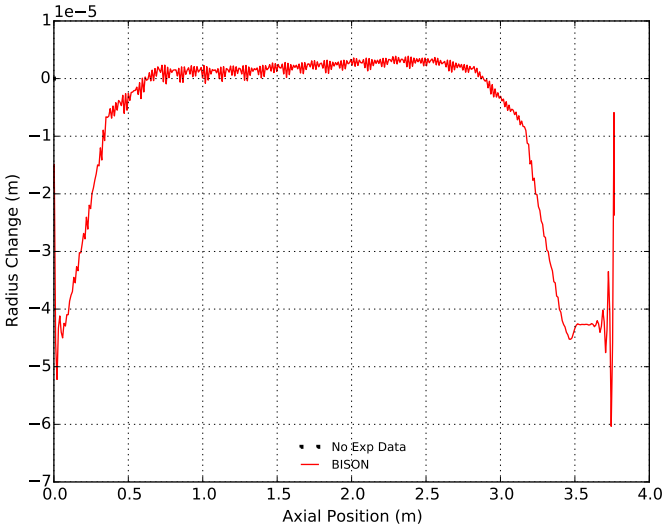

Figure A27.37: Cladding creep down strain comparisons for BEN013

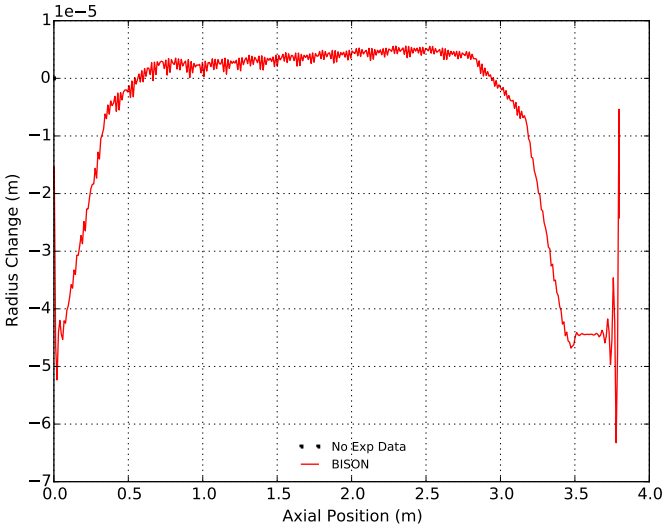

Figure A27.38: Cladding creep down strain comparisons for BFM073

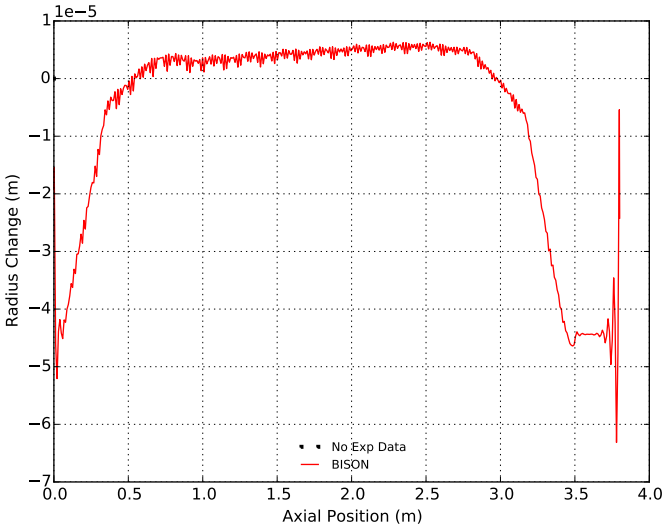

Figure A27.39: Cladding creep down strain comparisons for BFM070

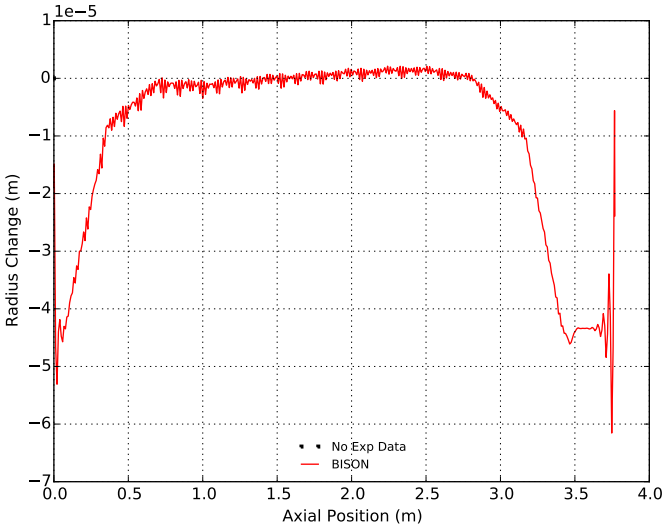

Figure A27.40: Cladding creep down strain comparisons for BFJ027

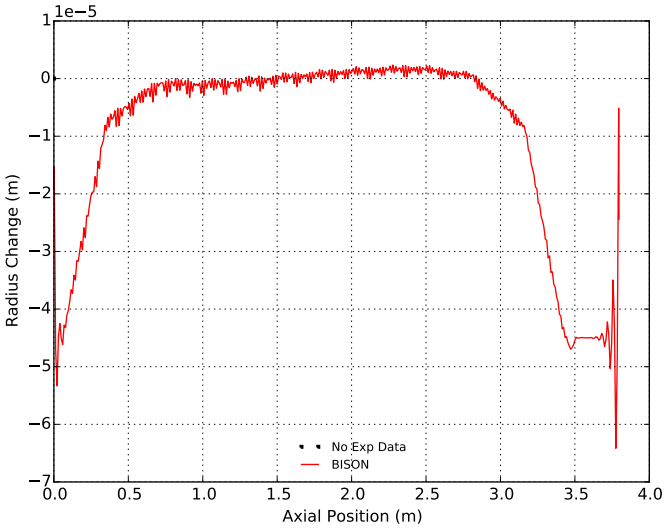

Figure A27.41: Cladding creep down strain comparisons for BFM071

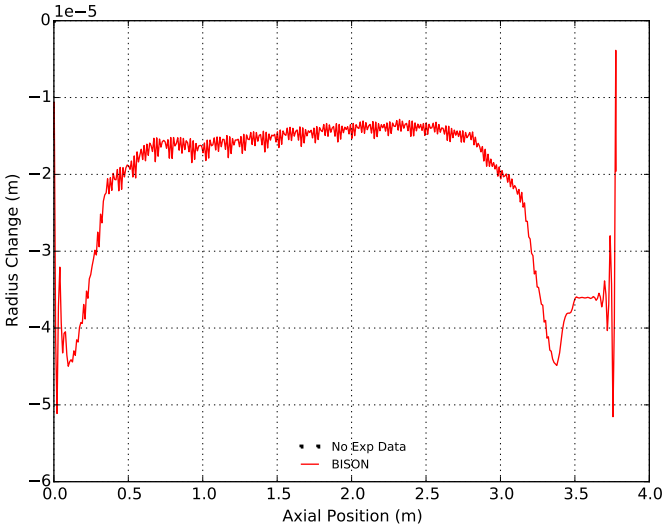

Figure A27.42: Cladding creep down strain comparisons for UFE019

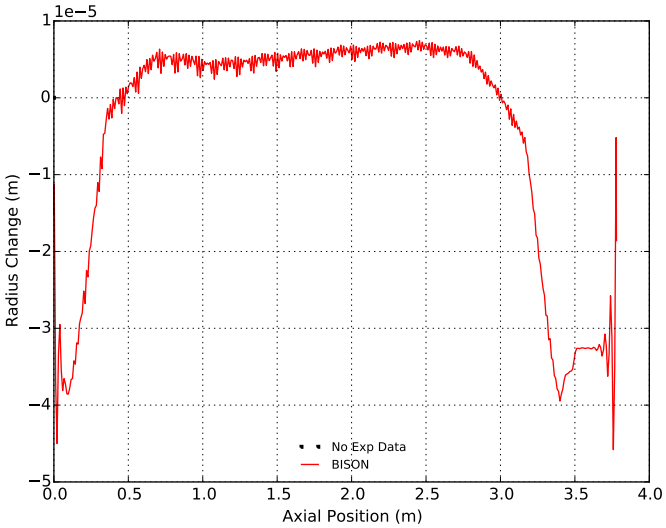

Figure A27.43: Cladding creep down strain comparisons for UFE067

A27.4.4 Cladding Oxide Thickness

The calculated cladding oxide thickness as a function of axial position is compared to measured data. Figures A27.44 to A27.54 show comparisons of BISON computed results to the measured cladding oxide thickness data for 11 out of the 13 selected test rods. Cladding oxide thickness data were not available for rods BFM070 and BFL031. The OxidationCladding model under the Materials block was used for the oxide thickness calculation. The results show BISON under predicts the peak oxide thickness for rods BFL009, BFM043, BEN013, BFM073, BFJ027, and BFM071, and over predicts the peak oxide thickness for rods BFM034, UFE019, and UFE067 by a significant margin compared to the measured results at the EOL. Only rods BFG092 and BFM156 were predicted with reasonable peak oxide thickness values compared to the measured result.

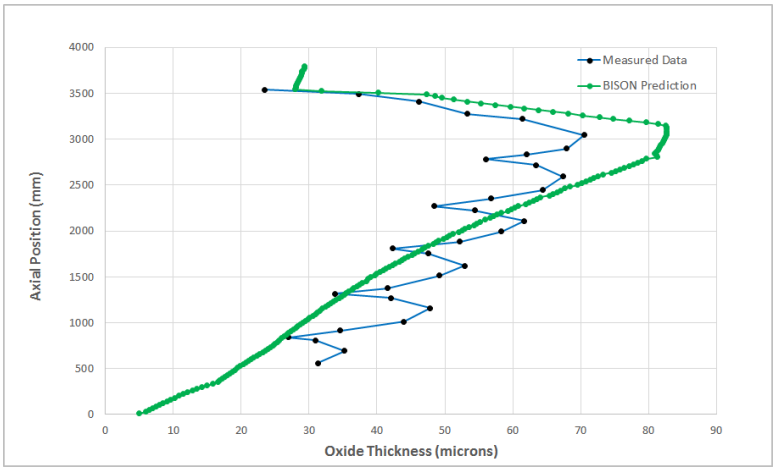

Figure A27.44: Cladding oxide thickness comparisons for BFM034

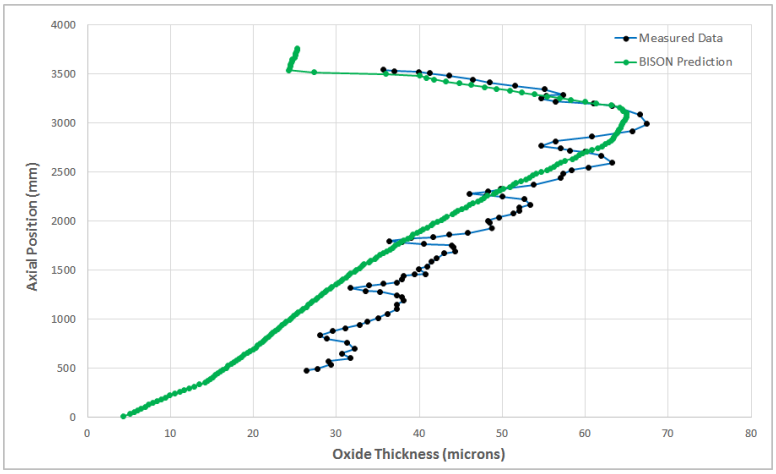

Figure A27.45: Cladding oxide thickness comparisons for BFG092

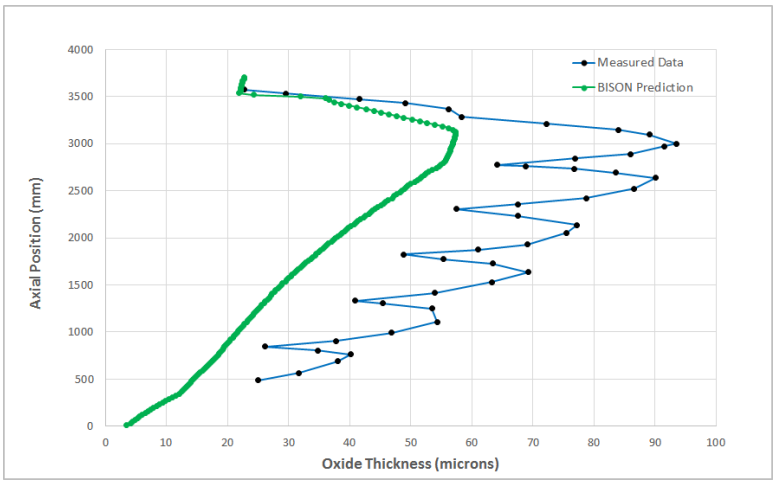

Figure A27.46: Cladding oxide thickness comparisons for BFL009

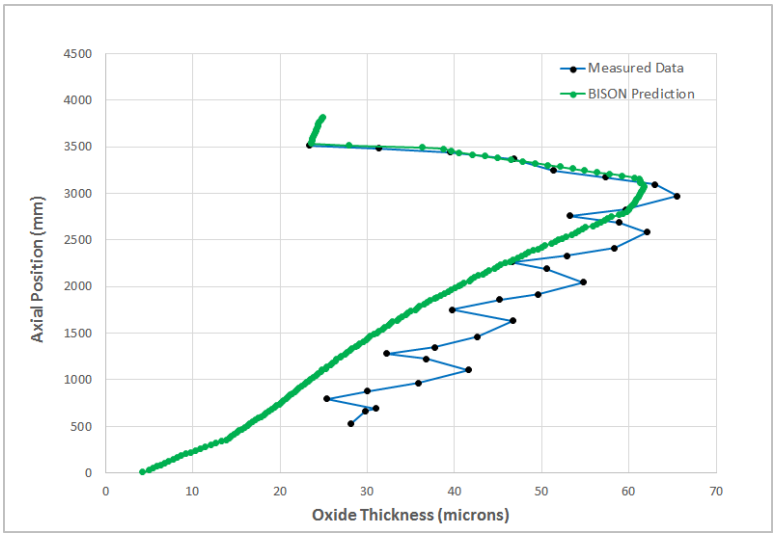

Figure A27.47: Cladding oxide thickness comparisons for BFM156

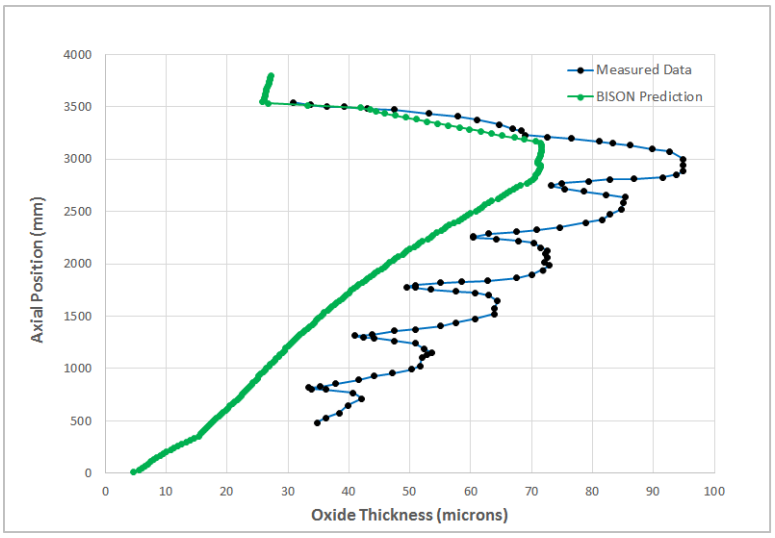

Figure A27.48: Cladding oxide thickness comparisons for BFM043

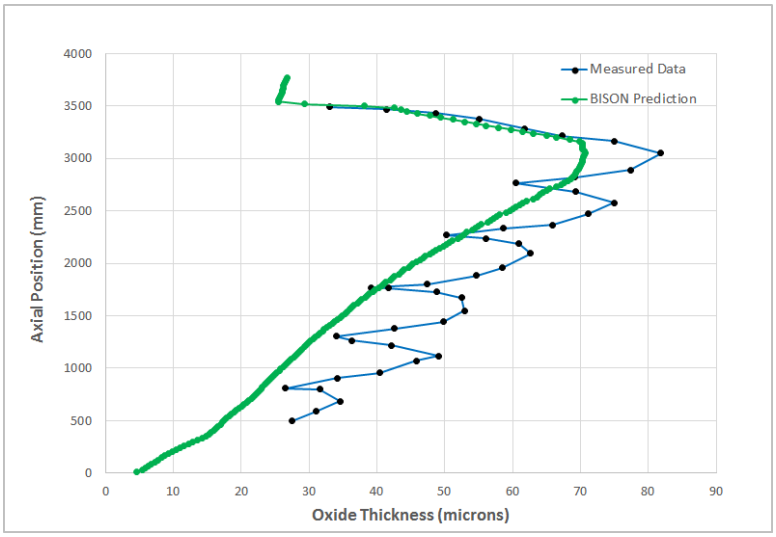

Figure A27.49: Cladding oxide thickness comparisons for BEN013

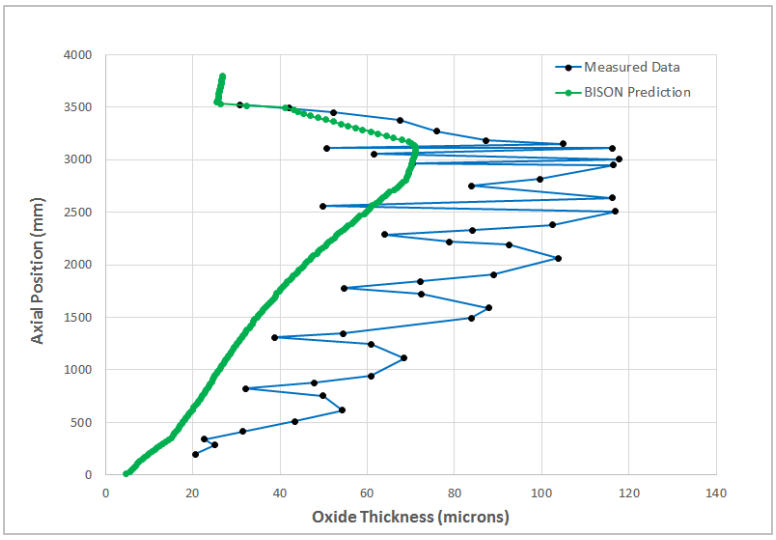

Figure A27.50: Cladding oxide thickness comparisons for BFM073

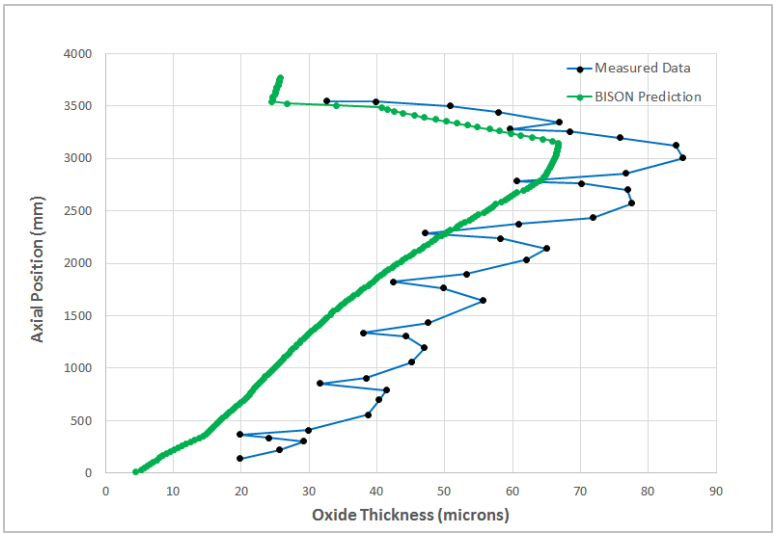

Figure A27.51: Cladding oxide thickness comparisons for BFJ027

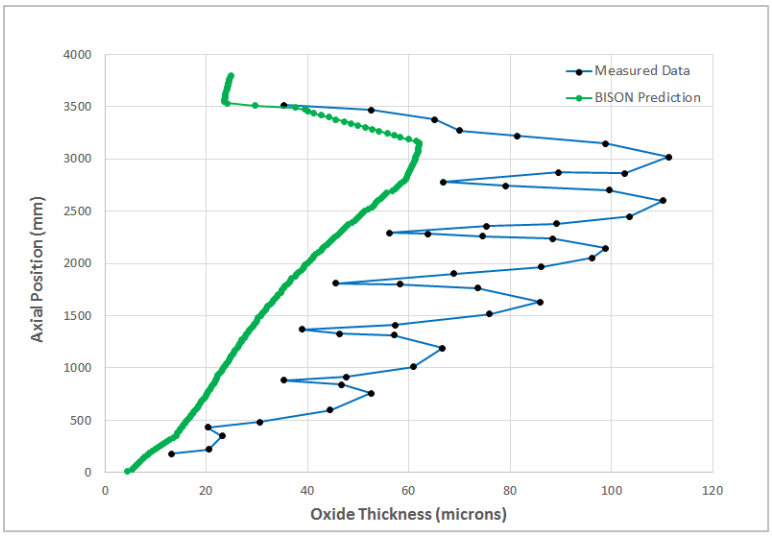

Figure A27.52: Cladding oxide thickness comparisons for BFM071

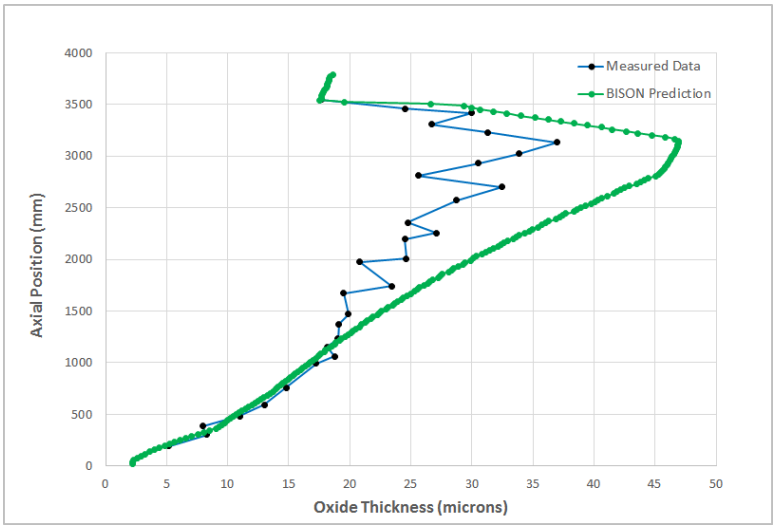

Figure A27.53: Cladding oxide thickness comparisons for UFE019

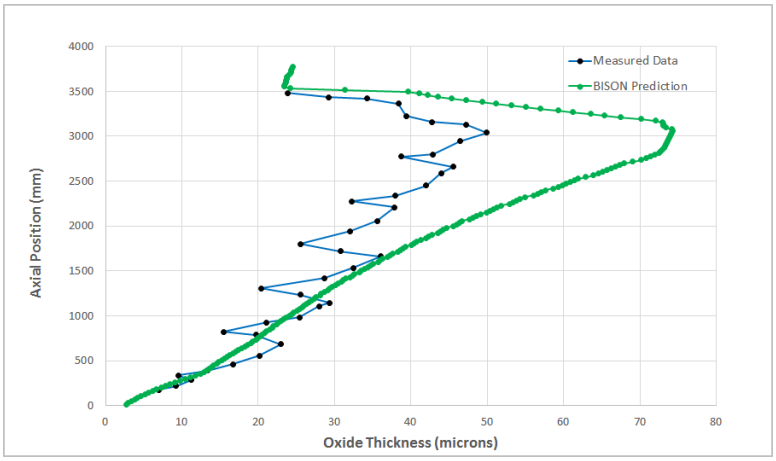

Figure A27.54: Cladding oxide thickness comparisons for UFE067

A27.4.5 Discussion

Based on the data presented above, several observations can be made regarding the results obtained from BISON analyses of the 13 selected Calvert Cliffs-1 test fuel rods.

- BISON consistently under predicts the EOL FGR by up to 2.1% for 12 out of the 13 selected test rods. The next step is to investigate inclusion of a high burnup gas release model in BISON.
- BISON consistently over predicts the EOL rod axial growth for all 13 selected test rods by an average of about 20%. This may be related to fuel/cladding interaction driven by friction (which is currently modeled using the tangential_penalty formulation) as well as application of axial creep strain and the axial growth model.
- BISON consistently over predicts the EOL cladding outer diameter for the 12 test rods with available data by a significant margin. This is likely related to fuel pellet behavior rather than cladding creep. More specifically, fuel pellet relocation and relocation recovery. Further review is recommended to determine the root cause of this behavior.

- Using the OxidationCladding model under the Materials block, BISON under predicts the EOL cladding oxide thickness for 6 out of the 11 test rods with available data by a significant margin. BISON also over predicts 3 out of the 11 test rods by a large margin. Further review of the cladding corrosion model, its input and implementation is warranted.

Based on the evaluation of these assessment cases, further evaluations of the fission gas release, cladding creep down strain, fuel relocation, rod axial growth and cladding oxide thickness characteristics in commercial rods are needed to extend the code's validation.

A28 Super Ramp PWR subprogram

A28.1 Overview

The Studsvik Super–Ramp project [70] investigated the behaviour of typical LWR test fuel rods when subjected to power ramps, after base irradiations to medium burnups. The Project consists of 28 fuel rods for the PWR subprogram and 16 for the BWR subprogram. In the following, only the PWR subprogram will be considered.

A28.2 Test Description

A28.2.1 The Super–Ramp PWR subprogram

The PWR test fuel rods (UO_2 pellets with Ziracaloy–4 claddings) were tested using high ramp rates. Tha main goal of the PWR Super–Ramp subprogram was to establish the damage threshold of the standard design PWR rods, with ramp tests performed at burnups above 30 GWd t^{-1}.

The irradiation experiments have been performed over 6 groups of PWR fuel rods, with different design specifications and different characteristics of both the fuel and the cladding materials. The rods have been base irradiated in the KWO (Obrigheim, Germany) and BR-3 (Mol, Belgium) commercial reactors, with linear heat rates between 9 and 27 kW m^{-1} and burnups between 28 and 45 GWd t^{-1}. Subsequently, the test rods underwent ramp tests in the R2 experimental reactor (Studsvik, Sweden).

The PWR subprogram includes 28 test rods, which can be subdivided in 6 groups according to specific design specifications. The rods analysed below belong to three different groups, as detailed in Table A28.1.

Table A28.1: Summary of the Super-Ramp PWR experiment rods. Burnup and linear heat rate refer to radial average values at axial peak position.

Rod group	Burnup (GWd t^{-1})	Linear heat rate (kW m^{-1})
PK1	33–36	19–26
PK2	41–45	17–25
PK6°	34–37	20–27

°Large grain

A28.2.2 Rod Design Specifications

In the following, the main design specifications of the analyzed fuel rods are reported. The rods were tested without undergoing a refabrication process between base irradiation and ramp test, hence the specifications in Table A28.2 correspond to the initial specifications.

Table A28.2: Analysed Super–Ramp PWR rods specifications

Rod group		PK1	PK2	PK6
Overall length	m	0.388	0.390	0.390
Fuel stack height	m	0.312	0.318	0.314
Nominal plenum height	m	0.032	0.032	0.033
Fill gas composition			He	
Fill gas pressure	MPa		2.25	
Fuel				
Material			UO_2	
Enrichment	wt.%	3.2	3.21	2.99
Density	%TD	94.6	94.3	95.1
Outer diameter	mm	9.11	9.14	9.14
Grain diameter (3D)	μm	9.36	8.58	34.3
Cladding				
Material			Zircaloy–4	
Outer diameter	mm	10.76	10.75	10.74
Inner diameter	mm	9.31	9.28	9.29

A28.2.3 Operating Conditions and Irradiation History

A typical power history for the base irradiation of the Super–Ramp PWR subprogram is reported in Figure A28.1 and a typical power history for the ramp test is reported in Figure A28.2. The rod axial power profile, clad surface temperature, coolant pressure and fast flux during experiments have been prescribed coherently with the data available in the International Fuel Performance Experiments database [57] and in the Super–Ramp final report [70].

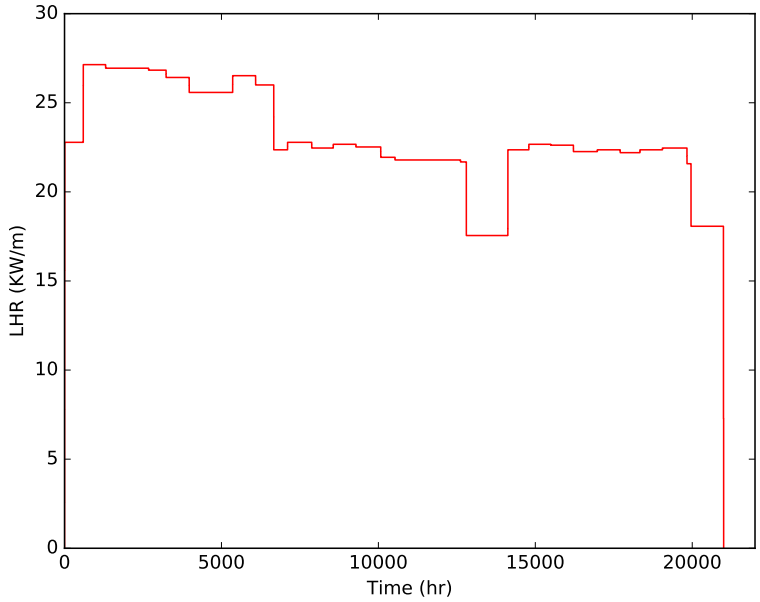

Figure A28.1: Typical base irradiation history for fuel rods from the Super–Ramp PWR subprogram.

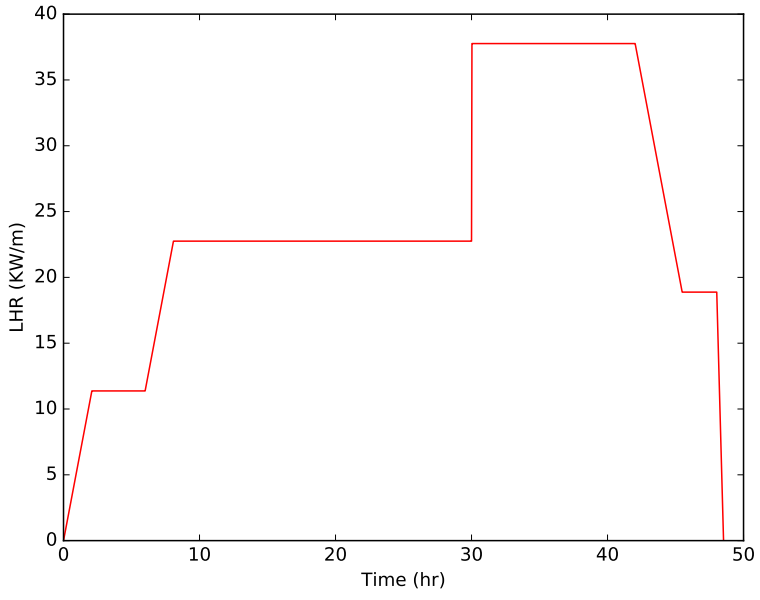

Figure A28.2: Typical ramp test (in terms of rod average linear heat rate) for fuel rods from the Super–Ramp PWR subprogram.

A28.3 Model Description

A28.3.1 Geometry and Mesh

The considered rods were modeled considering a smeared column of flat ended pellets (chamfering and dishing not considered in the geometry). The insulator pellets, placed in the experiments at both the ends of the fuel column, were neglected.

A 2-dimensional axisymmetric quadratic (Quad8 elements) mesh was used to model the geometry of the considered rods from the Super–Ramp PWR subprogram. The mesh scprit files employed to generate the meshes of the considered rods are included in each rod subfolder.

A28.3.2 Material and Behavioral Models

The following material and behavioral models were used for the UO_2 fuel:

- ThermalFuel - NFIR: temperature and burnup dependent thermal properties.
- RelocationUO2: relocation strains, relocation activation threshold power set to 5 kW m^{-1}.
- Sifgrs: fission gas release model with coupled gaseous swelling. The transient capability is considered, and the effective diffusion coefficient is calculated according to Turnbull et al. [59].

For the clad material, a constant thermal conductivity of 16 W $m^{-1}K^{-1}$ was used, and both thermal and irradiation creep were considered. Thermal expansion modeling utilized the CTHEXP sub-code with its correlations for Zircaloy [54].

A28.3.3 Boundary and Operating Conditions

The power history considered comprehends the base irradiation, shown in Figure A28.1, and the subsequent ramp test, reported in Figure A28.2. The temperature boundary conditions as a function of time was prescribed according to the files available in the IFPE databae [57]. The fast neutron flux in the clad during the base irradiation is available in [70], whereas during the ramp test was considered to be equal the last irradiation cycle during the base irradiation.

A28.3.4 Input files

The BISON input and all supporting files for these cases are provided with the code distribution at bison/assessment/Super_Ramp/analysis.

A28.4 Results

The considered fuel rod experiments from the Super–Ramp PWR subprogram are:

- PK1 series: rods PK1–1, PK1–2, PK1–3, PK1–4.
- PK2 series: rods PK2–1, PK2–2, PK2–3, PK2–4.
- PK6 series: rods PK6–2, PK6–3, PK6–S.

The results considered regard the integral fission gas release (FGR) calculated at the end of the tests. For the Super–Ramp PWR subprogram, the final, integral FGR measurement is available from the IFPE database.

A28.4.1 Fission Gas Release

The calculated integral fission gas release at the end of the irradiation for all considered cases is compared to the experimental data in Figure A28.3. The distance from the 45° line is a measure of the accuracy of the predictions. BISON results show a good agreement with the experimental data, in line with the intrinsic modelling uncertainties [20].

Moreover, detailed results of FGR as a function of the time for the simulation of PK1–1 and PK1–2 during the ramp tests are reported in Figures A28.4 and A28.5, respectively.

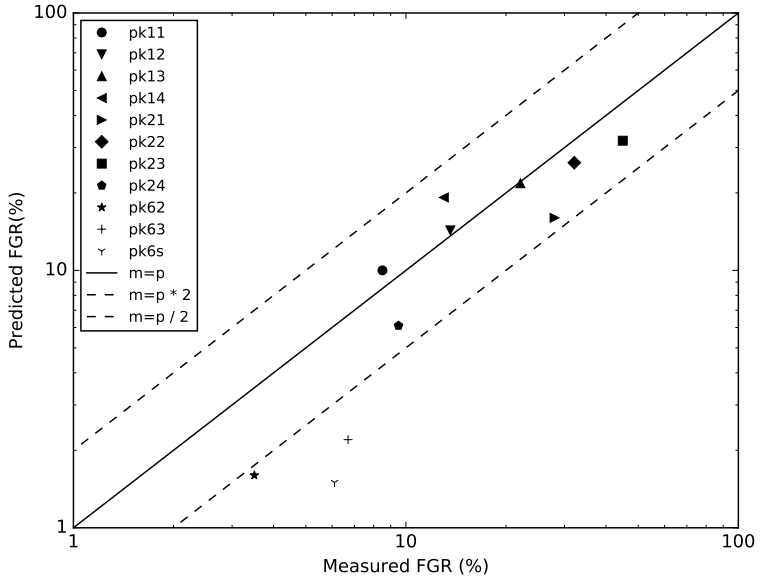

Figure A28.3: Comparison between the FGR calculated with BISON and the experimental data for all considered cases. The distance from the 45° line is a measure of the accuracy. Each point represents an irradiation experiment from the Super–Ramp PWR database. Acceptable bands are calculated with a factor of 2 [20].

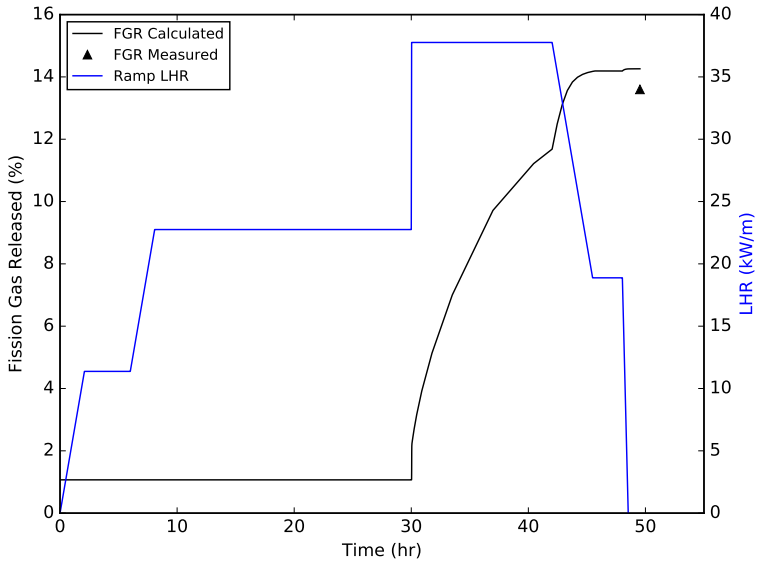

Figure A28.5: BISON calculated fission gas release during the ramp test (blue line) of the PK1–2 fuel rod experiment compared to the experimental data (green marker). The rod average linear heat rate is reported for completeness.

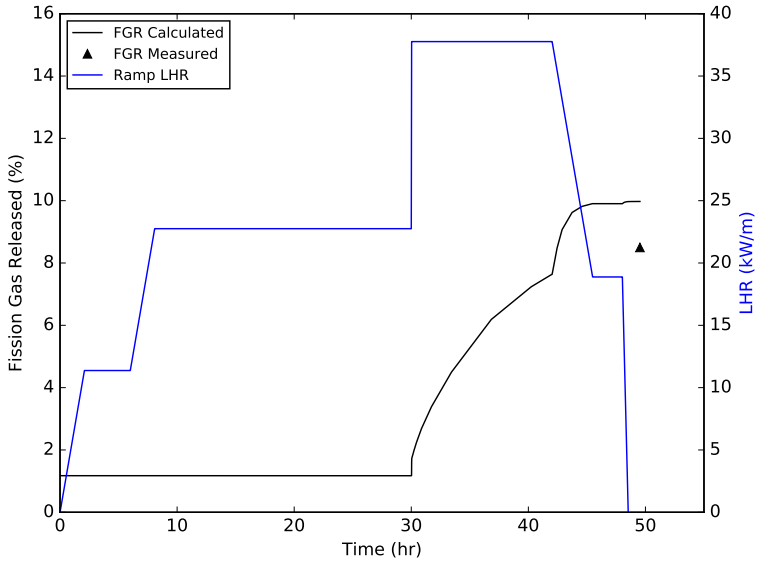

Figure A28.4: BISON calculated fission gas release during the ramp test (blue line) of the PK1–1 fuel rod experiment compared to the experimental data (green marker). The rod average linear heat rate is reported for completeness.

A29 HBEP R1 Rods A1/8-4, A3/6-4 and H8/36-4

A29.1 Overview

The purpose of the High Burnup Effects Programme (HBEP) Task 3 was to provide high burnup effects evaluations, fission gas sampling, and parameter effects [60]. Rods A1/8-4, A3/6-4 and H8/36-4 were selected for the assessment of BISON code; they were irradiated to 48.5 MWd/kgU, 47.8 MWd/kgU and 46.6 MWd/kgU respectively, in the TVO-1 boiling water reactor (BWR) [60].

A29.2 Test Description

The three rods in this series, manufactured by ASEA, have similar design characteristics but slightly different pellet and cladding diameter. The fuel stack consisted of solid pellets with an active length of 3.68 meters. This portion of the HBEP experiments designated as Task 3 was to provide well-characterised data on the evaluation of high burnup effects on different fuel characteristics with an emphasis on fission gas release.

Table A29.1: HBEP Test Rod Specifications (A1/8-4, A3/6-4, and H8/36-4)

Fuel Rod		
Fuel stack height	m	3.68
Nominal plenum height		
A1/8-4	mm	246
A3/6-4	mm	246
H8/36-4	mm	244
Number of pellets per rod		337
Pellet Height		
A1/8-4	mm	10.9
A3/6-4	mm	10.9
H8/36-4	mm	10.9
Fill gas composition		He
Fill gas pressure	MPa	.37
Fuel		
Material		UO_2
Enrichment		
A1/8-4	%	2.33
A3/6-4	%	3.08
H8/36-4	%	1.36
Density	%	95.6
Outer diameter		
A1/8-4	mm	9.939
A3/6-4	mm	10.439
H8/36-4	mm	9.939
Grain diameter		
All Rods	μm	6.6
Fuel densification		
All Rods	%	.43
Roughness		
All Rods	μm	1.1
Cladding		
Material		Zr-2
Outer diameter		
A1/8-4	mm	11.73
A3/6-4	mm	12.25
H8/36-4	mm	11.73
Inner diameter		
A1/8-4	mm	10.14
A3/6-4	mm	10.65
H8/36-4	mm	10.14
Roughness		
All Rods	μm	.35

A29.2.1 Operating Conditions and Irradiation History

Rods A1/8-4, A3/6-4 and H8/36-4 were irradiated in the TVO-1 commercial BWR Cycles 2 through 7 [60]. Reactor operating coditions were, coolant pressure of 7 MPa and coolant inlet temperature of 552 K [60]. Peak-in-life LHGR values occurred during the first and third operating cycles, with maximum rod-average LHGR values being approximately 18 to 27 KW/m. Rod-average burnups ranged from 44

to 50 MWd/kgM with rod-average FGR values ranging from 0.3 to 17.1%. Clad temperatures and local power histories were taken at 12 axial locations and obtained from the IFPE database. The plot below, Figure A29.1, shows the power histories for the A1/8-4, A3/6-4, and H8/36-4 rods.

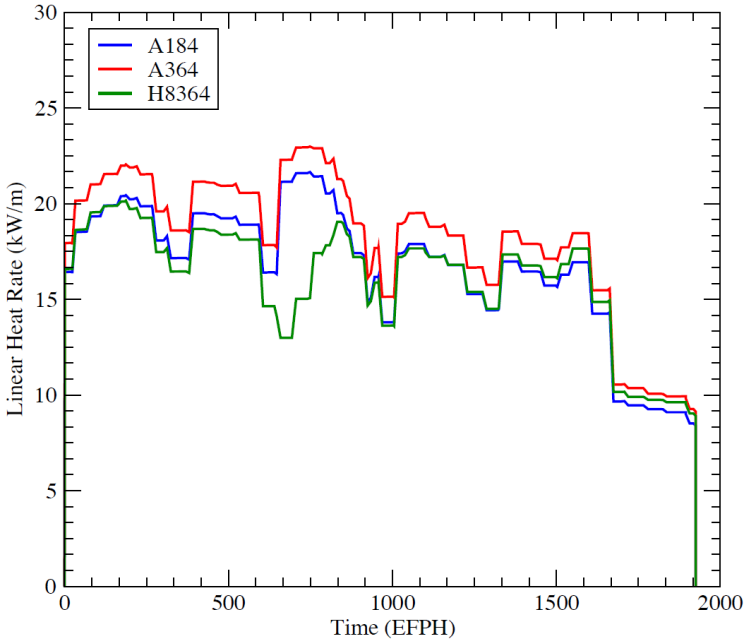

Figure A29.1: The linear heat rates for A1/8-4, A3/6-4 and H8/36-4.

A29.2.2 Geometry and Mesh

All three fuel rods were meshed using 2-D axisymmetric models with eight-node quadratic elements. For simplicity, the pellet stack was modeled as a single continuous fuel column (smeared mesh). The meshes were generated using BISON's automatic mesh generator. The fuel pellets had 200 axial elements and 12 radial elements, and the cladding consisted of 200 axial elements and 4 radial elements.

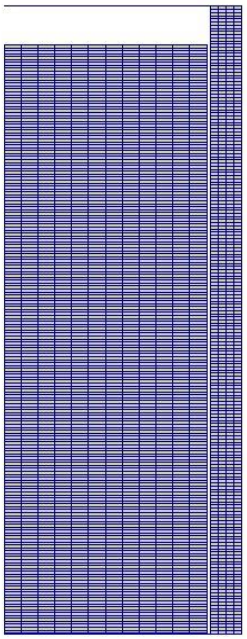

Figure A29.2: A BISON generated mesh showing the fuel and cladding mesh, axially minimized by 100 for visual purposes.

A29.2.3 Material and Behavioral Models

The following material and behavioral models were used for the UO_2 fuel:

- ThermalFuel - NFIR: For temperature and burnup dependent thermal properties.
- RelocationUO2: For relocation strains, the relocation activation threshold power is set to 5 kW/m.
- Sifgrs: A simplified fission gas release model (model 2) with a gaseous swelling model. The transient fission gas release model within Sifgrs was also utilized.

For the clad material, a constant thermal conductivity of 16 W/m-K was used and both thermal (primary and secondary) and irradiation creep were considered using the Limbäck creep model [36].

A29.2.4 Input files

The BISON input and all supporting files (power histories, axial power profile) are provided with the code distribution at bison/assessment/HBEP/analysis.

A29.3 Results

HBEP rods A1/8-4, A3/6-4, and H8/36-4 were designed and built to utilize well-characterized data on the effects of fuel temperature, burnup, power history, and different fuel characteristics with an emphasis on FGR. To achieve this the rods were built to the exact specification as described in the report. These rods were irradiated in the TVO-1 reactor for 6 cycles, and were then taken to a hot cell for fission gas characterization and diametral measurements.

Figure A29.3 and Figure A29.4 compare Bison calculations for both fission gas release and cladding diametral changes following irradiation. Bison's fission gas calculations slightly over predict for two of the cases and dramatically under predict for the H8/36-4 case. Cladding diametal comparisons vary from 12-55 microns.

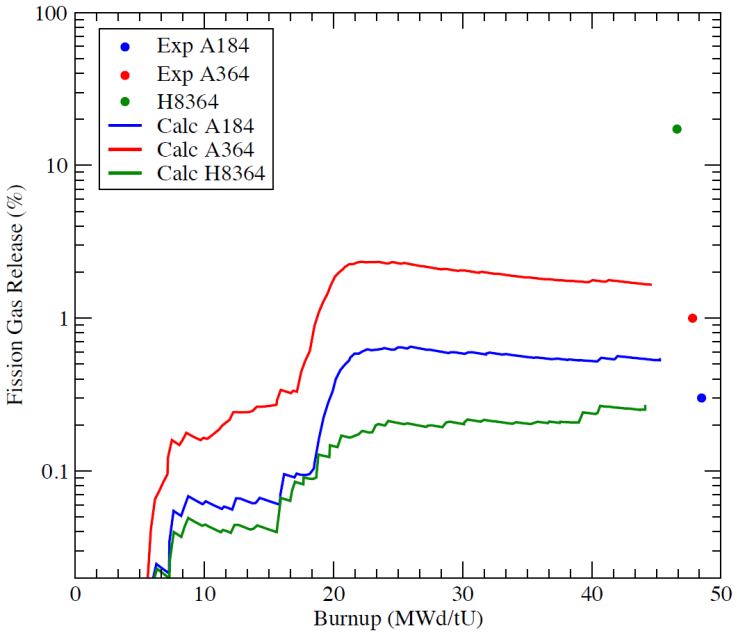

Figure A29.3: Comparison of measured fission gas release and the BISON calculations

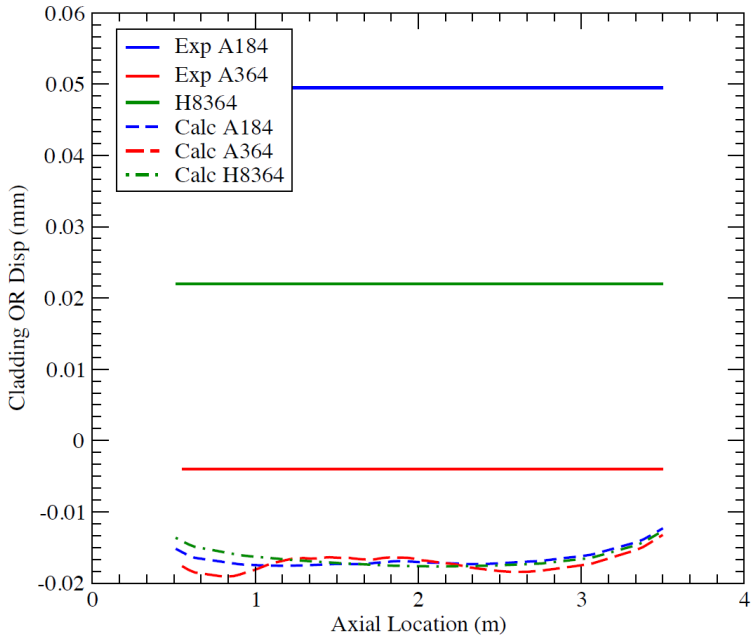

Figure A29.4: Comparison of measured cladding displacements and the BISON calculation; measured diameterchange was averaged over the region 500 to 3500 mm above the bottom of the fuel rod

Table 2.3 makes comparisons between BISON and measured fission gas, plenum pressure, clad elongation, free gas volume, and burnup. Table 2.4 and 2.5 compare Bison pellet-cladding gap calculations to the corisponding axilly measured pellet-clad gap values. Furthermore, Table 2.5 compares pellet OD's between experimental measurements and BISON calculations to better determine the differences between Table 2.4 pellet-clad gap comparisons.

Table A29.2: BISON Comparisons to Experimental Results

A1/8-4	Experiment	BISON	Units
Fission Gas Release	.3	0.54	%
Plenum Pressure	.48	.7	MPa
Clad Elongation	3.966	3.942	m
Free Gas Volume	27.9	21.1	cm^3
Burnup	48.5	45.2	MWd/kgU
A3/6-4	Experiment	BISON	Units
Fission Gas Release	1	1.68	%
Plenum Pressure	.64	.92	MPa
Clad Elongation	3.967	3.942	m
Free Gas Volume	28.5	22.8	cm^3
Burnup	47.8	44.5	MWd/kgU
H8/36-4	Experiment	BISON	Units
Fission Gas Release	17.3	.27	%
Plenum Pressure	2.86	.630	MPa
Clad Elongation	3.964	3.938	m
Free Gas Volume	29.2	21.64	cm^3
Burnup	46.6	43.2	MWd/kgU

Table A29.3: BISON Comparisons to Gap Experimental Measurements

H8/36-4		
Axial Location (cm)	Avg Exp Gap (microns)	BISON (microns)
220.5	24	14.3
170	20	19.2
48.2	48	46.2
23	48	55.3
A3/6-4		
Axial Location (cm)	Avg. Exp Gap (microns)	BISON (microns)
157	25	13

Table A29.4: BISON Comparisons Pellet OD to Experimental Measurements

H8/36-4			
Axial Location (cm)	Exp 0^o (mm)	Exp 90^o (mm)	BISON (mm)
220.5	10.067	10.116	10.058
170	10.105	10.121	10.049
48.2	10.014	10.066	10.002
23	10.068	10.07	9.988
A3/6-4			
Axial Location (cm)	Exp 0^o (mm)	Exp 90^o (mm)	BISON (mm)
157.5	10.536	10.554	10.577

Figure A29.5 shows the strong axial power dependence at times corresponding to axial control blade movements.

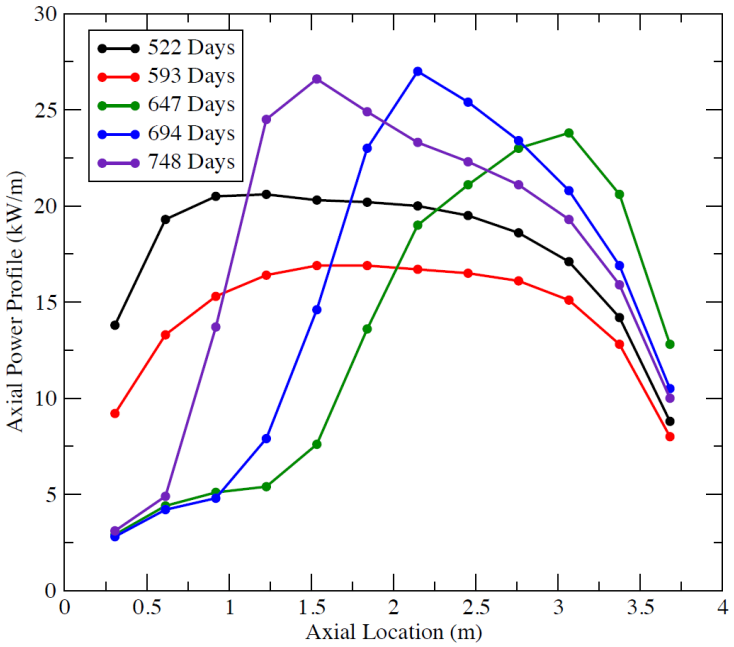

Figure A29.5: Axial Power Profile for H8/36-4 at selected times during the control blade insertion

A29.4 Discussion

Modeling these three rods was useful to the BISON development to validate the capability of modeling high burnup fuel rods. The HBEP report [60] stated, fission gas release was related to the rod location to the control blades. Rods closer to the control blades had significantly higher fission gas release than rods further away. Figure 2.5 shows, there is significant power changes caused by the blade movement, which could result in high fission gas release. BISON code appears to under calculate FGR under such conditions. Rods A1/8-4 and A3/6-4 were not located near a control blade.

During the PIE the cladding diameter was measured, and this value is the average value from 500-3500 mm. Furthermore, the cladding diameter does include the oxide thickness in the measurement. BISON's calculations are with in .07 to .02 mm of the measured value. There is no oxidation model in BISON to model the oxide growth of BWR fuel cladding, and this could also have implication on the calculations.

BISON calculated a lower free gas volume for all cases, and calulated a higher plenum pressure for A1/8-4, and A3/6-4 and a lower plenum pressure for H8/36-4. The difference between the calculated and measurement data on plenum pressure could be contributed to the difference in fission gas release. As for cladding elongation, BISON calculation is lower on all accounts. BISON currently does not consider the plenum spring or friction between the fuel and cladding. Both are driving mechanisms for cladding elongation.

A30 Hardy tube test

A30.1 Overview

The Hardy's experiment was performed to investigate the high temperature strain and rupture behaviour of Zircaloy-4 tubing to estimate the consequences of a hypothetical loss-of-coolant accident (LOCA). The transient-temperature tests were developed to study the effects of internal pressure and heating rate. The objective of the analysis is to validate the BISON code's prediction of clad deformation at high temperatures of Zircaloy-4 tube for internal pressures of 0.3, 1.4, and 5.5 MPa at a heating rate of 25 K/sec (25 C/sec from Hardy's experiment). Hardy test Rods 1, 2, and 3 correspond to Zircaloy tubes with internal pressures of 0.3, 1.4, and 5.5 MPa, respectively.

A30.2 Test Description

A30.2.1 Rod Design Specifications

The geometry of the cladding tube used for the Hardy test is shown in Table A30.1. The tubing material is Zircaloy-4 in a stress relieved condition with 50% cold work. The Zircaloy tubing has an outer diameter of 0.0152654 m (0.601 in) and a wall thickness of 0.000381 m (0.015 in). A schematic diagram of the apparatus used for the Hardy tube test is shown in Figure A30.1 [71]. The transient-temperature test designed to measure the expansion characteristics as a function of internal pressure and heating rate was done with pressurized Zircaloy-4 tubes to obtain mechanical property.

Table A30.1: Hardy Tube Test Rod Specifications

Cladding Tube		
Material		Zircaloy-4
Cold Work	%	50
Length	m	0.5
Inner diameter	mm	14.5054
Outer diameter	mm	15.2654
Wall thickness	mm	0.381
Fill gas pressure		
Rod 1	MPa	0.3
Rod 2	MPa	1.4
Rod 3	MPa	5.5

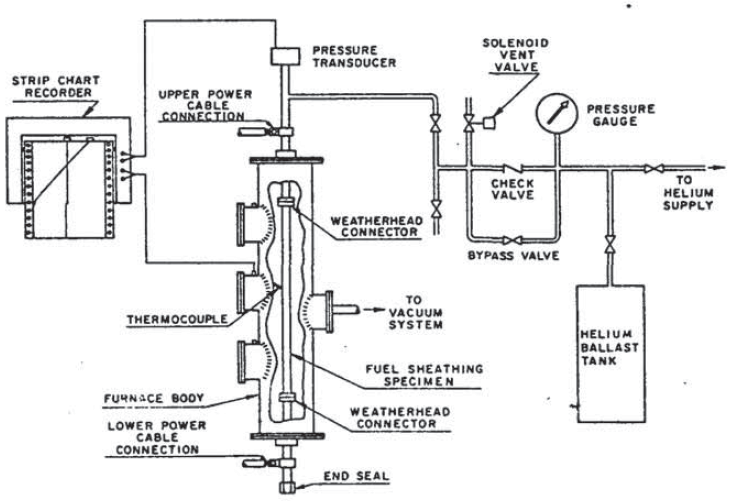

Figure A30.1: Schematic diagram of the Hardy Tube Test apparatus [71]

A30.2.2 Boundary and Initial Conditions

The boundary conditions are tabulated in Table A30.2. The Zircaloy tubes were pressurized with three internal gas pressures, 0.3, 1.4, and 5.5 MPa, for the Hardy tube test analysis.

Table A30.2: Boundary Conditions

Initial temperature	K	600
Heating rate	K/sec	25
External pressure	MPa	0.0
Temperature ramp	K	600-1600
Internal gas pressure		
Rod 1	MPa	0.3
Rod 2	MPa	1.4
Rod 3	MPa	5.5

A30.3 Model Description

A30.3.1 Geometry and Mesh

The geometry of the tube and mesh are shown in Figure A30.2. A single 8-node axisymmetric element was used to model the cladding tube. A full length model was used for the analysis. The length of the element was set at 0.5 m.

Figure A30.2: Scaled view of a single 8-node axisymmetric element mesh for Rods 1, 2 and 3.

A30.3.2 Material and Behavioral Models

The following material and behavioral models were used for the Zircaloy cladding tube:

- MechZry: option to model creep only or combined creep and instantaneous plasticity
- CreepZryModel: model primary and thermal creep of Zircaloy cladding

For the cladding material, a constant thermal conductivity of 16 W/m-K was used. Due to convergence issues at temperature around 900 K, the combined creep and instantaneous plasticity model for Zircaloy-4 cladding was not used in this simulation. Only the CreepZryModel was used to model the primary and thermal creep.

A30.3.3 Input files

The BISON input for the Hardy Tube Test are provided with the code distribution at bison/assessment/Hardy_Tube_Test/ar

A30.4 Results Comparison

A temperature transient thermal-mechanical analysis of the Zircaloy tube was conducted using BISON. The cladding stress-strain response for Rods 1, 2 and 3 to the three internal pressures of 0.3, 1.4, and 5.5 MPa, respectively, were examined. In each case, the internal pressures were kept constant while the temperature of the clad was raised uniformly from 600 K to 1600 K in 40 seconds, resulting in a heat rate of 25 K/sec. However, the solution code failed to converged for temperature above 1458 K for Rod 1, 1210 K for Rod 2, and 1005 K for Rod 3. Therefore, Rods 1, 2 and 3 were run to completion with the same ramp rate to a lower temperature of 1458 K, 1210 K and 1005 K, respectively.

An accuracy-controlling time step criterion was implemented through the MaterialTimeStep postprocessor. The maximum time step size was 1 second and the minimum time step size was 0.00000001 second.

A30.4.1 Strain

The comparison plots of the clad hoop strains as a function of clad temperature between BISON and experimental data from the Hardy tube test for Rods 1, 2 and 3 can be seen in Figures A30.3, A30.4, and A30.5, respectively. The results and test data are shown for cladding hoop strain of less than 0.05 m/m. The BISON results for the cladding hoop strain show that BISON predict the actual experimental values reasonably well for Rods 1, 2 and 3 for the temperature in which the code was able to converged to. For Rod 3 with 5.5 MPa internal pressure, the temp_standard_creep_end temperature of 500 K and temp_loca_creep_begin temperature of 501 K were used instead 700 K and 900 K, respectively. This eliminates the hoop strain deviation from the test data that was observed for Rod 3 when 700 K and 900 K were used as the upper limit of temperature where the standard thermal creep no longer applies and lower limit of temperature where the loca thermal creep model begins to apply, respectively. The deviations from the test data occurred in the temperature range of 700-900 K and may be due to the linear interpolation of the creep rate between the standard thermal creep and loca thermal creep models for internal pressure of 5.5 MPa.

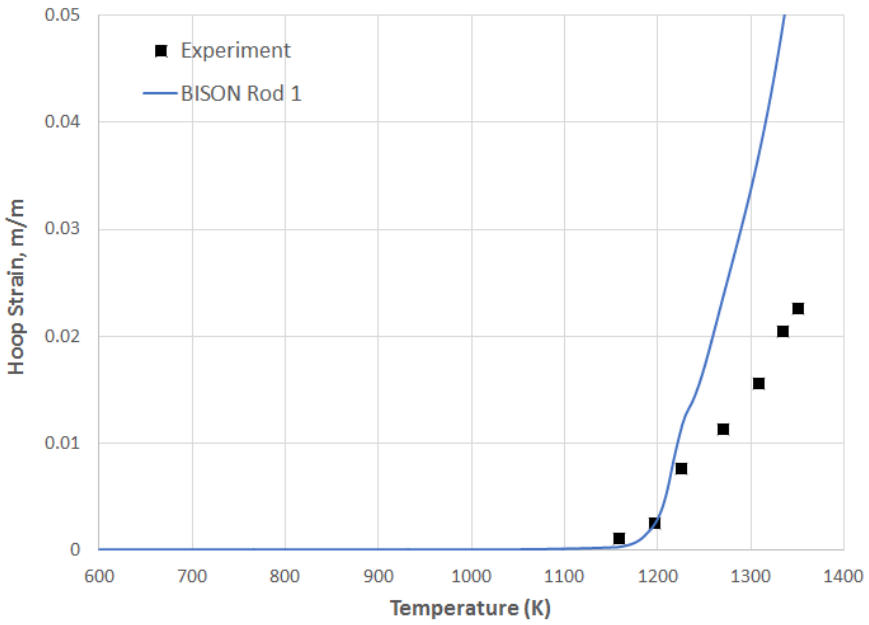

Figure A30.3: Cladding strain for Rod 1 with internal pressure of 0.3 MPa

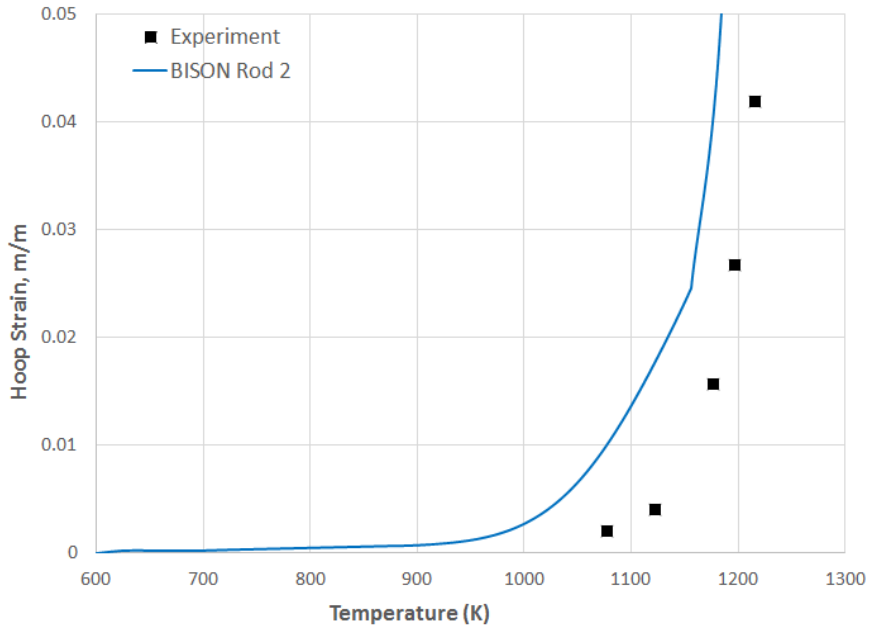

Figure A30.4: Cladding strain for Rod 2 with internal pressure of 1.4 MPa.

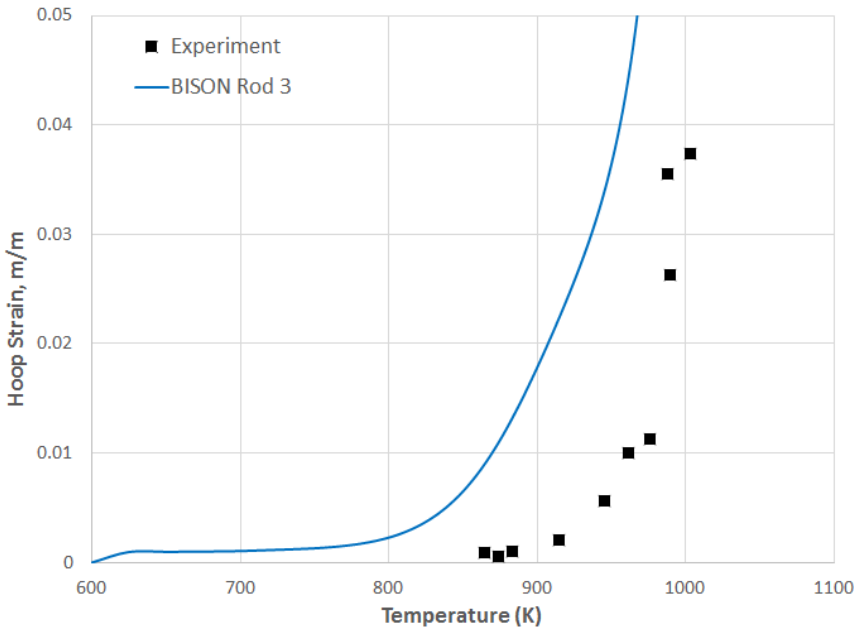

Figure A30.5: Cladding strain for Rod 3 with internal pressure of 5.5 MPa.

A30.5 Discussion

While the results show that BISON predict the cladding strain reasonably well for Rods 1, 2 and 3 compares to the experimental measurements for the temperature the code was able to converged to, there is a slight over prediction for all three rods. Convergence issues were observed for temperature approximately above 1458 K for Rod 1, 1210 K for Rod 2, and 1005 K for Rod 3. The hoop strains were expected to increase with increasing temperatures due to the differential pressure. When the cladding stresses exceeded the yield stress, plastic behavior and large increases in the hoop strains were expected. In addition, the temperature range of the applied heat spanned three material phases; each phase was characterized by a different set of material properties. The three phases are the alpha phase for temperatures lower than 1090 K (1500 F), the alpha+beta phase for temperatures between 1090 K (1500 F) and 1255 K (1800 F), and the beta phase for temperatures above 1255 K (1800 F). The Hardy tube test show that the alpha to beta transformation was found to have a significant effect on deformation characteristics of Zircaloy-4 tubing. Due to convergence issues in using the combined creep and instantaneous plasticity models, the instantaneous plasticity model was not used in this analysis. There are possible weaknesses in the combined creep and instantaneous plasticity model and should be tested further before using it for this simulation. Results and information from this simulation will help to guide future BISON developments.

A31 PUZRY ballooning tests

A31.1 Overview

Since the beginning of the 90s, several experimental series have been performed at the AEKI with Zr1%Nb (E110) and Zircaloy claddings [72]. The aims of these experiments were to study and to compare the mechanical properties of the cladding materials in the temperature range of 20–1200°C and to investigate the effect of oxidation and hydrogen uptake on the mechanical performance of the claddings. The objectives have been achieved through separate effect tests with well defined conditions. These cases are included in the IAEA Coordinated Research Project on Fuel Modeling in Accident Conditions (FUMAC). Limited to Zircaloy claddings (PUZRY test series), BISON simulations of these experiments have been performed.

The PUZRY single rod balloning tests were performed to investigate the mechanical behaviour and strength of Zircaloy cladding tubes and to provide adequate data for model validation. In particular, the effects of temperature and pressurization rate on the deformation and the failure (burst) pressure were investigated.

A31.2 Tests Description

Thirty-one short Zircaloy-4 tube samples were investigated in a resistance furnace providing isothermal conditions in the temperature range of 700–1200°C. The inner pressure of the test tube was increased linearly until the burst of the sample. The pressure history was monitored on-line by a computerized data acquisition system. The residual deformation of the samples was measured after the test.

For these experiments, the specimen was placed in a quartz test tube filled with inert gas (Ar) and heated up in an electrical furnace. The pressure of the inert gas in the quartz tube was kept at constant 1 bar by means of a buffer volume. After an approximately 1000 s heat-up period the sample was pressurized with Ar gas at a constant pressure gradient provided by choking with a capillary tube. Different pressurization rates between 0.005–0.263 bar/s could be achieved by using capillary tubes with different diameters. The temperature in the furnace and the cladding inner pressure were recorded by a PC with the data acquisition frequency of 10 records/s.

The specimens were 50 mm long pieces of Zircaloy-4 claddings. The specimens inner / outer diameters of 9.3 / 10.75 mm corresponded to the parameters of PWR fuel claddings. The samples were closed with Zircaloy end-plugs welded to the cladding in argon atmosphere. The pressurization was performed through a Zircaloy-4 pipe (2.15 mm diameter, 0.25 mm thickness) attached to one end of the specimen. The schematic drawing of the specimen is reported in Figure A31.1. The effect of corrosion on the mechanical performance of Zircaloy-4 cladding was not investigated.

The main characteristics of the PUZRY test series are summarized in Table A31.1.

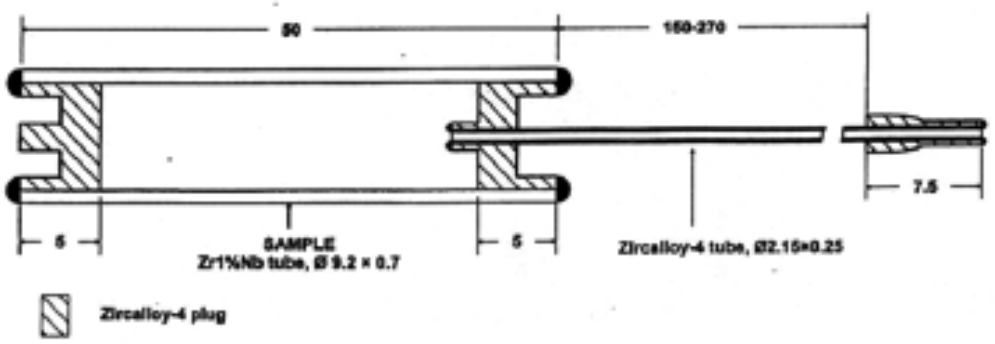

Figure A31.1: Drawing of the tube specimen for single-rod ballooning tests performed at AEKI [72]. Note that Zircaloy-4 tubes were used for the PUZRY tests.

Table A31.1: Main characteristics of the PUZRY test series [72].

Tube specimens	
Alloy	Zircaloy-4
Inner radius (mm)	4.65
Thickness (μm)	725
Length (mm)	50
ZrO_2 layer (μm)	0
End plugs	Zircaloy-4
Experimental conditions	
Temperature range (°C)	700–1200
Heating rate	isothermal tests
Pressure range (bar)	0–106
Pressurization rate (bar/s)	0.005–0.263
Atmosphere	Ar
Instrumentation	Pressure sensor, temperature sensor
Data acquisition (records/s)	10
Number of specimens tested successfully	31

A31.3 Modeling

A31.3.1 Setup of Calculations

2D axisymmetric BISON models of the cladding tubes tested during the PUZRY experiments were built. The presence of the end plugs was accounted for by applying zero radial displacement boundary conditions to the tube surfaces in correspondence of the plugs. The furnace heating was simulated by a temperature boundary condition applied to the tube outer wall and consistent with the experimental conditions. A slight, linear variation of the temperature along the tube length was considered, with the total temperature difference being 6°C [73]. The maximum temperature was considered at the tube mid-plane, which is consistent with visual inspections of the tested specimens showing ballooning around the mid-plane [72]. Taking advantage of the axial symmetry of the problem, only the lower half of the heated cladding length was modelled.

A31.3.2 Material and Behavioral Models

The following material and behavioral models were used for the Zircaloy-4 cladding:

- ThermalZry: Thermophysical material properties of Zircaloy.
- SolidModel: Solid mechanics models including elasticity, thermal expansion and creep. In particular, creep was calculated using a specific correlation for LOCA conditions (see MechZryModel).
- ZrPhase: Model for crystallographic phase transformation of Zircaloy as a function of temperature and time.
- Failure Cladding: Criterion for cladding failure due to burst, based on the calculated hoop stress and creep strain rate.

Constant values are used for the Youngś modulus ($E = 10^{11}$ Pa), Poisson ratio ($\nu = 0.3$) and linear thermal expansion coefficient ($\alpha = 5 \cdot 10^{-6}$) of the material.

A31.3.3 Input Files

The BISON inputs and all supporting files (temperature, pressure histories) for the simulations of the 31 PUZRY cases are provided with the code distribution at bison/assessment/PUZRY_ballooning_tests/analysis.

A31.4 Results

The simulation results for the 31 PUZRY cases are compared to the available experimental data in order to validate the BISON models for Zircaloy cladding behavior under LOCA accident conditions. Figures A31.2 and A31.3 show the comparisons between BISON predictions and experimental data of cladding inner pressure at failure and time to failure, respectively. The obtained accuracy is in line with the state of the art of fuel cladding modeling under LOCA conditions [74].

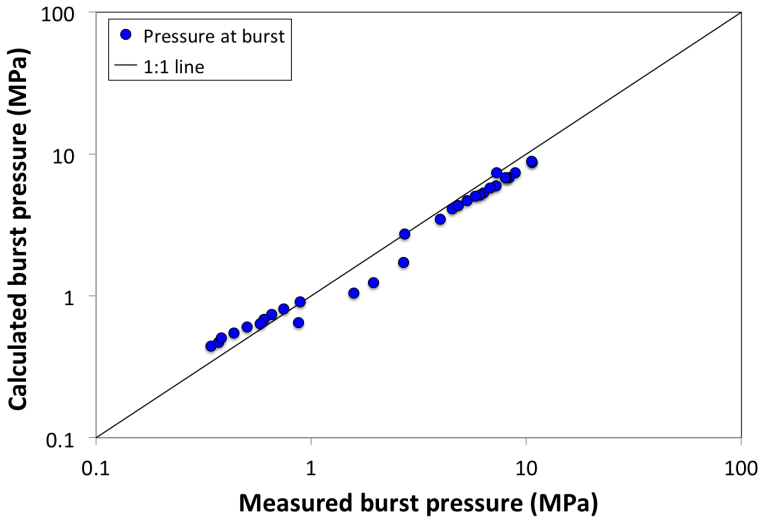

Figure A31.2: Comparison of calculated and measured tube inner pressures at burst for the PUZRY cases.

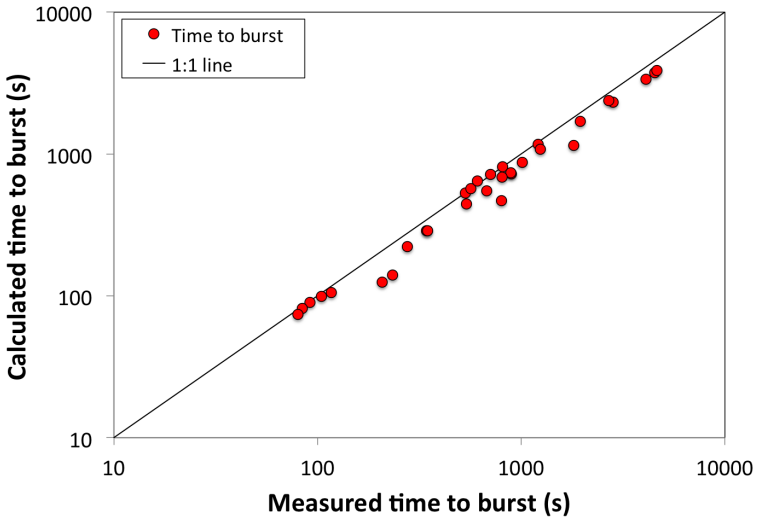

Figure A31.3: Comparison of calculated and measured time to burst for the PUZRY cases.

A32 REBEKA ballooning tests

A32.1 Overview

The REBEKA separate effects tests [75, 76, 77] are temperature transient tests in steam performed on single PWR–size Zircaloy–4 tubes at a variety of internal pressures and heating rates. The purpose of the tests was to establish data of cladding ballooning and burst with reference to LOCA conditions. The single-rod tests from the REBEKA program have been simulated with BISON for validation of code's modeling capabilities to reproduce cladding ballooning and burst under LOCA conditions.

A32.2 Test Description

A32.2.1 Experiment

The cladding tubes had a fabricated inner/outer diameter of 9.30/10.75 mm, with a 325 mm heated length, and were heated indirectly by conduction heating from inside, using an electrically insulated heater rod. A stack of alumina annular pellets (Al_2O_3) was used to simulate the fuel column in a fuel elements. The diametral c1earance between the cladding inner diameter and the pellets outer diameter was 0.15 mm. The axial gap distance between the end plugs and alumina pellets stack was 15 mm. Considering this magnitude and the change in the axiallength of the tube, it can be said that these experiments were carried out under axially unconstrained conditions. The test parameters covered a range of 1 to 14 MPa for the internal rod (He) pressure and 1 to 30 K s^{-1} for the heating rate. The test atmosphere was almost stagnant steam at atmospheric pressure and at a temperature of 473 K. The cladding temperatures were measured by thermocouples spot–welded on the outer surface of the cladding. More details on the experimental apparatus and conditions are given in [75, 76, 77].

A32.3 Model Description

A32.3.1 Geometry and Mesh

The considered cases are modeled considering only the cladding, while the allumina pellets are taken into account imposing a proper tempeature boundary conditions at the cladding inner radius, which accounts for the heat transfer through the inner components. For semplicity, only the heated portion of the rods was simulated.

A 2-dimensional axisymmetric quadratic (Quad8 elements) mesh was used to model the geometry of the considered rods. In addition, to investigate inherently three–dimensional aspects, such as the effect of azimuthal temperature differences, 3D simulations were conducted emplying hexahedral elements (Hex20 elements).

Taking advantage of the symmetry of the problem, only the lower half of the heated cladding length was modelled in the 2D simulations. For the 3D simulations, a quarter of the cladding circumference was modelled.

A32.3.2 Material Models

The following characteristic models were used for the Zircaloy–4 claddings in the considered conditions:

- High-temperature cladding oxidation calculated using the correlations of Leistikow [78] (in OxidationCladding model).
- Crystallographic phase transition model ZrPhase, which computes the volume fraction of β phase for Zr–based cladding materials as a function of time and temperature. The model is based on [79, 80].
- High-temperature creep model based on the correlations from [81, 75]. This allows for outward creep deformation of the cladding tube under the effect of internal pressurization and high temperature leading to cladding ballooning. The model accounts for the effect of crystallographic phase transition.
- The FailureCladding model, which evaluates the onset of cladding burst due to combined overstress and plastic instability [75, 74], and takes into account the effect of Zirconium phase transition and oxidation.

A32.3.3 Boundary Conditions

The internal electric heating was simulated by a time–dependent Dirichlet temperature boundary condition applied to the tube inner wall and consistent with the experimental conditions. In particular, a parabolic temperature profile symmetric with respect to the tube mid-plane was considered, which results from the uniform axial power generation in the heater rod [77]. To estimate the temperature variation over the heated length of the cladding, simplified calculations of axial heat conduction within the rod and convection to the outer steam atmosphere were performed, based on available information on materials and experimental conditions [75, 76, 77]. Pressure equal to the experimental value was applied at the tube inner wall.

A32.3.4 Input files

The BISON input and all supporting files for these cases are provided with the code distribution at bison/assessment/REBEKA/analysis.

A32.4 Results

Using the 2D axisymmetric model, simulations were conducted of the REBEKA experiments with a heating rate of 1 K s^{-1}, considering the full range of 1 to 14 MPa for the internal cladding pressure. As for the 3D model, only one case is here reported, in order to demonstrate BISON's ability to assess the impact of azimuthal temperature variations on cladding ballooning and burst.

A32.4.1 2D simulations

The predictions of burst temperature at the various internal cladding pressures are compared to the available experimental data in Figure A32.1. The trend of increasing burst temperature with decreasing internal pressure is reproduced, and the quantitative accuracy of predictions is reasonable. Nevertheless, a moderate but systematic under–prediction is observed. Such discrepancies may be due to uncertainties inherent in the cladding mechanics, oxidation and phase transformation modelling, three–dimensional effects (azimuthal temperature differences) that cannot be captured by 2D modelling, as well as measurement uncertainties.

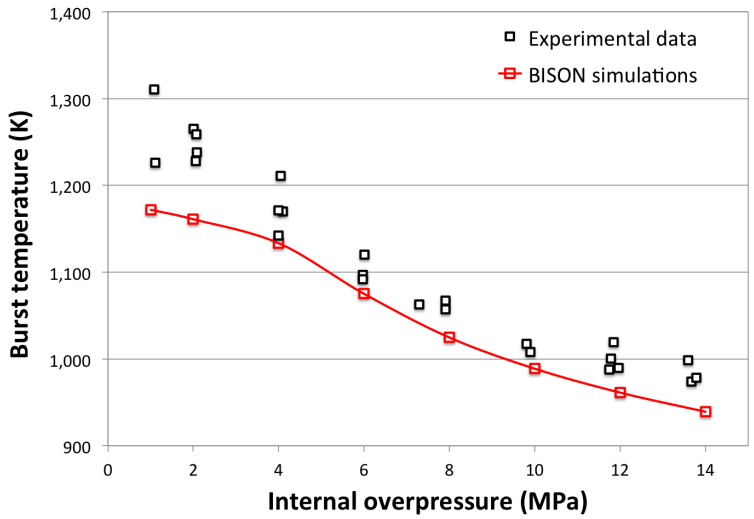

Figure A32.1: Comparison between BISON predictions and experimental data of cladding burst temperature for the simulations of the REBEKA tests with heating rate of 1 K s^{-1}.

Figure A32.2 shows contour plots of temperature, creep strain magnitude, and locations where the local stress reached the limiting burst stress for the case with 10 MPa internal pressure; results are shown at the time of cladding burst. The creep strain magnitude (-) is defined as

$$\varepsilon_{cr,mag} = \sqrt{\frac{2}{3}\,\overline{\overline{\varepsilon_{cr}}} : \overline{\overline{\varepsilon_{cr}}}} \tag{A32.1}$$

where $\overline{\overline{\varepsilon_{cr}}}$ is the creep strain tensor. The cladding ballooning effect as reproduced by BISON is obvious. Cladding failure due to burst is predicted at a temperature of about 993 K and a creep strain magnitude of about 1.1, which reasonably conform to experimental observations [75, 77]. The burst stress is first reached in the cladding mid–section of the cladding, which is characterized by the largest strain and hence by the highest thinning. The time evolution of the hoop stress and burst stress in the cladding mid–section in proximity of time of burst are plotted in Figure A32.3. The corresponding hoop strain is also shown. The stress increases under the effect of the constant inner pressure as the cladding wall thins due to the large creep strain. The burst stress decreases over time due to increasing temperature and progressive cladding oxidation (and in general also due to phase transformation, not observed at the

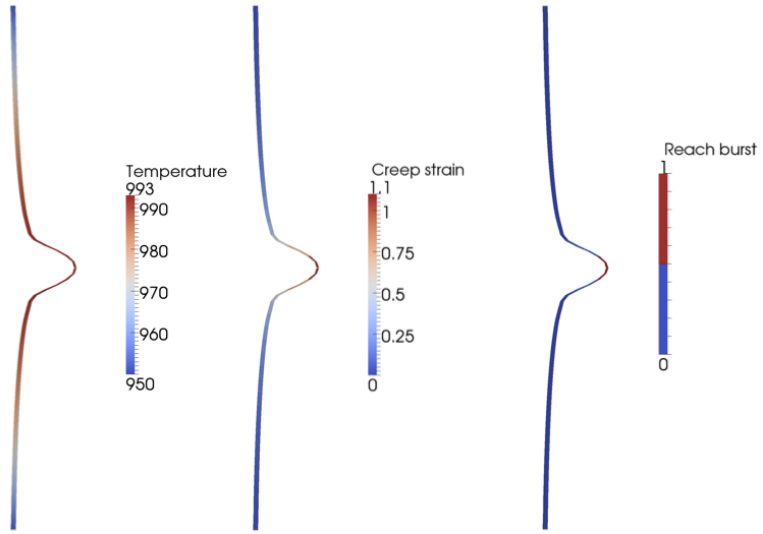

Figure A32.2: Contour plots for the BISON 2D simulation of the REBEKA test with 10 MPa internal pressure at the time of cladding burst. The results for the lower half of the heated cladding are mirrored to obtain a full-length view. The plots are magnified 4x in the radial direction for visualization.

temperatures reached in this specific case). The calculated time evolution of the cladding hoop strain is consistent with the experimental observations [77].

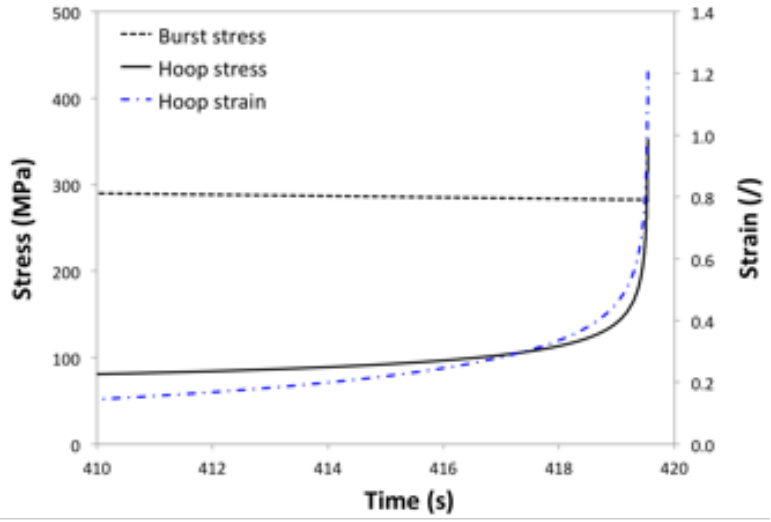

Figure A32.3: Time evolution of burst stress, hoop stress, and hoop strain at the cladding mid–section in proximity of time of burst. The results refer to the BISON simulation of the REBEKA test with 10 MPa internal pressure.

A32.4.2 3D simulation

In addition to above mentioned boundary conditions applied to the 2D simulations, in the 3D simulation an azimuthal temperature gradient was applied. A maximum azimuthal temperature variation of 30 K was considered, in conformity with the experimental indications from thermocouple measurements [76]. The results are presented for the exemplifying case of 10 MPa internal pressure at the time of cladding burst. Figure A32.4 shows contour plots of temperature, creep strain magnitude, and locations where the

local stress reached the limiting burst stress. The 3D simulation reproduces the non-uniform cladding ballooning and a localized burst on the hottest side of the cladding, which is consistent with experimental observations [76]. Note that the predicted burst temperature is higher (by about 10 K) than for the corresponding 2D simulation, thus indicating that capturing 3D aspects such as the effect of azimuthal temperature differences is of importance for fuel analysis during LOCA accidents.

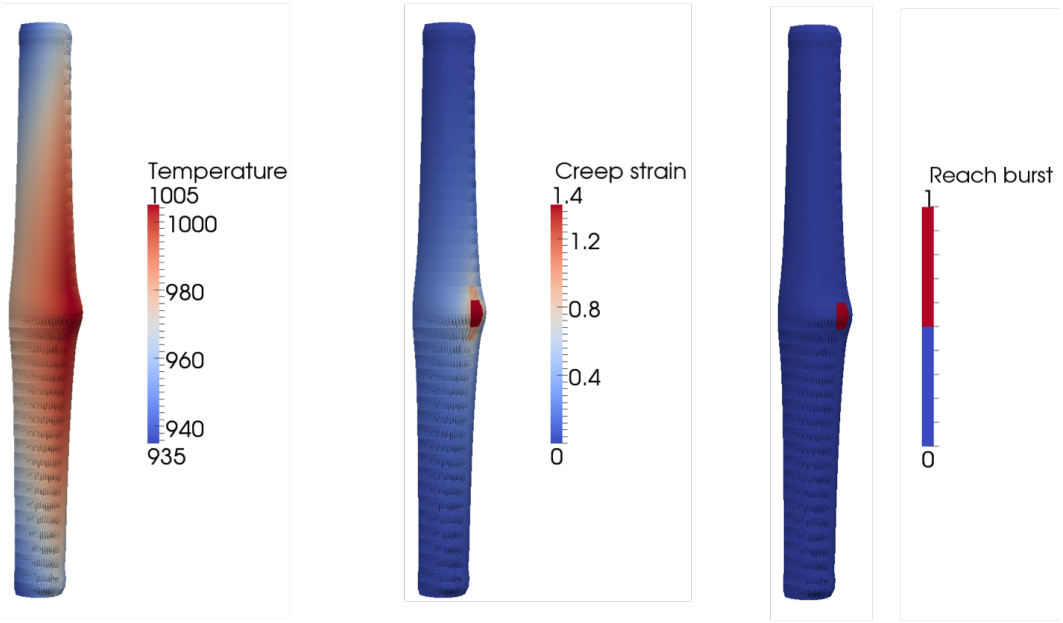

Figure A32.4: Contour plots for the BISON 3D simulation of the REBEKA test with 10 MPa internal pressure at the time of cladding burst. The results for the lower quarter of the heated cladding are mirrored to obtain a full-length, half circumference view. The plots are magnified 3x in the radial direction for visualization. The blur zones are due to the adopted visualization tool.

A33 IFA 650.2 integral LOCA test

A33.1 Overview

LOCA tests at Halden (IFA-650 series) are integral in-pile single rod tests. The second trial test run IFA-650.2 [82] was performed in May 2004.

A33.2 Test Description

A33.2.1 Rod Design Specifications

The test was carried out using a fresh, pressurized PWR rod and low fission power to achieve the desired temperature conditions. The rod plenum volume was made relatively large to be able to maintain stable pressure conditions during ballooning. The fabrication characteristics of the IFA-650.2 fuel rod are reported in Table A33.1.

Table A33.1: Design data of IFA-650.2 fuel rod [82]

Fuel material		UO_2
Fuel density	%TD	95.0
^{235}U enrichment	wt%	2.0
Active stack length	mm	500
Pellet OD	mm	8.29
Pellet ID	mm	0
Cladding material		Zy-4
Cladding ID	mm	8.36
Cladding OD	mm	9.50
Diametral gap	μm	70
Free volume	cm^3	17.4
Fill gas		He
Fill gas pressure	MPa	4.0

A33.2.2 Operating Conditions and Irradiation History

The fuel rod was located in a standard high-pressure flask in the IFA-650 test rig in the Halden reactor. A heater surrounding the rod was used to simulate the heat from adjacent rods. The flask was connected to a high-pressure heavy water loop and a blowdown system. During normal operation prior to the LOCA test, the rig was connected to the loop and forced circulation flow conditions existed. Then, the rig was disconnected. A natural convection phase began, with water flowing up between the fuel rod and flow separator (with heater) and down between flow separator and flask wall. Full pressure still existed in the rig. LOCA was initiated by opening the valves leading to the blowdown tank (blowdown phase). The initial pressure in the loop was $\sim$7 MPa and the counterpressure in the blowdown tank was $\sim$0.2 MPa. The channel pressure decreased to 3–4 bars, and the rig was practically emptied of water within 30–40 seconds. Stagnant superheated steam surrounding the rod provided inadequate cooling and the cladding temperature increased quickly (heat-up phase). A low fission power of 2.3 kW/m was used to simulate decay heat and achieve the desired temperature conditions. Cladding ballooning and rupture occurred during the heat up phase (burst at $\sim$800°C). Spray injection was started when the cladding temperature reached approximately 870°C, with the purpose to ensure enough steam for the oxidation process of the cladding. The target cladding temperature of 1050°C was reached and held for 264 seconds. The test was ended by a reactor scram.

The Halden IFA-650.2 test was selected for comparative fuel performance modelling in the IAEA FUMEX-III Project [45] and is being considered also within the IAEA FUMAC Project on Fuel Modelling under Accident Conditions [6].

A33.3 Model Description

A33.3.1 Geometry and Mesh

The rod geometry was modeled following the design specifications from [82] (Table A33.1). The enriched fuel pellet column was represeted with a smeared fuel column. Natural UO_2 pellets at the top and bottom of the fuel stack were also included. A single rod upper plenum was considered, whose volume is the sum of the various plenum volumes in the more complex real geometry [82]. A 2-dimensional axi-symmetric quadratic (Quad8 elements) finite element mesh was used. The enriched fuel column mesh consisted of 6 radial elements and 62 axial elements. Each natural UO_2 pellet mesh consisted of 6 radial elements and 1 axial element. The cladding mesh consisted of 256 axial elements and 3 radial elements. Figure A33.1 shows the finite element mesh used for the BISON anaysis of the IFA-650.2 fuel rod.

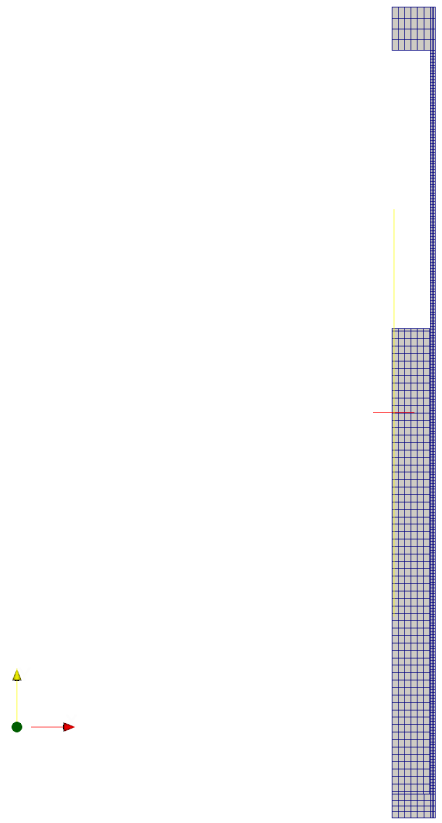

Figure A33.1: Finite element mesh for the IFA-650.2 fuel rod. The figure is scaled 10 times in the radial direction for visualization.

A33.3.2 Material and Behavioral Models

The following material and behavioral models were used for the UO_2 fuel:

- ThermalFuel - NFIR: temperature and burnup dependent thermal properties
- RelocationUO2: relocation strains, relocation activation threshold power set to 5 kW/m.
- VSwellingUO2: MATPRO models for fuel solid swelling and densification.
- Sifgrs: fission gas release model with the combined gaseous swelling model.

The following models were used for the Zircaloy–4 cladding that allow for representing ballooning and burst under LOCA conditions:

- High-temperature cladding oxidation calculated using the correlations of Leistikow [78] (in OxidationCladding model).
- Crystallographic phase transition model ZrPhase, which computes the volume fraction of β phase for Zr–based cladding materials as a function of time and temperature. The model is based on [79, 80].
- High-temperature creep model based on the correlations from [81, 75]. This allows for outward creep deformation of the cladding tube under the effect of internal pressurization and high temperature leading to cladding ballooning. The model accounts for the effect of crystallographic phase transition.

- The FailureCladding model, which evaluates the onset of cladding burst due to combined overstress and plastic instability [75, 74], and takes into account the effect of Zirconium phase transition and oxidation.

A33.3.3 Boundary and Operating Conditions

The boundary conditions (BCs) in terms of linear heat rate and rig pressure were provided by IFE-Halden.

Temperature BCs at the cladding outer surface were evaluated based on cladding outer temperatures which were measured at two axial positions during the experiment, and were also part of the Halden data. In particular, axial temperature profiles at the clad outer surface were obtained using some simplifying assumptions and imposing coincidence with the measured temperatures at measurement axial locations. The obtained profiles were used as outer cladding temperature BCs in absence of detailed thermal-hydraulics calculations. Details of the procedure and assumptions adopted for the calculation of the temperature BCs used for the BISON simulations of IFA-650.2 are given hereinafter.

Determination of the temperature boundary conditions

Clad outer temperature axial profiles are obtained based on the following assumptions:

- The effect of radiation is lumped into an 'effective' heat transfer coefficient. This is based on linearizing the radiative heat transfer law, $q'' \propto \left(T_1^4 - T_2^4\right)$, into $q'' \propto h_{rad}\,(T_1 - T_2)$, where q'' is the heat flux and $h_{rad} \propto T_{average}^3$ and has units of a heat transfer coefficient. The linearized equation is accurate if T_1 and T_2 are close enough. Under this assumption, the axial clad temperature profile can be written in a form as if heat transfer was purely convective

$$T(z) = T_{cool}(z) + q''(z)/h_{eff}(z) \tag{A33.1}$$

  where z is the axial coordinate, $T_{cool}(z)$ is the coolant temperature, and h_{eff} is the 'effective' heat transfer coefficient (convection+radiation).

- The coolant temperature is approximated as the heater temperature at the axial position z. This is estimated based on the Halden data of measured heater temperature at two axial location and a linear interpolation.

- The heat flux is proportional to the local linear heat rate, i.e., $q''(z) \propto q'(z)$. This is reasonable provided that the coolant channel conditions are reasonably uniform along the rod and that no axial fuel relocation takes place during the test. From this assumption and Eq. A33.1, it follows:

$$T(z) = T_{cool}(z) + q'(z)/h^*(z) \tag{A33.2}$$

  Where $h^*(z) = k h_{eff}(z)$ and k is a constant. The local linear heat rate, $q'(z)$, is obtained from the Halden data.

- $h^*(z)$ is determined based on the measured cladding temperatures. For this purpose, h^* is assumed to vary linearly along z

$$h^* = Az + B \tag{A33.3}$$

  The two equations needed to determine the coefficients A and B are the conditions of $T(z)$ (Eq. A33.2) being equal to the measured temperatures at the two measurement locations (thermocouples at clad outer wall).

The strongest simplification in the above approach is taking a linear fit of the heat transfer coefficient along the axial direction. When radiation is dominant, approximately $h^* \propto T_{average}^3$, which likely has a maximum at peak power position. However, the above approach based on measured temperatures may

be accurate enough in view of the uncertainties involved in determining thermal-hydraulic boundary conditions.

Figures A33.2 to A33.5 show examples of estimated clad outer temperature profiles at selected instants during different phases of the experiment. Using the measured temperatures and an axially varying heat transfer coefficient, actually, allows one to capture effects such as the higher temperature in the lower part of the rod during the blowdown phase, which are difficult to explain [82] or reproduce through thermal-hydraulics calculations.

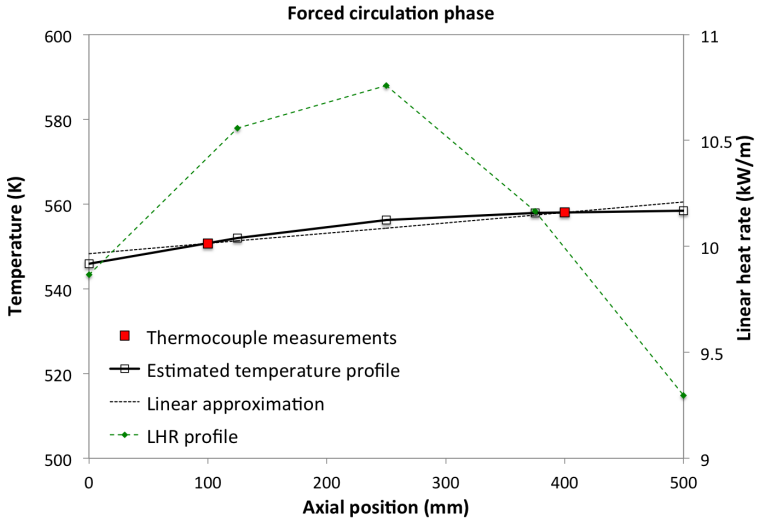

Figure A33.2: Estimated axial temperature profile at cladding outer surface at an instant during the forced circulation phase of the IFA-650.2 experiment. The measured temperatures at the thermocouple locations and the linear heat rate (LHR) profile interpolated from Halden data are also shown.

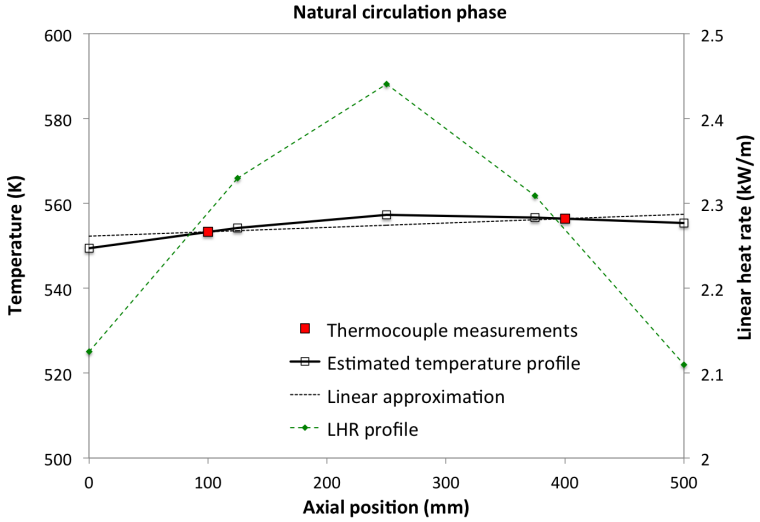

Figure A33.3: Estimated axial temperature profile at cladding outer surface at an instant during the natural circulation phase of the IFA-650.2 experiment. The measured temperatures at the thermocouple locations and the linear heat rate (LHR) profile interpolated from Halden data are also shown.

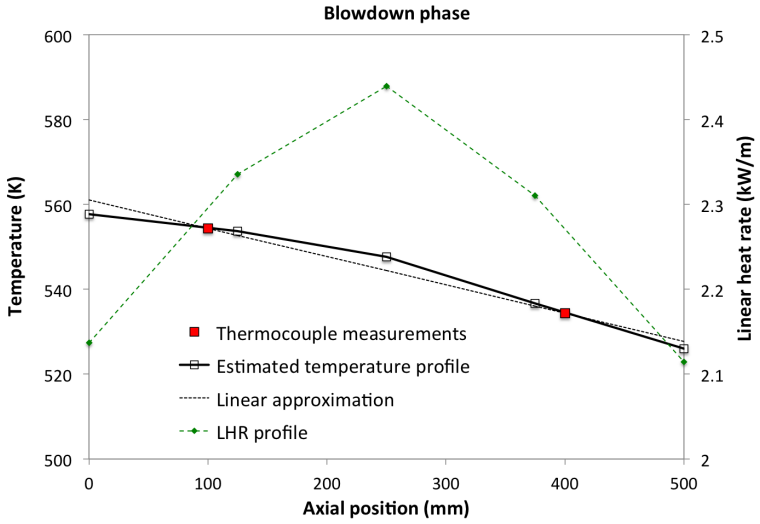

Figure A33.4: Estimated axial temperature profile at cladding outer surface at an instant during the blowdown phase of the IFA-650.2 experiment. The measured temperatures at the thermocouple locations and the linear heat rate (LHR) profile interpolated from Halden data are also shown.

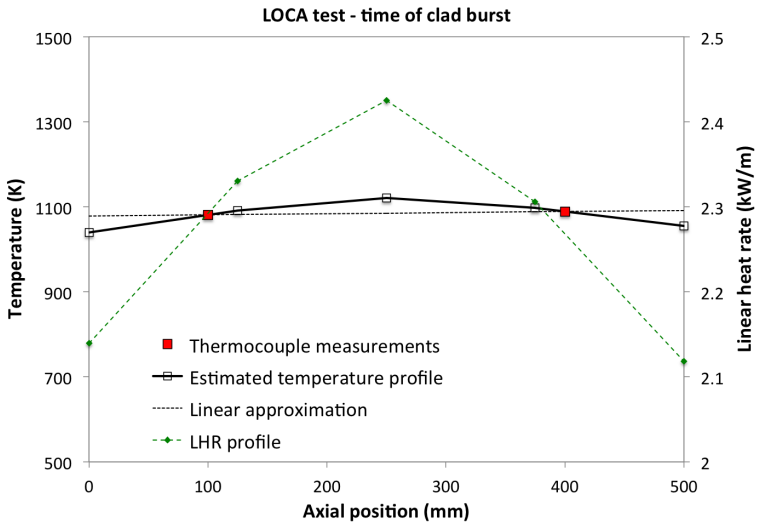

Figure A33.5: Estimated axial temperature profile at cladding outer surface at the time of cladding burst for the IFA-650.2 experiment. The measured temperatures at the thermocouple locations and the linear heat rate (LHR) profile interpolated from Halden data are also shown.

A33.3.4 Input files

The BISON input and all supporting files (power histories, axial power profile, fast neutron flux history, etc.) for this case are provided with the code distribution at bison/assessment/IFA_650_LOCA_tests/IFA_650.2/analysis.

A33.4 Results

We present comparison between calculated and experimental inner pin pressure and time to burst for the IFA-650.2 test. In Figure A33.6, calculated inner pin pressure is compared to the on-line experimental measurement, with predicted and experimental time to burst being also illustrated. The comparison points out that both quantities are reasonably well predicted by BISON. Rod pressure is slightly over-predicted during the heat-up phase of the test, which may be ascribed to discrepancies in the calculated plenum temperature and/or evolution of fuel rod inner volume during ballooning. Fission gas release is very low due to the test being performed with a fresh fuel rod and is not expected to affect rod pressure significantly.

Calculated time to burst is within 7 seconds of the experimental one.

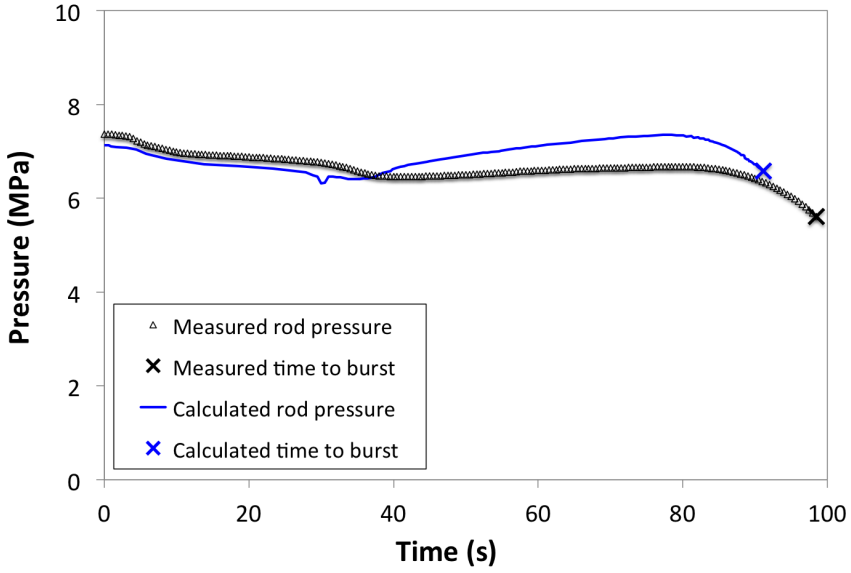

Figure A33.6: Comparison between measured and calculated fuel rod inner pressure and time to cladding bust for the Halden IFA-650.2 test. Time zero corresponds to the beginning of the blowdown phase.

A34 IFA 650.10 integral LOCA test

A34.1 Overview

The LOCA experiments performed in the Halden Research Reactor are integral in-pile single rod tests on fuel behavior under simulated LOCA conditions. The tenth LOCA test, i.e., IFA-650.10 [83], was carried out using a segment of a PWR rod that had been irradiated in a commercial PWR (Gravelines 5, 900 MWe, EDF, France) up to a burn-up of 61 MWd/kgU. During the test a low fission power (25 W/cm) was used to achieve the desired conditions for high cladding temperatures, ballooning and oxidation. A heater surrounding the rod and operating at 12 W/cm was used for simulating the heat from adjacent rods. The average cladding temperature increase rate during the heat-up was around 8 K/s. Cladding failure occurred ~249 seconds after blowdown at a cladding temperature of ~1025 K.

The Halden IFA-650.10 test was selected for comparative fuel performance modelling in the IAEA IAEA FUMAC Project on Fuel Modelling under Accident Conditions [6].

A34.2 Test Description

A34.2.1 Fuel rod characteristics and experimental setup

The fabrication characteristics of the IFA-650.10 fuel rod are reported in Table A34.1. The test rod was a segment from the commercially irradiated PWR mother rod. The fuel and cladding materials are UO_2 and Zircaloy-4, respectively, with typical PWR design specifications. The refabricated rod was filled with a gas mixture of 95 % argon and 5 % helium at 4 MPa. Argon was chosen to simulate the (low-conductivity) fission gases. The rod plenum volume (free gas volume) was made relatively large in order to maintain stable pressure conditions until cladding burst occurred. The total free gas volume (17 cm^3) was thus practically all located in the plenum, outside the heated region.

The fuel rod was located in a standard high-pressure flask in the IFA-650 test rig, which was connected to a high-pressure heavy water loop and a blowdown system. A schematic of the test rig with its instrumentation is shown in Fig. A34.1 and a cross-sectional view of the rig is shown in Figure A34.2.

The rod was located in the center of the rig and surrounded by an electrical heater inside the flask. The heater is part of a flow separator, which divides the space into a central channel surrounding the fuel rod and an outer annulus. The heater is used for simulating heat from the adjacent fuel rods in a power reactor core. Cladding temperature is influenced by both rod and heater powers. The flask was surrounded by a shroud and was placed inside the Halden reactor. The annulus between the shroud and the flask is filled with moderator (heavy water) at a pressure of 34 bar and a temperature of 235 C. One cladding surface thermocouple, TCC1, was located 9.5 cm above the fuel stack bottom, and the other two, TCC2 and TCC3, were attached 8 cm below the top of the stack. In IFA-650.10 the temperature of the heater was measured by two embedded thermocouples, i.e., TCH1 at the same elevation as TCC1, and TCH2 at ~2.6 cm below the fuel mid plane. A third thermocouple was placed on the outside surface at the axial midplane of the plenum. The axial power distribution was measured by three self-powered vanadium neutron detectors (ND) at three different elevations. The rig instrumentation also included a fuel pressure sensor (PF) and thermocouples at the inlet (TI) and outlet (TO) of the rig to measure the coolant temperatures.

Table A34.1: Design data of IFA-650.10 fuel rod [83, 84]

Fuel material		UO_2
Fuel density	%TD	95.32
^{235}U enrichment	wt%	4.487
Active fuel length	mm	440
Pellet OD	mm	8.21*
Pellet ID	mm	0
Pellet length	mm	10
Cladding material		Zy-4
Cladding ID	mm	8.36
Cladding OD	mm	9.50
Diametral gap	μm	150
Free volume	cm^3	17
Fill gas		Ar (95%), He (5%)
Fill gas pressure	MPa	4.0
Coolant temperature	K	508
Coolant pressure	MPa	7

* For consistency with the fuel-cladding diametral gap width [83, 84].

A34.2.2 Operation procedure and conditions

The experimental procedure for the IFA-650.10 test is detailed below [83]. Note that we refer here to the LOCA test performed in the Halden reactor on the pre-irradiated, refabricated PWR fuel rod. In the BISON simulation, we also considered the commercial base irradiation preceding the test, as described in Sections A34.3 and A34.4.

The general test scheme of IFA-650.10 consisted of the following phases:

- Preparatory phases. The test started with a preparatory irradiation with effective water cooling. This consisted of a forced circulation phase followed by a natural circulation phase. At the start of the test, the axial power distribution was symmetric with a peak to average power factor of ~1.05 (Fig. A34.3). The forced circulation phase started with steady state operation at a linear heat generation rate (LHGR) of 120-130 W/cm, with the outer loop connected and the pressure in the loop set to ~70 bar. Then the LHGR was decreased to ~25 W/cm by decreasing the reactor power. After reaching the correct fuel power level the electrical heater was turned on to the preset value ~12 W/cm. The power levels were chosen based on the previous test runs and pre-calculations to achieve the target peak cladding temperature (PCT) of 850 C during the heat-up phase of the test. Then the flow regime was switched to natural circulation by disconnecting the rig from the outer loop. The flow separator enabled natural convection flow in the test section of the rig: water flowed up between the fuel rod and flow separator (with heater) and down between flow separator and flask wall. Full pressure still existed in the rig. Temperatures in the rig were left to stabilize for three minutes before blowdown.

- Blowdown phase. Valves to the dump tank were opened (blowdown). The channel pressure decreased rapidly to ~4 bar as water flew out of the pressure flask. The rig was practically emptied of water in ~71 s, which corresponds to the end of the blowdown phase (beginning of the dry phase). The end of the blowdown phase is identified by the sudden increase in cladding and heater surface temperature. Also the temperature difference between the cladding and heater increases rapidly at end of the blowdown phase.

- Dry or heat-up phase. Stagnant superheated steam surrounding the test rod provided inadequate cooling and the fuel cladding temperature increased quickly. Much of the heat removal from the

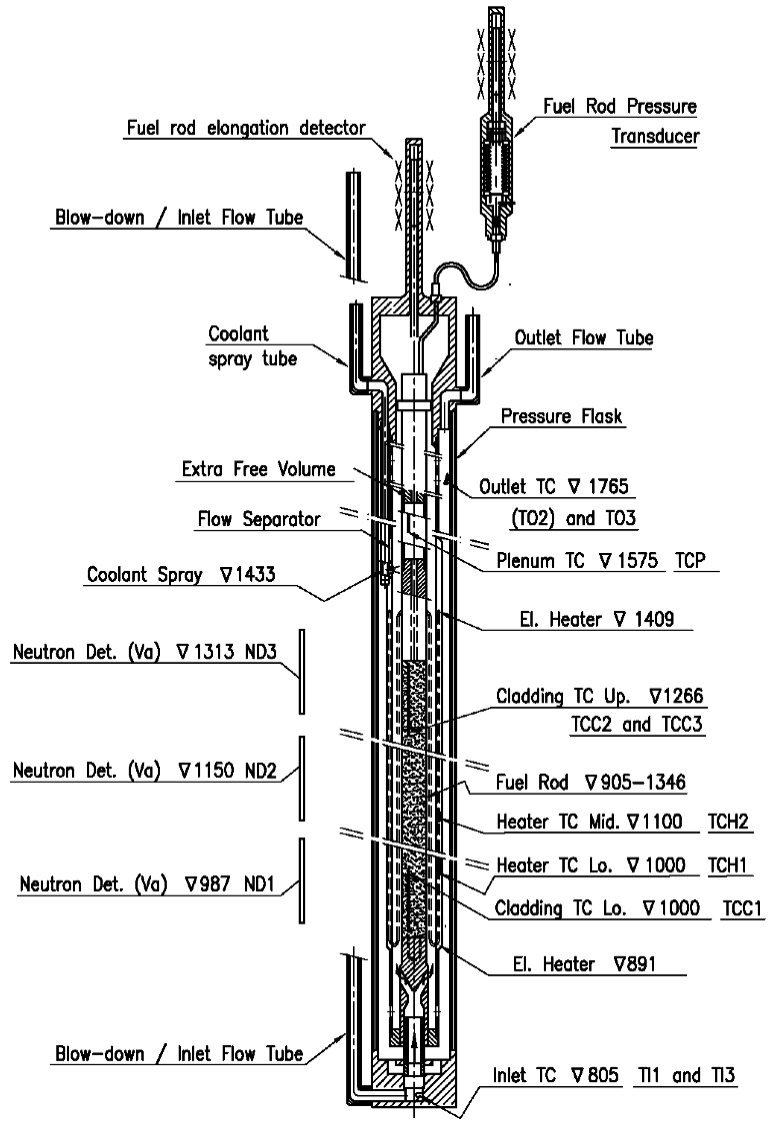

Figure A34.1: Schematic of the IFA-650.10 test rig with instrument elevations. Figure from [83]

.

test rod is by radiation to the surrounding heater. Small amounts of water are periodically sprayed into the rig to maintain a sufficient amount of steam for cladding oxidation during this phase. The influence of spraying on measured cladding, heater and coolant temperatures is reported to be weak, but no quantitative information on this issue is provided. Ballooning and burst occurred during the heat-up phase and were detected from pressure and temperature signals (burst at ~1025 K, ~249 s after blowdown). The test was ended by a reactor scram 418 s after the blowdown.

A34.2.3 Test results

The test was carried out successfully in May 2010. The test facility with its instruments worked well and cladding ballooning and burst occurred.

After the blowdown was completed (beginning of the dry or heat-up phase), an increase in the internal pressure and cladding temperatures was observed. At the beginning of the heat-up phase, and starting from a temperature of ~460 K, the average cladding temperature increase rate was ~5 K/s for TCC1 and ~4.3 K/s for TCC2 and TCC3. This rate slowly decreased until the burst, when it was approximately 1 K/s for all the thermocouples. The evolution of cladding, heater and coolant temperature signals during

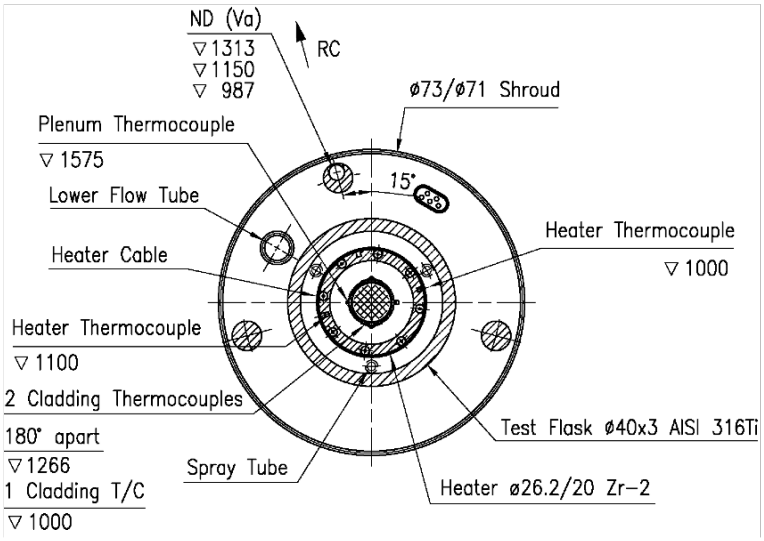

Figure A34.2: Cross sectional geometry of the IFA-650.10 test rig. Figure from [83]

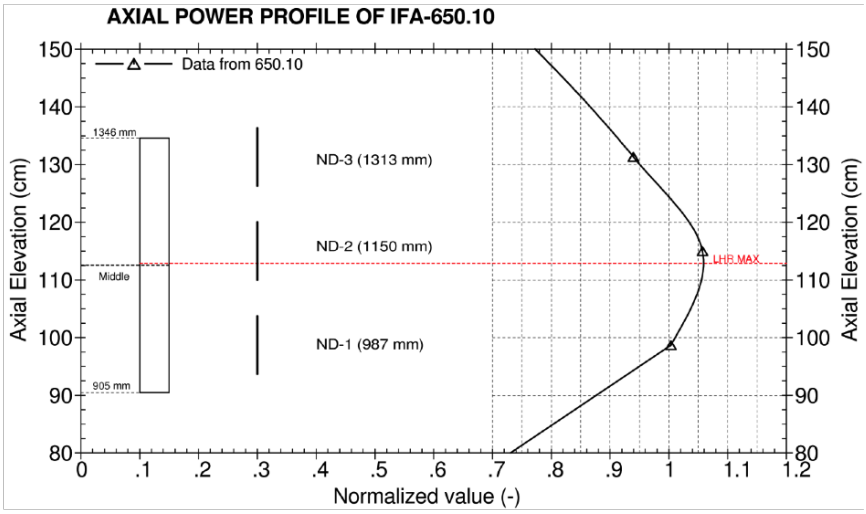

Figure A34.3: Axial power profile at the start of the test of IFA-650.10. Figure from [83]

the phases of the experiment are reported in Fig. A34.4.

Rod inner pressure in hot conditions was ~70 bar. Cladding ballooning started 228 seconds after the blowdown initiation (Fig. A34.5). The burst occurred 249 sec after the beginning of the blowdown. The burst time is recognizable as corresponding to the drop of the internal pressure signal and also, by the increase in activity indicated by the gamma monitor ~5 sec after the burst.

During post-irradiation examinations (PIE), the cladding outer diameter profile for IFA-650.10 was measured, which can be compared to code calculations for the mechanical behavior (ballooning) of the cladding. Figure A34.6 shown a visual inspection of the IFA-650 fuel rod around the burst opening.

A34.3 Model Description

A 2D BISON model of the IFA-650.2 fuel rod was constructed. The geometric parameters specified in Table A34.1 were used to develop a BISON finite-element mesh that suitably represents the experimental rod, including the fuel column, cladding tube, and plenum volumes.. The fuel was meshed as a smeared column with 12 radial elements and 88 axial elements. The cladding was meshed with 4 radial

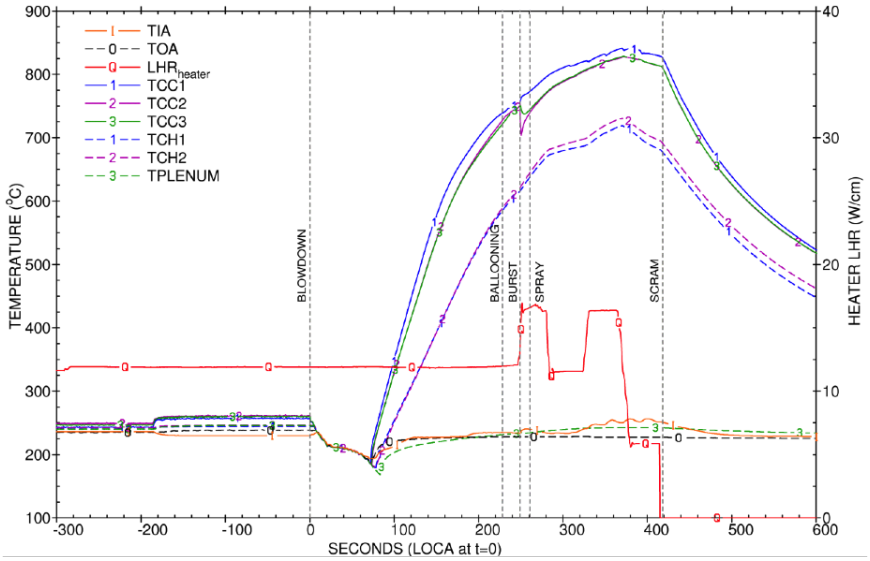

Figure A34.4: Signals for measured cladding (TCC), heater (TCH), coolant inlet (TIA) and outlet (TOA) temperatures, and heater power (LHR_{heater}) during the IFA-650.10 test. Taken from [83].

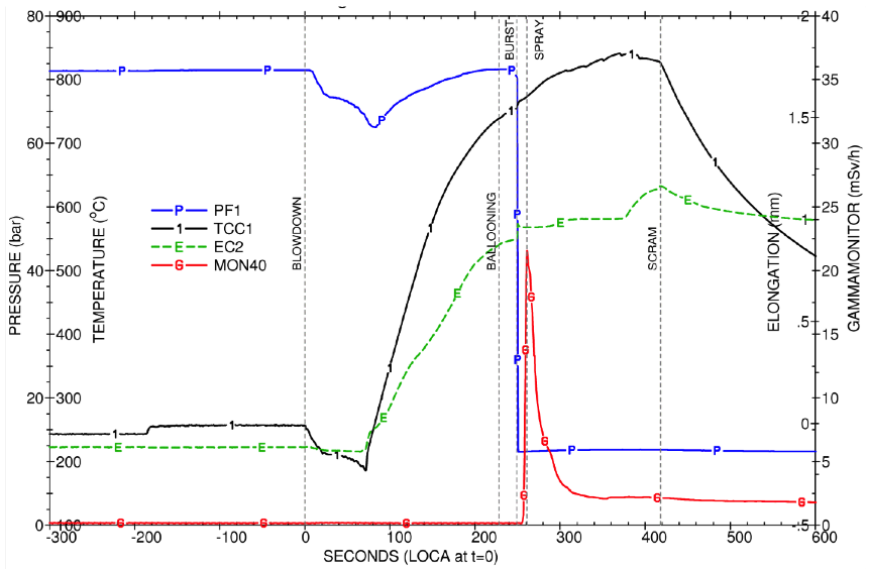

Figure A34.5: Signals for measured rod inner pressure (PF1), clad temperature (TCC), elongation (EC2) and gamma monitor response in the blow-down line (MON40). Taken from [83].

elements and 176 axial elements. Linear (Quad4) elements were used. The adopted mesh parameters are consistent with previous BISON validation work [85] and guarantee a high accuracy of the BISON thermo-mechanics solution. The plenum length was adjusted such that the initial rod inner volume is equal to the value of 17 cubic centimeters given in the documentation for the experiment [83, 84]. The BISON computational mesh for the simulation of IFA-650.10 is shown in Fig. A34.7.

The BISON input file was developed, which includes calls to the thermo-mechanics, material and behavioral models, fuel-cladding contact models, initial conditions, boundary conditions, coolant channel heat transfer models, and time discretization controls.

Refabrication in BISON is accounted for by specifying the refabrication temperature, pressure, and volume to suitably reset the rod conditions at the time of refabrication.

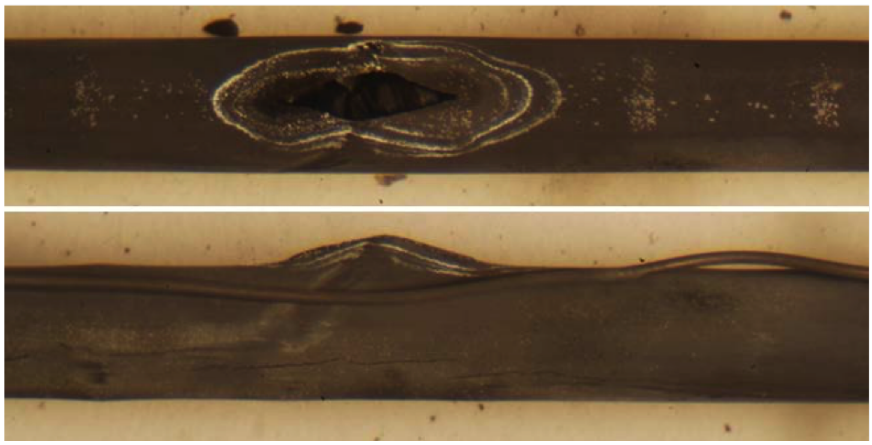

Figure A34.6: Post-test visual inspection for IFA-650.10 showing burst opening at two orthogonal orientations.

A34.3.1 Material and Behavioral Models

The following material and behavioral models were used for the UO_2 fuel:

- ThermalFuel - NFIR: temperature and burnup dependent thermal properties

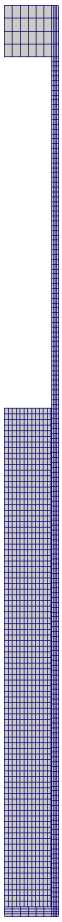

Figure A34.7: BISON computational finite-element mesh for the IFA-650.10 fuel rod. The view is magnified 10 times in the radial direction for improved visualization.

- RelocationUO2: relocation strains, relocation activation threshold power set to 5 kW/m.
- VSwellingUO2: MATPRO models for fuel solid swelling and densification.
- Sifgrs: fission gas release model with the combined gaseous swelling model.

The following models were used for the Zircaloy–4 cladding that allow for representing ballooning and burst under LOCA conditions:

- High-temperature cladding oxidation calculated using the correlations of Leistikow [78] (in OxidationCladding model).
- Crystallographic phase transition model ZrPhase, which computes the volume fraction of β phase for Zr–based cladding materials as a function of time and temperature. The model is based on [79, 80].
- High-temperature creep model based on the correlations from [81, 75]. This allows for outward creep deformation of the cladding tube under the effect of internal pressurization and high temperature leading to cladding ballooning. The model accounts for the effect of crystallographic phase transition.
- The FailureCladding model, which evaluates the onset of cladding burst due to combined overstress and plastic instability [75, 74], and takes into account the effect of Zirconium phase transition and oxidation.

A34.4 Development of time-dependent boundary conditions

As for the time-dependent boundary conditions such as linear power, coolant pressure histories, and thermal boundary conditions at the cladding outer wall, clearly their accurate determination is crucial to the reliability of the experiment simulation. For the Halden LOCA experiments, evaluating the time-dependent boundary conditions is a very significant task given the complexity of the experimental setup and procedure. The fuel rod power and coolant pressure histories need to be appropriately tabulated and supplied for the BISON calculation, which involves elaboration of the raw Halden data from neutron detector measurements. Determining the thermal boundary conditions at the cladding outer surface requires modeling heat transfer from the cladding to the coolant during the multiple phases of the IFA-650.10 experimental procedure, with each phase being characterized by a specific coolant condition, including forced and natural circulation, and the dry phase with the coolant becoming steam, the heat transfer being degraded and the heat transfer mode gradually switching from convection to radiation.

A BISON developer was stationed onsite at the Halden Reactor Project in Norway starting in October 2016. This researcher learned how to extract experimental data from the Halden data base plus use onsite data plotting programs. The IFA-650.10 experiment was discussed with Halden scientists to gain a better understanding of the experimental setup and available data. This information was been transferred to INL along with Halden raw data for the measured experimental conditions. Such data have been subsequently elaborated at INL in order to develop the boundary conditions (time-dependent inputs) for the BISON simulation of IFA-650.10. Because the raw measured data are available only at selected locations, while the fuel performance simulation requires boundary conditions at every location along the boundary of the computational domain, the development of such boundary conditions required a work of interpolation/extrapolation, involving the application of appropriate assumptions and physical sense in order to provide accurate inputs to the BISON code. An account of the work of development of the boundary conditions for each of the phases of the IFA-650.10 experiment is given in the following subsections.

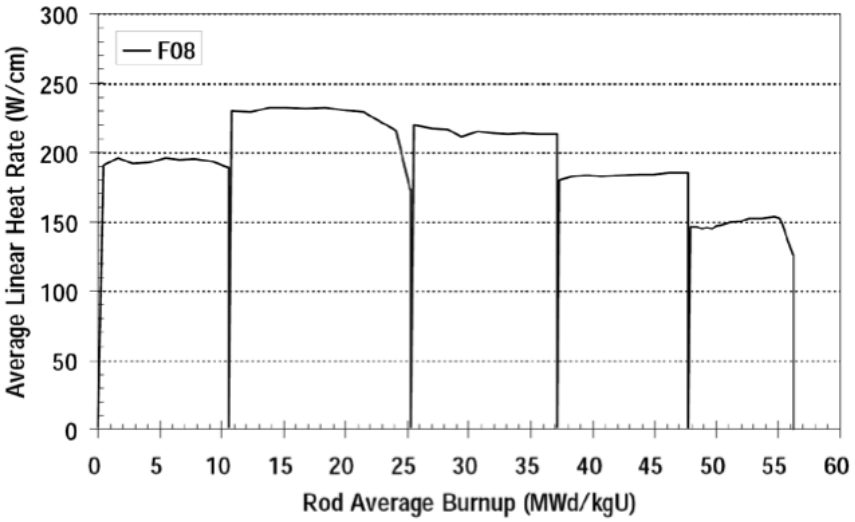

Figure A34.8: Power history for the commercial base irradiation of IFA-650.10

A34.4.1 Commercial base irradiation

As mentioned in Section A34.2.1, the IFA-650.10 experiment was carried out using a segment of a PWR rod that had been irradiated in a commercial PWR up to a burn-up of 61 MWd/kgU. Clearly, the commercial base irradiation needs to be included in a fuel performance simulation in order to account for the burnup dependent changes occurring in the fuel rod, hence providing the correct initial conditions for the simulation of the LOCA test in the Halden reactor. Simulation of the commercial base irradiation was included in the BISON analysis of IFA-650.10. The power history for the base irradiation was made available by the Halden Project in chart form and is reported in Fig. A34.8. The power data were digitized from this chart and tabulated for usage as input to BISON. For simplicity, the base irradiation was simulated on the geometry of the refabricated IFA-650.10 rod rather than on the geometry of the original commercial mother rod. As for the coolant conditions during the base irradiation, typical PWR parameters were adopted, i.e.: water at a pressure of 15.5 MPa, an inlet temperature of 580 K and an inlet mass flux of 3800 kg/m^2-s was considered. The heat transfer from the cladding to the coolant was modeled using BISON's internal coolant channel model for convective heat transfer under PWR conditions.

A34.4.2 Halden test – Preparatory phases

As outlined in Section A34.2.2, the Halden test began with preparatory phases of fuel rod irradiation under coolant conditions of forced circulation, first, and natural circulation, afterwards. To determine the temperature boundary conditions at the cladding outer surface, rather than explicitly modeling the cladding-to-coolant heat transfer during these preparatory phases, we chose a pragmatic approach in which we used the measured temperatures available from the Halden data. In particular, for these initial phases of the experiment, we considered an axially flat temperature profile, with the (time dependent) temperature value being the average of the temperature data measured at two different axial locations (Section A34.2.1). The temperature profile along the plenum length is also considered as flat, with the temperature value being equal to the temperature measured by the third thermocouple, which was placed at the axial midplane of the plenum (Section A34.2.1).

This approach guarantees good accuracy as the temperature values are derived directly from the measurements. The downside of this approach is that axial temperature peaking (which is associated with power peaking) is not allowed as an axially flat profile is used. This makes such an approach less suitable for the post-blowdown phases of the test (i.e., the blowdown phase and the heat-up phase), when cladding ballooning occurs that presents an axial dependence (localized ballooning and burst in corre-

spondence of the hottest axial position). This is a consequence of the axial temperature peaking in the cladding and the strong temperature dependence of Zircaloy thermal creep and the associated cladding ballooning. Hence, a more detailed approach with a physically based modeling of heat transfer is needed for the post-blowdown phases (see Sections A34.4.3 and A34.4.4). However, axial peaking is not anticipated to be important during the low-temperature, preparatory phases of the test, when no ballooning of the cladding is involved. Basically, the simulation of the preparatory phases only serves the purpose of determining the initial temperature and rod inner pressure conditions for the subsequent post-blowdown phases. Therefore, the approach based on measured temperatures is thought to be ideal as it allows one to minimize uncertainty in the temperature boundary condition for the simulation utilizing an axially flat profile, sufficient for the purpose of analyzing the preparatory phases of the test.

As for the post-blowdown phases, a more detailed approach is developed, which is described in the next sections. Since radiative heat transfer to structural components surrounding the rod becomes important (dominant) during the hot phase (while it is negligible for fuel performance simulations under normal reactor conditions), extending BISON's coolant channel model to include the radiative contribution was necessary. This work is briefly described in Section A34.4.3. Then, we applied the extended model to the determination of the cladding thermal boundary conditions during the post-blowdown phases of the experiment, as discussed in Section A34.4.4.

Switching between different approaches to prescribing the thermal boundary conditions (i.e., convection calculations for the base irradiation, prescribed temperatures during the preparatory phases, and convection-radiation calculations during the post-blowdown phases) was made possible by a recently developed MOOSE capability (called 'Controls') [86].

As for the rod LHGR and coolant pressure histories, these were also obtained from Halden as measured time-dependent data and tabulated for usage to inform the BISON simulation.

A34.4.3 Extension of the BISON coolant channel model

At high temperature, radiative heat transfer can occur from the cladding outer surface to the surrounding core structural components. In simulated LOCA tests at Halden, heat can be transferred to the heating element as well. Indeed, radiation is the dominant mode of heat transfer during the dry phase of the experiment.

Radiative heat transfer was implemented in BISON for modeling heat transfer in Halden LOCA tests. A new heat transfer mode was added to the code to compute radiative heat transfer. For this purpose, the effective emissivity parameter is needed. The value chosen for this parameter for the IFA-650.10 simulation is 0.6, which is the typical surface emissivity of oxidized zirconium alloy cladding [87].

The radiation heat transfer coefficient is described by the following equation:

$$h_r = \varepsilon\sigma(T_c^2 + T_s^2)(T_c + T_s) \tag{A34.1}$$

$$\varepsilon = \varepsilon_c\varepsilon_h R_h(\varepsilon_c R_c + \varepsilon_h R_h - \varepsilon_c\varepsilon_h R_c)^{-1} \tag{A34.2}$$

Where σ is the Stefan-Boltzmann constant (5.670410^{-8} W/m^{2}K^4), T_c and T_s the temperatures of the two heat exchanging surfaces, ε_c and ε_h the surface emissivities of the cladding and heater, respectively, and R_c and R_h the radii of the cladding and heater surfaces.

A34.4.4 Halden test – Blowdown and heat-up phases

Measured temperatures at different locations in the IFA-650 rig during the post-blowdown phases of the test (outer cladding surface along the fuel stack and in correspondence of the upper plenum mid-plane, heater surface) are plotted in Fig. A34.9. The cladding temperatures start increasing ~71 s after blowdown, i.e., when the rig is emptied of water and heat transfer from the cladding to the coolant (i.e., steam at this point) is degraded. This time identifies the end of the blowdown phase and the beginning of the heat-up or dry phase. As expected, the temperature at the plenum is very close to the coolant inlet/outlet temperatures, since there is no power generation at the plenum. The plot also includes

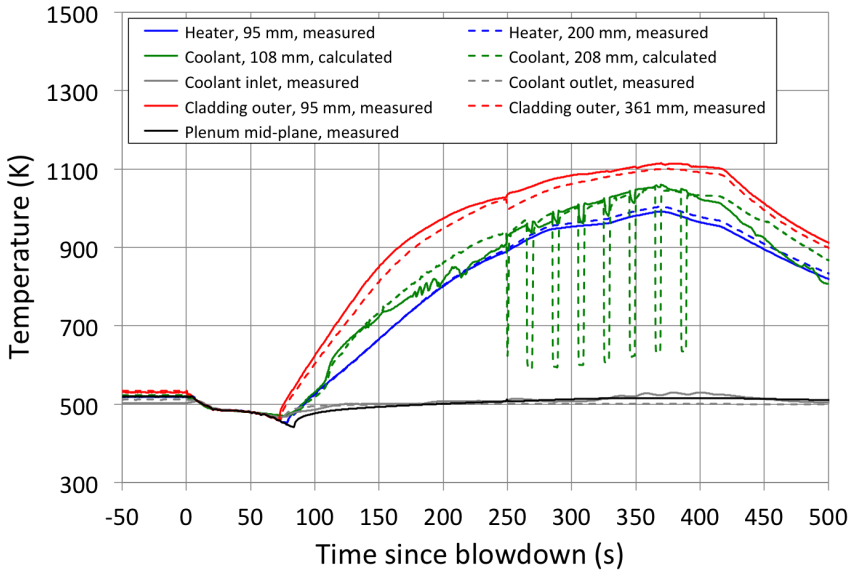

Figure A34.9: Measured temperatures at different locations in the IFA-650 rig during the post-blowdown phases of the test. Calculated coolant temperatures (FUMAC project) are also shown. Positions are axial distances from the bottom of the fuel stack. Note that the fuel stack length is 440 mm (Table A34.1).

calculated coolant temperatures at axial positions that approximately correspond to the positions of the heater temperature measurements. These calculations were provided through the FUMAC project. The comparison demonstrates that during the post-blowdown phases of the test, the coolant temperature is close to the heater temperature. This justifies the assumption, which was made in the present work, of considering the coolant temperature as equal to the heater temperature for the purpose of estimating the radiative heat transfer from the cladding to the heater. In particular, we considered the coolant temperature along the fuel rod length and up to the top of the heater as equal to the average of the heater temperatures measured with the two heater thermocouples (Section A34.2.1).

Above the top of the heater, i.e., in correspondence of the top portion of the fuel rod plenum, the coolant temperature was approximated as equal to the measured coolant outer temperature. The validity of such hypothesis is confirmed by the comparison between measured coolant outlet temperature and temperature at plenum mid-plane in Fig. A34.9. Since we expect the coolant temperature along the plenum to be close to the temperature of the cladding at the same position (because there is no heat generation at the plenum), the comparison indicates that the measured coolant temperature at outlet position is a good approximation for the coolant temperature along the plenum.

As for the linear heat generation rate (LHGR) history for the rod, this was obtained from Halden as raw data from neutron detector measurements. In particular, Halden provided experimental measurements as a fast-scan recording (two per second). The time-dependent LHGR raw data were tabulated for usage in BISON. The data were provided at 5 axial locations. The full information, i.e., data at all locations, was used for the BISON simulation in order to allow for the axial power peaking profile, with the maximum power being close to the axial mid-plane of the fuel stack. Linear interpolation of the data along the axial direction was performed in order to obtain the rod power profile at each time step. Power peaking determines the axially varying heat transfer and ultimately is reflected in the axial peaking of the cladding temperature profile. As mentioned in Section, A34.4.2, such axial peaking is important during the dry phase of the test, when cladding ballooning occurs with the maximum ballooning and burst location being at the hottest axial position. These localized effects occur in spite of the power and temperature peaking effects being low, and result from the strong temperature dependence of Zircaloy thermal creep and the associated cladding ballooning. Hence, detailed consideration of the axial power

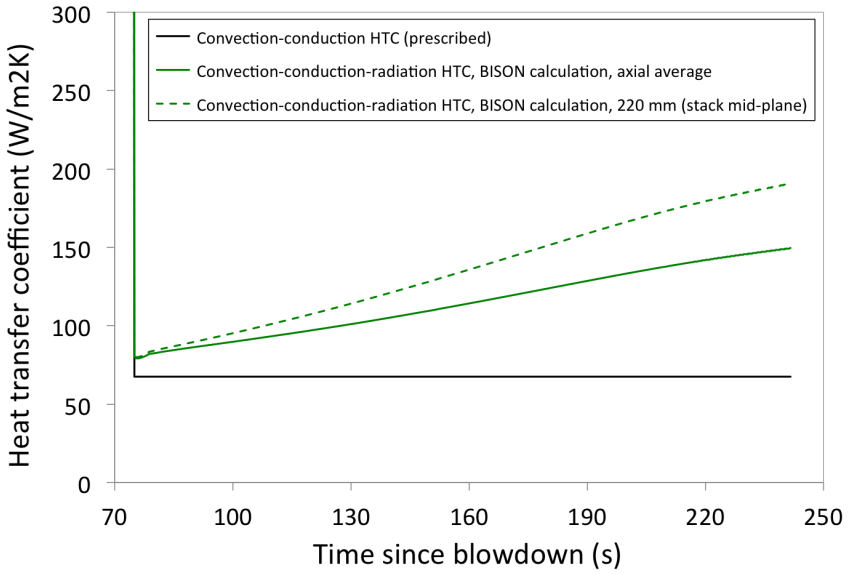

Figure A34.10: Heat transfer coefficients for the BISON calculation of thermal boundary conditions during the post-blowdown phase of the IFA-650.10 test. Positions are axial distances from the bottom of the fuel stack.

and temperature profiles is necessary in order to accurately capture cladding ballooning and burst during a LOCA simulation.

Based on the coolant temperatures estimated as above and the prescribed LHGR profile, the calculation of the heat transfer from the cladding to the coolant (or the heater, for the radiative contribution) was performed in the present work using the extended BISON coolant channel model (Section A34.4.3). Such calculation enabled the determination of the thermal boundary conditions at the cladding outer wall. Some further details of this calculation are discussed hereafter.

Figure A34.10 shows the heat transfer coefficient (HTC) for the BISON simulation of IFA-650.10 during the post-blowdown phase of the test. The figure only illustrates the time span after the end of blowdown (when the water coolant flashes to steam, heat transfer is rapidly degraded and the cladding temperature consequently starts increasing, i.e., 71 seconds after valves opening [83]). The extended BISON coolant channel model (Section A34.4.3) allows for combined convective, conductive and radiative heat transfer, as is necessary to model the dry phase of the experiment. As for the HTC for convection and conduction, we prescribe values dropping from 20,000 W/m^{2}K during the first 71 seconds after valves opening [88] to 67.5 W/m^{2}K over four seconds. The latter value represents the average of best-estimate values for the dry phase of the test [88]. BISON's coolant channel model computes the radiative HTC and calculates the thermal boundary condition at the cladding outer surface considering all contributions to heat transfer. The overall HTC is also plotted in Fig. A34.10. Average values along the active rod length as well as the value at the mid-plane of the active length are included. The value at the mid-plane is higher because the radiative HTC is roughly proportional to the cubed average of the temperatures of the heat exchanging bodies (i.e., the cladding and the heater in this case), which is highest near the mid-plane of the active length.

Note that the experimental transient continued beyond the time of burst (Fig. A34.9), but we stop the simulation at burst time. After burst, factors such as the geometry of the burst opening, fuel rod depressurization, and possible fuel dispersal all affect fuel rod behavior. Accounting for these additional aspects is beyond the scope of this work, where we rather focus on predicting pre-burst fuel rod behavior (temperatures, ballooning) as well as the time to burst. Burst time is directly related to the coping time for reactor operators during a LOCA accident; hence, its accurate prediction is a capability of primary importance for a fuel performance code.

The quantitative accuracy of the calculated cladding temperature boundary conditions with the code development and procedure described above is demonstrated in Section A34.5, where the Halden temperature measurements are compared to BISON calculated temperatures.

A34.4.5 Input files

The BISON input and all supporting files (power histories, axial power profile, etc.) for this case are provided with the code distribution at bison/assessment/ IFA_650_LOCA_tests/IFA_650.10/analysis.

A34.5 Results

The BISON simulation covers all of the the phases of the IFA-650.10 experiment (Section A34.2.2), from the base irradiation to the LOCA transient up to the burst failure of the fuel rod cladding.

A34.5.1 Temperature distributions in the fuel rod

Figure A34.11 shows the comparison of the cladding outer temperatures calculated in BISON for the IFA-650.10 test compared to the Halden measurements at the axial locations where the measurements were performed. The plot covers the blowdown and heat-up phases up to cladding burst. A very good agreement between the calculated temperatures (BISON boundary conditions) and the measurements is demonstrated. Cladding temperature drives thermally activated processes of cladding creep and ballooning, and ultimately cladding failure due to burst, hence, the accurate determination of the temperature boundary conditions at the cladding outer surface is a prerequisite for realistic fuel performance simulations. Indeed, correctly determining the thermal boundary conditions for a LOCA experiment involves significant additional complexity compared to normal reactor operating conditions, due to the different phases of the experiment which are associated with different heat transfer regimes and, mostly, the importance of radiative heat transfer, which is negligible in normal operating conditions but becomes the dominant mode during the heat-up phase of the Halden LOCA experiments. Therefore, the significant work performed on the thermal boundary conditions (Section A34.4), also involving an ad-hoc extension of BISON's coolant channel model to introduce the effect of radiative heat transfer (Sections A34.4.3 and A34.4.4) was of paramount importance for the successful completion of the present milestone.

Figure A34.12 illustrates calculated axial profiles of cladding outer temperature at three instants during the IFA-650 test. Temperature starts increasing at the end of the blowdown phase (beginning of heat-up). Increasing temperature causes cladding ballooning due to high-temperature Zircaloy creep until burst failure occurs. Note that an (albeit slight) axial peaking of the cladding outer temperature profile is predicted during the heat-up phase. This originates in the axial peaking of the rod power, which is accounted for in the simulation, and ultimately leads to localized ballooning and burst. Hence, with these boundary conditions and BISON's capabilities for fuel rod high-temperature behavior during LOCAs, we expect to be able to predict localized ballooning and burst through the BISON simulation. This is confirmed by results, as discussed in subsection A34.5.2.

Figure A34.13 shows contour plots of calculated fuel temperatures in the fuel rod at the time during the simulations that corresponds to the predicted cladding burst failure. Besides the full rod, separate plots for the fuel and cladding are shown with specific color scales. The temperature in the fuel is lower than for normal PWR operation, because of the lower power generation during a LOCA (decay power, which is simulated by a low fission power in the Halden LOCA experiments). The cladding, instead, reaches very high temperatures compared to normal PWR operation values of around 600 K because of the degraded heat transfer to the coolant during a LOCA that ultimately causes cladding heat-up and ballooning due to thermal creep. These effects are consistently reproduced in the BISON simulation.

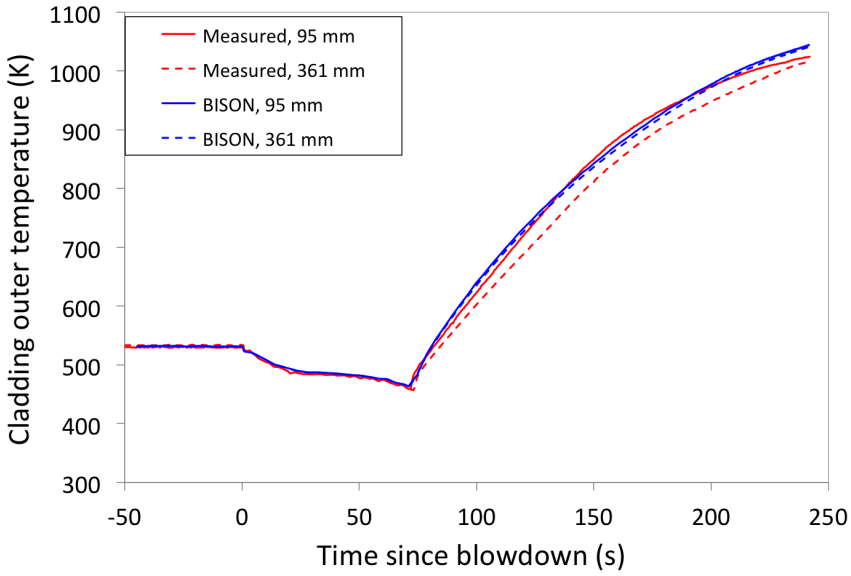

Figure A34.11: Measured cladding outer temperatures at two different axial locations in the IFA-650.10 rod during the post-blowdown phases of the test and calculated temperatures in BISON (with an extended coolant channel model, Section A34.4.3) at corresponding locations. Positions are axial distances from the bottom of the fuel stack.

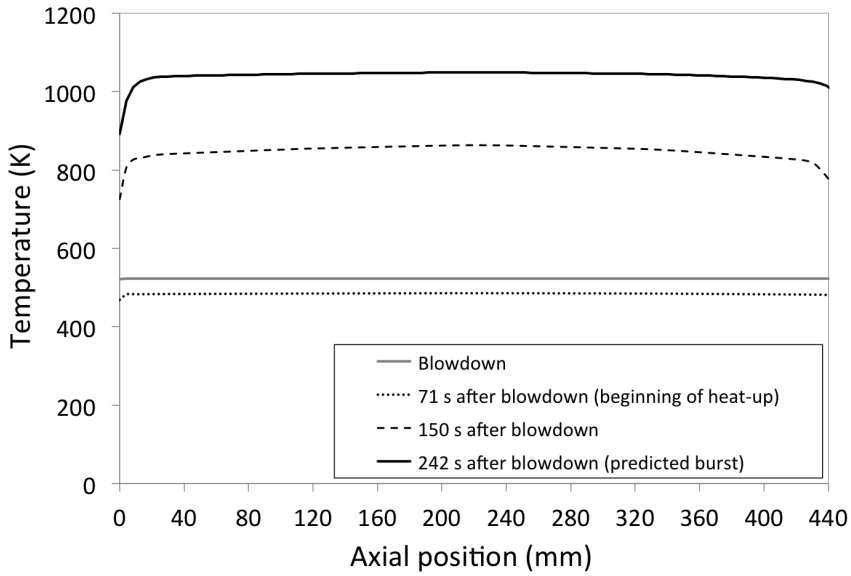

Figure A34.12: Calculated axial profiles of cladding outer temperature at three instants during the IFA-650.10 test, i.e., blowdown (valves opening), beginning of heat-up and time of predicted burst failure.

A34.5.2 Cladding ballooning and burst behavior

Figure A34.14 shows a contour plot of calculated hoop strain at the time of burst. This corresponds to the final time of the simulation and occurs in hot conditions during the LOCA transient, at the peak of cladding strain. The figure demonstrates how cladding ballooning, with large cladding strain and a maximum localized near the axial mid-plane of the fuel stack, is properly reproduced by BISON.

In order to give an account of the kinetics of the ballooning process as reproduced in the simulation, Fig. A34.15 shows the calculated time evolution of the hoop strain in the cladding (specifically, at the

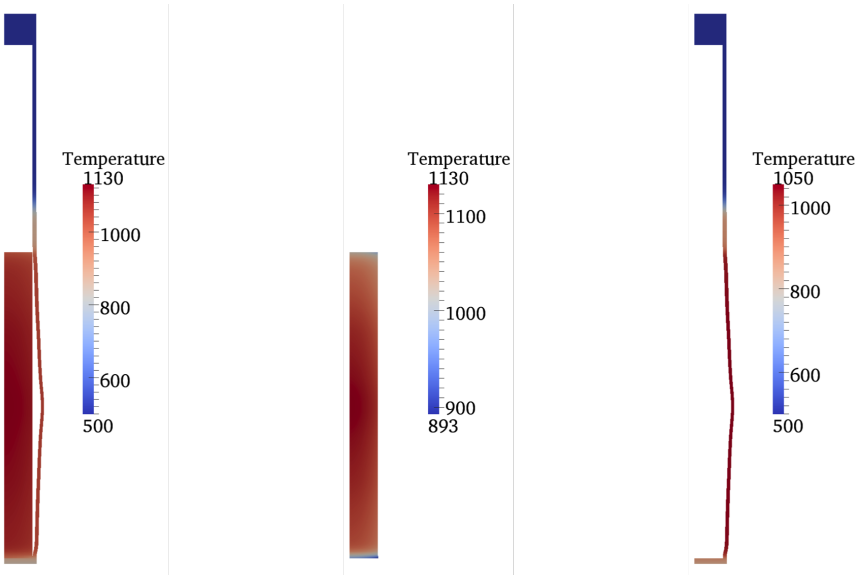

Figure A34.13: Contour plots of calculated temperature in the in the IFA-650.10 fuel rod at the time of cladding burst failure. Full rod (left), fuel only (center) and cladding only (right).

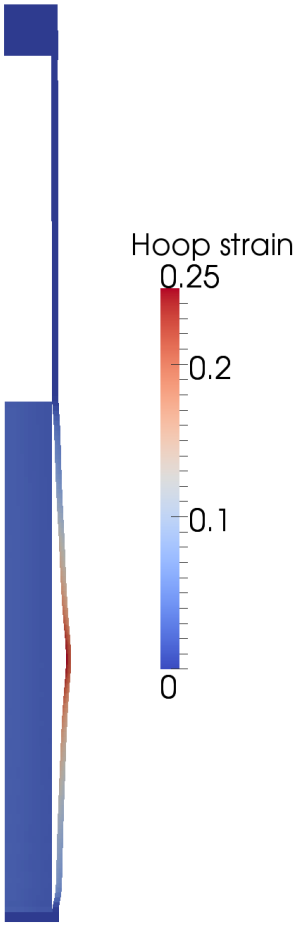

Figure A34.14: Contour plot of calculated hoop strain in the IFA-650.10 fuel rod at the time of cladding burst failure. Cladding ballooning as reproduced in the simulation is evident. The view is magnified 10 times in the radial direction for improved visualization.

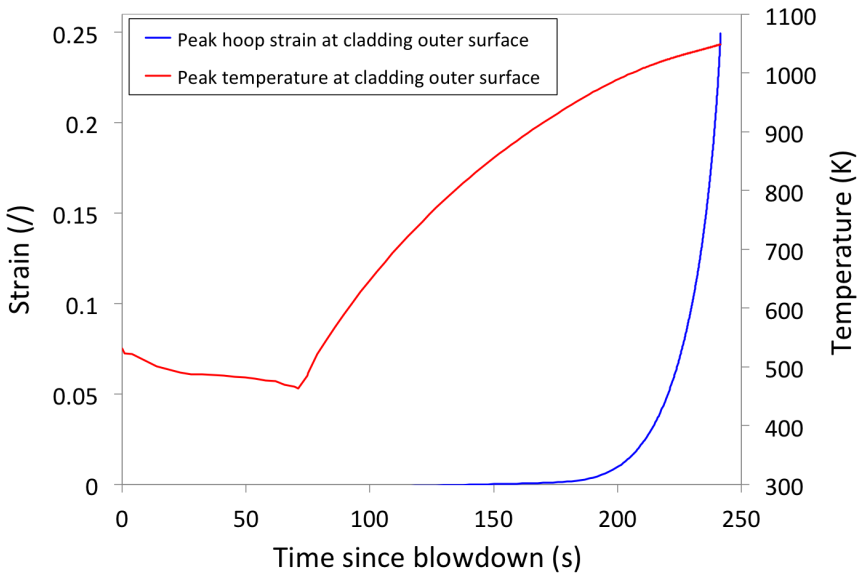

Figure A34.15: Calculated hoop strain and cladding temperature at peak axial position during the post-blowdown phases of IFA-650.10.

outer surface) during the heat-up phase of the IFA-650.10 experiment. The corresponding peak outer cladding temperature is also shown. The cladding strain rapidly accelerates (ballooning) with increasing temperature during the last ~100 s before burst. This behavior ensues primarily from the exponential dependence of Zircaloy cladding creep upon temperature. This kinetics is qualitatively consistent with the behavior observed experimentally during separate-effects cladding ballooning tests [77]. Hence, BISON reproduces cladding ballooning during the LOCA test as expected. Rapid thermal creep and ballooning continue until the cladding fails due to burst at the location of maximum strain. BISON predicts cladding burst failure according to the plastic instability criterion as the strain rate reaches the limit level. Cladding burst is predicted to occur ~242 seconds after blowdown, i.e., about 7 seconds before the time observed experimentally. Such an agreement of the simulation with the experimental behavior is very good. Furthermore, BISON's prediction is conservative as cladding is predicted to fail before it was experimentally observed.

The accuracy of the solution during the very high strain rate period is guaranteed by the automatic time step control in BISON specifically developed for this work, which progressively reduces the time step length as the strain rate increases. Just before the time of burst (maximum strain rate), the time step length is $\sim 3 \times 10^{-2}$ s. Note that time steps up to the order of 10^5 are used during the simulation of a base irradiation. This highlights the variety of time scales that are involved and need to be properly accounted for in a complete simulation of this experiment.

Figure A34.16 shows the axial profile of the cladding diameter at the end of the simulation compared with the experimental data from post-irradiation examinations. BISON is able to predict cladding ballooning with a physically meaningful profile and with the position of maximum strain being reasonably close to the experimental observation. However, an over-prediction of cladding outward strain along the rod is observed. Note that many variables determine the exact location of maximum strain and burst, not all of which can be accounted for in a deterministic calculation. For example, water spraying, which was active during the experiment, likely had an effect on the cladding temperature profile, hence on the location of maximum temperature and thermal creep strain. However, no quantitative information on this issue was provided by the Halden Project [83]. In conclusion, the cladding diameter results are considered reasonable, in view of the involved uncertainties and complexities. Indeed it is well known that prediction of dimensional changes is a difficult area for fuel performance codes, and BISON results are in line with the state of the art [45, 74]. Improvements may be achieved with further developments of the

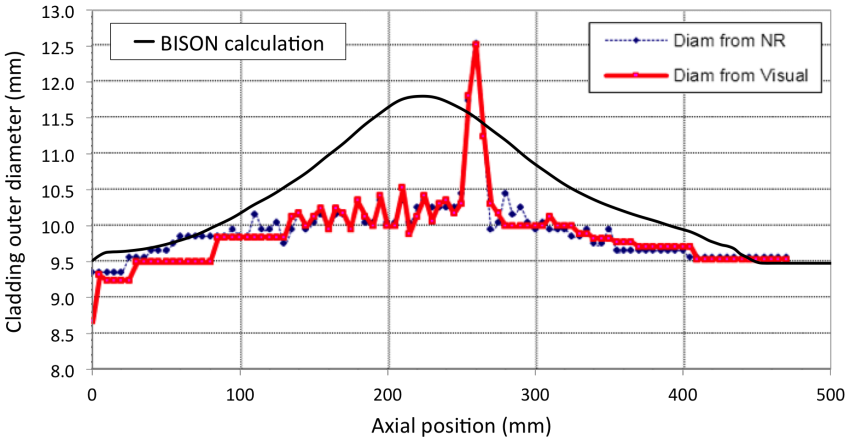

Figure A34.16: Calculated cladding outer diameter profile for IFA-650.10 at the end of the simulation compared to the PIE experimental data.

cladding behavior models in BISON, in particular for cladding creep. One aspect that can be considered for future work is the anisotropic creep behavior of Zircaloy [75, 81]. This will require modifications to the BISON mechanical model to allow for anisotropic behavior.

A34.5.3 Rod inner pressure evolution

In Figure A34.17, the time evolution of rod inner pressure during the post-blowdown phases of the IFA-650.10 experiment is compared to the experimental (pressure transducer) data from Halden. BISON reproduces the experimental behavior with a good accuracy. A moderate over-prediction of the rod pressure during the heat-up phase is observed, which may be partly due to a discrepancy between the calculated and actual plenum temperature (which together with rod inner volume and gas content determines the plenum pressure) in consequence of the assumptions made for the estimation of the temperature boundary conditions (Section A34.4). Also, the calculated pressure as burst time is approached decreases more rapidly than experimentally observed. This is expected to be a consequence of calculated cladding outward deformation (ballooning) and the associated increase in rod inner volume being more pronounced than occurred experimentally. This circumstance is confirmed by the calculated cladding diameter profile at the end of the simulation shown in Fig. A34.16. An improved treatment of cladding creep that allows for anisotropic behavior, and a refined calculation of the plenum temperature, may improve our results even further.

As already mentioned above, the time to burst failure is predicted to be 7 seconds before experimentally observed, which is both accurate and conservative.

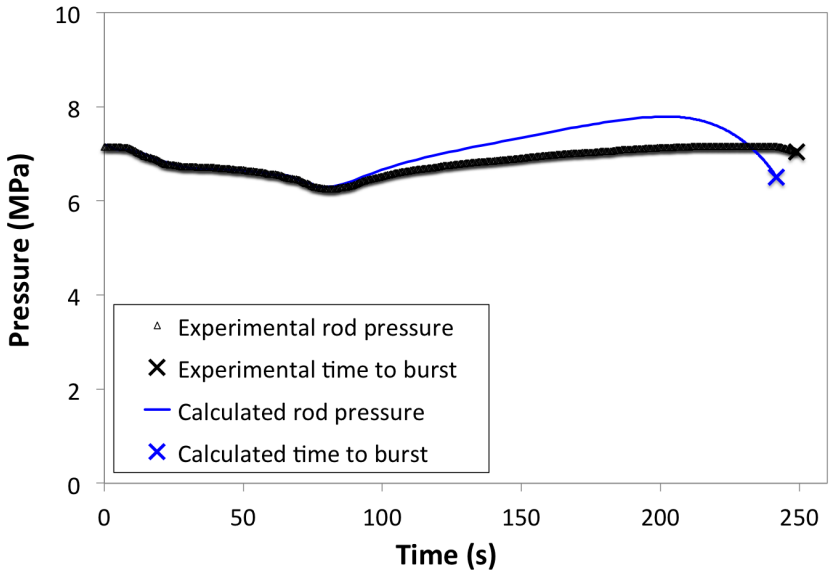

Figure A34.17: Rod inner pressure evolution during the post-blowdown phase of IFA-650.10 and time to cladding burst. BISON results are compared to the Halden experimental data.

A35 OECD/NEA/WGFS RIA Fuel Codes Benchmark Case 5

A35.1 Overview

In September 2009 the Organization for Economic Co-operation and Development (OECD)/Nuclear Energy Agency (NEA)/Committee on the Safety of Nuclear Installations (CSNI) organized a technical workshop on Nuclear Fuel Behavior during Reactivity Initiated Accidents. One conclusion from a session in the workshop devoted to RIA safety criteria was that fuel rod performance codes are heavily used during the processes of assessing revised safety criteria for the RIA design basis accident. Therefore, as a conclusion of the workshop it was recommended that a benchmark (RIA benchmark Phase I) between fuel performance codes used for assessing RIAs be organized by the Working Group on Fuel Safety (WGFS).

The RIA Fuel Codes Benchmark was organized into two activities [26]. The one of interest here is to compare the results of different simulations on simplified cases in order to provide additional bases for understand the differences in modeling of the concerned phenomena. Detailed specifications were prepared in order to prevent as much as possible the variability between the applied model among the different institutions and codes. The full detailed specifications can be found in [26].

Aside from the benchmark case 5 was selected to perform a closer comparison between BISON and FRAPTRAN [27]. The simplified model will be described below.

A35.2 Model Description

In order to limit the variability in initial states and properties of high burnup fuel, the cases are limited to a fresh 17x17 PWR type fuel rod. All cases start from ambient conditions and ramp to normal operating conditions during the first 50 seconds and stabilize at those conditions until 100 s, at which point the RIA transient starts. The simulation is concluded at 200 s.

A35.2.1 Geometry and Mesh

The fuel is standard UO2 fuel pellets with a diameter of 8.26 mm and a height of 1 cm. No dishing or chamfer is considered in the model. A total fissile column height of 10 cm is specified resulting in a 10 pellet stack. The fuel has a theoretical density of 10970 kg/m^3 with 4% porosity. The cladding is standard Zircaloy-4 material and is 570 μm thick. In case 5 the fuel rod is initialized with no initial gap (to simulate a high burnup rod) and the fuel and cladding are considered bonded (no slipping occurs) when the fuel is in contact with the cladding. The plenum volume is defined as 2 cm^3 and is filled with helium at either a low value (20 bar) or a high value (50 bar) at 20 C.

The geometry described in the benchmark specifications was interpreted into a 2D-RZ model for BISON. Owing to the simplicity of the model specified in the benchmark the internal BISON module (SmearedPelletMesh) was used to generate the mesh. The fuel was defined with 10 radial mesh elements and 40 axial elements. The cladding was defined with 5 radial elements and 40 axial elements. The cladding height was defined to achieve a plenum volume of 2 cm3. The geometry is shown in Figure A35.1.

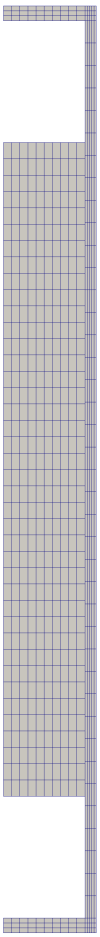

Figure A35.1: BISON fuel rod geometry and mesh. Representation is magnified 3X in the radial direction for clarity.

A35.2.2 Material and Behavioral Models

The fuel is modeled using an Elastic model with a Modulus of Elasticity of 200 GPa, a Poisson ratio of 0.345 and thermal expansion coefficient as defined in MATPRO [89]. The thermal properties of the fuel are defined using the built-in ThermalFuel module (NFIR correlation) with a porosity of 0.04. The transient power pulse is applied to the fuel as a uniform heat source using the HeatSource module in the Kernels block.

The cladding is modeled using the SolidModel module with the Modulus of Elasticity applied as a function of temperature and a Poisson ratio of 0.3. The thermal properties were defined with the ThermalZry module and the thermal expansion coefficient was applied as a function of temperature from MATPRO. An IsotropicPlasticity module was also applied to the cladding to capture the effect of instantaneous plasticity resulting from the rapid expansion of the fuel into the cladding due to thermal expansion. The yield strength of the cladding was defined as a function of temperature from [90]. No creep models were used due to the small time scales involved in RIA transients.

A35.2.3 Boundary and Operating Conditions

For case 5 the benchmark specified PWR Conditions for the thermal-hydraulic conditions. These conditions are water coolant at hot zero power (HZP) conditions of 280 C, 155 bar, velocity of 4.0 m/s and a water channel radius of 7.5 mm. For these conditions the CoolantChannel module in BISON was used.

The power pulse will start from zero power at t=100 s and is approximated with a triangular shape. The pulse width will be 30 ms full width at half max (FWHM). The maximum power was defined as 1.0 MW, aimed at initiating departure from nucleate boiling (DNB). The power pulse will result in 531.6 J/g (127.06 cal/g) of energy injected into the fuel. All the power is injected into the UO2 and no contribution will be released in the cladding or coolant. The radial and axial profiles in the fuel are supposed to be flat.

A35.2.4 Input files

The BISON input and all supporting files (power histories, axial power profile, fast neutron flux history, etc.) for this case are provided with the code distribution at bison/assessment/RIA_benchmark/case_5/analysis.

A35.3 Results Comparison

A complete compilation of all the results for all cases and codes was compiled by the OECD [91] comparing each output parameter of interest defined in the benchmark. This report will present and compare the results of BISON and FRAPTRAN simulations for case 5 of the benchmark.

A35.3.1 Radial Average Enthalpy

An important parameter to consider when discussing RIA transients is the amount of energy injected into the fuel and the resulting fuel radial average enthalpy. Historically the US Nuclear Regulatory Commissions (USNRC) acceptance criterion for reactivity excursions has been based upon the maximum radial average fuel enthalpy in the fuel rod [92]. Therefore, for safety considerations it is necessary to be able to accurately model the fuel radial average enthalpy of the rodlet. The first two parameters of interest in the benchmark were the energy injected into the rodlet and the variation of radial average enthalpy from the starting conditions at time zero. The energy injected, fuel radial average enthalpy, and power pulse are shown in Figure A35.2. Figure A35.3 shows the fuel radial average enthalpy over a longer duration to show the good agreement between the two codes. Good agreement on the radial average enthalpy of the fuel shows that both codes are calculating comparable radial profiles throughout the fuel pellet during the entire simulation.

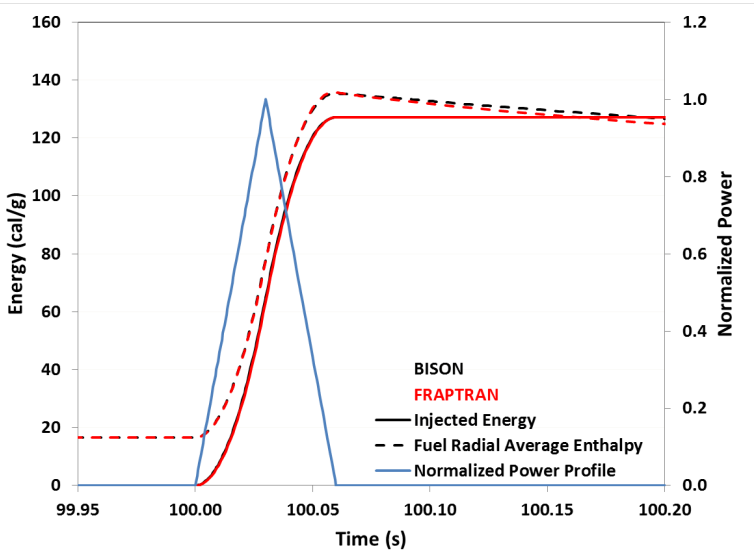

Figure A35.2: Profile comparisons between FRAPTRAN and BISON for the energy injected into the rodlet and fuel radial average enthalpy shown with the simplified 30 ms FWHM power profile.

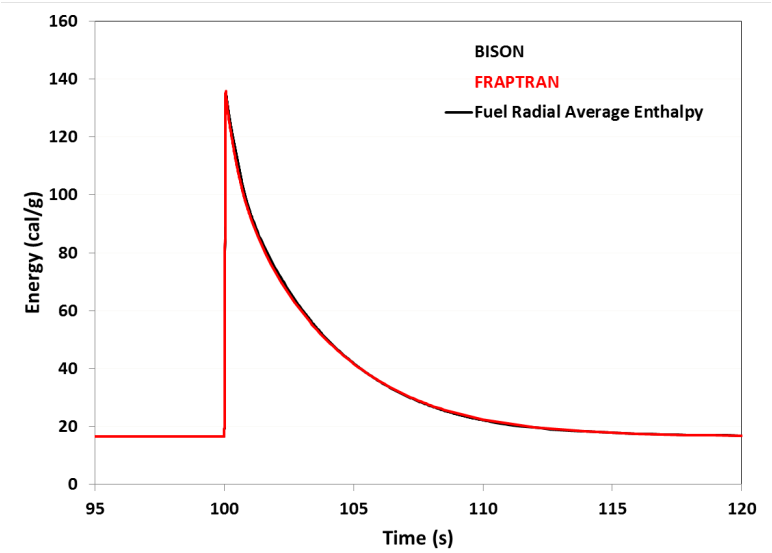

Figure A35.3: Fuel radial average enthalpy shows excellent agreement between BISON and FRAPTRAN.

A35.3.2 Temperatures

The temperature profiles at different radial locations in the rodlet are shown in Figure A35.4. The fuel centerline temperature shows good agreement between the two codes over the entire transient. The fuel surface and cladding surface temperatures deviate slightly between the two codes. Due to the complexity of the problem and the multiphysics simulation involved it is difficult to pinpoint the cause of the temperature differences between the two codes. There are large variations between the fuel to cladding gap conductance and cladding to coolant heat transfer coefficient between the two codes that will cause differences in temperatures. Also, differences in mechanical models have effects on various mechanisms that affect the energy transport, such as the gap width between the fuel and cladding.

A35.3.3 Hoop Stress and Strain

The combination of such a large and rapid temperature increase and the fuel having a coefficient of thermal expansion twice that of the cladding, results in large hoop strains being applied to the cladding. The hoop strain and corresponding hoop stress at the outer surface of the cladding are shown in Figure A35.5. During a RIA event the cladding is forced to expand and conform to the expansion of the fuel, therefore the cladding undergoes a displacement controlled problem. The cladding total hoop strain is controlled by the radial expansion of the fuel until separation occurs during cooling. As such, the total hoop strain shows some variation between the codes. They have very similar evolutions, but FRAPTRAN predicts approximately 0.4% more strain than BISON after the pulse. This variation correlates to a difference in the maximum outer radius, 4.209 mm in BISON and 4.219 mm in FRAPTRAN. This is likely due to multiple reasons. First, FRAPTRAN assumes a rigid pellet that cannot yield, while BISON assumes a compliant fuel pellet. Also differences in fuel thermal expansion and plasticity models between codes could result in the variations in calculated strain.

Each code predicted a maximum hoop stress of approximately 340 MPa and were within 20 MPa of each other throughout the transient. The two codes agree reasonably well on the stress, except for a short time just after the power pulse. During this time just after the pulse (100.06-101.0s) there is a complicated trade-off between elastic strain and the development of plastic strain. The increase in plastic strain is due to the decrease of the Zircaloy yield strength as the temperature increases. The temperature dependent yield strength capability was added to BISON as a result of participation in this

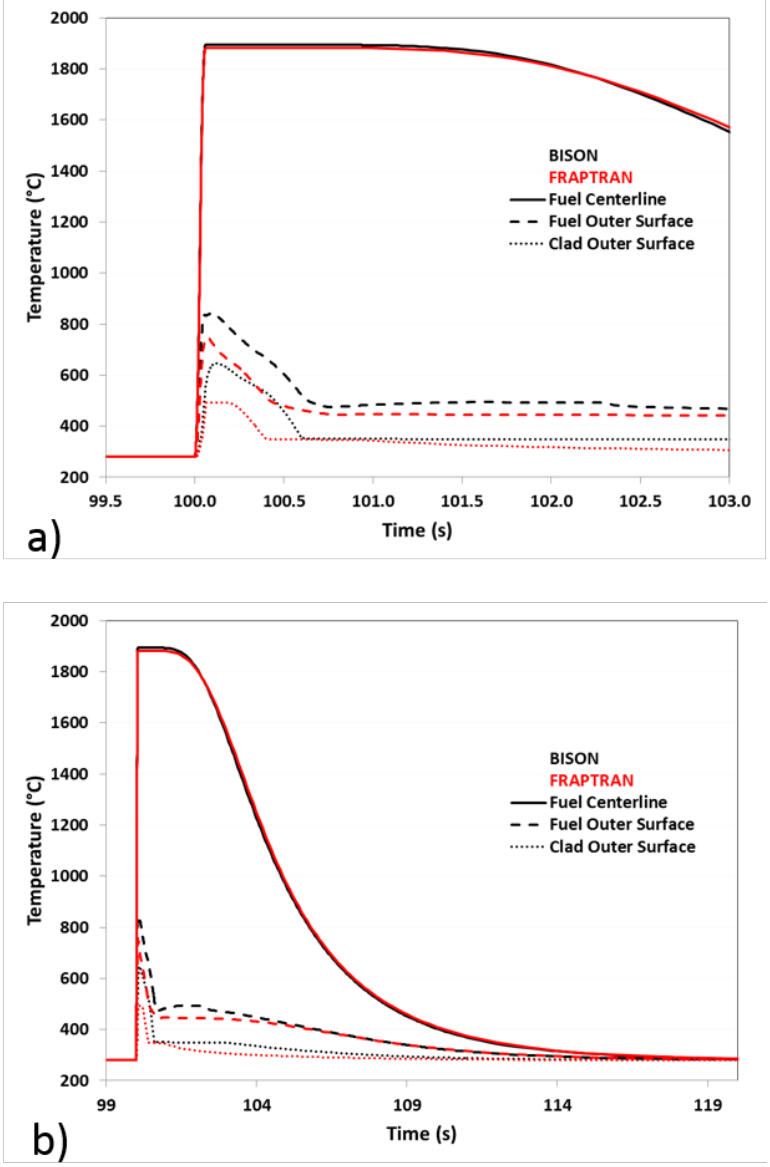

Figure A35.4: Temperature profiles at different radial locations on the rodlet. a) Temperature profiles during a smaller temporal scale around the power pulse and b) larger temporal scale showing temperature profiles during the cooling of the rodlet.

OECD benchmark.

A35.4 Summary

A simplified RIA case for a simulated high burnup LWR fuel rod has been successfully modeled using FRAPTRAN and BISON. When comparing different outputs, the trends in both codes for temperature and stresses and strains are similar, and the quantitative agreement is reasonably good. On the other hand there are large differences between the two codes when calculating the HTCs between the fuel and cladding and cladding to water. The large variations in the HTC help explain the small variations in the temperature profiles between the two codes. The differences between the stress and strain profiles can be explained due to differences in the plasticity models and how the mechanics in the fuel are treated (rigid vs. elastic) between the two codes.

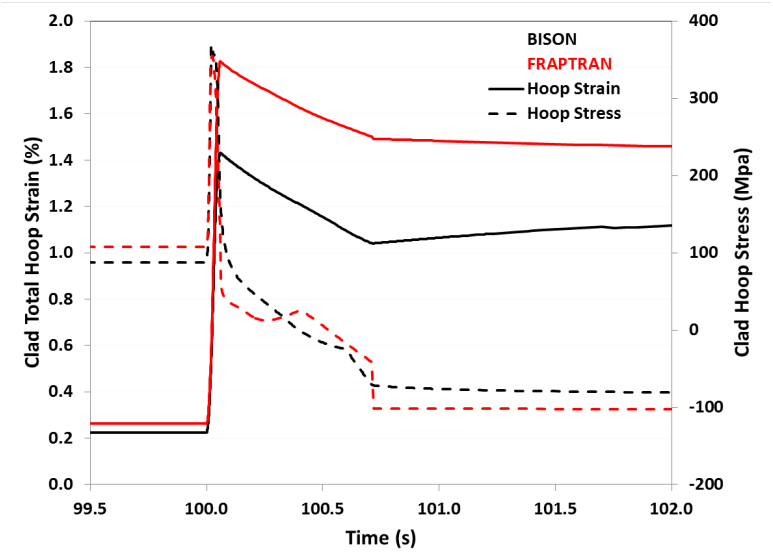

Figure A35.5: Hoop stress and total hoop strain at the outer surface of the claddingTemperature profiles at different radial locations on the rodlet.

Overall, the similarities and differences between the outputs of the two codes provide some insight into the behavior of fuel rods in a RIA scenario. They also emphasize the importance of incorporating all the physics of interest in these fuel performance codes and having proper correlations for the material properties. Code verification and validation remains an important task to ensure safe nuclear fuel development and safety criteria.

A36 CABRI REP Na RIA Cases

A36.1 Overview

Over the past few decades the average fuel cycle lengths have been extended and thus the average fuel burnups have increased. Experimental data from test reactors indicate that fuel performance during reactivity-initiated accidents (RIA) decreases with higher burnups [93]. Therefore the ability to accurately predict the phenomena of interest during these types of accidents will be necessary for safe operation of reactors with fuel at higher burnup levels. To date, more than a thousand pulse irradiation tests prototypic of RIA events have been carried out on previously unirradiated (fresh) fuel. About 140 tests have been done on pre-irradiated samples, but that data is limited beyond burnup levels of 40 GWd/tU and is based on older fuel rod designs. Only a few tests have been performed on rods at extended burnup and these have been performed at the CABRI facility in France and the Nuclear Safety Research Reactor (NSRR) in Japan. The purpose of these programs was to provide data for high burnup fuels that can be used to develop safety criteria at extended burnup levels and to provide data to validate analytical codes.

The RIA tests at the CABRI reactor facility began in 1992 by the Institut de Protection et de Sûreté Nucléaire (IPSN which is now IRSN) in collaboration with Electricité de France (EDF), Framatome, CEA, and with participation of the US NRC. A total of twelve tests were performed within the CABRI REP sodium loop using preirradiated fuel rods having burnups ranging between 33 and 65 GWd/tU. Of the twelve, eight contained UO2 fuel and four were MOX. The cladding for all tests was Zircaloy 4 except test 11 which was M5. Following the CABRI REP program, another series of tests have been initiated under the CABRI International Program (CIP) to test high burnup fuel with advanced cladding alloys.

The CABRI test reactor is a pool-type Light Water Reactor (LWR) designed with a central area that can accept the insertion of a test device. The central area was originally designed to study fast reactor transients and contains a sodium coolant loop. During the experiment, the test rod is placed inside a test capsule which contains the in-pile instrumentation. Due to the sodium coolant loop, the test capsule temperature and pressure are different from LWR conditions, but the tests are considered appropriate to study the response of the rodlet up to the departure from nucleate boiling point. Under these conditions the effects of pellet cladding mechanical interaction (PCMI) can be tested.

The tests chosen for evaluation in this study include the CABRI REP Na-2, 3, 5, and 10 cases with UO2 fuel. Each will be discussed in detail in the following section. Details of the modelling options will then be discussed followed by a comparison of the results. For this validation study a majority of the comparisons are against results from the FALCON fuel performance code [37] (performed by the Electric Power Research Institute (EPRI)) as access to the experimental data is limited to members of the CABRI International Program.

A36.2 Test Description

An overview of the four REP Na tests chosen for the BISON simulations are shown in Table A36.1 [94, 95, 96], including as-manufactured cladding and pellet geometry. A detailed description of the rodlet history for each case will be discussed below. Details on the case geometry and base irradiation conditions were taken from FRAPTRAN-1.5 Integral Assessment [97]. During all the REP Na tests the sodium coolant is heated to 280°C at the test capsule inlet and pressurized to 0.5 MPa. The sodium flows at a velocity of 4 m/s.

Table A36.1: Overview of REP Na cases

Test (date)	REP Na-2 (6/94)	REP Na-3 (10/94)	REP Na-5 (5/95)	REP Na-10 (7/98)
Fuel Type	17x17 UO_2	17x17 UO_2	17x17 UO_2	17x17 UO_2
Cladding Type	Std Zy-4	Std Zy-4	Std Zy-4	Std Zy-4
Initial enrichment (^{235}U/U %)	6.85	4.5	4.5	4.5
Internal gas pressure (MPa, 20°C)	0.101	0.31	0.302	0.301
Active length (mm)	1004.9	440.8	563.5	559
Max. burnup (GWd/tU)	33	53.8	64	63
Corrosion thickness (μm)	10	35-60	15-25	60-100
Pulse width FWHM (ms)	9.6	9.5	8.8	31
Energy deposit (J/g) [cal/g]	865 [207]	511 [122.2]	435 [104]	453 [108.3]
Cladding OD (mm)	9.51	9.55	9.51	9.51
Cladding thickness (mm)	0.637	0.596	0.578	0.575
Pellet OD (mm)	8.05	8.19	8.19	8.19
Pellet height (mm)	11.99	13.69	13.74	14.25
Diametral fuel-cladding gap (μm)	186	164	164	164

A36.2.1 REP Na-2

All the test rods in the CABRI REP Na tests were short segments refabricated from 17x17 PWR-type fuel rods irradiated under nominal PWR conditions, except the Na 2 test. REP Na-2 was a 1 m long rod base irradiated to 33 GWd/tU in the BR3 reactor. The fuel rod had a uniform 10μm oxide thickness after the base irradiation. The test rod was not refabricated prior to the power pulse except to replace the internal gas pressure to 0.101 MPa.

During the CABRI transient test the rodlet was pulsed with a Gaussian-type pulse with a full-width-at-half-maximum (FWHM) of 9.6 ms and a total energy deposited into the fuel of 865 J/g at 0.4 seconds after the beginning of the pulse.

A36.2.2 REP Na-3

The REP Na-3 rodlet was obtained from a segmented FRAGEMA low-tin cladding parent rod irradiated for 4-cycles in the Gravelines reactor to 50 GWd/tU. The 440.8 mm REP Na-3 section had a local burnup of 53.8 GWd/tU. The rodlet section had oxide thickness ranging from 35-60μm over the length of the rod. The rod was refabricated from the 5th span using the FABRICE procedure [93, 98] and backfilled with He to 0.31 MPa.

The CABRI test characteristics are similar to REP Na-2. The pulse was Gaussian-type with a FWHM pulse width of 9.5 ms depositing 511 J/g of energy into the fuel.

A36.2.3 REP Na-5

The REP Na-5 rodlet was obtained from rod EDF1065 which was irradiated in Gravelines for 5 cycles to a rod average burnup of 62 GWd/tU. The test rod was refabricated from a fuel segment removed from the 2nd-3rd spacer grid span. The rodlet fuel length was 563.5 mm and the oxide thickness varied between 15-25μm over the length of the rodlet. The FABRICE method was used to refabricate the rod and refill the plenum to 0.302 MPa. The local average burnup of the REP Na-5 sample was 64 GWd/tU.

The rod was tested with a FWHM pulse width of 8.8 ms and depositing 435 J/g of energy into the fuel.

A36.2.4 REP Na-10

The REP Na-10 rodlet was refabricated from a 5-cycle fuel rod in Gravelines. The local burnup of the 559 mm segment was 63 GWd/tU. The rod was taken from the 5th span of the parent rod and had approximately 60-100μm of oxide with some initial spalling of the oxide. The rod was refabricated with an initial plenum gas pressure of 0.301 MPa.

The REP Na-10 pulse was a much broader pulse with a FWHM of 31 ms depositing 453 J/g of energy into the fuel. Of the four cases being simulated, REP Na-10 was the only rod that experienced failure during the test. No evidence of fuel ejection was observed and no gas bubbles were detected in the sodium channel indicating a tight crack with a slow gas leak.

A36.3 Model Description

A36.3.1 Geometry and Mesh

The rod specifications and geometry in Table A36.1 and FRAPCON input files [97] were used to define the geometry for the cases. The 4 cases were modeled using a two-dimensional, axisymmetric (2D-RZ) mesh with quadratic elements. The mesh consists of 15 radial elements with 11 in the fuel and 4 in the cladding. Four axial elements were used per pellet length. Element axial lengths in the cladding were slightly longer, as required for the contact algorithm. The mesh for REP Na-3, typical for the four rods considered, is shown in Figure A36.1 (scaled 15x in radial direction).

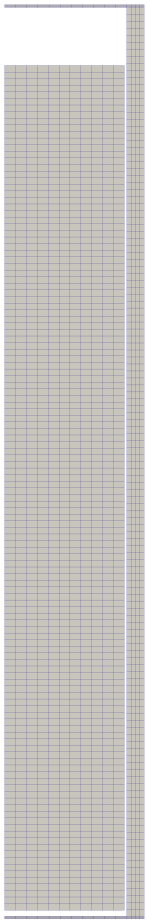

Figure A36.1: Fuel rod mesh (scaled 15x in radial direction)

A36.3.2 Base Irradiation Material and Behavior Models

Proper initial conditions prior to the RIA transient are very important to being able to accurately predict and analyze the results from the transient correctly. A base irradiation of the fuel was performed in BISON according to the reactor operating conditions specified in FRAPCON input files [97]. The following material and model options were used for the base irradiation for all cases [10, 9]:

- Frictionless contact model
- GapHeatTransferLWR thermal contact model with a fuel and cladding roughness of 2 and 0.5 microns, respectively
- CoolantChannel model for thermal hydraulic calculations with coolant pressure, temperature and mass flux specified in the respective FRAPCON input files
- ThermalFuel-NFIR: temperature and burnup dependent properties
- Elastic fuel model
- RelocationUO2: relocation strains, relocation activation threshold power set to 5 kW/m
- Sifgrs and VSwellingUO2: fission gas release model with the combined gaseous swelling model
- ThermalZry: thermal conductivity and specific heat for Zircaloy
- MechZry: model mechanical deformation for Zircaloy-4 used with the CombinedCreepPlasticity as the constitutive model
- CreepZryModel: model for thermal and irradiation creep and irradiation growth for Zircaloy-4
- ZryPlasticity: model for instantaneous plasticity of Zircaly-4. This material model provides cladding yield strength estimations and includes options for either a PNNL model [90] or EPRI model [99] based on a modified version of MATPRO [89]. In this work only the EPRI model was used.

A36.3.3 Transient Test Material and Behavior Models

All the model and material options listed above were used during the RIA with the following exceptions:

- CoolantChannel model was changed to sodium coolant with 0.5 MPa and 280°C pressure and temperature conditions, and a velocity of 4 m/s
- RelocationUO2: burnup_relocation_stop was used to specify the average burnup during the base irradiation when contact was made between the fuel and cladding. This prevents more relocation during the RIA.
- Sifgrs: transient_option = 1 used in this study to perform an initial assessment of this model applied to the analysis of RIAs.
- CreepZryModel: was disabled during the RIA due to the small time scales

A36.3.4 Input Files

The BISON input file and all supporting files (axial power profiles and power histories) for all four CABRI REP Na cases are provided with the code distribution at bison/assessment/CABRI_REP_Na/analysis.

A36.4 Results Comparison

Without membership in the CABRI International Program there is limited acces to the CABRI REP experimental data. So to the extent possible, BISON results are compared against those CABRI REP experimental data reported in the open literature [94, 95, 96]. To provide more detailed comparisons, BISON results are also compared against FALCON calculations for the same cases, as extracted from two EPRI reports [93, 100].

A36.4.1 REP Na-2

REP Na-2 was base irradiated to an average burnup of 33 GWd/tU and had an initial enrichment of 6.85% which allowed for higher energy depositions than the other cases. The energy deposited into the fuel during the RIA CABRI test was reported as 866 J/g (207 cal/g). Assuming a Gaussian-type pulse with a FWHM of 9.6 ms resulted in 205 cal/g of energy injected into the fuel at the peak power node (PPN) in BISON. The calculated maximum change in radial averaged fuel enthalpy from 20°C is 217 cal/g compared to 200 cal/g calculated by FALCON and 199 cal/g reported by IRSN. The BISON power pulse, energy injected, and radial averaged enthalpy are plotted in Figure A36.2 (Note: unless otherwise stated all BISON data reported or plotted is at the PPN).

The fuel and cladding temperature histories are plotted in Figure A36.3 with comparison between FALCON results for the fuel centerline and cladding inner temperature in Figure A36.4. A complete list of the BISON results compared against FALCON calculations and experimental/reported values from IRSN found in literature is shown in Table A36.2. BISON is able to predict thermal results very well when compared against FALCON or the reported values. All temperature predictions are within 3% of values computed by FALCON and the peak fuel radial average enthalpy is within 10% of FALCON and reported values.

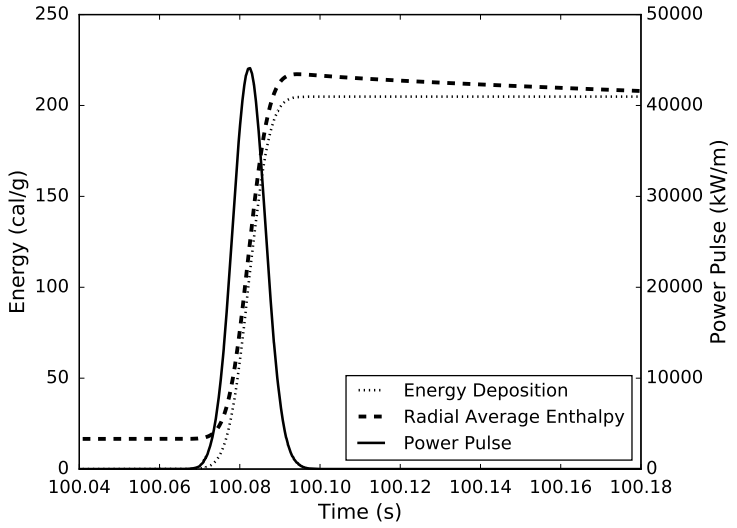

Figure A36.2: BISON power pulse, energy deposited and computed radial averaged fuel enthalpy at PPN for REP Na-2 case

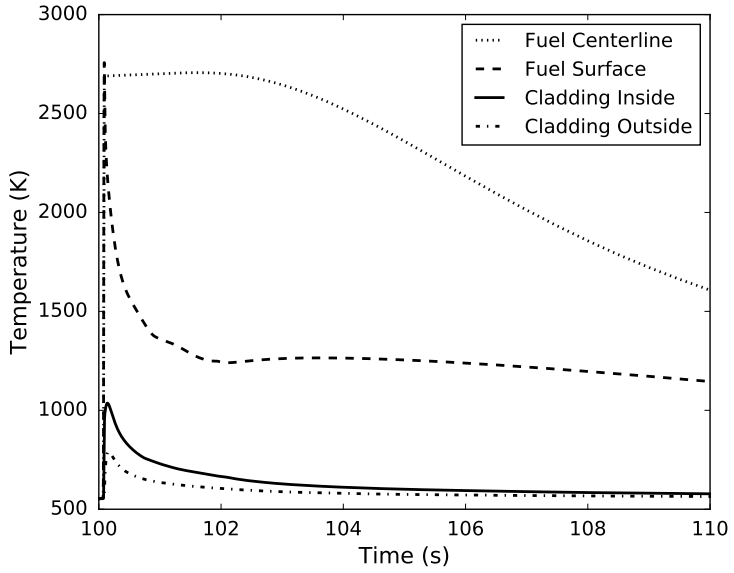

Figure A36.3: Fuel and cladding temperature profiles at PPN for the REP Na-2 case

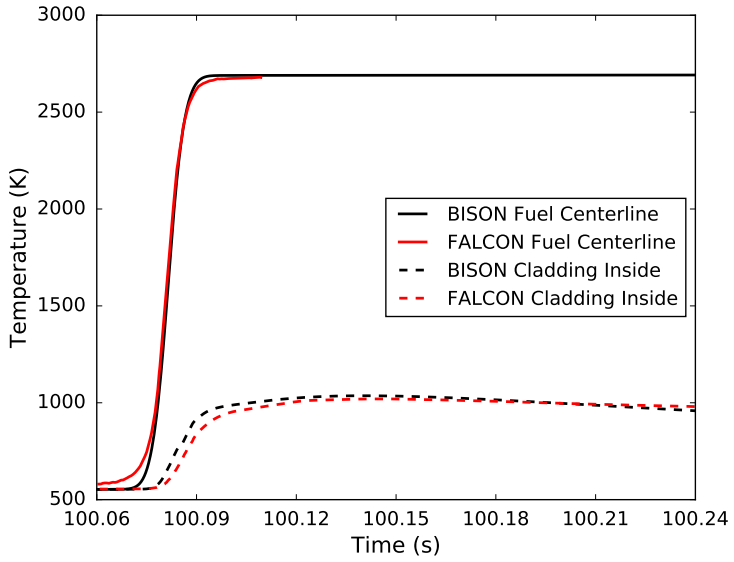

Figure A36.4: Fuel centerline and cladding inside temperature at PPN comparisons with FALCON

Although thermal behavior is well-predicted by BISON, mechanical results deviate significantly from both FALCON calculations and measured values. As shown in Table A36.2, BISON predicts less than half the residual cladding radial displacement and hoop strain as compared to FALCON and measured values. BISON and FALCON outer cladding surface hoop strain histories are shown in Figure A36.5. Post-test measurements of the cladding diameter compared against BISON calculations are shown in Figure A36.6 [96]. The oscillations in the post-test measurements are due cladding ridging at the pellet-pellet interfaces, which are not seen in the BISON results due to the smeared fuel approximation. It should also be noted that due to the temporary frictionless contact restriction, axial elongation comparisons will not be made at this time. Without frictional contact we expect significant discrepancies to FALCON or experimental results.

There are a number of postulated reasons for the discrepancies in the mechanical results. As previously stated, the frictionless contact option greatly impacts the axial displacement predictions but it also influences the plastic hoop strain estimation in BISON. The plasticity model in BISON compares the von

Table A36.2: BISON calculations compared against FALCON calculations and experimental/reported values found in literature for REP Na-2.

Property	BISON	FALCON	Experimental/ Reported Values	% Difference (FALCON)	% Difference (Experimental)
Energy Deposition (cal/g)	205	-	207	-	-1.0
Peak Fuel Enthalpy (cal/g)	217	200	199	8.7	9.2
Max Fuel Temperature (K)	3024	2948	-	2.6	-
Max Fuel Centerline Temp. (K)	2707	2775	-	-2.5	-
Clad Max Inside Temp. (K)	1036	1020	-	1.6	-
Max Hoop Strain (%)	1.36	2.60	3.5	-48	-61
Residual Hoop Strain (%)	0.46	2.20	-	-79	-
Max Clad Radial Disp. (μm)	64	135	-	-53	-
Clad Radial Disp. Residual (μm)	21	102	135	-79	-78
Fission Gas Released (%)	7.1	-	5.5	-	29
Corrosion thickness (μm)	5	-	4-10	-	-

Mises stress against the cladding yield stress; without friction the axial stress component is negligible resulting in lower von Mises stress and less plastic strain accumulation. Another important factor that has a significant impact on the cladding stress and strain state is the initial fuel-to-clad gap width prior to the RIA [91]. BISON calculates this gap from the base-irradiation simulation used to provide the initial fuel rod state prior to the RIA, whereas FALCON and SCANAIR begin with no initial fuel-to-cladding gap.

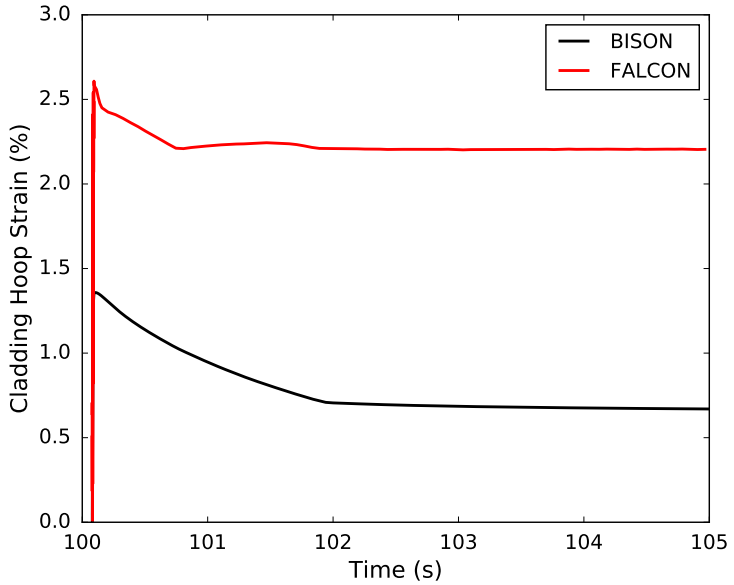

Figure A36.5: Cladding hoop strain evolutions at PPN for BISON and FALCON

The predictions for the fission gas release (FGR) during the transient are very promising. BISON predicted a final FGR of 7.1% compared to the measured value of 5.5%. A plot of the FGR is shown in Figure A36.7 along with the fuel centerline temperature plotted on the right ordinate. The inset shows the FGR and fuel temperature during the time period of the pulse. The initial large increase in FGR is highly correlated to the fast increase in fuel temperature. Fission gas release and gaseous swelling are computed by a physics-based model from Pastore et al. [101, 102]. This model also captures the rapid

FGR (burst release) during transients, which is interpreted as driven by fuel micro-cracking [103, 104]. Micro-cracking during RIA transients has been observed experimentally (e.g., [105]) and may account for the majority of FGR during a RIA, where the high FGR observed (5-20%, approximately) cannot be interpreted as diffusion-based in view of the short time scale of the event. Note that traditional FGR models typically only account for diffusion-based FGR and will thus tend to strongly underpredict FGR during the short duration of a RIA event. This is demonstrated by comparison with the results from a purely diffusion based model that differs from the complete BISON model only in that the specific transient (micro-cracking) capability is deactivated. This is shown in Figure A36.7 with no burst release due to micro-cracking. In this case the FGR still increases due to diffusion-based FGR because of the very high temperatures in the fuel reaching between 2700-3000 K. Hence, the recently developed transient release capability of the BISON model may represent an important step towards better capturing FGR during RIAs.

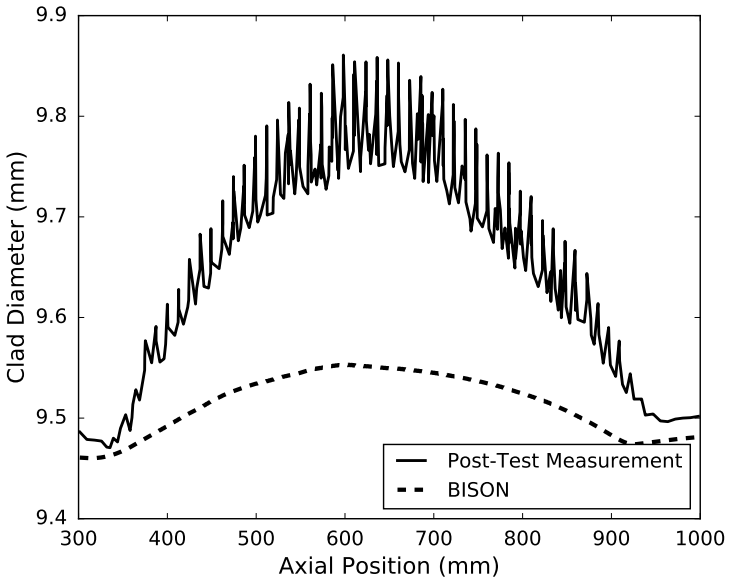

Figure A36.6: Residual outer cladding diameter calculations from BISON compared against Post-Test measurements.

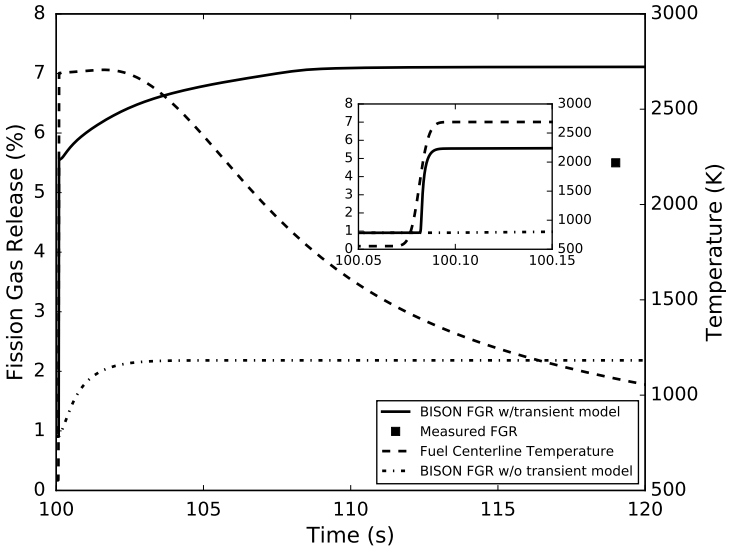

Figure A36.7: Fission gas release plotted with the measured post-test value at 5.5% for REP Na-2. The Inset shows a shorter time scale of the FGR plotted with the fuel centerline temperature (K) showing the high fission gas release rate correlates to the fast increase in temperature.

A36.4.2 REP Na-3

The REP Na-3 test rod was base irradiated to a burnup of 53 GWd/tU and tested in CABRI with 9.5 ms FWHM pulse targeting 511 J/g (122 cal/g). The maximum change in fuel radial averaged enthalpy at the PPN in BISON was 136 cal/g compared to 118 cal/g calculated in FALCON and 124 cal/g reported by IRSN. The Gaussian-type power pulse with the energy injected and radially averaged enthalpy are plotted in Figure A36.8 with all the results from literature tabulated in Table A36.3. BISON over estimates the radial averaged enthalpy by 10-15% in this case compared to the reported values and FALCON.

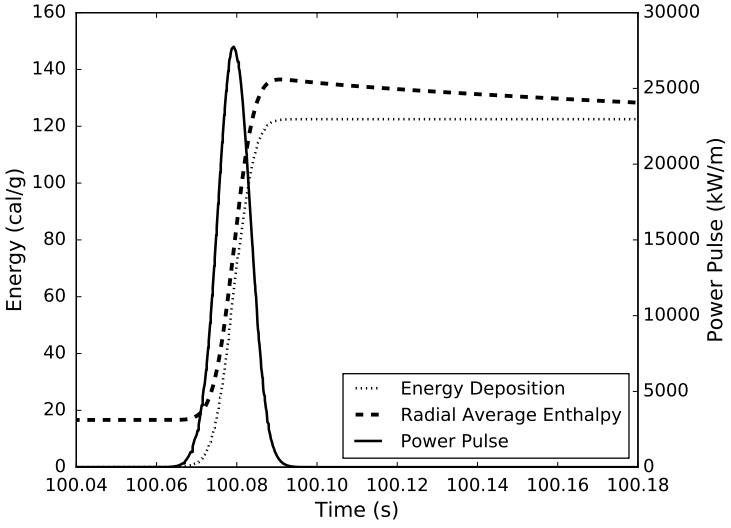

Figure A36.8: Power pulse, energy deposition and radial averaged fuel enthalpy at PPN for REP Na-3 case

The computed fuel centerline, fuel surface, cladding inside, and cladding outer surface temperature histories are plotted in Figure A36.9. The fuel centerline reaches a maximum temperature of just above 1900 K and the maximum temperature in the fuel reaches 2600 K which occurs a few microns in from

Table A36.3: BISON calculations at PPN compared against FALCON calculations and experimental/reported values found in literature for REP Na-3.

Property	BISON	FALCON	Experimental/ Reported Values	% Difference (FALCON)	% Difference (Experimental)
Energy Deposition (cal/g)	122	-	122	-	0
Peak Fuel Enthalpy (cal/g)	136	118	124	15	10
Max Fuel Temperature (K)	2599	2480	-	4.8	-
Max Fuel Centerline Temp. (K)	1904	1960	-	-2.9	-
Clad Max Inside Temp. (K)	1002	935	-	7.1	-
Max Hoop Strain (%)	1.19	1.5	2.2	-21	-46
Residual Hoop Strain (%)	0.40	1.10	-	-64	-
Max Clad Radial Disp. (μm)	56	81	-	-31	-
Clad Radial Disp. Residual (μm)	18	51	55	-64	-67
Fission Gas Released (%)	9.8	-	13.7	-	-29
Corrosion thickness (μm)	51	-	35-60	-	-

the fuel surface due to the high burnup rim effect. The pellet surface achieves a maximum temperature of 2300 K. The temperature calculations by BISON agree very well, within 7% of the FALCON calculations.

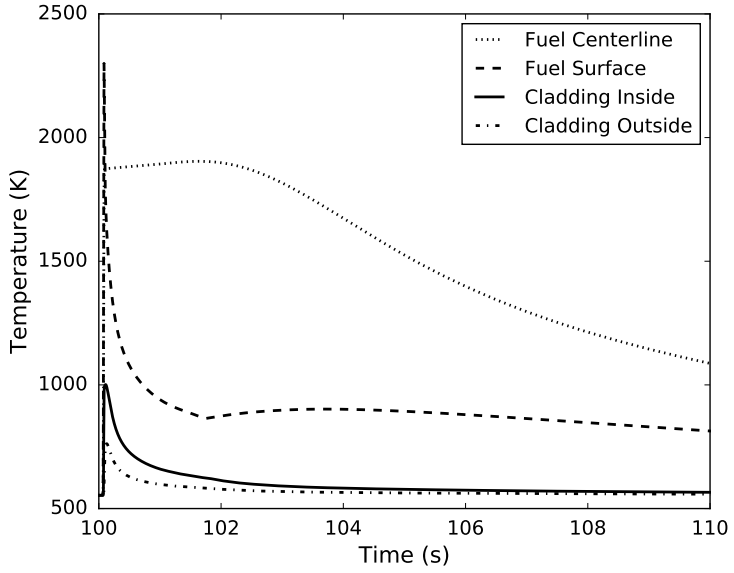

Figure A36.9: Fuel and cladding temperature histories at PPN for the REP Na-3 case

BISON has again shown to do very well in predicting the temperatures in the fuel and the cladding for this case. The fuel enthalpy BISON calculated was 16% higher than calculated by FALCON even though the fuel centerline temperature differed by less. The higher radial averaged fuel enthalpy calculation in BISON is likely due to a different fuel radial power profile in BISON resulting in more energy deposited into the rim region and thus higher fuel temperatures.

The cladding hoop strain calculations by BISON are again under-predicted compared to the results from FALCON and experimental data reported by IRSN. The cladding hoop strain evolution compared against FALCON is plotted in Figure A36.10. The maximum values are approximately 20% less than FALCON and almost half the measured values. The residual hoop strain calculation in BISON is less than half the FALCON calculation which means BISON is not estimating the amount of plastic deforma-

tion correctly. The residual cladding displacement is plotted with the FALCON results and the post-test measurements in Figure A36.11.

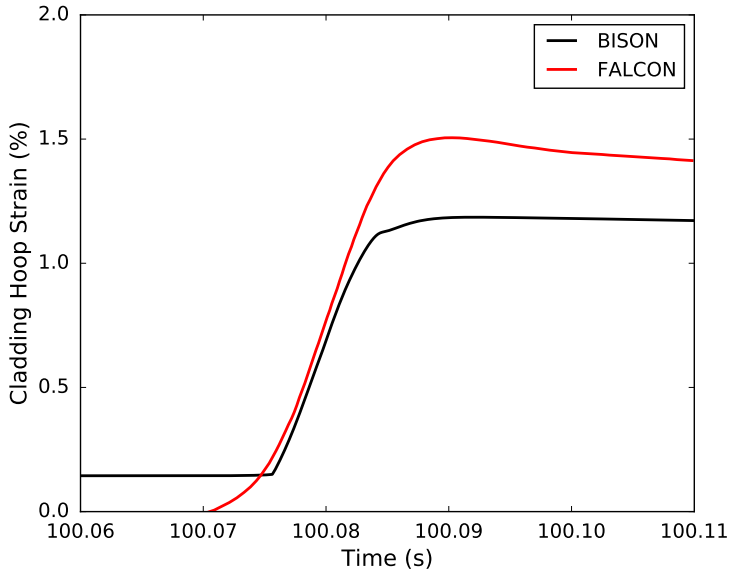

Figure A36.10: BISON and FALCON calculated cladding hoop strain evolutions at PPN

The fission gas release progression with and without the transient model is plotted in Figure A36.12 with the fuel centerline temperature. BISON calculated a final fission gas release of 9.8% compared to the measured 13.7%. Figure A36.12 shows the influence of the burst release component in the BISON fission gas release model for the transient. During the initial temperature increase in the fuel, the fission gas release increases from just under 2% (the end result from the base irradiation) to 5.5% in approximately 10 ms. The fission gas release continues to increase over the next 4 seconds likely due to a combination of increased diffusion from the elevated fuel temperatures and the transient burst release model. In contrast, the FGR without the transient model shows very small increase throughout the simulation. The diffusion-based contribution is much smaller in this case than in Figure A36.7 because the fuel temperatures are much lower during this transient.

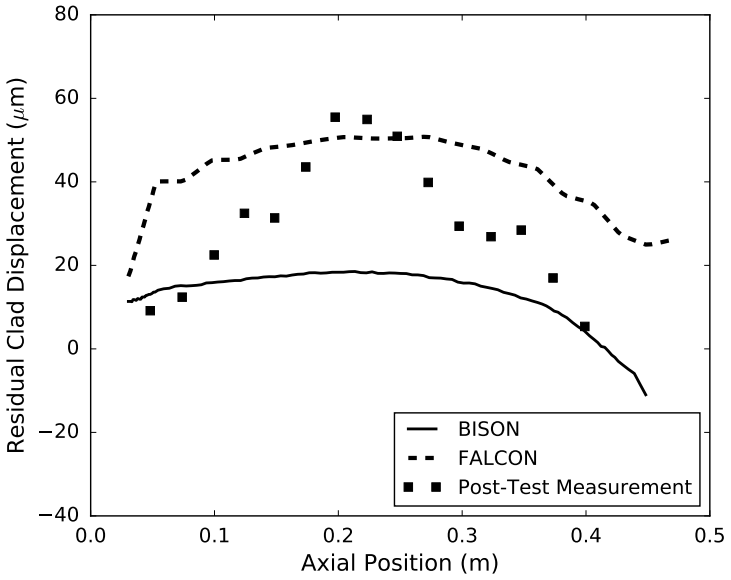

Figure A36.11: Residual cladding displacement calculations for BISON and FALCON against post-test measurements

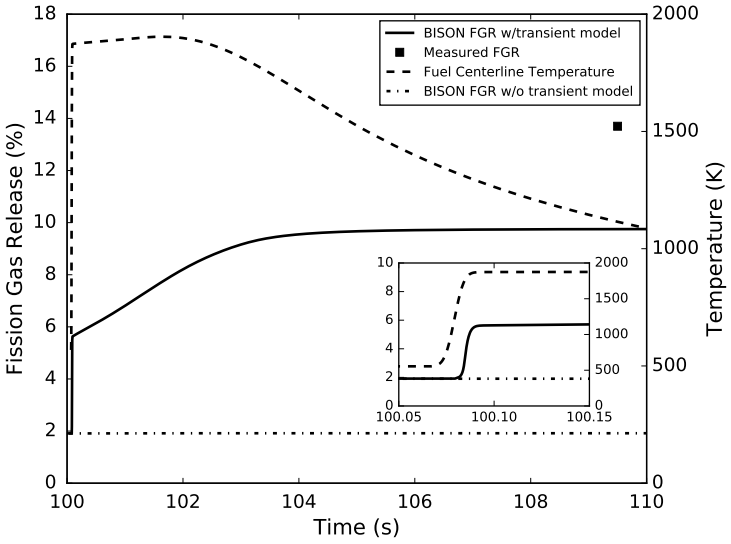

Figure A36.12: Fission gas release plotted with fuel centerline temperature and measured post-test result for REP Na-3

A36.4.3 REP Na-5

REP Na-5 was base irradiated during 5 cycles to a local rodlet burnup of 64 GWd/tU. The CABRI test targeted an energy deposition of 435 J/g (104 cal/g) during an 8.8 ms FWHM pulse. Even with the high burnup of the REP Na-5 rodlet the oxidation thickness only varied between 15-25 microns because it was taken from between the 2nd and 3rd spacers from the parent rod. The energy deposited into the rodlet was reported as 104 cal/g from the IRSN and 112 cal/g at 1.2 seconds for FALCON. FALCON also reported that the energy deposition was 105 cal/g up through 0.4 seconds. The resulting max increase in radial averaged enthalpy calculated in BISON was 116.8 cal/g compared to 115 cal/g from FALCON and 108 cal/g reported from IRSN. These results are plotted in Figure A36.13 and tabulated in Table A36.4.

A more detailed comparison with FALCON shows the time progression of the injected energy and

radial average enthalpy in Figure A36.14. The data available from the FALCON results is limited out to 120 ms after the start of the transient but up to that time the results between BISON and FALCON show very good agreement.

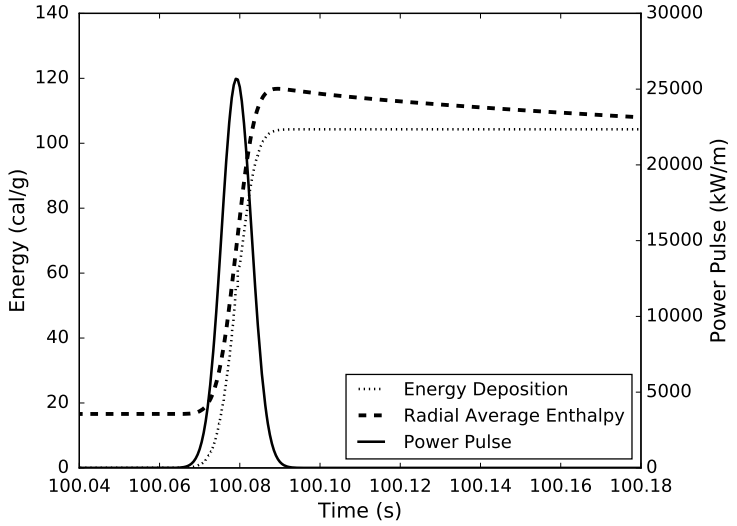

Figure A36.13: Power pulse, energy deposited and radial averaged fuel enthalpy at PPN for REP Na-5 case

The temperature histories for the fuel and cladding are plotted in Figure A36.15 with the maximum reported values for the fuel and cladding shown in Table A36.4. The cladding inside and outside temperatures for BISON and FALCON are plotted in Figure A36.16. The results here again show very good agreement between the two codes for temperature predictions.

Table A36.4: BISON calculations compared against FALCON calculations and experimental/reported values found in literature for REP Na-5.

Property	BISON	FALCON	Experimental/ Reported Values	% Difference (FALCON)	% Difference (Experimental)
Energy Deposition (cal/g)	104.3	112	104	-6.9	0.3
Peak Fuel Enthalpy (cal/g)	116.8	115	108	1.5	8.1
Max Fuel Temperature (K)	2444	2387	-	2.4	-
Max Fuel Centerline Temp. (K)	1684	1757	-	-4.1	-
Clad Max Inside Temp. (K)	1104	1020	-	8.2	-
Max Hoop Strain (%)	1.34	1.21	1.1	10.5	22
Residual Hoop Strain (%)	0.48	0.85	-	-44	-
Peak Cladding Hoop Stress (MPa)	713	867	-	-18	-
Fission Gas Released (%)	5.3	-	15.1	-	-65
Corrosion thickness (μm)	19	-	15-25	-	-

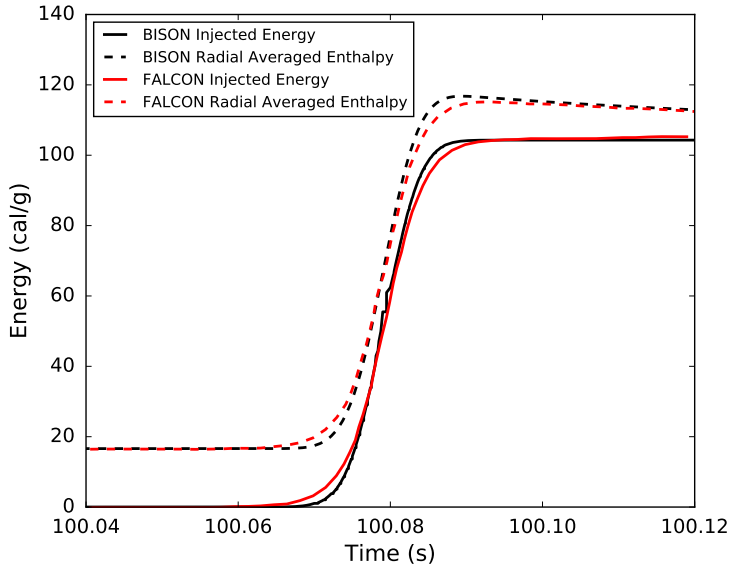

Figure A36.14: Injected energy and radial averaged enthalpy at PPN comparisons between BISON and Falcon for REP Na-5

The cladding outer surface hoop strain is shown in Figure A36.17. BISON shows a very good agreement with FALCON on the total hoop strain during the transient, 1.34% compared to 1.21%. Even though the total amount of hoop strain predicted by BISON is much closer to FALCON for this case, the residual hoop strain is still under predicted. FALCON calculates a residual cladding hoop strain of 0.85% compared to BISON with a prediction of 0.48% at the PPN.

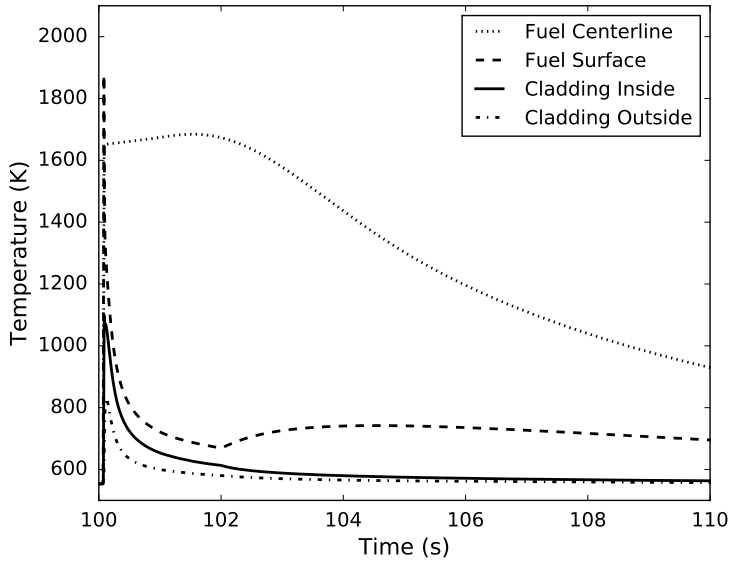

Figure A36.15: Fuel and cladding temperature histories at PPN for REP Na-5

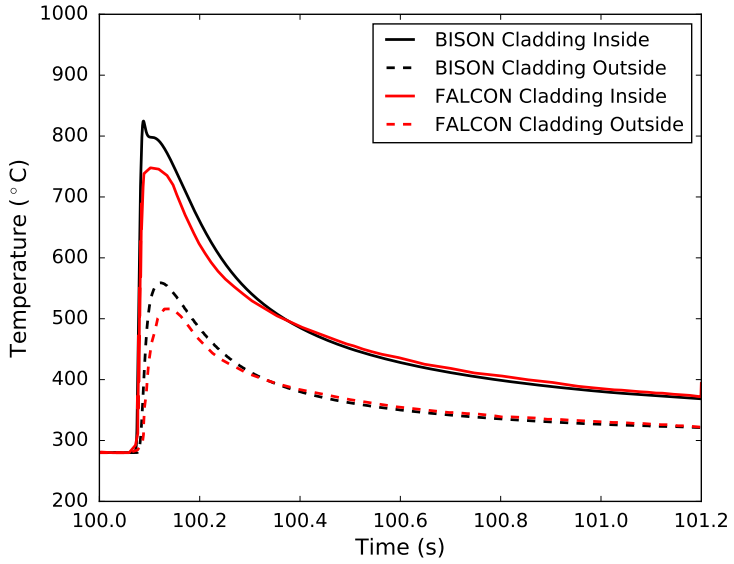

Figure A36.16: Cladding temperature at PPN comparisons between BISON and FALCON for REP Na-5

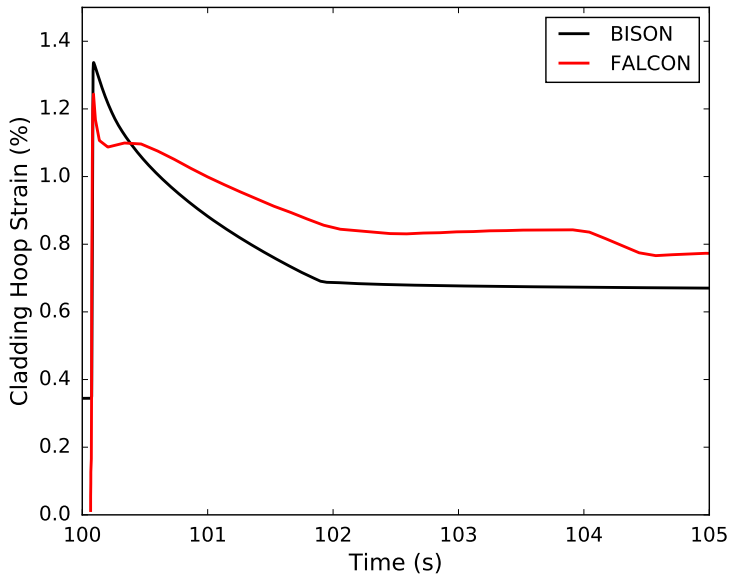

Figure A36.17: Cladding hoop strain at PPN comparisons between BISON and FALCON for REP Na-5

The fission gas release prediction for BISON was 5.3% at the conclusion of the test compared to the measured 15.1% post-test measurement. During this test the initial burst release was much less than the previous two cases, from 1.6% to 1.9% during the initial temperature rise in the fuel (Figure A36.18). The majority of the fission gas was released when the fuel centerline temperature was around its maximum of approximately 1650 K.

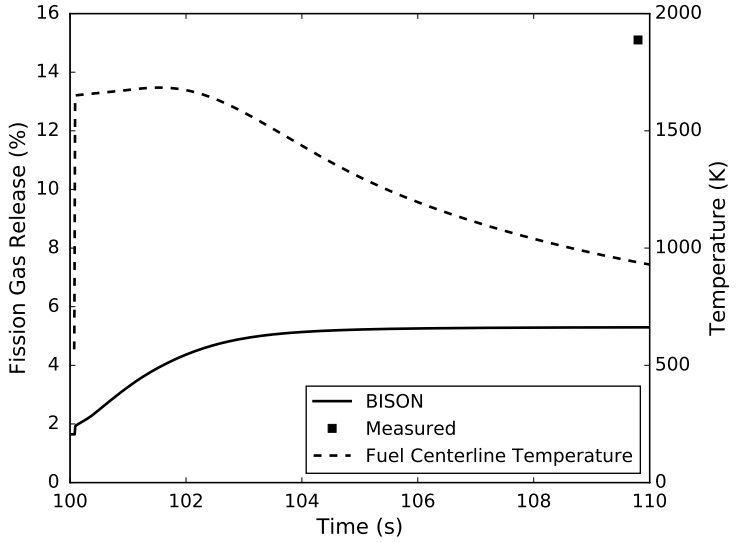

Figure A36.18: Fission gas release plotted with fuel centerline temperature and the measured post-test result for REP Na-5

A36.4.4 REP Na-10

The REP Na-10 rodlet was irradiated to 63 GWd/tU with an oxide thickness ranging from 60-100 μm. The CABRI test targeted 453 J/g (108.3 cal/g) of energy deposited into the fuel in a 31 ms FWHM pulse. During the test the microphones in the test capsule detected a strong signal indicating that cladding failure had occurred. The microphones detected that the failure originated at an axial location 255 mm from the bottom of the fuel column. The injected energy at time of failure was 75 cal/g at the PPN and 74 cal/g at the location of failure. There was no indication of fuel ejection during the remaining 30 cal/g of energy injection.

BISON does not currently have a failure model for RIA type accidents so the results presented are assuming no failure in the rodlet and as a result there are no comparisons to experimental measurements for this test. The BISON simulation resulted in 109 cal/g of energy deposited into the rodlet compared to 103 cal/g in FALCON and 108 cal/g reported by IRSN. The resulting calculated maximum increase in radial average fuel enthalpy was 118 cal/g in BISON, 109 cal/g in FALCON and a reported value of 98 cal/g by IRSN. These values result in an 8% difference between BISON and FALCON and a 20% difference from the reported value. All these values are shown in Table A36.5. A more detailed comparison of the injected energy and radial average enthalpy between BISON and FALCON is shown in Figure A36.20. The profiles are very similar with the BISON results predicting slightly higher results than FALCON. These results would be much closer if the energy injected was the same. The pulse in BISON was targeted to deposit 108 cal/g of energy into the fuel at the PPN. If this value was scaled back to match the 103 cal/g in FALCON the results would be closer.

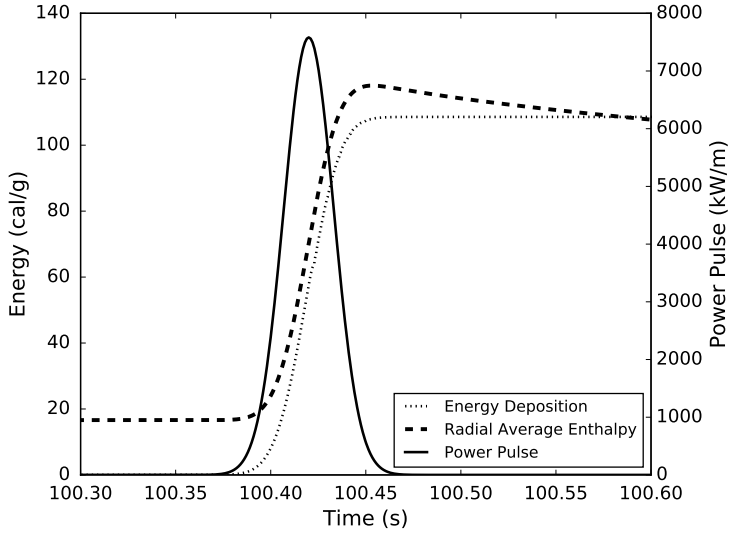

Figure A36.19: Power pulse, energy deposited and radial averaged fuel enthalpy at PPN for REP Na-10 case

Table A36.5: BISON calculations compared against FALCON calculations and experimental/reported values found in literature for REP Na-10.

Property	BISON	FALCON	Experimental/ Reported Values	% Difference (FALCON)	% Difference (Experimental)
Energy Deposition (cal/g)	109	103	108	5.4	0.3
Peak Fuel Enthalpy (cal/g)	118	109	98	8.0	20
Max Fuel Temperature (K)	2215	2046	-	8.2	-
Max Fuel Centerline Temp. (K)	1748	1662	-	5.2	-
Clad Max Inside Temp. (K)	1091	1080	-	1.0	-
Max Hoop Strain (%)	1.19	1.00	-	19	-
Residual Hoop Strain (%)	0.52	0.73	-	-29	-
Peak Cladding Hoop Stress (MPa)	656	773	-	-15	-
Fission Gas Released (%)	5.6	-	Rod burst	-	-
Corrosion thickness (μm)	87	-	60-100	-	-

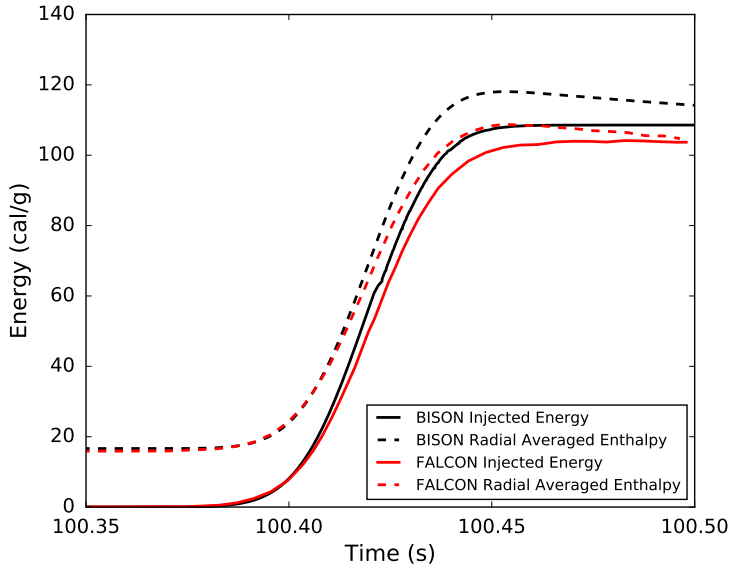

Figure A36.20: Injected energy and radial averaged enthalpy at PPN comparisons between BISON and Falcon for REP Na-10

The fuel and cladding temperature profiles are plotted together in Figure A36.21. An interesting observation comparing Figures A36.21 and A36.15 is the much lower fuel surface temperature in the REP Na-10 case. The maximum fuel temperature is still greater than the fuel centerline temperature and that happens just inside the fuel surface, but due to the much longer pulse in REP Na-10 the fuel surface temperature does not exceed the centerline temperature. Figure A36.22 shows a more detailed comparison of the cladding temperature histories between BISON and FALCON with good agreements between the two codes.

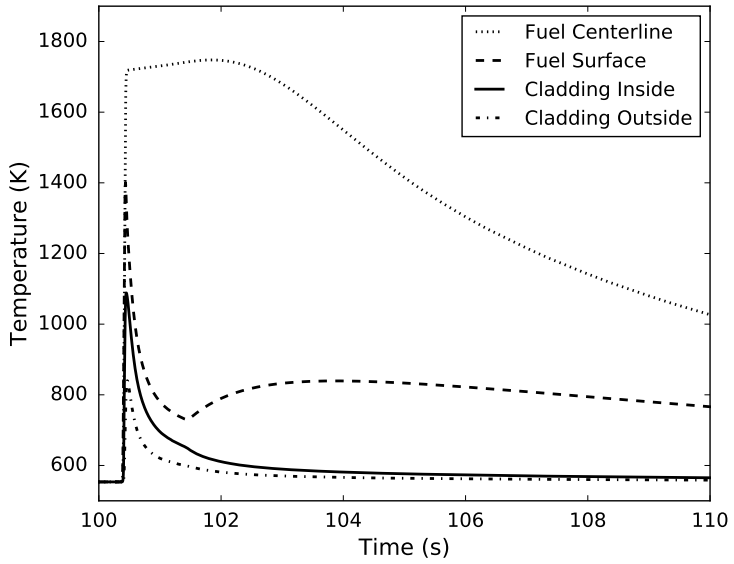

Figure A36.21: Fuel and cladding temperature evolutions at PPN for REP Na-10

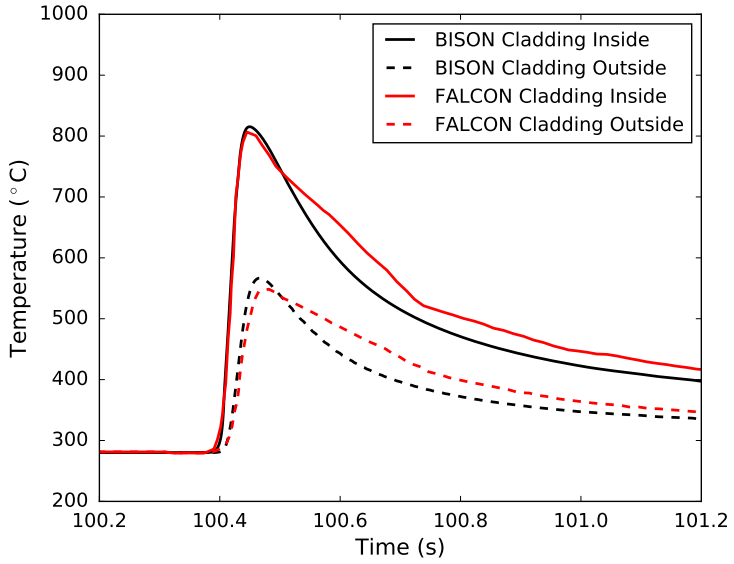

Figure A36.22: Cladding temperature at PPN comparisons between BISON and FALCON for REP Na-10

There are no measured mechanical results available, but for this case BISON again predicts a higher cladding hoop strain than FALCON, 1.19% compared to 1.0%. The residual hoop strains are under predicted indicating a slight difference in the calculated plastic strain between the two codes. The two codes show good agreement on the maximum cladding hoop stress calculated. BISON predicts 656 MPa versus 773 MPa for FALCON, only 15% difference.

Since the fuel rod failed there is no experimental results for fission gas release to compare to, but BISON predicted a 5.6% fission gas release at the end of the transient. The fission gas release looked very similar to REP Na-5 (Figure A36.18) with a very small increase during the initial fuel temperature increase.

A36.5 Discussion

There are several observations that can be made on the results presented above for the CABRI REP Na cases for RIA validation.

- BISON tends to slightly over predict the estimated fuel radial average enthalpy compared to FALCON and the reported values (predicted using SCANAIR). The results typically compare within 10% of FALCON and reported values, with slightly higher differences for REP Na-3 FALCON and REP Na-10 SCANAIR results.

- BISON agrees very well with FALCON on the temperature predictions. The maximum fuel temperature (located in the high burnup rim region) and the maximum temperatures calculated for the fuel centerline and cladding inside temperatures were all within 10% of FALCON, with many of the results well within 5%.

- In general the mechanical results do not show similar close agreement with FALCON or measured values. BISON generally under predicts the max hoop strain in the cladding outer surface. The max hoop strain results look reasonable for REP Na-5 and 10, but generally the strains reported are referenced from cold zero power conditions prior to the transient. This removes any accumulated plastic or creep strain from the base irradiation. The results presented for BISON are the absolute strains and this can be seen in Figures A36.10 and A36.17 where the BISON results do not start from zero as the FALCON results do. Referencing these results from zero would result in an even

greater under-prediction, but these results show the absolute strain because it was not explicitly stated whether the FALCON or measured results are referenced to a pre-RIA condition.

- Similar to the total hoop strain in the cladding the plastic strain accumulation is also under predicted. This is evident in Figures A36.6 and A36.11 showing the residual displacement or clad diameter and in Tables A36.2 through A36.5.

- The fission gas release calculations show good agreement with measured values, with only REP Na-5 showing a sizable difference.

Based on the results presented so far for the CABRI REP Na RIA cases the results show promise with the thermal predictions but improvements can be made in regards to the mechanical results. There are a lot of important details concerning the FALCON modeling procedure and results that are not known and many assumptions are made during the comparison. For example the FALCON and reported values for fuel radial averaged enthalpy do not specify if these are results at the peak power node or rod averaged. It is assumed the results are for the PPN; the BISON results are at the PPN.

The post base-irradiation conditions have a significant impact on the mechanical results. One of the most significant initial conditions prior to the RIA test is the fuel-to-clad gap distance. In all cases the BISON base-irradiation calculation predicted fuel-to-clad gaps of 14.9-17.5 μm at CZP conditions after the base irradiation. Those gaps were reduced to between 9.6-14 μm at HZP conditions prior to the transient. All these cases were for high-burnup fuel (excluding REP Na-2) which should result in a closed or very small gap after the base-irradiation. In a recent study benchmarking BISON and SCANAIR calculations against the CIP0-1 rodlet RIA test, a micrograph of a high-burnup fuel rod clearly shows fuel-zirconia bonding (Figure 3 in [106]). In that study the SCANAIR simulation assumed a closed gap, as the micrograph indicated, prior to the RIA pulse while the BISON simulation began with a 14 μm gap. The resulting under-estimated strains are similar to those observed in this study. As a thought project, assuming no initial gap on REP Na-3, hand calculations were performed on the results from the cladding hoop strain (Figure A36.10) to add the 16.4 μm gap to the displacement thus estimating the resulting total hoop strain. The results are shown in Figure A36.23 and the magnitude of the results compare much better to the FALCON results.

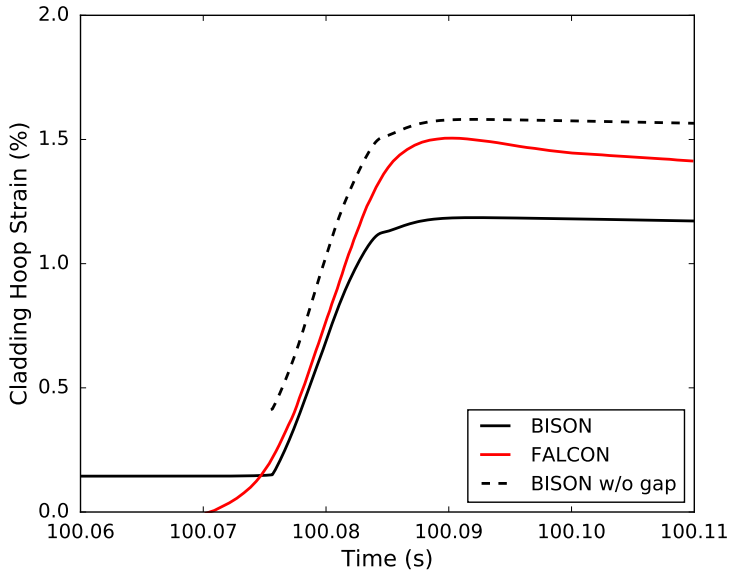

Figure A36.23: BISON and FALCON calculated cladding hoop strain evolutions at PPN with the estimated BISON results assuming no initial fuel-to-cladding gap

A36.6 Recommended Future Work

There is a lot of work to be improved upon with regards to the RIA validation modeling. Some of the improvements include:

- Frictional contact will improve axial displacement predictions that can be compared against experimental results and FALCON calculations. Frictional contact will also improve plastic strain predictions in the cladding.
- Discrete pellet mesh will provide more prototypic results and better comparisons to measured data such as in Figure A36.6
- Including fuel creep and cracking during the base irradiation
- Fuel-clad bonding occurs with high-burnup cases and results in a much different estimation of the fuel-to-cladding gap after the base irradiation. During cold zero power conditions this could likely result in a closed gap between the fuel outer surface and the cladding inner surface with gaps opening up inside the fuel cracks. Understanding and accounting for this could likely have a big impact on the estimation of pellet-clad-mechanical-interactions during RIAs and other transient events.
- Implement a failure model for RIA applications to predict when failure occurs during fast transients such as RIAs

A37 NSRR FK RIA Tests

A37.1 Overview

NSRR is a modified TRIGA (Training, Research, Isotopes, General Atomics) ACPR (Annular Core Pulse Reactor) with a dry space located in the center of the core. In a simulated RIA test for an irradiated fuel, a single instrumented fuel rod in a water-filled capsule is placed in the center of the core, and is pulse irradiated.

A large number of experiments on simulated RIA have been performed at the test facility of NSRR to evaluate the fuel rod behavior and failures at different energy depostion, burnup, fuel design, and coolant condition. Since 1989, tests on medium and high burnup fuels in NSRR have been started and continued; recent experiments moved towards the testing on high burnup fuel with advanced corrosion resistant cladding alloys such as MDA and Zirlo^{TM} [107]. Pulse irradiation tests were normally performed in stagnant coolant water at room temperature (˜20°C) and atmospheric pressure (˜0.1 MPa) under a narrow power pulse with Full Width at Half Maximum (FWHM) of approximately 5 ms. Recent tests were performed at high coolant temperature (280°C) and high pressure (up to 6.4 MPa) to provide measurements on fuel failures at conditions close to Hot Zero Power (HZP) condition. The current evaluation was performed on early RIA tests conducted at room temperature and atmospheric pressures; a number of tests on BWR type fuels with burnup from 41 to 61 GWd/tU (three and four cycles) were selected for the validation of BISON code based on published information from JAEA (formerly known as JAERI) [108, 109].

A37.2 Test Description

A37.2.1 Rod Design Specifications

An overview of NSRR FK cases selected for BISON assessment is shown in Table A37.1. All the fuel types are UO_2 fuel enriched to 4.5% with zirconium-lined recrystallized Zircaloy-2 cladding, and were refabricated into short rodlets to fit into the NSRR test capsule. All the test rods selected for evaluations are short rodlets with an active fuel stack length of 102 mm (10 pellets) or 128 mm (12 pellets).

Table A37.1: Overview of NSRR FK cases

Test	FK1	FK2	FK3	FK4	FK5	FK6	FK7	FK8	FK9
Clad thickness (mm)	0.86	0.86	0.86	0.86	0.86	0.86	0.86	0.86	0.86
Fuel density (%TD)	0.97	0.97	0.97	0.97	0.97	0.97	0.97	0.97	0.97
U235 enrichment (%)	4.5	4.5	4.5	4.5	4.5	4.5	4.5	4.5	4.5
Burnup (GWd/tU)	45	45	41	56	56	61	61	61	61
Fill gas pressure (MPa)	0.3	0.3	0.3	0.5	0.5	0.1	1.5	1.5	1.5
Energy deposit (cal/g)	167	95	186	180	100	168	166	90	119
Peak fuel enthalpy (cal/g)	129.52	69.8	144.5	139.5	69.8	130.5	128.6	64.8	89.8
Power Pulse width (ms)	4.5	7	4.5	4.3	7.3	4.3	4.3	7.3	5.7
Failure enthalpy (cal/g)	-	-	-	-	-	70	62		86

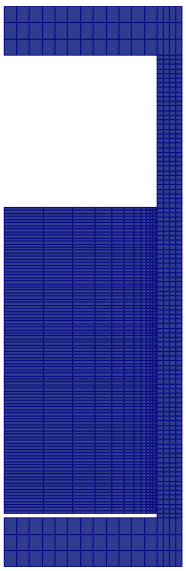

Figure A37.1: Finite Element Grid for the BISON Analyses of the NSRR RIA Tests

A37.2.2 Operating Conditions and Irradiation History

Fuel rod segements for Tests FK-1, FK-2, and FK-3 were irradiated in Fukushima Daiichi Unit 3 for three cycles to a burnup level of 41 to 45 GWd/tU, and FK-4 – FK-9 were irradiated in Fukushima Daini Unit 2 to a burnup level of 56 to 61 GWd/tU [108, 109]. The short fuel segment for each rod has a flat axial burnup profile from base irradiation, and a uniform axial power profile in the RIA transient.

Those rodlets were tested in NSRR reactor at room temeprature (˜20°C) and atmospheric pressure (˜0.1 MPa) condition with stagnant flow.

A37.3 Model Description

A37.3.1 Geometry and Mesh

The rod specifications and geometry in Table A37.1 and were used to define the geometry for the cases. The 9 cases were modeled using a two-dimensional, axisymmetric (2D-RZ) mesh with eight-node quadratic elements.

The mesh consists of 16 radial elements with 12 in the fuel and 4 in the cladding. 100 axial elements were used for modeling in the axial direction. A typical finite element grid for the RIA tests is illustrated in Figure A37.1.

A37.3.2 Material and Behavioral Models

The material and behavior model options used for modeling the RIA test cases are listed below:

- Fuel thermal conductivity: NFIR thermal conductivity model is used
- Fuel mechanical models: elastic fuel is assumed for the modeling
- Fission gas release and swelling: fission gas release and swelling models are turned off
- Thermal model of clad: MATPRO model on thermal conductivity and specific heat for Zircaloy is used (ThermalZry)
- Clad mechanical model: plastic deformation model of Zircaloy (ZryPlasticity) is used

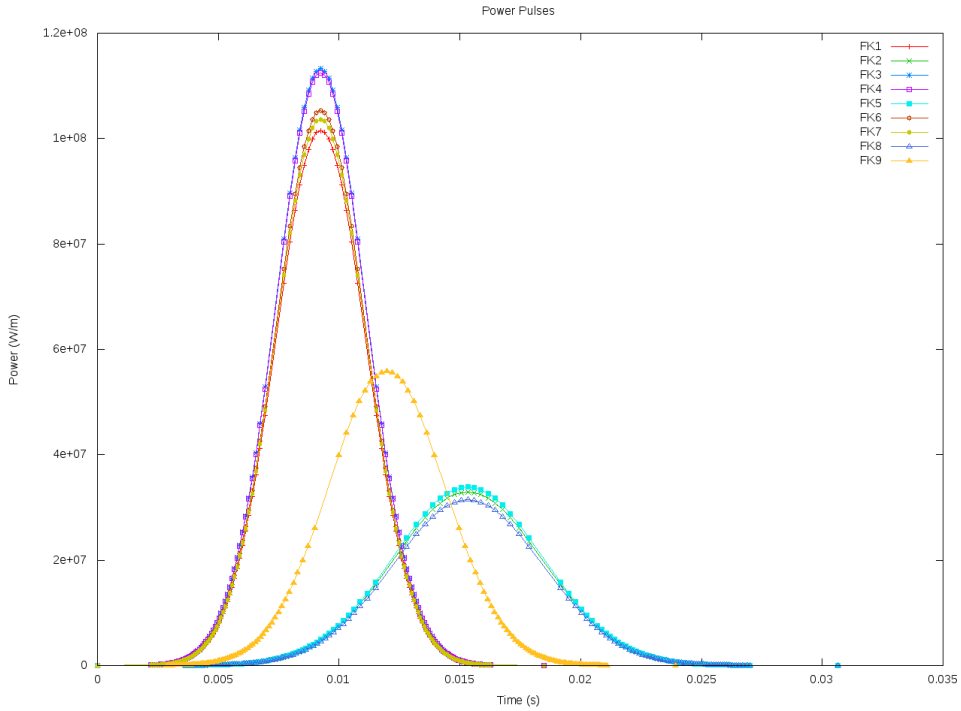

Figure A37.2: Power Pulses for the NSRR BWR RIA Tests.

A37.3.3 Boundary and Operating Conditions

The thermal and mechanical boundary condtions used for the test cases are described as follows:

- Mechanical contact model: frictionless model is used
- Thermal contact model: GapHeatTransferLWR thermal contact model is used
- Thermal boundary condition: clad temperature is specified for all test cases; one example of using coolant channel model is provided for modeling DNB for test case FK-3

The power history during the simulated RIAs for the test cases are plotted in Figure A37.2.

Base irradiation simulation was performed for the BWR rods with the design geometry and material of the test rods to provide the parameters of gap size and fast neutron fluence for modeling the RIA transients. Radial power and burnup profiles at the end of base irradiation were taken from [110] for preparing the pre-transient conditions.

Since the RIA test cases were prepared based on conditions after base irradiation, the variables describing the as-irradiated conditions such as burnup, fast neutron fluence, gap size, and radial power rofiles are inputs in those test cases. However, fission gas inventory at fuel grain boundaries can not be easily established using such methodology; therefore fission gas release and swelling were not modeled in those test cases. It would be of interest to develop a simple model in BISON to compute the pre-transient fission gas inventory for predicting the fission gas release in a fast transient in the future.

The coolant channel model was tested for the modeling of DNB in a RIA for one selected test case FK-3.

A37.3.4 Input files

The BISON input and all supporting files (power histories, axial power profile, fast neutron flux history, etc.) for NSRR FK cases are provided with the code distribution at bison/assessment/NSRR_FK/analysis.

Table A37.2: Summary of Fuel Temperatures of the FK cases

Case	Peak Clad Inner Surface Temperature (°C)	Peak Rim Temperature by Falcon (°C) [100]	Peak Centerline Temperature by Falcon (°C) [100]	Peak Rim Temperature (°C)	Peak Centerline Temperature (°C)
FK-1	645	2529	1569	2353	1583
FK-2	386	1360	880	1390	902
FK-3	678	2691	1737	2574	1723
FK-4	730	2747	1591	2616	1652
FK-5	407	1290	852	1450	884
FK-6	509	2696	1510	2723	1521
FK-7	503	2648	1509	2699	1501
FK-8	274	1339	788	1595	804
FK-9	367	2007	1146	2122	1082

Table A37.3: Summary of Clad Hoop Strains of FK cases

Case	[H_{fail}] H_p (cal/g)	Peak SED or SED at failure (MJ/m^3)	Calculated Peak Hoop Strain by Falcon [111] (%)	Calculated Peak Hoop Strain (%)	Measured Residual Strain (%)	Calculated Residual Hoop Strain (%)
FK-1	130	4.25	1.30	0.84	0.85	0.22
FK-2	70	2.28	0.4	0.65	0	0.00
FK-3	145	4.11	1.55	0.84	1.47	0.18
FK-4	140	4.14	1.75	0.84	1.25	0.17
FK-5	70	2.35	0.41	0.65	0	0.00
FK-6	[70] 131	4.03	1.7	0.84	Failed	0.18
FK-7	[62] 129	3.98	1.6	0.84	Failed	0.18
FK-8	65	2.04	0.6	0.62	0	0.00
FK-9	[86] 90	3.70	1.0	0.84	Failed	0.05

A37.4 Results

This section describes results of the evaluation of NSRR RIA tests using BISON code. Results of temprature predictions on NSRR FK cases calculated by BISON along with Falcon predictions are summarized in Table A37.2. Results of clad hoop strains calcuated by BISON is shown in Table A37.3 in comparison to Falcon results [111].

Figure A37.3 provides the radial temperature profiles for FK-1 – FK-9 at the time of peak rim temperature. Figure A37.4 provides the radial temperature profiles for FK-1 - FK-9 at the time of peak fuel centerline temperature.

Those results have shown the typical thermal response during a RIA; the pellet has an initial edge-peaked profile, and then decreases rapidly while the fuel centerline features a more gradual temperature reduction. This is futher illustrated in the example of case FK3 in Figure A37.5 which provides calculated temperature at fuel centerline, fuel outer surface, and clad inner surface.

A37.5 Discussion

BISON calculations on the fuel temperatures matches closely to Falcon results for most cases, except for a few cases on peak rim temperature predictions. Using same power history as Falcon code, the

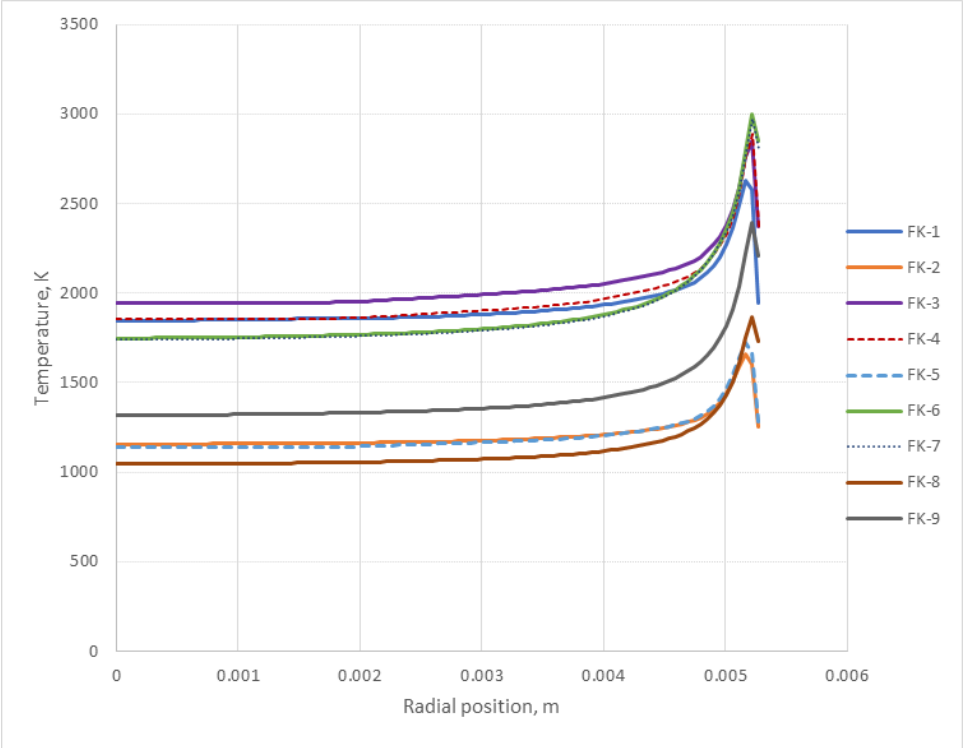

Figure A37.3: Radial Fuel Temperature Profiles for the FK 1-9 Fuel Rods at the Time and Elevation of Peak Fuel Temperature in the Rim Region

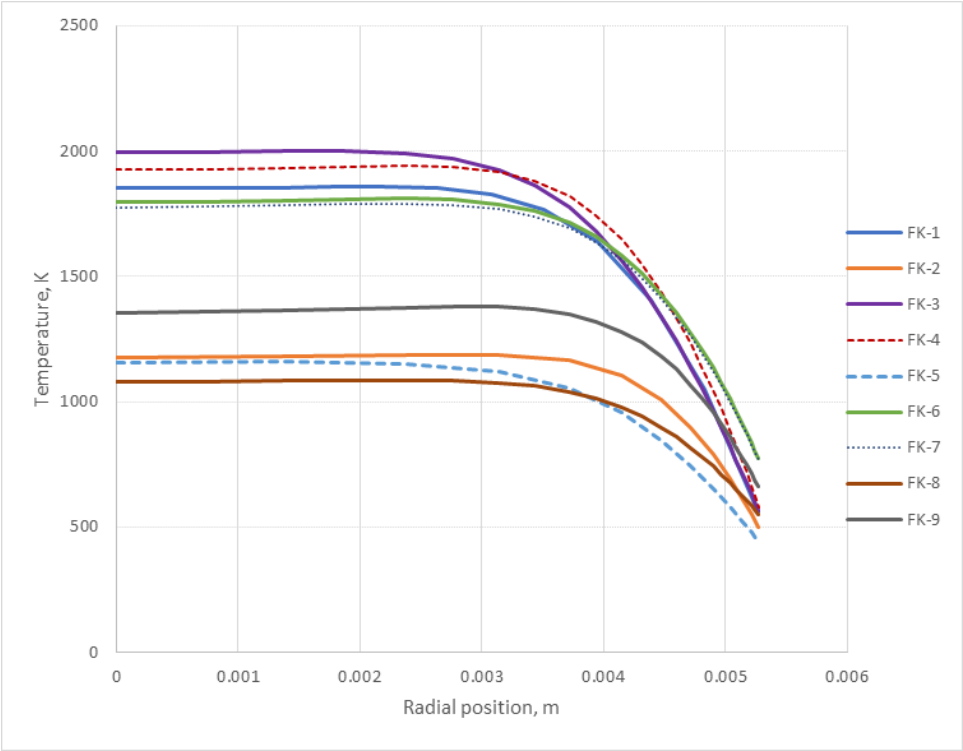

Figure A37.4: Radial Fuel Temperature Profiles for the FK 1-9 Fuel Rods at the Time and Elevation of Peak Fuel Ceneterline Temperature

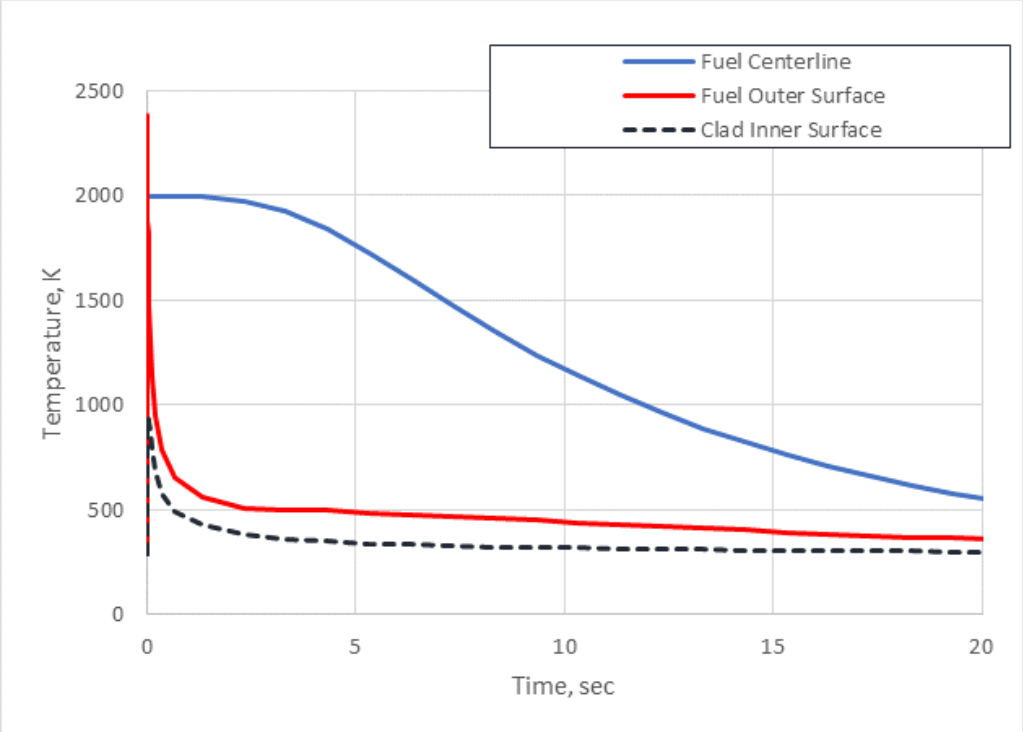

(a) 0-20 sec

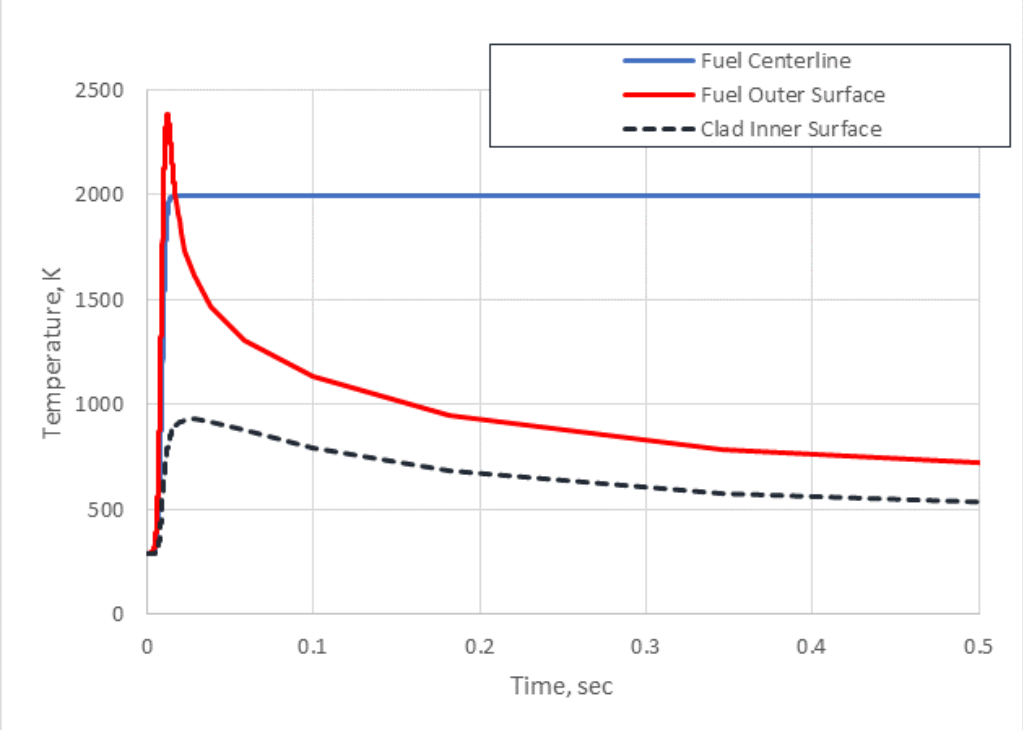

(b) 0-0.5 sec

Figure A37.5: Temperature at fuel centerline, fuel outer surface, and clad inner surface for test case FK-3

calculated enthaly by BISON in general is higher than the reported value from experiments, with a maximum over-prediction of 10%.

Clad permanent hoop strains calculated by BISON are smaller than measurements and Falcon code results. This could be caused by the gap size used for the pre-transient conditions from BISON calculations at the end of base irradiation, which is larger than the gap size assumed in Falcon analysis.

The current thermal boundary condtion uses specified cladding temperature which is same as the one used in [100], and this is considered to be adequate to predict the Pellet Clad Mechanical Interaction (PCMI) phase in the RIA since cladding outer surface temeprature changes little during the power pulse. In some tests (FK-1, FK-3, FK-4, and FK-9), cladding temperature escalation was observed after the power pulse phase, which was considered to be caused by the Departure from Nucleate Boiling (DNB). The coolant channel model was tested for the modeling of DNB in a RIA for case FK-3, it was found that the model under-predict the CHF , which empirically scales the Zuber correlation to match the measured CHF from transient pool boiling tests [112]. By lowering the scaling factor to force the DNB to occur, the current coolant model tends to over-predict the clad temperature. The reason could be the lack of the considerations of the radiation heat transfer in the film boiling phase or the under-prediction of the rewetting temperature. Further model and code changes would be needed to improve the prediction of cladding temperature during DNBs.

Frictional model was tested but failed to converge, and therefore a frictionless model was used instead, and for this reason, no comparison to measurements on the axial fuel elongation was performed.

A37.6 Conclusion

Simulated RIA tests on irradiateiond BWR rods FK-1 – FK-9 were modeled using BISON code. BISON calculations results were compared to measurements and Falcon code results. A few observations can be made with regard to the current validation:

- BISON tends to over-predict the peak fuel enthalpy in comparison to Falcon code.
- BISON agrees well with Falcon on the temperature predictions, and could capture the characteristics of the temperature profile during a pulse irradiation.
- BISON tends to under-predict the clad permanent hoop strain as compared to Falcon code and experiements; this could be caused the relatively larger pre-transient gap size used in the BISON calculations.
- The clad permanent axial strain is also under-predicted, which can be attributed to the pre-transient gap size as well as the lack of frictional contact in modeling those test cases.
- BISON tends to under-predict the CHF compared to the measured CHF in pool boling tests [112];

Current results indicate some input, such as gap size and rod power, of those test cases might need to be refined, and further code improvements, e.g. the contact model and the coolant channel model, would be needed to augment the capability for the applications to modeling RIA transients.

Bibliography

[1] R. L. Williamson, J. D. Hales, S. R. Novascone, M. R. Tonks, D. R. Gaston, C. J. Permann, D. Andrs, and R. C. Martineau. Multidimensional multiphysics simulation of nuclear fuel behavior. *Journal of Nuclear Materials*, 423:149–163, 2012.

[2] J. D. Hales, R. L. Williamson, S. R. Novascone, D. M. Perez, B. W. Spencer, and G. Pastore. Multidimensional multiphysics simulation of TRISO particle fuel. *Journal of Nuclear Materials*, 443:531–543, November 2013.

[3] Pavel Medvedev. Fuel performance modeling results for representative FCRD irradiation experiments: Projected deformation in the annular AFC-3A U-10Zr fuel pins and comparison to alternative designs. Technical Report INL/EXT-12-27183 Revision 1, Idaho National Laboratory, 2012.

[4] S. A. Pitts, S. R. Novascone, H. Chen, B. W. Spencer, S. Satpathy, R. J. Gardner, and J. D. Hales. Verify and validate 1.5d capability. Technical Report CASL-U-2017-1380-000, Consortium for Advanced Simulation of LWRs, 2017.

[5] J. Killeen, E. Sartori, and T. Tverberg. FUMEX-III: A new IAEA coordinated research project on fuel modeling at extended burnup, paper 2176. In *Proceedings of Top Fuel 2009*, Paris, France, Sept 6-10, 2009.

[6] J. Zhang and M. Veshchunov. Status Update of the IAEA FUMAC Project. Presented at the OECD/NEA Expert Group on Reactor Fuel Performance (EGRFP), Paris, France, February 2016.

[7] J. C. Killeen, J. A. Turnbull, and E. Sartori. Fuel modelling at extended burnup: IAEA coordinated research project FUMEX-II. In *Proceedings of the 2007 International LWR Fuel Performance Meeting*, San Francisco, California, Paper 1102, September 30–October 3 2007.

[8] IAEA. Advances in high temperature gas cooled reactor fuel technology. Technical Report IAEA-TECDOC-1674, International Atomic Energy Agency, 2012.

[9] J. D. Hales, S. R. Novascone, G. Pastore, D. M. Perez, B. W. Spencer, R. L. Williamson, and R. J. Gardner. BISON theory manual: The equations behind nuclear fuel analysis. Technical Report INL/EXT-13-29930 Rev. 1, Idaho National Laboratory, September 2014.

[10] J. D. Hales, S. R. Novascone, G. Pastore, D. M. Perez, B. W. Spencer, R. L. Williamson, and R. J. Gardner. BISON users manual. Technical Report INL/MIS-13-30307 Rev. 2, Idaho National Laboratory, September 2014.

[11] A. Soba, A. Denis, L. Romero, E. Villarino, and F. Sardella. A high burnup model developed for the DIONISIO code. *Journal of Nuclear Materials*, 433:160–166, 2013.

[12] A. Soba and A. Denis. Personal communication, 2017.

[13] J.B. Ainscough, B.W. Oldfield, and J.O. Ware. Isothermal grain growth kinetics in sintered UO_2 pellets. *Journal of Nuclear Materials*, 49:117–128, 1973.

[14] A. M. Ross and R. L. Stoute. Heat transfer coefficient between UO_2 and Zircaloy-2. Technical Report AECL-1552, Atomic Energy of Canada Limited, 1962.

[15] C. M. Allison, G. A. Berna, R. Chambers, E. W. Coryell, K. L. Davis, D. L. Hagrman, D. T. Hagrman, N. L. Hampton, J. K. Hohorst, R. E. Mason, M. L. McComas, K. A. McNeil, R. L. Miller, C. S. Olsen, G. A. Reymann, and L. J. Siefken. SCDAP/RELAP5/MOD3.1 code manual, volume IV: MATPRO–A library of materials properties for light-water-reactor accident analysis. Technical Report NUREG/CR-6150, EGG-2720, Idaho National Engineering Laboratory, 1993.

[16] D. D. Lanning and C. R. Hann. Review of methods applicable to the calculation of gap conductance in zircaloy-clad uo2 fuel rods. Technical Report BWNL-1894, UC-78B, Pacific Northwest National Laboratory, 1975.

[17] A. Marion (NEI) letter dated June 13, 2006 to H. N. Berkow (USNRC/NRR). Safety Evaluation by the Office of Nuclear Reactor Regulation of Electric Power Research Institute (EPRI) Topical Report TR-1002865, "Topical Report on Reactivity Initiated Accidents: Bases for RIA Fuel rod Failures and Core Coolability Criteria". http://pbadupws.nrc.gov/docs/ML0616/ML061650107.pdf, 2006.

[18] T. Tverberg, M. Amaya. Study of thermal behavious of UO_2 and (U,Gd)O_2 to high burnup (IFA-515). Technical Report HWR-671, Halden, February 2001.

[19] P. Lösönen. Early-in-life irradiation of IFA-562.2 (The Ultra High Burn-up Experiment). Technical Report HWR-247, Halden, December 1989.

[20] Giovanni Pastore, L. P. Swiler, J. D. Hales, S. R. Novascone, D. M. Perez, B. W. Spencer, L. Luzzi, P. Van Uffelen, and R. L. Williamson. Uncertainty and sensitivity analysis of fission gas behavior in engineering-scale fuel modeling. *Journal of Nuclear Materials*, 456:398–408, 2015.

[21] IAEA. Fuel Modelling at Extened Burnup (FUMEX-II): Report of a Coordinated Research Project 2002-2007. Technical Report IAEA-TECDOC-1687, International Atomic Energy Agency, 2002-2007.

[22] G. Pastore, S. R. Novascone, R. L. Williamson, J. D. Hales, B. W. Spencer, and D. S. Stafford. Modelling of fuel behaviour during loss-of-coolant accidents using the BISON code. In *Proc. of the LWR Fuel Performance Meeting, Zurich, Switzerland, September 13–17*, 2015.

[23] G. Pastore, R.L. Williamson, S. R. Novascone, B. W. Spencer, and J. D. Hales. Modelling of LOCA tests with the BISON fuel performance code. In *Enlarged Halden Programme Group Meeting, Fornebu, Norway, May 8–13*, 2016.

[24] R. L. Williamson, C. P. Folsom, G. Pastore, and S. Veeraghavan. Reactivity insertion accident (RIA) capability status in the BISON fuel performance code. Technical Report CASL-X-2016-1104-000, Oak Ridge National Laboratory, USA, July 2016.

[25] G. Pastore, D. Pizzocri, S. R. Novascone, D. M. Perez, B. W. Spencer, R.L. Williamson, P. Van Uffelen, and L. Luzzi. Modelling of transient fission gas behaviour in oxide fuel and application to the BISON code. In *Enlarged Halden Programme Group Meeting, Røros, Norway, September 7–12*, 2014.

[26] Reactivity Initiated Accident (RIA) Fuel Codes Benchmark Phase-II Report-Volume 2: Task No. 1 Specifications. Technical Report NEA/CSNI/R(2016)6, OECD/NEA, 2016.

[27] K. J. Geelhood. FRAPTRAN–1.5: A Computer Code for the Transient Analysis of Oxide Fuel Rods. Technical Report NUREG/CF-7023 Vol.1, Rev.1, U.S. Nuclear Regulatory Commission, 2014.

[28] G. K. Miller, D. A. Petti, J. T. Maki, and D. L. Knudsen. PARFUME theory and model basis report. Technical Report INL/EXT-08-14497, Idaho National Laboratory, 2009.

[29] M. Phelip, F. Michel, M. Pelletier, G. Degeneve, and P. Guillermier. The ATLAS HTR fuel simulation code objectives, description and first results. In *2nd International Topical Meeting on High Temperature Reactor Technology*, pages 1–10, Beijing, China, September 2004.

[30] D. G. Martin. Considerations pertaining to the achievement of high burn-ups in htr fuel. *Nuclear Engineering and Design*, 213:241–258, 2002.

[31] E. Proksch, A. Strigl, and H Nabielek. Production of carbon monoxide during burn-up of UO_2 kerneled HTR fuel particles. *Journal of Nuclear Material*, 107:280–285, 1982.

[32] C. Vitanza, E. Kolstad, and U. Graziani. Fission gas release from UO_2 pellet fuel at high burnup. In *Proceedings of the American Nuclear Society Meeting on Light Water Reactor Fuel Performance*, page 361, Portland, Oregon, Apr 29 to May 3, 1979.

[33] E. R. Bradley, M. E. Cunningham, and D. D. Lanning. Final data report for the instrumented fuel assembly (IFA)-432. Technical Report NUREG/CR-2567, PNNL-4240, Pacific Northwest National Laboratory, 1982.

[34] C. R. Hann, D. D. Lanning, E. R. Bradley, R. K. Marshall, M. E. Cunningham, and R. E. Williford. Data Report for the NRC/PNL Halden Assembly IFA-432. Technical Report NUREG/CR-0560, PNL-2673, Pacific Northwest National Laboratory, 1978.

[35] Wolfgang Wiesenack, September 2012. IFA-431 Rods 1, 2, and 3 Halden data.

[36] M. Limbäck and T. Andersson. A model for analysis of the effect of final annealing on the in- and out-of-reactor creep behavior of zircaloy cladding. In *Zirconium in the Nuclear Industry: Eleventh International Symposium*, ASTM STP 1295, pages 448–468, 1996.

[37] Y Rashid, R Dunham, and R Montgomery. Fuel Analysis and Licensing Code: FALCON MOD01. Technical report, Electric Power Research Institute, December 2004.

[38] L. P. Swiler, R. L. Williamson, and D. M. Perez. Calibration of a fuel relocation model in BISON. In *Proceedings of the International Conference on Mathematics and Computational Methods Applied to Nuclear Science and Engineering*, Sun Valley, Idaho, May 5-9, 2013.

[39] Wolfgang Wiesenack, November 2012. IFA-432 Rods 1, 2, and 3 Halden data.

[40] J. A. Turnbull. Concluding Report on Three PWR Rods Irradiated to 90 MWd/kgUO2 in IFa-519.9: Analysis of Measurements Obtained In-Pile and By PIE. Technical Report HWR-668, Halden, January 2001.

[41] I. Matsson. The Effects of Grain Size on FGR and PCMI in High Burnup Fuel (IFA-534.14). Technical Report HWR-558, Halden, February 1999.

[42] Wolfgang Wiesenack, April 2014. IFA-534 Rods 18 and 19 Halden data.

[43] Halden. Qa report for halden ifa-534.14, May 2003. Revision 1.

[44] Glyn Rossiter. Iaea fumex-iii co-ordinated research programme: Nnl final report. Technical Report NNL (12) 12172, National Nuclear Laboratory, 2012.

[45] IAEA. Improvement of Computer Codes Used for Fuel Behaviour Simulation (FUMEX-III): Report of a Coordinated Research Project 2008-2012. Technical Report IAEA-TECDOC-1697, International Atomic Energy Agency, 2008-2012.

[46] T. Tverberg, B. Volkov, and J. C. Kim. Final report on the UO_2-Gd_2O_3 fuel performance test in IFA-636. Technical Report HWR-817, Halden, September 2005.

[47] M. Vankeerbergen. The Integral Fuel Rod Behaviour Test IFA-597.2: Pre-characterization and Analysis of measurements. Technical Report HWR-442, Halden, March 1996.

[48] I. Matsson and J. A. Turnbull. The Integral fuel rod behaviour test IFA-597.3: Analysis of the Measurements. Technical Report HWR-543, Halden, January 1998.

[49] D. R. Packard. Preirradiation characterization of ginna/eseerco lead fuel assemblies containing barrier cladding and annular pellets. Technical Report XN-NF-85-79(P) Revision 1, Exxon Nuclear Company Inc., June 1986.

[50] Siemens Power Corporation. Annular-pellet barrier-clad fuel assemblies at the r. e. ginna pwr: Hotcell examinations. Technical Report EP 80-17 volume 1, Empire State Electric Energy Research Corporation, April 1997.

[51] Ifpe/spc-re-ginna database. Technical report, OECD Nuclear Energy Data Bank, May 2002.

[52] A. S. Giurgiuman and T. E. Wickersham. Annular-pellet barrier-clad fuel r. e. ginna reactor lead fuel assemblies poolside examination. Technical Report EP 80-17, Empire State Electric Energy Research Corporation, August 1994. Final Report.

[53] The Third Risø Fission Gas Project: Bump Test AN2 (CB6). Technical Report Risø-FGP3-AN2, Risø, September 1990.

[54] PE MacDonald and LB Thompson. Matpro-9 a handbook of materials properties for use in the analysis of light water reactor fuel behaviour. Technical Report TREE-NUREG-1005, SEE CODE-9502158 EG and G Idaho, Inc., Idaho Falls (USA). Idaho National Engineering Lab., 1976.

[55] The Third Risø Fission Gas Project: Bump Test AN3 (CB8-2R). Technical Report Risø-FGP3-AN3, Risø, September 1990.

[56] The Third Risø Fission Gas Project: Bump Test AN4 (CB7-2R). Technical Report Risø-FGP3-AN4, Risø, September 1990.

[57] E. Sartori, J. Killeen, and J. A. Turnbull. International Fuel Performance Experiments (IFPE) Database. OECD-NEA, 2010, available at http://www.oecd-nea.org/science/fuel/ifpelst.html.

[58] The Third RisøFission Gas Project: Bump Test AN8 (CB10). Technical Report Risø–FGP3–AN8, Risø, september 1990.

[59] J. A. Turnbull, C. A. Friskney, J. R. Findlay, F. A. Johnson, and A. J. Walter. The diffusion coefficients of gaseous and volatile species during the irradiation of uranium dioxide. *Journal of Nuclear Materials*, 107:168–184, 1982.

[60] HBEP. Summary of the High Burn-up Effects Programme as abstracted from the Programme Final Report. Technical report, High Burn-up Effects Programme, December 2002.

[61] The risø transient fission gas release project: Bump tests with ge fuel. Technical Report Riso-TFGP-R10, Risø, June 1986.

[62] The Third Risø Fission Gas Project: Bump Test II3 (STR014-3R). Technical Report Risø-FGP3-II3, Risø, September 1990.

[63] The Third Risø Fission Gas Project: Bump Test GE7 (ZX115). Technical Report Risø-FGP3-GE7, Risø, September 1990.

[64] Ifpe/osiris r3 database. Technical report, OECD Nuclear Energy Data Bank, May 2002.

[65] M. Lippens and D. Boulanger. Tribulation international programme: Final report. Technical Report 89/79, BelgoNucleaire, September 1989.

[66] Oecd nuclear energy data bank. Technical report, Database, IFPE/Tribulation, May 2002.

[67] Jr G. P. Smith, E.J. Ruzauskas, R. C. Pirek, and M. Griffiths. Hot cell examination of extended burnup fuel from calvert cliffs-1 volume 1. Technical Report TR-103302-V1, Electric Power Research Institute, November 1993.

[68] G. P. Smith Jr, R. C. Pirek, and M. Griffiths. Hot cell examination of extended burnup fuel from calvert cliffs-1 volume 2. Technical Report TR-103302-V2, Electric Power Research Institute, July 1994.

[69] ABB Combustion Engineering-Nuclear Fuel. Examination of the prototype and 1h038 assemblies after reactor cycle 9 in calvert cliffs unit 1. Technical Report CE NPSD-493-NP, Electric Power Research Institute, November 1992.

[70] Seved Djurle. Final Report of the Super–Ramp Project. Technical Report STSR–32, Studsvik Energiteknik, AB, 1984.

[71] D.G. Hardy. High Temperature Expansion and Rupture Behaviour of Zircaloy Tubing. In *CSNI Proceeding of the Specialist Meeting on Safety of Water Reactor Fuel Elements in Saclay*, Saclay, France, October 22-24 1973.

[72] E. Perez-Feró, Z. Hózer, T. Novotny, G. Kracz, M. Horváth, I. Nagy, A. Vimi, A. Pintér-Csordás, Cs. Győri, L. Matus, L. Vasáros, P. Windberg, and L. Maróti. Experimental Database of E110 Claddings under Accident Conditions. Technical Report EK-FRL-2012-255-01/02, Centre for Energy Research, Hungarian Academy of Sciences, Budapest, Hungary, May 2013.

[73] K. Kulacsy. personal information.

[74] V. Di Marcello, A. Schubert, J. van de Laar, and P. Van Uffelen. The TRANSURANUS mechanical model for large strain analysis. *Nuclear Engineering and Design*, 276:19–29, 2014.

[75] F. J. Erbacher, H. J. Neitzel, H. Rosinger, H. Schmidt, and K. Wiehr. Burst criterion of Zircaloy fuel claddings in a loss-of-coolant accident. In *Zirconium in the Nuclear Industry, Fifth Conference, ASTM STP 754, D.G. Franklin Ed.*, pages 271–283. American Society for Testing and Materials, 1982.

[76] M. E. Markiewicz and F.J. Erbacher. Experiments on ballooning in pressurized and transiently heated Zircaloy-4 tubes. Technical Report KfK 4343, Kernforschungszentrum Karlsruhe GmbH (Germany, Kernforschungszentrum Karlsruhe, Germany, 1988.

[77] F.J. Erbacher, H.J. Neitzel, and K. Wiehr. Technical Report KfK 4781, Kernforschungszentrum, Karlsruhe, 1990.

[78] S. Leistikow, G. Schanz, H. v. Berg, and A.E. Aly. Comprehensive presentation of extended Zircaloy-4/steam oxidation results 600-1600 C. In *CSNI/IAEA specialists meeting on water reactor fuel safety and fission product release in off-normal and accident conditions*, Riso Nat. Lab., Denmark, 1983.

[79] A.R. Massih. Transformation kinetics of zirconium alloys under non-isothermal conditions. *Journal of Nuclear Materials*, 384:330–335, 2009.

[80] Ali R Massih and Lars Olof Jernkvist. Transformation kinetics of alloys under non-isothermal conditions. *Modelling and Simulation in Materials Science and Engineering*, 17(5):055002, 2009.

[81] H. J. Neitzel and H. Rosinger. The development of a burst criterion for zircaloy fuel cladding under loca conditions. Technical Report KfK 4343, Kernforschungszentrum Karlsruhe GmbH (Germany, Kernforschungszentrum Karlsruhe, Germany, 1980.

[82] M. Ek. LOCA Testing at Halden; The Second Experiment IFA-650.2. Technical Report HWR-813, OECD Halden Reactor Project, 2005.

[83] A. Lavoil. LOCA Testing at Halden; The Tenth Experiment IFA-650.10. Technical Report HWR-974, OECD Halden Reactor Project, 2010.

[84] A. Lavoil. LOCA Experiments IFA-650.10. Technical Report EP-1650.10, OECD Halden Reactor Project, 2010.

[85] R. L. Williamson, K. A. Gamble, D. M. Perez, S. R. Novascone, G. Pastore, R. J. Gardner, J. D. Hales, W. Liu, and A. Mai. Validating the BISON fuel performance code to integral LWR experiments. *Nuclear Engineering and Design*, 301:232–244, 2016.

[86] Open-source MOOSE software. http://mooseframework.org.

[87] J. Stuckert. On the thermo-physical properties of Zircaloy-4 and ZrO_2 at high temperature. Technical Report FZKA 6739, Kernforschungszentrum Karlsruhe, Germany, 2002.

[88] L. Jernkvist. Estimation of thermo-hydraulic boundary conditions for the Halden IFA-650 LOCA tests. Technical report, Quantum Technologies AB, 2016.

[89] L. J. Siefken et al. SCDAP/RELAP5/MOD3.3 Code Manual: MATPRO–A Library of Materials Properties for Light-Water-Reactor Accident Analysis. Technical Report NUREG/CR-6150, Vol.4, Rev.2, U.S. Nuclear Regulatory Commission, 2001.

[90] K.J. Geelhood, C.E. Beyer, and W.G. Luscher. PNNL Stress/Strain correlation for Zircaloy. Technical Report PNNL-17700, Pacific Northwest National Laboratory, 2008.

[91] Reactivity Initiated Accident (RIA) Fuel Codes Benchmark Phase-II Report-Volume 1: Simplified Cases Results, Summary and Analysis. Technical Report NEA/CSNI/R(2016)6, OECD/NEA, 2016.

[92] Assumptions Used for Evaluating a Control Rod Ejection Accident for Pressurized Water Reactors. Technical Report Regulatory Guide 1.77, U.S. Atomic Energy Commission, 1974.

[93] R. O. Montgomery and Y. R. Rashid. Evaluation of irradiated fuel during RIA simulation tests. Technical Report TR-106387, Electric Power Research Institute, August 1996.

[94] J. Papin, B. Cazalis, J. Frizonnet, J. Desquines, F. Lemoine, V. Georgenthum, F. Lamare, and M. Petit. Summary and interpretation of the CABRI REP-Na program. *Nuclear Technology*, 157(3):230–250, 2007.

[95] J. Papin, B. Cazalis, J. Frizonnet, E. Federici, and F. Lemoine. Synthesis of CABRI-RIA tests interpretation. In *Eurosafe Meeting 2003*, Paris, France, 2003.

[96] F. Schmitz and J. Papin. High burnup effects on fuel behaviour under accident conditions: the tests CABRI REP-Na. *Journal of Nuclear Materials*, 270(1):55–64, 1999.

[97] K. J. Geelhood and W. Luscher. FRAPTRAN–1.5: Integral Assessment. Technical Report NUREG/CR-7023 Vol.2, Rev.1, U.S. Nuclear Regulatory Commission, 2014.

[98] J. Y. Blanc and M. Vouillot. Presentation of the fabrice process and refabrication experience up to 1994. Technical Report IAEA-TECDOC-822, International Atomic Energy Agency, 1995.

[99] W. Liu. Zirconium alloy clad yield stress model in bison-casl code. Technical Report ANA-P1400138-TN02 Rev.1, ANATECH Corp., December 2015.

[100] R. Montgomery and D. Sunderland. Analysis of reactivity initiated accident-simulation tests conducted at the CABRI and NSRR facilities in france and japan. Technical Report 1002863, Electric Power Research Institute, December 2003.

[101] G. Pastore, L. Luzzi, V. Di Marcello, and P. Van Uffelen. Physics-based modelling of fission gas swelling and release in UO_2 applied to integral fuel rod analysis. *Nuclear Engineering and Design*, 256:75–86, 2013.

[102] G. Pastore, L.P. Swiler, J.D. Hales, S.R. Novascone, D.M. Perez, B.W. Spencer, L. Luzzi, P. Van Uffelen, and R.L. Williamson. Uncertainty and sensitivity analysis of fission gas behavior in engineering-scale fuel modeling. *Journal of Nuclear Materials*, 465:398–408, 2015.

[103] G. Pastore, D. Pizzocri, J. D. Hales, S. R. Novascone, D. M. Perez, B. W. Spencer, R. L. Williamson, P. Van Uffelen, and L. Luzzi. Modeling of transient fission gas behavior in oxide fuel and application to the BISON code. In *Enlarged Halden Programme Group Meeting*, Røros, Norway, September 7–12 2014.

[104] T. Barani, E. Bruschi, D. Pizzocri, G. Pastore, P. Van Uffelen, R.L. Williamson, and L. Luzzi. Analysis of transient fission gas behaviour in oxide fuel using BISON and TRANSURANUS. *Journal of Nuclear Materials*, 486:96–110, 2017.

[105] T. Nakamura, H. Sasajima, T. Fuketa, and K. Ishijima. Fission gas induced cladding deformation of lwr fuel rods under reactivity initiated accident conditions. *Journal of Nuclear Science and Technology*, 33(12):924–935, 1996.

[106] V. Georgenthum, C. Folsom, A. Moal, O. Marchand, R. Williamson, H. Ban, and D. Wachs. SCANAIR-BISON benchmark on CIP0-1 RIA test. In *to be published in 2017 Water Reactor Fuel Performance Meeting*, Jeju Island, Korea, September 10–14 2017.

[107] Masaki Amaya, Fumihisa Nagase, Tomoyuki Sugiyama, Yutaka Udagawa, Takafumi Narukawa, and Akihiko Sawada. Current Studies at JAEA on Fuel Behaviors under Accident Conditions. In *Proceedings of WRFPM 2014*, Sendai, Japan, September 14–17 2014.

[108] T. Nakamura, K. Kusagaya, T. Fuketa, and H. Uetsuka. High-burnup BWR Fuel Behavior under Simulated Reactivity-initiated Accident Conditions. *Nuclear Technology*, 138(3):246–259, 2002.

[109] T. Nakamura, M. Yoshinaga, M. Takahashi, K. Okonogi, and K. Ishijima. Boiling Water Reactor Fuel Behavior under Reactivity-initiated-accident Conditions at Burnup of 41 to 45 GWd/tonne U. *Nuclear Technology*, 129(2):141–151, 2000.

[110] Takehiko Nakamura, Masato Takahashi, and Makio Yoshinaga. Evaluation of burnup characteristics and energy deposition during nsrr pulse irradiation tests on irradiated bwr fuels. Technical Report JAERI-Research 2000-048, JAERI, September 2000.

[111] Wenfeng Liu, John Alvis, Robert Montgomery, and Ken Yueh. Analysis of High Burnup Fuel Failures at Low Temperatures in RIA Tests Using CSED. In *Proceedings of 2010 LWR Fuel Performance*, Orlando, Florida, USA, Sepember 26–29 2010.

[112] V. Bessiron. Modeling of Clad-to-coolant Heat Transfer for RIA Applications. *Journal of Nuclear Science and Technology*, 44(2):211–221, 2007.